



MINISTÉRIO DA  
CIÊNCIA, TECNOLOGIA  
E INOVAÇÕES



PÁTRIA AMADA  
**BRASIL**  
GOVERNO FEDERAL

sid.inpe.br/mtc-m21c/2021/02.10.14.12-TDI

**ANALYSIS OF EXTREME PRECIPITATION EVENTS  
ESTIMATED BY SATELLITE AND ITS RELATIONSHIP  
WITH MESOSCALE CONVECTIVE SYSTEMS OVER  
SOUTH AMERICA**

Rayana Santos Araujo Palharini

Doctorate Thesis of the Graduate  
Course in Meteorology, guided  
by Dr. Daniel Alejandro Vila,  
approved in February 24, 2021.

URL of the original document:

[<http://urlib.net/8JMKD3MGP3W34R/4465CAB>](http://urlib.net/8JMKD3MGP3W34R/4465CAB)

INPE  
São José dos Campos  
2021

**PUBLISHED BY:**

Instituto Nacional de Pesquisas Espaciais - INPE  
Coordenação de Ensino, Pesquisa e Extensão (COEPE)  
Divisão de Biblioteca (DIBIB)  
CEP 12.227-010  
São José dos Campos - SP - Brasil  
Tel.:(012) 3208-6923/7348  
E-mail: pubtc@inpe.br

**BOARD OF PUBLISHING AND PRESERVATION OF INPE  
INTELLECTUAL PRODUCTION - CEPPII (PORTARIA Nº  
176/2018/SEI-INPE):****Chairperson:**

Dra. Marley Cavalcante de Lima Moscati - Coordenação-Geral de Ciências da Terra  
(CGCT)

**Members:**

Dra. Ieda Del Arco Sanches - Conselho de Pós-Graduação (CPG)  
Dr. Evandro Marconi Rocco - Coordenação-Geral de Engenharia, Tecnologia e  
Ciência Espaciais (CGCE)  
Dr. Rafael Duarte Coelho dos Santos - Coordenação-Geral de Infraestrutura e  
Pesquisas Aplicadas (CGIP)  
Simone Angélica Del Ducca Barbedo - Divisão de Biblioteca (DIBIB)

**DIGITAL LIBRARY:**

Dr. Gerald Jean Francis Banon  
Clayton Martins Pereira - Divisão de Biblioteca (DIBIB)

**DOCUMENT REVIEW:**

Simone Angélica Del Ducca Barbedo - Divisão de Biblioteca (DIBIB)  
André Luis Dias Fernandes - Divisão de Biblioteca (DIBIB)

**ELECTRONIC EDITING:**

Ivone Martins - Divisão de Biblioteca (DIBIB)  
André Luis Dias Fernandes - Divisão de Biblioteca (DIBIB)





MINISTÉRIO DA  
CIÊNCIA, TECNOLOGIA  
E INOVAÇÕES



sid.inpe.br/mtc-m21c/2021/02.10.14.12-TDI

**ANALYSIS OF EXTREME PRECIPITATION EVENTS  
ESTIMATED BY SATELLITE AND ITS RELATIONSHIP  
WITH MESOSCALE CONVECTIVE SYSTEMS OVER  
SOUTH AMERICA**

Rayana Santos Araujo Palharini

Doctorate Thesis of the Graduate  
Course in Meteorology, guided  
by Dr. Daniel Alejandro Vila,  
approved in February 24, 2021.

URL of the original document:

[<http://urlib.net/8JMKD3MGP3W34R/4465CAB>](http://urlib.net/8JMKD3MGP3W34R/4465CAB)

INPE  
São José dos Campos  
2021

## Cataloging in Publication Data

---

Palharini, Rayana Santos Araujo.

P175a      Analysis of extreme precipitation events estimated by satellite and its relationship with mesoscale convective systems over South America / Rayana Santos Araujo Palharini. – São José dos Campos : INPE, 2021.

xxx + 170 p. ; (sid.inpe.br/mtc-m21c/2021/02.10.14.12-TDI)

Thesis (Doctorate in Meteorology) – Instituto Nacional de Pesquisas Espaciais, São José dos Campos, 2021.

Guiding : Dr. Daniel Alejandro Vila.

1. Satellite. 2. Extreme rainfall. 3. Estimates. 4. MCS. I.Title.

CDU 551.577(8)

---



Esta obra foi licenciada sob uma Licença [Creative Commons Atribuição-NãoComercial 3.0 Não Adaptada](#).

This work is licensed under a [Creative Commons Attribution-NonCommercial 3.0 Unported License](#).

MINISTÉRIO DA  
CIÊNCIA, TECNOLOGIA  
E INOVAÇÕES**INSTITUTO NACIONAL DE PESQUISAS ESPACIAIS**

Pós Graduação

Meteorologia

**ATA DE REUNIÃO****DEFESA FINAL DE DISSERTAÇÃO: RAYANA SANTOS ARAUJO PALHARINI - REGISTRO 125989/2016****BANCA: 029/2021**

No dia 24 de fevereiro, às 14h00, por videoconferência, a aluna mencionada acima defendeu seu trabalho final, intitulado **"ANALYSIS OF EXTREME PRECIPITATION EVENTS ESTIMATED BY SATELLITE AND ITS RELATIONSHIP WITH CONVECTIVE MESOSCALE SYSTEMS ON SOUTH AMERICA"** (apresentação oral seguida de arguição) perante uma Banca Examinadora, cujos membros estão listados abaixo. A aluna foi **APROVADA** pela Banca Examinadora, por unanimidade, em cumprimento ao requisito exigido para obtenção do Título de Doutora em Meteorologia.

A banca sugere incorporar as observações dos membros na tese, bem como mudança do título para:

**Título: "ANALYSIS OF EXTREME PRECIPITATION EVENTS ESTIMATED BY SATELLITE AND ITS RELATIONSHIP WITH MESOSCALE CONVECTIVE SYSTEMS OVER SOUTH AMERICA."**

Eu, Manoel Alonso Gan, como Presidente da Banca Examinadora, assino esta ATA em nome de todos os membros.

**Membros da Banca**Dr. Daniel Alejandro Vila (**orientador**) - CPTEC – INPEDr. Manoel Alonso Gan (**Presidente**) - CPTEC - INPEDr. Nelson Ferreira de Jesus (**Convidado**) - CPTEC - INPEDr. Daniele Tôrres Rodrigues (**Convidado**) - Universidade Federal do Rio Grande do NorteDr. Enrique Vieira Mattos (**Convidado**) - Universidade Federal de Itajubá (UNIFEI)

Documento assinado eletronicamente por **Manoel Alonso Gan, Pesquisador**, em 26/02/2021, às 14:26 (horário oficial de Brasília), com fundamento no art. 6º do [Decreto nº 8.539, de 8 de outubro de 2015](#).

A autenticidade deste documento pode ser conferida no site <http://sei.mctic.gov.br/verifica.html>, informando o código verificador **6574589** e o código CRC **807F34CF**.



---

**Referência:** Processo nº 01340.000654/2021-88

SEI nº 6574589

*“A Terra ofereceria ao homem sempre o necessário, se com o necessário soubesse o homem contentar-se.”*

O LIVRO DOS ESPÍRITOS  
ALLAN KARDEC  
1857



Queridos leitores,

*Escrevo em português, minha língua materna, pois é mais fácil expressar meus sentimentos.*

*Ao longo de meu doutoramento, tive a oportunidade de sentir muitos sentimentos diferentes, alguns nunca sentidos antes na minha trajetória de vida.*

*Vi muitas situações injustas dentro e fora da pós-graduação. Vi pessoas agirem de forma corrupta, vi outras sendo corruptíveis pois deveriam pensar: "Se é bom para mim, porque não?!" Com isso poucos se beneficiaram e muito se prejudicaram. Mas pouco importava, pois erámos apenas estudantes sem direito algum.*

*No começo lutei muito, por meus direitos e de meus colegas, briguei por achar que mudaria o sistema corrompido, mas depois de perder as forças de tanto lutar, percebi que sozinha nada mudaria.*

*Percebi que a mudança deve ocorrer primeiro dentro de cada indivíduo. Só assim, viveremos em um mundo regenerado onde os conceitos de respeito e justiça nascem dos atos de todas as pessoas e não apenas de algumas.*

*Passei por muitas situações difíceis, desde dores constantes nas costas, dores de estômago, enxaquecas, dor de dente, muitas espinhas no rosto, descobrimento de novos fios de cabelo branco e de uma doença auto-imune, tudo isso desencadeado pelo estresse e pressão que estão associados a obtenção do tão sonhado título de PhD.*

*Não bastasse as doenças físicas, ainda surgiram as doenças psicológicas. Em muitos momentos achei que não conseguiria e que a vida não tinha nenhum sentido. Me perguntei muitas vezes qual seria o verdadeiro sentido da vida e qual seria a minha missão nesse mundo que muitas vezes parece ser tão caótico.*

*E por falar em caótico, eis que surge o ano de 2020 que estará marcado na minha vida e na vida de muitos habitantes deste planeta chamado Terra. Ano marcado pela pandemia do corona vírus, que abalou emocionalmente não só a mim mas a muitas pessoas. Tivemos que nos adaptar e aprender com os obstáculos colocados pela vida.*

*Muitos tiveram suas vidas ceifadas, inclusive um membro de minha família, para nos mostrar quão pequeninos somos perante a um vírus invisível. Alguns aproveitaram essa oportunidade de aprendizado, outros... nem tanto!*

*Com a ajuda de amigos/irmãos e do grande mestre Jesus, descobri que essa vida é apenas uma passagem, apenas um caminho para acharmos o que existe de mais importante e essencial em todo o universo: O AMOR*

*Por tudo isso, dedico esta tese a meus pais que me deram a oportunidade de vir a esse mundo, ao meu esposo que me deu a oportunidade do aprendizado e crescimento espiritual dia a dia, e a todos os amigos espirituais que estavam e estão comigo em todos os momentos da minha vida com um apoio e amor incondicional. Se eu pudesse resumir tudo o que sinto em uma palavra, essa seria GRATIDÃO.*





## **ACKNOWLEDGEMENTS**

I express my gratitude to my advisor, Daniel Vila, for believing in me in the realization of this work. I send my eternal gratitude to the family members, friends, and other professors of PGMET who directly and indirectly collaborated in the work and provided me with inspiration along the journey. To Dr. Cintra and Dra. Sheila for taking care of my psychological state. To Rodrigo for your steady love and for always being patient with me, and for helping me at all times. I am sure that I have learned and will learn a lot being beside you! Finally, I thank the Brazilian government for the financial support of the National Council for Scientific and Technological Development (CNPq) and the Coordination for the Improvement of Higher Education Personnel (CAPES) through my Ph.D. fellowship and the sponsorship of my program at the National Institute for Space Research (INPE).



## ABSTRACT

Climate change is increasing the intensity and frequency of extreme events around the world and our society is vulnerable to the dangers of natural disasters. According to the Brazilian Atlas of Natural Disasters, a total of 38,996 disasters were recorded during the period 1991-2012. According to this database, approximately 40% of hydrometeorological events were caused by floods, landslides, hail, local storms and windstorms. One of the main meteorological variables associated with natural disasters is precipitation. Understanding the behavior and improving the prediction of these events is of fundamental importance as heavy rainfall causes irreparable damage and causes great economic losses for a country. With the objective of improve the understanding about extreme rainfall of Brazil a daily  $1^\circ \times 1^\circ$  gridded precipitation database was used to assess the performance of different precipitation products to retrieval extreme rainfall at different regions of Brazil, as well as an analysis of the Mesoscale Convective Systems and their influence on extreme rain. The products evaluated in this investigation were 3B42 RT v7.0, 3B42 RT v7.0 uncalibrated, CMORPH V1.0 RAW, CMORPH V1.0 CRT, GSMAP-NRT-no gauge v6.0, GSMAP-NRT- gauge v6.0, CHIRP V2.0, CHIRPS V2.0, PERSIANN CDR v1 r1, CoSch and TAPEER v1.5 from Frequent Rainfall Observations on GridS (FROGS) database. Some products considered in this investigation are adjusted with rain gauge values and others only with satellite information. In this study, these two sets of products were considered. In addition, gauge-based daily precipitation data, provided by Brazil's National Institute for Space Research, were used as reference in the analyses. In order to compare gauge-based daily precipitation and satellite-based data for extreme values, statistical techniques were used to evaluate the performance the selected satellite products over the tropical region of South America. According to the results, the threshold for rain to be considered an extreme event in South America presented high variability, ranging from 20 to 150 mm/day, depending on the region and the percentile threshold chosen for analysis. In addition, the results showed that the ability of the satellite estimates to retrieve rainfall extremes depends on the geographical location and large-scale rainfall regimes. Each region of Brazil is characterized by extremes of rain with different intensities. The regions with the highest values are south and north regions of Brazil with values around 125.0 mm/day. In both regions, the GSMAP product (with and without rain gauges adjustments) have a better performance. On the other hand, the regions with the lowest intensities are the northeastern region (inland and coast) with more frequent extreme values around the 35.0 mm/day. In those regions 3B42RT v7.0 and 3B42RT v7.0 uncalibrated demonstrated a better performance respectively. It is worth mentioning that the precipitation values found in this work do not necessarily cause disasters or generate impacts in the analyzed regions, they were considered extreme from a statistical point of view, considering the analyzed database. In order to describe the morphological characteristics of the MCS and identify the influence of these systems on extreme rain during the period 2012-2016 in the

tropical region of South America, the dataset used in this investigation was the CACATOES dataset. It is a level-3 product derived from the Tracking Of Organized Convection Algorithm through 3D segmentation (TOOCAN). According to results, small systems with a duration smaller than 12 hours are the ones that occurred with a higher frequency. However, systems that have duration above 12 hours are the ones that most contributed to the extreme rain. A significant influence of the MCS was identified over a large part of the South America regions. In addition, the influence of the MCS over the investigated region presented a significant variability. In order to analyze five case studies associated to extreme rain which caused natural disaster in five different regions of Brazil was analysed. The regions were defined based on previous studies according to the climatological distribution of rainfall in each region. To be considered statistically extreme, the cases were analyzed considering rain values above the 99th percentile during the period 2012-2016. Three databases were used: Precipitation from (i) rain gauges stations and (ii) different satellite-based estimates and (iii) Mesoscale convective tracking data. The methodology was based in identifying events, analyzing the performance of satellite precipitation estimates to detect the observed extreme rain and finally quantifying the influence of convective systems on the extreme rain that occurred. Although all regions of Brazil are subject to the occurrence of natural disasters caused by extreme rains, the results suggest that the impacts caused in each region have different magnitudes. It was noticed that the convective systems influenced above 90.0 % of the extreme rains in the case analysed in South region of Brazil while it influenced about 60.0 % to 90.0 % of the extreme rains in the case analysed in Northeast region of Brazil. In general, satellite products have identified rain events, however, in the southern region of Brazil, products have tended to overestimate rainfall, while other regions have tended to underestimate extreme rain values. It can be seen then that it is still a challenge for the methods used in the satellite precipitation estimation products to accurately identify specific extreme rain events.

Keywords: Satellite. Extreme rainfall. Estimates. MCS.

# **ANÁLISE DE EVENTOS EXTREMOS DE PRECIPITAÇÃO ESTIMADOS POR SATÉLITE E SUA RELAÇÃO COM SISTEMAS CONVECTIVOS DE MESOESCALA SOBRE A AMÉRICA DO SUL**

## **RESUMO**

As mudanças climáticas estão aumentando a intensidade e a frequência de eventos extremos em todo o mundo. Cada vez mais, a sociedade está vulnerável aos perigos dos desastres naturais. De acordo com o Atlas Brasileiro de Desastres Naturais, um total de 38.996 desastres foram registrados no período de 1991 a 2012. De acordo com esta base de dados, aproximadamente 40% dos eventos hidrometeorológicos foram causados por inundações, deslizamentos de terra, granizo, tempestades locais e vendavais. Uma das principais variáveis meteorológicas associadas aos desastres naturais é a precipitação. Entender o comportamento e melhorar a previsão desses eventos é de fundamental importância, pois chuvas intensas causam danos irreparáveis e grandes perdas econômicas para um país. Com o objetivo de melhorar o entendimento sobre as chuvas extremas do Brasil, um banco de dados diário de precipitação em grade de  $1^\circ \times 1^\circ$  foi usado para avaliar a habilidade de diferentes produtos de estimativas de precipitação por satélite em detectar as chuvas extremas em diferentes regiões do Brasil, bem como a análise da sistemas convectivos de mesoescala e sua influência nas chuvas extremas. Os produtos avaliados nesta investigação foram 3B42 RT v7.0, 3B42 RT v7.0 não calibrado, CMORPH V1.0 RAW, CMORPH V1.0 CRT, GSMAP-NRT-sem pluviômetro v6.0, GSMAP-NRT-com pluviômetro v6.0, CHIRP V2.0, CHIRPS V2.0, PERSIANN CDR v1 r1, CoSch e TAPEER v1.5 do banco de dados Frequent Rainfall Observations on GridS (FROGS). Alguns produtos considerados nesta investigação são ajustados com valores de pluviômetro e outros apenas com informações de satélite. Neste estudo, esses dois conjuntos de produtos foram considerados. Além disso, dados de precipitação diária baseados em indicadores, fornecidos pelo Instituto Nacional de Pesquisas Espaciais do Brasil, foram usados como referência nas análises. A fim de comparar a precipitação diária baseada em pluviômetro e os dados de satélite para valores extremos, técnicas estatísticas foram usadas para avaliar o desempenho dos produtos de satélite selecionados na região tropical da América do Sul. De acordo com os resultados, o limiar para chuva ser considerada um evento extremo na América do Sul apresentou grande variabilidade, variando de 20,0 a 150,0 mm/dia, dependendo da região e do limiar de percentil escolhido para análise. Além disso, os resultados mostraram que a capacidade das estimativas de satélite de recuperar os extremos de chuva depende da localização geográfica e dos regimes de chuva em grande escala. Cada região do Brasil é caracterizada por extremos de chuva com intensidades diferentes. As regiões com os maiores valores são as regiões Sul e Norte do Brasil com valores em torno de 125,0 mm / dia. Em ambas as regiões, o produto GSMAP (com e sem ajustes de pluviômetros) tem melhor desempenho. Por outro lado, as regiões com as menores intensidades são a região Nordeste (interior e litoral) com valores extremos mais frequentes em torno dos 35,0 mm/dia. Nessas regiões, o 3B42RT v7.0 e o 3B42RT v7.0 não calibrado demonstraram um melhor desempenho, respectivamente. Vale ressaltar que os

valores de precipitação encontrados neste trabalho não necessariamente causam desastres ou geram impactos nas regiões analisadas, foram considerados extremos do ponto de vista estatístico, considerando a base de dados analisada. Com o objetivo de descrever as características morfológicas do MCS e identificar a influência desses sistemas nas chuvas extremas durante o período de 2012-2016 na região tropical da América do Sul, o conjunto de dados utilizado nesta investigação foi o conjunto de dados CACATOES. É um produto de nível 3 derivado do Algoritmo de Rastreamento de Convecção Organizada por meio da segmentação 3D (TOOCAN). De acordo com os resultados, pequenos sistemas com duração inferior a 12 horas são os que ocorreram com maior frequência. Porém, os sistemas que têm duração acima de 12 horas são os que mais contribuem para as chuvas extremas. Foi identificada uma influência significativa do MCS em grande parte das regiões sul-americanas. Além disso, a influência do MCS sobre a região investigada apresentou uma variabilidade significativa. Com o objetivo de analisar cinco estudos de caso associados às chuvas extremas que causaram desastres naturais em cinco diferentes regiões do Brasil foram analisados. As regiões foram definidas com base em estudos anteriores de acordo com a distribuição climatológica das chuvas em cada região. Para serem considerados estatisticamente extremos, os casos foram analisados considerando-se valores de chuva acima do percentil 99 durante o período de 2012-2016. Três bancos de dados foram usados: Precipitação de (i) estações pluviométricas e (ii) diferentes estimativas baseadas em satélite e (iii) dados de rastreamento convectivo de mesoescala. A metodologia baseou-se na identificação de eventos, na análise do desempenho das estimativas de precipitação por satélite para detectar as chuvas extremas observadas e, por fim, quantificar a influência dos sistemas convectivos nas chuvas extremas ocorridas. Embora todas as regiões do Brasil estejam sujeitas à ocorrência de desastres naturais causados por chuvas extremas, os resultados sugerem que os impactos causados em cada região têm magnitudes diferentes. Percebeu-se que o sistema convectivo influenciou acima de 90,0 % das chuvas extremas no caso analisado na região Sul do Brasil enquanto influenciou cerca de 60,0 % a 90,0 % das chuvas extremas no caso analisado na região Nordeste do Brasil. Em geral, os produtos de satélite identificam eventos de chuva, no entanto, na região sul do Brasil, os produtos tendem a superestimar as chuvas, enquanto outras regiões tendem a subestimar os valores extremos de chuva. Pode-se ver então que ainda é um desafio para os métodos usados nos produtos de estimativa de precipitação por satélite identificar com precisão eventos específicos de chuva extrema.

Palavras-chave: Satellite. Extreme rainfall. Estimates. MCS.

## LIST OF FIGURES

	<u>Page</u>
1.1 Thesis structure. . . . .	4
2.1 (a) The world's first satellite Sputnik-1 launched in October 4,1957 by Russia. (b) The The world's first meteorological satellite TIROS-1 launched in April 1,1960 by USA. . . . .	10
2.2 Satellites with meteorological objectives already placed launched in orbit. (a) TRMM, (b) GPM, (c) GOES. . . . .	11
3.1 Topography map of the studied region. . . . .	19
3.2 Percentage of days with, at least, one rain gauge in every grid point for the period 2012-2016. White color represent no gauges for that grid point for the whole period (a) GPCC dataset and (c) INPE dataset. Pixels with a frequency larger than 90% of in the temporal series for 2012 to 2016 period (b) GPCC dataset and (d) INPE dataset. . . . .	23
3.3 ECDF of Percentiles (a) 99.0, (b) 99.5, (c) 99.9 and (d) MAX values from South America. . . . .	29
3.4 Zonal mean precipitation over South America. . . . .	31
3.5 Zonal precipitation (a) and number of grid points by latitude (b) of maximum values over South America. . . . .	33
3.6 PDF of maximum rainfall [mm/day] of satellite products from South America (345 grid points). The histograms represent the empirical distribution. The curves represent the density estimated by the kernel method. . . . .	34
3.7 Statistical comparison between gridded rain gauge data and satellite-derived rainfall products over a period of 5 years (2012-2016) described by Taylor Diagram of maximum rainfall (a) and Bias bars (b). RMSE is represented with curved lines in green, STD is represented with curved lines blue and r is represented with straight lines in black. . . . .	36
3.8 Spacial distribution of maximum rainfall [mm/day] of each products. . .	37
3.9 Spacial distribution of Estimated - Observed maximum precipitation [mm/day] of each products. . . . .	39
3.10 Zonal precipitation (a) and number of grid points by latitude of the mean values of all values above 99th percentile over South America. .	40

3.11 PDF of 99th percentile of rainfall [mm/day] of satellite products from South America (345 grid points). The histograms represent the empirical distribution. The curves represent the density estimated by the kernel method. . . . .	41
3.12 Statistical comparison between gridded rain gauge data and satellite-derived rainfall products over a period of 5 years (2012-2016) described by Taylor Diagram of P99th rainfall (a) and Bias bars (b). RMSE is represented with curved lines in green, STD is represented with curved lines blue and $r$ is represented with straight lines in black. . . .	43
3.13 Spacial distribution of 99th percentile rainfall [mm/day] of each products.	44
3.14 Spacial distribution of Estimated - Observed 99th percentile of rainfall [mm/day] of each products. . . . .	45
4.1 Frequency of wet days ( $> 1.0$ mm/day) over Brazil during the study period (2012-2016) using rain gauges dataset at National Institute for Space Research (INPE) . . . . .	52
4.2 The five regions of Brazil according to homogeneous rainfall regime. .	56
4.3 Grid points with more than 90% of rain gauges data in the temporal series for 2012 to 2016 period of INPE dataset with 317 valid grid points.	61
4.4 PDF of Maximum rainfall [mm/day] from satellite products for five regions in Brazil: Southern Brazil (R1); Central Region (R2); Northeastern (R3); Northeast Coast (R4); North Brazil (R5). . . . .	63
4.5 PDF of P99th rainfall [mm/day] from satellite products for five regions in Brazil: (a) Southern Brazil-R1; (b) Central Region-R2; (c) Northeastern-R3; (d) Northeast Coast-R4; (e) North Brazil-R5. . . . .	64
4.6 Statistical comparison between gridded rain gauge data (INPE) and satellite-derived rainfall products over a period of 5 years (2012-2016): Taylor Diagram of Maximum (a), P99th rainfall (b), bias bars of Maximum (c), and P99th rainfall (d). RMSE is represented by green curved lines, STD is represented by blue curved lines and $r$ is represented by black straight lines. . . . .	66
4.7 Seasonal empirical cumulative distribution function of (a) maximum rainfall and (b) extreme rainfall above P99th threshold [mm/day] of satellite products from R1 - Southern Brazil - 31 grid points. . . . .	67



4.8	Statistical comparison between gridded rain gauge data and satellite-derived rainfall products over a period of 5 years (2012-2016): Taylor Diagram of Maximum (a), P99th rainfall (b), bias bars of Maximum (c), and P99th rainfall (d). RMSE is represented by green curved lines, STD is represented by blue curved lines and $r$ is represented by black straight lines. . . . .	68
4.9	Seasonal empirical cumulative distribution function of (a) maximum rainfall and (b) extreme rainfall above P99th threshold [mm/day] of satellite products from R2 - Central Region- 171 grid points. . . . .	69
4.10	Statistical comparison between gridded rain gauge data and satellite-derived rainfall products over a period of 5 years (2012-2016): Taylor Diagram of Maximum (a), P99th rainfall (b), bias bars of Maximum (c), and P99th rainfall (d). RMSE is represented by green curved lines, STD is represented by blue curved lines and $r$ is represented by black straight lines. . . . .	70
4.11	Seasonal empirical cumulative distribution function of (a) maximum rainfall and (b) extreme rainfall above P99th threshold [mm/day] of satellite products from R3 - Northeastern - 53 grid points. . . . .	71
4.12	Statistical comparison between gridded rain gauge data and satellite-derived rainfall products over a period of 5 years (2012-2016): Taylor Diagram of Maximum (a), P99th rainfall (b), bias bars of Maximum (c), and P99th rainfall (d). RMSE is represented by green curved lines, STD is represented by blue curved lines and $r$ is represented by black straight lines. . . . .	72
4.13	Seasonal empirical cumulative distribution function of (a) maximum rainfall and (b) extreme rainfall above P99th threshold [mm/day] of satellite products from R4 - Northeast Coast - 6 grid points. . . . .	73
4.14	Seasonal empirical cumulative distribution function of (a) maximum rainfall and (b) extreme rainfall above P99th threshold [mm/day] of satellite products from R5 - North Brazil- 39 grid points. . . . .	74
4.15	Statistical comparison between gridded rain gauge data and satellite-derived rainfall products over a period of 5 years (2012-2016): Taylor Diagram of Maximum (a), P99th rainfall (b), bias bars of Maximum (c), and P99th rainfall (d). RMSE is represented by green curved lines, STD is represented by blue curved lines and $r$ is represented by black straight lines. . . . .	75
4.16	Summary table indicating the products that showed a better performance over the different regions of Brazil. . . . .	78

5.1	Topography map of South America. . . . .	81
5.2	Grid points with more than 90% of rain gauges data in the temporal series for 2012 to 2016 period of INPE dataset with 345 valid grid points. . . . .	84
5.3	Schematic flowchart to describe variable extracted from CACATOES dataset and rain gauges dataset considering the rainfall values above percentile 99th (P99th). . . . .	87
5.4	Distribution of life time duration of MCS represented by (a) Probability distribution function and (b) Cumulative distribution function. . . . .	88
5.5	Distribution of maximum cold cloud surface reached by the MCS along its life cycle at 235K represented by (a) Probability distribution function and (b) Cumulative distribution function. . . . .	89
5.6	Distribution of population of MCS which are included partially or totally within a 1°/1day grid point represented by (a) Probability distribution function and (b) Cumulative distribution function. . . . .	90
5.7	Distribution of eccentricity of the ellipse at a 235K threshold and at time of the maximum extent from MCS represented by (a) Probability distribution function and (b) Cumulative distribution function. . . . .	91
5.8	Distribution of minimum brightness temperature of MCS represented by (a) Probability distribution function and (b) Cumulative distribution function. . . . .	91
5.9	Probability Distribution Function bi-dimensional of morphological attributes of MCS over South America (land + ocean). The colours shading corresponds to the joint frequency of variables in log-normal. . . . .	93
5.10	(a) Spatial distribution of the fraction of the time occupied by MCS during all period of duration 2012-2016. (b) Spatial distribution of the fraction of the time occupied by MCS > 12 hr of duration. (c) Spatial distribution of the fraction of the time occupied by MCS > 24 hr of duration. . . . .	94
5.11	(a) Scatter plot of accumulated extreme rainfall (values above P99) and accumulated rainfall influenced by MCS occurred during 2012-2016 and marginal histograms of respectively variables. (b) Plot of relationship between contribution of MCS in extreme rainfall and fraction of time occupied by MCS, the size of points represent the total number of MCS occurred . . . . .	97
5.12	(a) Accumulated extreme rainfall (values above P99) recorded during 2012 to 2016 over tropical region of South America. (b) Number of MCS events recorded in 5 years (2012-2016).(c) Contribution of MCS for extreme rainfall. . . . .	98

6.1	The five regions of Brazil according to climatological rainfall regime. Southern Brazil (R1-blue), Central Region (R2-green), Northeastern (R3-black), Northeast Coast (R4-yellow) and North Brazil (R5-red). . .	104
6.2	Schematic flowchart to describe variable extracted from CACATOES dataset and rain gauges dataset considering the rainfall values above percentile 99th (P99th). . . . .	109
6.3	Municipalities affected by extreme rains. (a) Flooding in municipality of Iraí located north of Rio Grande do Sul state. (b) Flooding in municipality of Chapecó located west of Santa Catarina state. Photographs: Fernando Sucolotti/G1 and Marcio Cunha/RBS. . . . .	111
6.4	Fields of atmospheric patterns from GFS model over South America for <b>20140626 12UTC</b> . <b>(a)</b> Satellite GOES-13 infrared image; <b>(b)</b> Potential temperature (shaded, K) and wind barbs (knots) in the dynamic tropopause, 925–850-hPa layer-averaged cyclonic relative vorticity (black contours); <b>(c)</b> 250-hPa wind speed (m s <sup>-1</sup> , shaded according to color bar), 250-hPa potential vorticity (gray contours), 250-hPa relative humidity (%), shaded according to gray scale), 600–400-hPa layer averaged ascent (red contours); <b>(d)</b> 250-hPa wind speed (m s <sup>-1</sup> , shaded according to color bar), 1000–500-hPa thickness (dashed contours), Sea Level Pressure (solid contours), total precipitable water (mm, shaded according to gray scale). . . . .	112
6.5	(a) Accumulated rainfall recorded during 24/06/2014 to 28/06/2014 over South region of Brazil (R1). (b) Fraction of rain from rain gauges on days that had MCS record by rain accumulated in 5 days. (c) Number of MCS events recorded in 5 days. (d) Fraction of the days that had MCS record by 5 days. (e) Indicative map of the location of the analyzed region. . . . .	113
6.6	Case of extreme precipitation occurred over South region of Brazil (R1) during 24/06/2014 to 28/06/2014. . . . .	114
6.7	Bar graphs of (a) Probability Of Detection (POD), (b) Miss Rate (MR), (c) False Alarm Ratio (FAR), (d) Threat Score (TS), (e) Frequency Bias Index (FBI) and (e) Proportion Correct (PC) for 5 days accumulated precipitation over South region of Brazil during 24/06/2014 to 28/06/2014. . . . .	116

6.8	Municipalities affected by the extreme rain. (a) Flooding in municipality of Muriaé on Minas Gerais state, (b) Collapse of houses in municipality of Duque de Caxias on Rio de Janeiro state. Photographs: Adir de Freitas Valentim Junior/VC no G1 and Vladimir Platonov/ABr/exame.com. . . . .	117
6.9	Fields of atmospheric patterns from GFS model over South America for <b>20120102 00UTC</b> . <b>(a)</b> Satellite GOES image; <b>(b)</b> Potential temperature (shaded, K) and wind barbs (knots) in the dynamic tropopause, 925–850-hPa layer-averaged cyclonic relative vorticity (black contours); <b>(c)</b> 250-hPa wind speed ( $\text{m s}^{-1}$ , shaded according to color bar), 250-hPa potential vorticity (gray contours), 250-hPa relative humidity (% , shaded according to gray scale), 600–400-hPa layer averaged ascent (red contours); <b>(d)</b> 250-hPa wind speed ( $\text{m s}^{-1}$ , shaded according to color bar), 1000–500-hPa thickness (dashed contours), Sea Level Pressure (solid contours), total precipitable water (mm, shaded according to gray scale). . . . .	119
6.10	(a) Accumulated rainfall recorded during 01/01/2012 to 05/01/2012 over Central Region of Brazil (R2). (b) Fraction of rain from rain gauges on days that had MCS record by rain accumulated in 5 days. (c) Number of MCS events recorded in 5 days. (d) Fraction of the days that had MCS record by 5 days. (e) Indicative map of the location of the analyzed region. . . . .	120
6.11	Case of extreme precipitation occurred over Central Region of Brazil (R2) during 01/01/2012 to 05/01/2012. . . . .	122
6.12	Bar graphs of (a) Probability Of Detection (POD), (b) Miss Rate (MR), (c) False Alarm Ratio (FAR), (d) Threat Score (TS), (e) Frequency Bias Index (FBI) and (e) Proportion Correct (PC) for 5 days accumulated precipitation over Central region of Brazil during 01/01/2012 to 05/01/2012. . . . .	123
6.13	Municipalities affected by the extreme rain. (a) Flooding in municipality of São Gabriel in Bahia state, (b) Flooding in municipality of Santa Maria da Vitoria in Bahia state. Photographs:Fabiano Pereira/Fotografe o tempo and Divulgação/Correios. . . . .	124

6.14	Fields of atmospheric patterns from GFS model over South America for <b>20160124 06UTC</b> . <b>(a)</b> Satellite GOES image; <b>(b)</b> Potential temperature (shaded, K) and wind barbs (knots) in the dynamic tropopause, 925–850-hPa layer-averaged cyclonic relative vorticity (black contours); <b>(c)</b> 250-hPa wind speed ( $\text{m s}^{-1}$ , shaded according to color bar), 250-hPa potential vorticity (gray contours), 250-hPa relative humidity (% , shaded according to gray scale), 600–400-hPa layer averaged ascent (red contours); <b>(d)</b> 250-hPa wind speed ( $\text{m s}^{-1}$ , shaded according to color bar), 1000–500-hPa thickness (dashed contours), Sea Level Pressure (solid contours), total precipitable water (mm, shaded according to gray scale). . . . .	126
6.15	(a) Accumulated rainfall recorded during 20/01/2016 to 24/01/2016 over Northeastern region of Brazil (R3). (b) Fraction of rain from rain gauges on days that had MCS record by rain accumulated in 5 days. (c) Number of MCS events recorded in 5 days. (d) Fraction of the days that had MCS record by 5 days. (e) Indicative map of the location of the analyzed region. . . . .	128
6.16	Case of extreme precipitation occurred over Northeastern region of Brazil (R3) during 20/01/2016 to 24/01/2016. . . . .	129
6.17	Bar graphs of (a) Probability Of Detection (POD), (b) Miss Rate (MR), (c) False Alarm Ratio (FAR), (d) Threat Score (TS), (e) Frequency Bias Index (FBI) and (e) Proportion Correct (PC) for 5 days accumulated precipitation over Northeastern region of Brazil during 20/01/2016 to 24/01/2016. . . . .	130
6.18	One of the municipalities affected by the extreme rain. (a) Flooding in Municipality of João Pessoa in Paraíba state, (b) Collapse of houses in municipality of João Pessoa in Paraíba state. Photograph: Natalia Xavier/G1 and Walter Paparazzo/G1). . . . .	131

6.19	Fields of atmospheric patterns from GFS model over South America for <b>20160416 12UTC</b> . <b>(a)</b> Satellite GOES image; <b>(b)</b> Potential temperature (shaded, K) and wind barbs (knots) in the dynamic tropopause, 925–850-hPa layer-averaged cyclonic relative vorticity (black contours); <b>(c)</b> 250-hPa wind speed (m s <sup>-1</sup> , shaded according to color bar), 250-hPa potential vorticity (gray contours), 250-hPa relative humidity (% , shaded according to gray scale), 600–400-hPa layer averaged ascent (red contours); <b>(d)</b> 250-hPa wind speed (m s <sup>-1</sup> , shaded according to color bar), 1000–500-hPa thickness (dashed contours), Sea Level Pressure (solid contours), total precipitable water (mm, shaded according to gray scale). . . . .	133
6.20	(a) Accumulated rainfall recorded during 14/04/2016 to 18/04/2016 over Northeast Coast of Brazil (R4). (b) Fraction of rain from rain gauges on days that had MCS record by rain accumulated in 5 days. (c) Number of MCS events recorded in 5 days. (d) Fraction of the days that had MCS record by 5 days. (e) Indicative map of the location of the analyzed region. . . . .	135
6.21	Case of extreme precipitation occurred over Northeast Coast of Brazil (R4) during 14/04/2016 to 18/04/2016. . . . .	136
6.22	Bar graphs of <b>(a)</b> Probability Of Detection (POD), <b>(b)</b> Miss Rate (MR), <b>(c)</b> False Alarm Ratio (FAR), <b>(d)</b> Threat Score (TS), <b>(e)</b> Frequency Bias Index (FBI) and <b>(e)</b> Proportion Correct (PC) for 5 days accumulated precipitation over <b>Northeast Coast region of Brazil during 14/04/2016 to 18/04/2016</b> . . . . .	137
6.23	One of the municipalities affected by the extreme rain. (a) and (b) Collapse of houses in municipality of Monte Alegre in Pará state. Photographs: Arney Barreto/G1 and Reprodução/TV Tapajós). . . . .	139
6.24	Fields of atmospheric patterns from GFS model over South America for <b>20160503 00UTC</b> . <b>(a)</b> Satellite GOES image; <b>(b)</b> Potential temperature (shaded, K) and wind barbs (knots) in the dynamic tropopause, 925–850-hPa layer-averaged cyclonic relative vorticity (black contours); <b>(c)</b> 250-hPa wind speed (m s <sup>-1</sup> , shaded according to color bar), 250-hPa potential vorticity (gray contours), 250-hPa relative humidity (% , shaded according to gray scale), 600–400-hPa layer averaged ascent (red contours); <b>(d)</b> 250-hPa wind speed (m s <sup>-1</sup> , shaded according to color bar), 1000–500-hPa thickness (dashed contours), Sea Level Pressure (solid contours), total precipitable water (mm, shaded according to gray scale). . . . .	140

6.25 (a) Accumulated rainfall recorded during 29/04/2016 to 03/05/2016 over North Brazil (R5). (b) Fraction of rain from rain gauges on days that had MCS record by rain accumulated in 5 days. (c) Number of MCS events recorded in 5 days. (d) Fraction of the days that had MCS record by 5 days. (e) Indicative map of the location of the analyzed region. . . . .	141
6.26 Case of extreme precipitation occurred over North Brazil (R5) during 29/04/2016 to 03/05/2016. . . . .	142
6.27 Bar graphs of (a) Probability Of Detection (POD), (b) Miss Rate (MR), (c) False Alarm Ratio (FAR), (d) Threat Score (TS), (e) Frequency Bias Index (FBI) and (e) Proportion Correct (PC) for 5 days accumulated precipitation over North region of Brazil during 29/04/2016 to 03/05/2016.	143





## LIST OF TABLES

	<u>Page</u>
3.1 Description table of satellite products. . . . .	22
4.1 Description table of satellite products . . . . .	60
5.1 Description of parameters from TOOCAN dataset selected for analysis in this work. The dimensions Time and nmaxMCS represent the num- ber of days within a month and the maximum number of MCS within a 1°1day grid point (set at 25) respectively. . . . .	83
6.1 Description table of satellite products. . . . .	106
6.2 Summarized table with the cases of extreme rainfall events analyzed from each region. . . . .	107
6.3 Contingency table considering P99th threshold by grid point . . . . .	109
6.4 Statistical measures obtained by contingency table . . . . .	110



## CONTENTS

	<u>Page</u>
<b>1 INTRODUCTION . . . . .</b>	<b>1</b>
1.1 Objectives . . . . .	3
1.2 Thesis structure . . . . .	4
<b>2 LITERATURE REVIEW . . . . .</b>	<b>5</b>
2.1 Overview of satellite based rainfall estimation methods . . . . .	5
2.2 Definitions of extreme rainfall . . . . .	12
2.3 Mesoscale Convective Systems . . . . .	13
2.4 Natural disasters . . . . .	14
<b>3 ASSESSMENT OF THE EXTREME PRECIPITATION BY SATELLITE ESTIMATES - PART 1: SOUTH AMERICA . . . . .</b>	<b>17</b>
3.1 Introduction . . . . .	17
3.2 Materials and methods . . . . .	19
3.2.1 Study area . . . . .	19
3.2.2 Data . . . . .	20
3.2.2.1 Rainfall Satellite-Based Products . . . . .	20
3.2.2.2 Rainfall ground-based data . . . . .	22
3.2.3 Methodology . . . . .	24
3.2.3.1 Assessment of satellites products : statistical analysis . . . . .	24
3.2.3.2 Characterization of extreme rainfall . . . . .	27
3.3 Results and discussion . . . . .	30
3.3.1 Extreme rain from maximum daily values . . . . .	32
3.3.2 Extreme rain from 99th percentile threshold . . . . .	39
3.4 Conclusions . . . . .	45
<b>4 ASSESSMENT OF THE EXTREME PRECIPITATION BY SATELLITE ESTIMATES - PART 2: REGIONAL ANALYSIS . . . . .</b>	<b>49</b>
4.1 Introduction . . . . .	49
4.2 Methodology . . . . .	51
4.2.1 Study area . . . . .	55
4.2.2 Analyzed data . . . . .	58
4.2.2.1 Satellite Precipitation Products (SPP) . . . . .	58

4.2.2.2	Rainfall ground-based data . . . . .	60
4.3	Results and discussion . . . . .	61
4.3.1	Southern Brazil - R1 . . . . .	64
4.3.2	Central Region - R2 . . . . .	67
4.3.3	Northeastern - R3 . . . . .	69
4.3.4	Northeast Coast - R4 . . . . .	71
4.3.5	North Brazil - R5 . . . . .	73
4.4	Conclusions . . . . .	75
<b>5</b>	<b>Characteristics of Mesoscale Convective Systems and its relation with extreme precipitation over South America using an Eulerian Tracking approach . . . . .</b>	<b>79</b>
5.1	Introduction . . . . .	79
5.2	Study area . . . . .	81
5.3	Datasets . . . . .	82
5.3.1	Mesoscale convective systems dataset . . . . .	82
5.3.2	Rain gauge dataset . . . . .	83
5.4	Methodology . . . . .	84
5.5	Results and discussion . . . . .	87
5.5.1	Characterization mesoscale convective systems over South America . . . . .	87
5.5.2	Influence of MCS on extreme rain . . . . .	95
5.6	Conclusions . . . . .	98
<b>6</b>	<b>Analysis of extreme rainfall events in different regions of Brazil : Case studies . . . . .</b>	<b>101</b>
6.1	Introduction . . . . .	101
6.2	Materials and Methods . . . . .	103
6.2.1	Study area . . . . .	103
6.2.2	Rain gauges dataset . . . . .	105
6.2.3	Satellite Precipitation Products (SPP) . . . . .	106
6.2.4	TOOCAN dataset . . . . .	107
6.2.5	Methodology . . . . .	107
6.3	Results and discussion . . . . .	110
6.3.1	Case study for Southern Brazil - R1 . . . . .	110
6.3.2	Case study for Central Region - R2 . . . . .	116
6.3.3	Case study for Northeastern - R3 . . . . .	123
6.3.4	Case study for Northeast Coast - R4 . . . . .	130
6.3.5	Case study for North Brazil - R5 . . . . .	137

6.4 Conclusions . . . . .	143
<b>7 MAIN CONCLUSIONS AND FUTURE WORK . . . . .</b>	<b>147</b>
<b>REFERENCES . . . . .</b>	<b>149</b>



## 1 INTRODUCTION

In the last years, severe weather events have caused significant economic and human losses. Climate change have increased the intensity and frequency of extreme weather events around the world in the last decades ([MARCELINO, 2008](#); [MIN et al., 2011](#); [SENEVIRATNE et al., 2012](#); [DONAT et al., 2016](#)) and the societies are vulnerable to hazards caused by natural disasters. In this way, accurate weather predictions are of fundamental importance to alert the population to the risks of occurrence of extreme events. A deep understanding of such phenomena may improve their prediction in an effective manner, and, most importantly, mitigate the impact of weather extreme events in our daily life.

Natural disasters such as flooding and landslides events are one of most wide-reaching costly hazards. They may be triggered by meteorological events like extreme rainfall and amplified by human intervention such as deforestation and/or urban development ([SMITH; WARD, 1999](#); [KIRSCHBAUM et al., 2015](#); [KIRSCHBAUM; STANLEY, 2017](#)). However, many definitions of natural disasters can be found in the literature. Some studies define a natural disaster as the result of the impact of extreme or intense natural phenomena on a social system, causing serious damages and losses that exceed the capacity of the community or society to deal with ([ALEXANDER, 1993](#); [ALCÁNTARA-AYALA, 2002](#); [UNDP, 2004](#); [MARCELINO, 2008](#)). This definition of natural disasters is used in the present investigation.

One of the main meteorological variable associated with natural disasters is the precipitation. Weather systems are complex and evolve rapidly. In addition, isolated storms, in which rain showers occur in one place and not another, makes reliable ground-based precipitation measurements over entire regions a challenging problem ([LAU; WU, 2003](#)).

Extreme precipitation events are most often related to severe storms that produce intense rain, strong winds and hail. When these storms are well organized, they are called Mesoscale Convective Systems (MCS). The MCS are clusters of deep convective clouds that are wider than individual storms, often accompanied by an extensive stratiform cloud in the lower troposphere in the form of anvil hundreds of kilometers away. In South America, MCS are responsible for most of the precipitation in the tropics and in several regions of mid-latitudes during the warm season ([VELASCO; FRITSCH, 1987](#); [MACHADO; LAURENT, 2004](#))

Many remote sensing techniques have been developed in order to estimate pre-

cipitation in a efficient manner. The main objective of the remote sensing technique is to obtain information over an area or object located at certain distance from a measurement equipment. The most common equipment used for this purpose is the weather radars and environmental satellites. The satellites sense the radiation to indicate the presence of clouds, water vapour, and surface features, while the radar senses electromagnetic radiation to indicate the presence of precipitation.

The data obtained by weather radars and satellites are of significant importance to the investigation of extreme events since this data fill the spatial and temporal gaps left by the ground rain gauge network. There is a necessity to improve the characterisation of precipitation extremes combining satellite with ground-based measurements. In addition, due to large gaps in instrument coverage over oceans, which cover 70% of the Earth's surface, tracking rain globally is exceptionally difficult.

Due to the problems mentioned above, the use of satellite data is essential and their use has been increased over the last years. Missions such as the Tropical Rainfall Measuring Mission (TRMM) (KUMMEROW et al., 1998), the Global Precipitation Measurement (GPM) (HOU et al., 2014), and Geostationary Operational Environmental Satellite - R series (GOES-R) (GOODMAN et al., 2012) were launched in order to provide a global coverage and a better quantitative description of rain processes. New satellite rainfall products were developed for this missions and have been improved constantly since the satellites launch; however, there is necessity to validate the algorithms used to post-processing the data obtained by these satellites. In the present work, the validation process is performed by comparing the satellite data with rain gauges data.

It is observed that in situations of extreme precipitation, satellite estimates fall short of expectations. Usually when the systems are shallow convective and disorganized, satellite estimates tend to be underestimated and when they are systems the organized deep convective are overestimated (PETKOVIĆ; KUMMEROW, 2017). Several limitation on data sampling (due to the time-space intermittent of the precipitation) sensor design (due to resolution spatial, temporal and spectral) and algorithm development can be considered generators of the uncertainties of satellite-based retrievals (FERRARO, 2007; MASSARI; MAGGIONI, 2020).

Another challenge is found when it is necessary to estimate warm rain. According to (CHEN et al., 2011),(CALHEIROS, 2013) many algorithms have problems to detect



warm rain. In Brazil, for example, it is seen that a strong signal of warm rain modulates rainfall over the coastal areas of Northeast of Brazil and adjacent ocean (PALHARINI; VILA, 2017). Most studies on precipitation estimation with satellite data over land focus on rain involving ice formation; however, it is necessary a deeper investigation about warm rain.

Satellite precipitation products (SPP) are of great utility and a large number of researches have been using them for different purposes. Nonetheless, a validation process of these products, by a inter-comparison of various existing SPPs, for extreme rain events over South America has not yet been done yet. In doing so, the question that motivated this research is: Are the satellites able to correctly estimate extreme rainfall values over South America?

In addition, the present investigation intend to answer other question: since MCS may be the cause of severe storms and that the extremes of precipitation can be related to these systems (DURKEE et al., 2009; MATTOS; MACHADO, 2009; ROCA; FIOLEAU, 2020), what is the influence of MCS for extreme rainfall over South America?

## **1.1 Objectives**

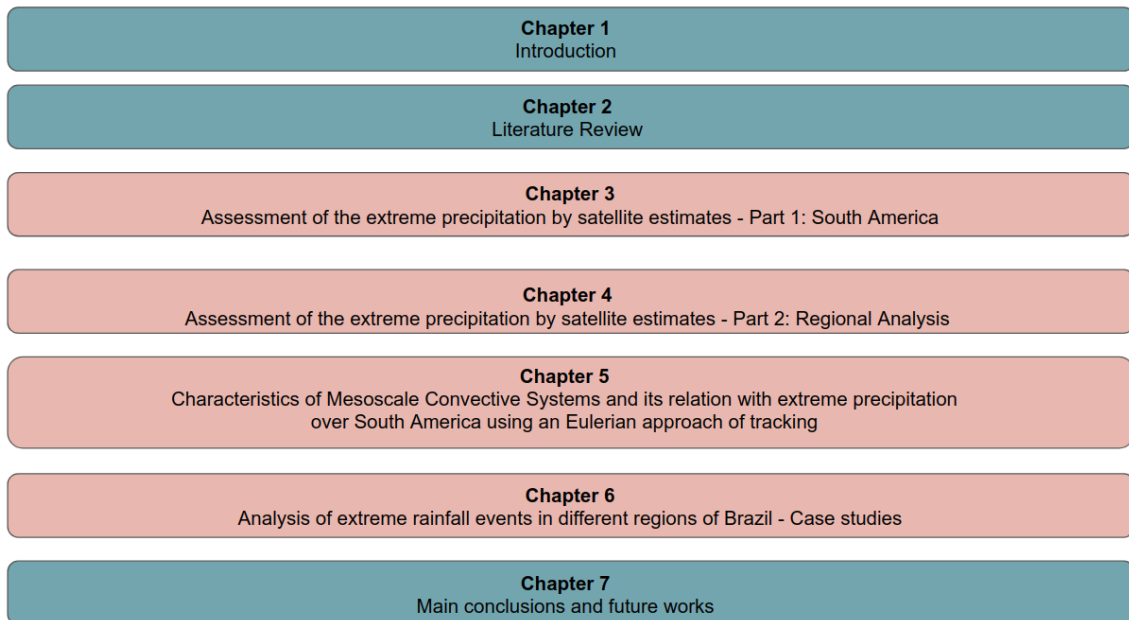
The main objective of this investigation is to assess the ability of different satellite-based algorithms to retrieval extreme precipitation and analyze the Mesoscale Convective Systems (MCS) behavior to identify the influence of these systems on the extreme rainfall occurred over South America. The specific objectives of this research are the following:

- (i) Assess the ability of Satellite Precipitation Products (SPP) to capture the characteristics of extreme precipitation over the tropical region of South America and at different regions of Brazil and compare satellite precipitation estimation products with the rain gauge dataset from a period ranging from 2012 to 2016;
- (ii) Describe the characteristics of Mesoscale Convective Systems (MCS) acting on the study regions by using tracking algorithm with Eulerian approach;
- (iii) Analyze five study cases of extreme rain events that caused natural disasters in five different regions of Brazil and compare with the results generated in items i) and ii).

## 1.2 Thesis structure

The structure of the thesis is divided into seven chapters. A introduction to the problem attacked in this investigation and the main scientific questions that motivated this research was shown in this chapter (chapter 1). Chapter 2 presents a literature review, which provides a general overview of the characteristics of extreme rainfall and convective systems, natural disasters, satellite precipitation estimation techniques. Chapters 3 to 6 are structured as published journal papers or paper under preparation to be submitted for publication in near future. Chapter 3 presents the assessment of the extreme precipitation by satellite estimates for South America. Chapter 4 presents the assessment of the extreme precipitation by satellite estimates for different regions of Brazil. Chapter 5 presents an analysis of Mesoscale Convective Systems characteristics and their relation with extreme rainfall. Chapter 6 presents five study cases on extreme events occurred in different regions of Brazil. Finally, the conclusions and future works are described in Chapter 7. Figure 1.1 shows a flowchart of the topics covered in each chapter in this investigation.

Figure 1.1 - Thesis structure.



Source: Author's production.

## 2 LITERATURE REVIEW

This work address topics such as natural disasters, extreme precipitation, convective systems, and satellite precipitation estimation techniques. The present chapter presents a literature review on the main concepts related to the topics covered in the thesis.

### 2.1 Overview of satellite based rainfall estimation methods

Remote sensing is the science that seeks to obtain information about an object from a certain distance. There are different ways to collect data and different sensors that can be used for this purpose. One of the main remote sensing tool employed in meteorology are environmental satellites. They can carry instruments or sensors that measure the electromagnetic radiation coming from the Earth-atmosphere system. The radiation emitted from the Sun is reflected, absorbed, and emitted by the Earth's atmosphere or surface. Satellite sensors are calibrated to detect several wavelengths along the electromagnetic spectrum (YAMASOE; CORRÊA, 2016).

Along the last 60 years, significant improvements have been made in the area of remote sensing using satellite. The first satellite, Sputnik 1 (Figure 2.1a), was launched into space by the Soviet Union in order to access the capabilities of launching payloads for space and the effects of weightlessness and radiation on living organisms. Nowadays, satellites play a fundamental role on our daily life providing real time images, communication, internet, and so on.

In 1960, the first meteorological satellite, called Television Infrared Observation Satellites (TIROS-1), Figure 2.1b), was launched by the USA. With this satellite it was possible to observe, for the first time, clouds layer from space. It was a great advance for science to be able to see meteorological systems and their evolution on a wide spatial scale. This program was NASA's first experimental step to determine if satellites could be useful for remote sensing applications. However, even with all technological development along the last years, precipitation measurements by satellite still a difficult task.

Accurate meteorological information are essential for the development of effective alert system. In doing so, the improvement of satellite estimates are of fundamental importance for extreme rainfall detection. Efforts have being made by several research centres to ensure that high-resolution scientific data are available to

help them to identify these events. Missions such as Tropical Rainfall Measuring Mission (TRMM) (KUMMEROW et al., 1998) (Figure 2.2a) and the Global Precipitation Measurement (GPM) (HOU et al., 2014) (Figure 2.2b) use a constellation of Low-Earth Orbit (LEO) satellites or missions like Geostationary Operational Environmental Satellite (GOES), composed by Geosynchronous Equatorial Orbit (GEO) satellites (GOODMAN, 2019) (Figure 2.2c), provide a global coverage and a quantitative description of rain processes.

Launched on November 1997 and designed for a lifetime of 3 years, the Tropical Rainfall Measuring Mission (TRMM) satellite produced over 17 years of valuable scientific data. A joint mission of National Aeronautics and Space Administration (NASA) and the Japan Aerospace Exploration Agency (JAXA), the TRMM dataset became the space standard for measuring precipitation and helped researcher to understand the physics of tropical cyclone structure and evolution, convective system properties, lightning-storm relationships, climate and weather modeling, and human impacts on rainfall (KUMMEROW et al., 1998).

Launched on February 27th of 2014 and carrying advanced instruments for precipitation measurements, the Global Precipitation Measurement (GPM) mission has contributed for the advancement of our understanding of Earth's water and energy cycles and has improved the forecasting of extreme events that cause natural disasters. A consortium of international space agencies, including the National Aeronautics and Space Administration (NASA), Japan Aerospace Exploration Agency (JAXA), the Centre National d'Etudes Spatiales (CNES), the Indian Space Research Organization (ISRO), the National Oceanic and Atmospheric Administration (NOAA), the European Organization for the Exploitation of Meteorological Satellites (EUMETSAT), and others (<https://pmm.nasa.gov/GPM>) (HOU et al., 2014) organized this mission. The main objective of GPM is to provide next-generation observations of rain and snow worldwide every three hours, continuing the work done by the TRMM's mission.

Since 1975, Geostationary Operational Environmental Satellites (GOES) have provided images and data on atmospheric conditions and solar activity. GOES data products have led to accurate weather forecasts and better understanding of long-term climate conditions. The NASA designed and launched the GOES missions and the National Oceanic and Atmospheric Administration (NOAA) have operated them. In October 2015, NOAA celebrated the 40th anniversary of the launch of the first GOES satellite (GOODMAN, 2019).

These satellites are equipped with several sensors that have the objective of measure irradiated energy around the globe utilizing waves frequency in channel of visible, infrared, radar and microwave. Based on these frequencies was been built all the products for the different applications. Some of the applications of these products are: climate prediction, agriculture, land surface models, extreme weather among others. A description of some of the sensors used for remote sensing is given below.

In the Visible (VIS) channel the precipitation rate is estimated by reflected radiation from the top of the clouds. The disadvantages are related to the estimates are indirect and based on empirical methods. It is not possible to obtain measures in the night period because the brightness of a cloud is affected by the angular position of the cloud in relation to the sensor and the Sun.

The thermal infrared (IR) is based on energy emitted by the Earth's surface and the atmosphere. The energy emitted is proportional to the temperature, in this way, with the temperature of the top of the clouds, it is possible to evaluate the evolution of precipitating systems composed of clouds of great vertical development. It has a high temporal resolution, however, these estimates can be contaminated by cirrus clouds that are cold and shallow clouds.

The passive microwave sensor (PMW) provides direct measurement of precipitation rates. The main disadvantages are related to low spatial and temporal resolutions. In the case of active microwaves (AMW) or radar, these sensor provide direct measurements of the vertical structure of the precipitation. However, there are limitations related to the narrow range of data obtained by low-orbit satellites (LEO).

In order to improve the deficiencies of each technique used to post-process the measured data from different sensors, most of the satellite rain estimation algorithms use hybrid techniques and create products using AMW and PMW techniques associated with IR and VIS data. In addition, surface data corrections are employed in order to minimize uncertainties. The inconsistency in the performance of satellite products has been observed in different climatic and topographic at different regions, timescales, and precipitation intensities. In doing so, a significant effort need to be done to the sensors measurements and to post-process the data (MUHAMMAD et al., 2018).

Some studies evaluate the uncertainties of the precipitation products by satellite

considering an average rainfall. In the investigation conducted by ([SAPIANO; ARKIN, 2009](#)), the authors have performed a sub-daily inter-comparison of high-resolution datasets CMORPH technique; TMPA; Naval Research Laboratory (NRL) blended technique; PERSIANN with existing sub-daily gauge data over the United States and the Pacific Ocean. The results showed that the biases are relatively high for most of the datasets over land and ocean with a general tendency to overestimate warm season rainfall over the United States and to underestimate rainfall over the tropical Pacific Ocean.

In the work performed by [Tian et al. \(2009\)](#), the authors devised a scheme to separate the total errors in a satellite-based data set into three independent components, hit bias, missed precipitation and false precipitation. The authors analysis produced the spatio-temporal distribution of these error components and their magnitudes for each product.

[Falck et al. \(2016\)](#) valuated the simulation results of a multidimensional stochastic satellite precipitation error model (SREM2D) for several algorithms to estimate satellite precipitation in the Tocantins-Araguaia river basin. The authors showed that the set obtained through the achievements of the SREM2D model reduced the bias of satellite precipitation estimation algorithms for large drainage area basins.

In addition to the works cited above, there are some studies that evaluated the estimates when heavy or extreme rainfall events occurred. [Aghakouchak et al. \(2011\)](#) evaluate the performance of four satellite derived precipitation products (CMORPH, PERSIANN, TMPA-RT, and TMPA-V6) for the central United States region. According to the authors, the performance of all satellite products tended to decrease as the extreme precipitation threshold increased. The authors suggested that extensive efforts are necessary to develop algorithms that can capture extremes in a reliable manner.

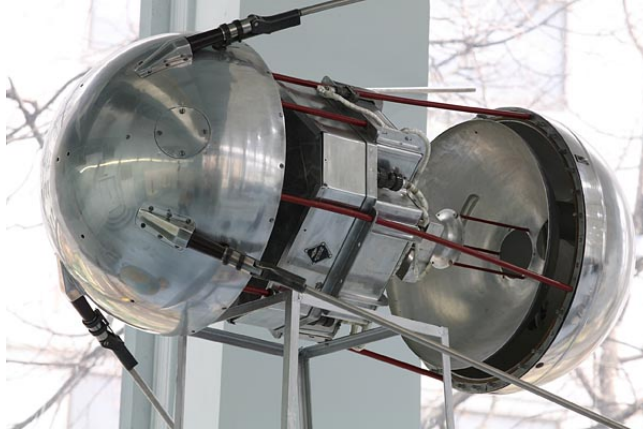
[Mehran and Aghakouchak \(2014\)](#) investigated the capability of satellite precipitation datasets to detect heavy precipitation rates over different temporal accumulations. The authors compared the products from TMPA-RT, PERSIANN, and CMORPH dataset. According to them, the results showed that none of the high temporal resolution datasets are ideal for detecting heavy precipitation rates.

[Prakash et al. \(2016\)](#) investigated the use of satellite products to estimate heavy rainfall across India using the Multi-satellite Precipitation Analysis (TMPA/TRMM),

and the Integrated Multi-satellite Retrievals (IMERG/GPM). The satellite product were compared with gauge-based observations. According to the authors, TMPA has problems in detecting and estimating heavy rainfall over northern and south-east India and that IMERG showed a notable improvement over TMPA as compared to gauge-based observations.

[Sanò et al. \(2018\)](#) described a new algorithm based on the Passive microwave Neural network Precipitation Retrieval approach (PNPR v3). According to the author, PNPR v3 is a global rainfall retrieval algorithm able to optimally exploit the GMI multi-channel response to different surface types and precipitation structures around the globe.

Figure 2.1 - (a) The world's first satellite Sputnik-1 launched in October 4,1957 by Russia.  
(b) The The world's first meteorological satellite TIROS-1 launched in April 1,1960 by USA.



(a) Sputnik 1

Source: Federal Space Agency of Russia.



(b) TIROS 1

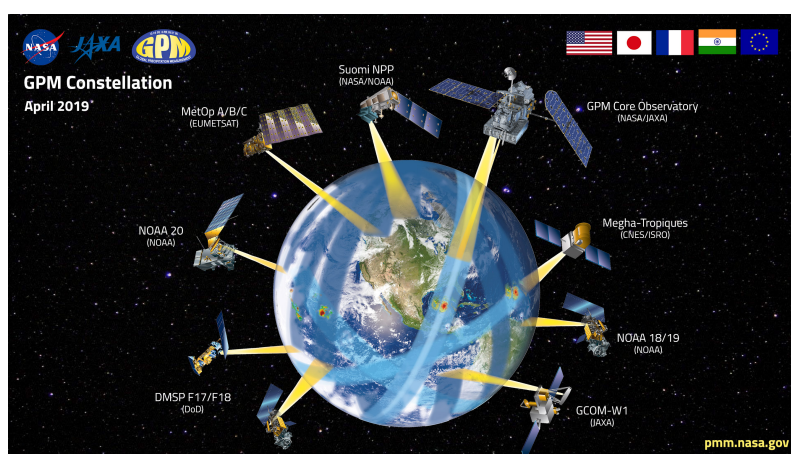
Source: NASA (1960).



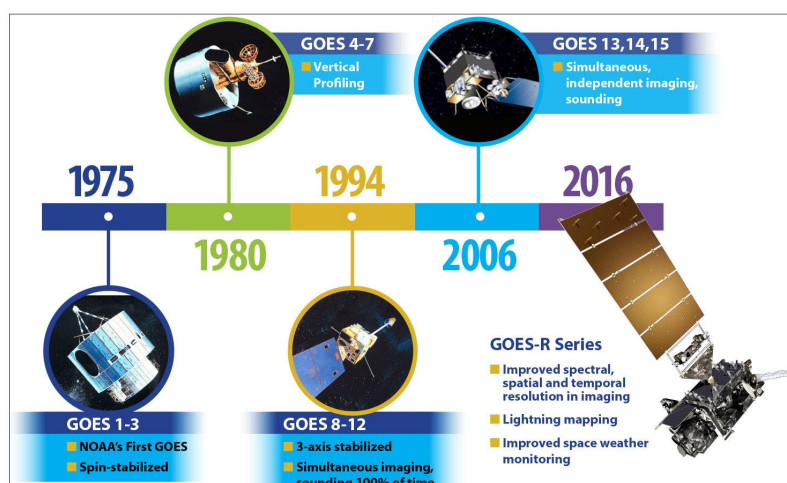
Figure 2.2 - Satellites with meteorological objectives already placed launched in orbit. (a) TRMM, (b) GPM, (c) GOES.



(a) TRMM



(b) GPM-constellation



(c) History of GOES

Source: NASA/NOAA (2016).

## 2.2 Definitions of extreme rainfall

According to the Intergovernmental Panel Climate Change (IPCC) Glossary extreme weather event is defined as "an event that is rare at a particular place and time of year. Definitions of rare vary, but an extreme weather event would normally be as rare as or rarer than the 10th or 90th percentile of a probability density function estimated from observations" (FIELD et al., 2012).

The extreme events can be characterised by some attributes such as rate of occurrence (probability per unit time), magnitude (intensity), temporal duration and timing, spatial scale (footprint) and multivariate dependencies" (DIAZ; MURNANE, 2008).

Diaz and Murnane (2008) explained that the term "extreme event" can be confused with other concepts. According to this work the use of expressions such as rare, severe, extreme, and high-impact events are commonly used in the same context, however, they should not. In an attempt to clarify these terms, the author describes these definitions in a separate manner:

**Severe events** are events that create large losses in measures such as a number of lives, financial capital, or environmental quality (e.g., loss of species). The severity can be measured by the expected long-term loss, which is known as the risk.

**Rare events** are events that have a low probability of occurrence. Because of the rarity of these events, human societies (and other ecosystems) are often not well adapted to them and so suffer large amounts of damage when they do occur.

**Extreme events** are events that have extreme values of certain important meteorological variables. Damage is often caused by extreme values of certain meteorological variables, such as large amounts of precipitation (e.g., floods), high wind speeds (e.g., cyclones), high temperatures (e.g., heat waves), etc. Extreme is generally defined as either taking maximum values or exceedance above pre-existing high thresholds.

**High-impact events** are severe events that can be either short-lived weather systems (e.g., severe storms) or longer-duration events such as blocking episodes that can lead to prolonged heat waves and droughts.

The number of researches related to extreme events and their implications have increased in the last years. About 2000 articles related to keywords "rainfall" and "extreme events" or "precipitation" and "extreme events" were published from 1980 to 2016 according to bibliometric mapping carried out by Pereira et al.

(2017).

These studies range from regional scales to local ones, such as [Manton et al. \(2001\)](#) that used some indices to analyze the tendency of extreme precipitation in a period of 38 years for the regions of Southeast Asia and the South Pacific. It was found that the intensity of the extreme events has increased. However, the frequency of occurrence of the events have decreased.

[Teixeira and Satyamurty \(2011\)](#) analysed the average rainfall based on cluster analysis and area average rainfall series for southern and southeastern regions of Brazil. In this investigations, the authors found that the annual heavy and extreme rainfall events frequencies present increasing trends in the 45-yr period.

[Liebmann et al. \(2001\)](#), studied the interannual variability of extreme precipitation in the state of São Paulo. In their investigations, it was found that there is a positive correlation between the number of extreme events in the entire state and SST anomalies in the central and eastern Pacific.

Recently [Demirdjian et al. \(2018\)](#), [Zhou et al. \(2015\)](#) proposed an methodology for the statistical modeling of extreme precipitation monitoring system using the TRMM dataset. According to the authors, the application of the developed methodology led a better estimates of the regional average recurrence interval maps. This information is of fundamental importance to identify how rare a particular precipitation event is.

[Wang et al. \(2017\)](#) have compared a regional frequency analysis of precipitation extremes in Mainland China with fuzzy c-means and L-moments approaches and Generalized Extreme Value (GEV) distribution results fitted to each site. According to the authors, at some regions GEV distribution have a better accuracy than others.

### **2.3 Mesoscale Convective Systems**

Mesoscale Convective Systems (MCS) are clusters of deep convective clouds that are wider than individual storms. They are often accompanied by an extensive stratiform cloud in the lower troposphere in the form of anvil of hundreds of kilometers ([ORLANSKI, 1975](#)). According to [Orlanski \(1975\)](#), [Zipser \(1981\)](#), [HOUZE JUNIOR. \(2004\)](#), [HOUZE \(2018\)](#), the MCS are cloud systems that occur in connection with a group of storms and produce continuous precipitation over areas of the order of 100 km on the horizontal scale. According to the au-

thors, these systems have typical periods of life around 6 to 12 hours and storms embedded in their interior of these systems are possible sources of intense precipitation, strong winds, tornadoes, hail, and intense electrical activity.

The Squall lines and the Mesoscale Convective Complexes (MCC) can be considered as particular types of MCS because they have different shapes. Squall lines have a linear shape while MCC have a circular shape (MADDOX, 1980). The Squall lines are identified by a vigorous line of convective cells extending up to hundreds of kilometers along a horizontal axis. They interact with each other and are connected by a stratiform region. They are usually formed close to the interface between a mass of hot humid air and a mass of cold air producing very strong winds on the surface. Due to the displacement of the system, as clouds dissipate, new clouds are formed so that the storm can last for several hours (COTTON, 1990).

The MCCs have an circular shape and typical diameters of 300 to 400 km with hundreds of individual storms interconnected inside covered by an extensive layer of Cirrus clouds, originated from mature Cb clouds. These systems occur mainly at night with a typical duration of around 10 to 12 hours (MADDOX, 1980).

Thus, MCS in general are basically made up of a convective and a stratiform region. The first is characterized by strong convection and high cloud top, while the second region has clouds of great horizontal extension and low cloud top with the appearance of an anvil (COTTON, 1990).

The strong convergence of humidity at low levels precedes the formation of MCS by several hours (FRANK, 1978). In the case of squall lines, the organization of convective cells provides hot and humid air and the strong vertical wind shear separates regions of updraft and downdraft. The development of MCC is associated with a low level jet in a weak wind regime that provides hot and humid air to the convective cells coupled to a high level jet (VELASCO; FRITSCH, 1987).

## **2.4 Natural disasters**

The lack or excess of rains events are part of the natural variability of the climate. However, if we consider the impacts, this is the consequence of human actions, since building in areas at risk or exposed to extreme rainfall can lead to natural disasters. A survey performed by the World Bank and GFDRR, with of 117 countries, emphasized the urgency of climate-smart policies to protect the

most vulnerable people as they are often exposed to natural disasters. The report also assessed the benefits of interventions to increase resilience in these countries which include insurance policies, social protection systems, and early warning systems to mitigate the impact of extreme disaster events ([HALLEGATTE et al., 2016](#)).

From the social point of view, extreme events are those that cause extreme impacts in the society causing deaths, homelessness, and property damage. Losses caused by catastrophes, defined by the property insurance industry as storms that causes insured losses bigger then 5 million in the year of occurrence, have grown steadily in the United States from 100 million annually in the 1950s to 6 billion per year in the 1990s. ([EASTERLING, 2000](#)).

In Brazil, according to Global Facility for Disaster Reduction and Recovery (GF-DRR), the average annual losses caused by natural disasters are estimated at 3.9 billion. The most vulnerable populations are located at large cities in Brazil. Between 2009 and 2014, nearly every highly populated municipality in Brazil were affected by floods and about 50000 low-income homes were destroyed ([TORO et al., 2014](#)).

Currently, in Brazil, there is a natural disaster alert system via text messages (SMS). This natural disaster alert system is coordinated by the National Center for Risk and Disaster Management (Cenad) and the Ministry of Integration in partnership with Civil Defense of the States, the National Telecommunications Agency (ANATEL), and the telephone operators. The system aims to prevent accidents, to guide and advise the population on procedures that should be adopted in view of the risk of floods, storms or landslides, among other occurrences. The system began operating in February 2017 and it has already registered that 2.6 million citizens received notices for free. To receive the notices, the citizens need to be registered in a database by sending the zip code of their address to the number 40199 via SMS. Alerts are sent by SMS to cell phones registered in case of imminent natural disasters.

Knowing the importance of alert systems, some authors have deepened their studies on this topic. According to [Sorensen \(2000\)](#), an alert system, regardless of the type of disaster, provides crucial information to people that lives in risky areas and help them to make decisions and to take actions. In this way, alert systems should provide useful and timely information to risk-exposed individuals and mitigate or avoid human losses during the occurrence of a natural disaster.



Currently several countries have flood warning systems. Some of the system are: the Flood Forecast Center in England ([WERNER et al., 2009](#)), the NOAA Automated Flood Warning Systems in the USA ([NATIONAL WEATHER SERVICES, 2009](#)), and the European Flood Alert System (EFAS) for all Western European countries ([THIELEN et al., 2008](#)). All of these systems work in conjunction with hydrological modeling data from weather forecasts generated by atmospheric models.

In Brazil, [Pereira Filho and Santos \(2006\)](#) used radar data to estimate precipitation and river level data to develop a hydrometeorological forecasting system based on neural networks with the objective of simulating and detecting flash flood events in the drainage basin of the Tamanduateí River, state of São Paulo. This study demonstrated good results in the prediction of extreme events in the drainage basin considered in the investigation.

Recently, [Machado \(2015\)](#) proposed a Severe Weather Forecast and Observation System (SOS-CHUVA) to reduce the vulnerability of the population to extreme rainfall events through the analysis of very short term forecast (nowcasting). With this system, the meteorological information should reach the population in an adequate and fast way in order to reduce losses of life and material assets in landslides and flood risks.

In this way, the reduction of natural disasters has been on the agenda of the United Nations (UN) in the last two decades. The United Nations General Assembly implemented a program called International Strategy for Disaster Reduction (ISDR). Through this program, it was possible to raise awareness of the public authorities of several countries in the face of disasters and to increase the efforts to investigate these phenomena ([BONACHEA PICO, 2006](#)). The program believes that a organized national and local strategies for disaster risk reduction must be multi-sectoral. These strategies should link policies in areas such as land use, building codes, public health, education, agriculture, environmental protection, energy, water resources, poverty reduction and climate change adaptation.

Another program from the World Meteorological Organization (WMO) also support the global agenda on sustainable development, climate change adaptation and disaster risk reduction. Protection of livelihoods and property from the risks related to weather, climate and water events are the main priorities in this program. In addition, WMO have emphasized that the development of reliable tools to predict these events is of fundamental importance for any country.

### 3 ASSESSMENT OF THE EXTREME PRECIPITATION BY SATELLITE ESTIMATES - PART 1: SOUTH AMERICA

#### 3.1 Introduction

Precipitation is one of the most important meteorological variables to investigate in the hydrological cycle context. When precipitation occurs in a very intense or extreme way, it can cause significant social, economic and environmental impacts. The meteorological systems responsible for intense rainfall are complex and evolve rapidly, making measurement difficult. In addition, due to the morphology of these systems, rainfall can occur in one place and not in others, which makes precipitation measurements in certain regions a real challenge (LAU; WU, 2003).

In recent decades, the interest in investigating the impact of extreme events has been growing due their effects on daily life (ALCÁNTARA-AYALA, 2002); (MARCELINO, 2008). In this scenario, different techniques have been developed to monitor precipitation using satellites. However, extreme precipitation data collected by the satellites are difficult to process, requiring complex algorithms for this task (MASUNAGA et al., 2019). Improvement of these algorithms for data retrieval is essential to quantify extreme events in terms of frequency and intensity, and to generate useful information for decision-makers.

The use of satellite-based retrievals is promising, and their use has increased since the launch of missions such as the Tropical Rainfall Measuring Mission (TRMM) (KUMMEROW et al., 1998) and the Global Precipitation Measurement (GPM) mission (HOU et al., 2014). These initiatives provide quasi-global coverage and better quantitative description of rain processes. Although the quality of satellite rainfall products has improved in recent years, their algorithms require validation studies through comparisons with observational data and physical process approaches.

Some studies have observed that satellite-based retrievals for extreme precipitation events, usually caused by convective systems, fall short of expectations (MASUNAGA et al., 2019) and that South America experiences some of the most intense mesoscale convective systems (MCSs) on Earth (ZIPSER et al., 2006).

---

<sup>0</sup>Palharini, R.S.A.; Vila, D.A.; Rodrigues, D.T.; Quispe, D.P.; Palharini, R.C.; de Siqueira, R.A.; de Sousa Afonso, J.M. Assessment of the Extreme Precipitation by Satellite Estimates over South America. Remote Sens. 2020, 12, 2085. <https://doi.org/10.3390/rs12132085>

In general, satellite observations tend to underestimate the rainfall when convective systems are shallow and overestimate them when convective systems are deep (PETKOVIĆ; KUMMEROW, 2017). Furthermore, the presence of complex topography in South America, like the Andes mountain range with its snow-covered surfaces and heavy precipitation from warm clouds in areas such as northeastern Brazil and the Amazon, makes satellite estimation a very difficult task (ZAMBRANO-BIGIARINI et al., 2017); (SALIO et al., 2015); (PALHARINI; VILA, 2017); (LIU; ZIPSER, 2009). It is a particular challenge to estimate warm rain, and most studies of precipitation estimation with satellite data over land focus in rain-ice processes, making it hard to detect warm rain by the algorithms (CHEN et al., 2011); (CALHEIROS, 2013). In Brazil, for example, about 80% of the clouds over the coastal areas of the Northeast region and adjacent ocean are classified as shallow convective, responsible for generating extreme warm rain events (PALHARINI; VILA, 2017). (RODRIGUES et al., 2019) showed that the quality of extreme satellite estimates in northeastern Brazil depends on the season, location, and time scale in which the precipitation events occur. Their study indicated that accumulated rain in two days showed better results for the quality of the extreme precipitation estimates coming from the satellite. However, those results cannot be extrapolated to other regions and rainfall regimes, as shown by other researchers who have performed global analysis (HUFFMAN et al., 2001); (MASUNAGA et al., 2019).

Several limitations of data sampling (due to the intermittent time-space behavior of precipitation), sensor design (due to spatial, temporal and spectral resolution) and algorithm design are also sources of uncertainties for extreme satellite-based retrievals. At the same time, the use of satellite-based datasets is fundamental to provide global coverage and a better quantitative description of rain processes. In this respect, the quality of satellite rainfall products has improved in recent decades. Satellite rainfall products (SRPs hereafter) have been improved in terms of temporal and spatial resolution. However, their performance needs to be understood across space–time scales and other uncertainty factors should be identified. Some studies have already evaluated the ability of satellite-based rain estimation products to estimate average rainfall values. These investigations have revealed very close estimates to observed data, such as (DEMBÉLÉ; ZWART, 2016), (WANG et al., 2017), (SHARIFI et al., 2018) and (SHI et al., 2020). These have analyzed different satellite-based rainfall estimation for Africa, Austria and China, by evaluating the average behavior of rain intensity over the respective time series chosen by the authors. But further investigation is needed of the ability of these satellite-based products to estimate extreme rainfall values.

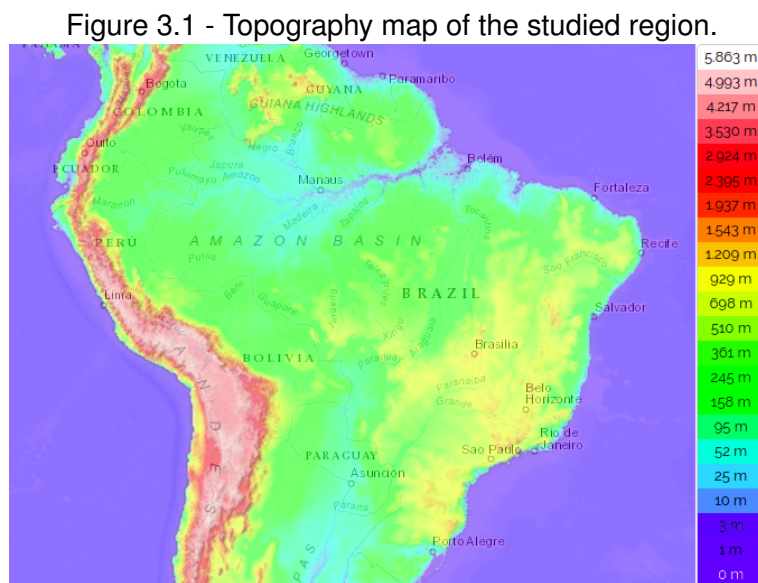


In this context, the main goal of this study is to assess the ability of satellite-based precipitation products to capture the characteristics of extreme precipitation over the tropical region of South America using different satellite precipitation estimation products from a new dataset called Frequent Rainfall Observations on GridS (FROGS) (ROCA et al., 2019), and to compare them with the rain gauge dataset from the National Institute for Space Research (INPE) for the period 2012-2016. To compare SRPs and rain-gauge data, maximum values and 99th percentiles of time series were used to identify extreme events. Statistical metrics such as bias, correlation and mean square error were used.

## 3.2 Materials and methods

### 3.2.1 Study area

South America has an area of about 17.8 million  $km^2$ , contains 6% of the world's population, and is divided into 12 countries. The precipitation in South America is influenced by a large number of meteorological systems, which in turn can be influenced by the topographic characteristics in the region, as shown in Figure 3.1. A review of the atmospheric systems and a schematic representation of all the systems that occur in the low and high troposphere over South America is available in (REBOITA et al., 2010).



Source: Author's production.

The domain analyzed in this investigation is contained in the coordinates from 30°S to 15°N and from 90°W to 30°W, corresponding to the tropical region of South America. We considered a period of five years, ranging from 2012 to 2016.

### **3.2.2 Data**

#### **3.2.2.1 Rainfall Satellite-Based Products**

The Frequent Rainfall Observations on GridS (FROGS) dataset (DOI:10.14768/06337394-73A9-407C-9997-0E380DAC5598), which is composed of daily precipitation gridded products that include satellites, ground-based and reanalysis products adjusted to a common 1°x1° grid resolution, were used in this study. The dataset was downloaded from the ESPRI/IPSL repository.

The FROGS database was built to put all products from different groups such as NASA, NOAA, JAXA among others, in a common resolution (ROCA et al., 2019). Each product was originally formulated with different purposes, considering different areas and different time scales and resolutions. Some products contain global information, others quasi-global and still others specific regions. Also, there are products that consider only the ocean or land areas, and others that consider both. For this reason, the FROGS dataset was built to offer accessible data on daily precipitation products with a common grid of 1°x1°, to provide support to clarify some uncertainties that are inherent in all precipitation products by making them comparable. The FROGS database is formed by 32 products, where the files are produced in NETCDF-4 format and contain information such as longitude, latitude, time and rain intensity. To perform this investigation, we considered the subset of SRPs for the period ranging from 2012 to 2016.

The SRPs selected in this study are described below.

The 3B42RT is a near-real-time product, also known as the TRMM multi-satellite Precipitation Analysis (TMPA) algorithm - Real-Time (HUFFMAN et al., 2007), where passive microwave (PMW) and infrared (IR) data are combined and the historical rain gauge information is incorporated in the calibrated product;

The Global Satellite Mapping of Precipitation (GSMAP) product (KUBOTA et al., 2006) is based on microwave estimation of rainfall but also use IR geostationary imagery to extrapolate the PMW estimates. Rain gauge observations are used to correct for bias;

The Climate Prediction Center morphing technique (CMORPH) (XIE et al., 2017) is a product that combines PMW and IR data to 'morph' the PMW estimated fields. A bias correction technique, using Climate Prediction Center (CPC) rain gauge analysis (XIE et al., 2003), is applied over land surfaces for the V1.0 CRT version;

The Combined Scheme approach (CoSch) (VILA et al., 2009) is a product that uses the Real-Time - TRMM Multi-satellite Precipitation Analysis (TMPA) algorithm and rain gauge data from the Global Telecommunications System (GTS) and multiple institutions in Latin America to remove the bias from TMPA;

The Tropical Amount of Precipitation with an Estimation of ERror (TAPEER) is a product based on the GOES precipitation index technique (CHAMBON et al., 2013), which merges geostationary infrared images with microwave instantaneous rain rate estimates;

The Climate Hazards Infrared Precipitation (CHIRP) (FUNK et al., 2015) is a product based on infrared observations from geostationary observations in a GOES. The CHIRPS product is a merger of rain station information with CHIRP estimates using a weighted average of the closest stations;

The Precipitation Estimation from Remotely Sensed Information using Artificial Neural Networks - Climate Data Record (PERSIANN-CDR) (ASHOURI et al., 2015) is an infrared-based product that uses neural networks to obtain rain rate information.

The short names and version of products used are: 3B42 RT v7.0, 3B42 RT v7.0 uncalibrated, CMORPH V1.0 RAW, CMORPH V1.0 CRT, GSMAP-NRT-no gauge v6.0, GSMAP-NRT- gauge v6.0, CHIRP V2.0, CHIRPS V2.0, PERSIANN CDR v1 r1, CoSch and TAPEER v1.5. From here on they will be called, respectively, 3B42g, 3B42, CMORPH, CMORPHg, GSMAP, GSMAPg, CHIRP, CHIRPSg, PERSIANNg, COSCHg and TAPEER, where sub-index 'g' represents the versions with gauge correction. Table 6.1 below reports some characteristics of the satellite products used.

Table 3.1 - Description table of satellite products.

Satellite product version	Spatial coverage	Use rain gauges	Use IR sensor	Use MW sensor	References
CHIRP v2.0	50°S-50°N 180°W-180°E Land only	No	Yes	No	(Funk et al. 2015)
CHIRPS v2.0	50°S-50°N 180°W-180°E Land only	Yes	Yes	No	(Funk et al. 2015)
PERSIANN CDR v1 r1	50°S-50°N 180°W-180°E	Yes	Yes	No	(Ashouri et al., 2015) (Sorooshian et al., 2014)
3B42 RT v7.0 uncalibrated	50°S-50°N 180°W-180°E	No	Yes	Yes	(Huffman et al. 2007)
3B42 RT v7.0	50°S-50°N 180°W-180°E	Yes	Yes	Yes	(Huffman et al. 2007)
GSMAP-NRT-no gauges v6.0	50°S-50°N 180°W-180°E	No	Yes	Yes	(Kubota et al., 2007)
GSMAP-NRT-gauges v6.0	50°S-50°N 180°W-180°E	Yes	Yes	Yes	(Kubota et al., 2007)
CMORPH V1.0, RAW	60°S-60°N 180°W-180°E	No	Yes	Yes	(Xie et al., 2017)
CMORPH V1.0, CRT	60°S-60°N 180°W-180°E	Yes	Yes	Yes	(Xie et al., 2017)
TAPEER v1.5	30°S-30°N 180°W-180°E	No	Yes	Yes	(Roca et al, 2018)
COSCH	60°S-33°N 120°W-30°W Land only	Yes	Yes	Yes	(Vila et al., 2009)

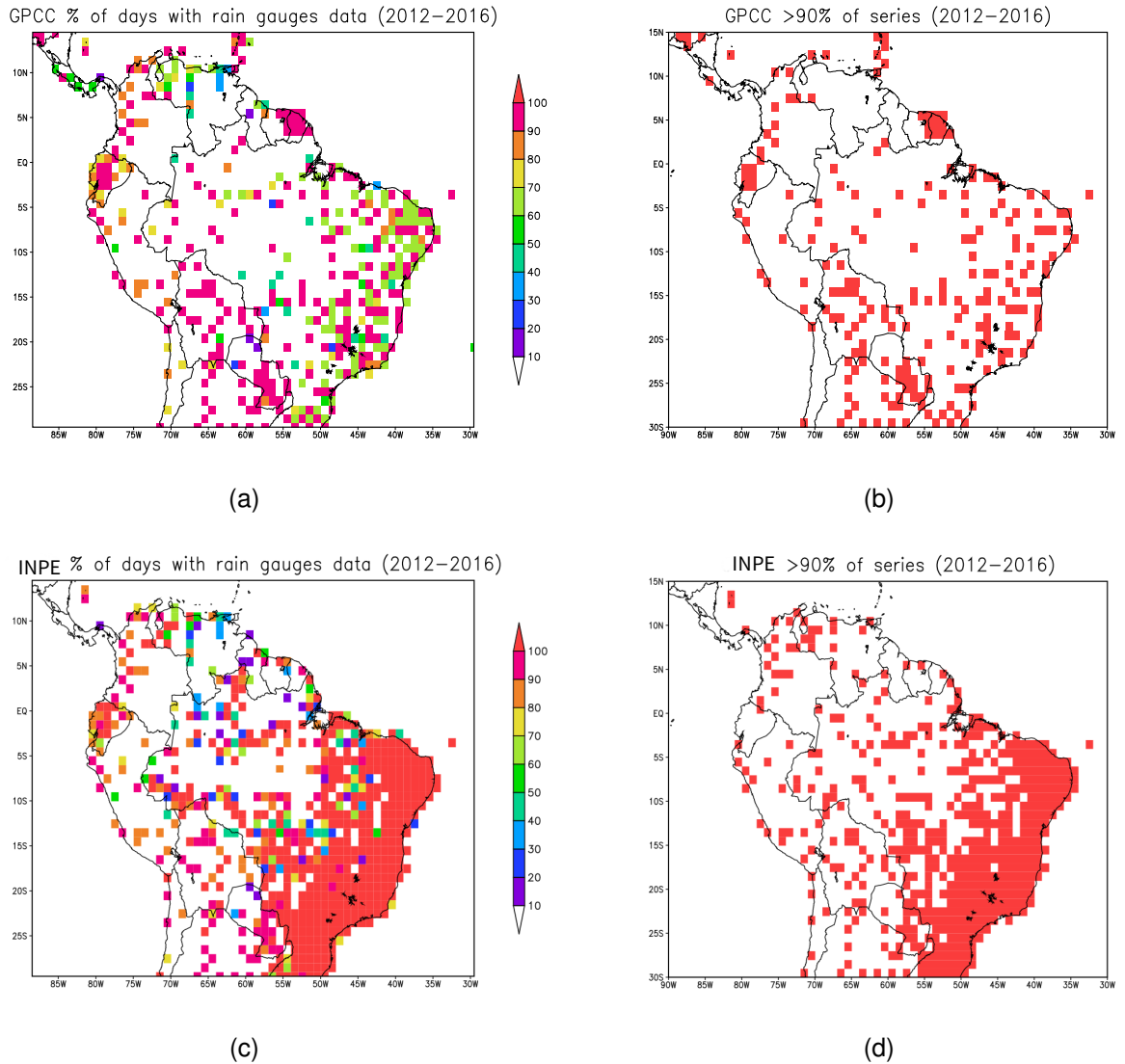
Source: Roca et al (2019).

### 3.2.2.2 Rainfall ground-based data

In this study, two different ground-based databases were analyzed. The first database came from Global Precipitation Climatology Center (GPCC), which is included in the FROGS product. This product is available in a grid with a resolution of  $1^\circ \times 1^\circ$ , considers rainfall information from around the globe from the Global Precipitation Climatology Center (GPCC), and uses a modified SPHEREMAP interpolation scheme (BECKER et al., 2013). The second database was provided by Brazil's National Center for Space Research (INPE) and contains data from automatic and conventional rain gauges/stations from different networks in South America. This database is in DAT format and has been interpolated for regular  $1^\circ \times 1^\circ$  grids using the simple average and then converted to NETCDF format, ensuring the consistency of spatial and temporal resolutions for comparisons.

In order to consider only the grid points representative of the entire time series period, only 10 of the missing data was allowed for each grid point. Figures 3.2 (a) and (c) show the percentage of the number of days where at least one gauge was reported for that grid point in the GPCC and INPE databases, respectively, and Figures 3.2 (b) and (d) identify the grid points with a frequency larger than 90% from Figures 3.2 (a) and (c). In the latter case, the GPCC and INPE databases have 220 and 345 valid grid points respectively.

Figure 3.2 - Percentage of days with, at least, one rain gauge in every grid point for the period 2012-2016. White color represent no gauges for that grid point for the whole period (a) GPCC dataset and (c) INPE dataset. Pixels with a frequency larger than 90% of in the temporal series for 2012 to 2016 period (b) GPCC dataset and (d) INPE dataset.



Source: Author's production.

Grid points with more than 90% of days with gauge information ( $\text{rain} \geq 0.0$ ) were used. In this analysis, 220 grid points were accounted for from the GPCC FROGS database and 345 grid points from the INPE database. Analysis of the rain gauge data sets for GPCC and INPE revealed that the INPE database had greater spatial coverage. Comparison between the two datasets (not shown here) indicated a small difference between them. For this reason, we decided to choose the dataset

provided by INPE to perform this work. So, the INPE rainfall database will be used hereafter as the reference for validation of satellite precipitation estimates for different products. It is important to mention there is no complete coverage of rain gauges in the study area in both databases considered. However, the INPE database covered a more complete data network with more grid points represented by rain gauges.

To ensure data quality, INPE performs an automatic data quality control that considers four steps: (i) range test, which seeks to eliminate gross errors outside the confidence interval; (ii) step test, which considers a maximum difference between consecutive values; (iii) internal consistency test, which makes an association between different meteorological parameters; and (iv) persistence test, which identifies the variability of measurements over a long period of time (COSTA et al., 2017).

### 3.2.3 Methodology

#### 3.2.3.1 Assessment of satellites products : statistical analysis

Statistical analysis was performed to compare satellite data with the gauge-based rainfall data. The objective of this comparison was to evaluate the ability of different algorithms to estimate extreme rainfall. In doing so, we considered the following statistical measures(WILKS, 2011), (MEHRAN; AGHAKOUCHAK, 2014), (MUHAMMAD et al., 2018), (LIU et al., 2019):

a) *The correlation coefficient ( $r$ )* refers to the agreement between satellite-based rainfall and gauge-based rainfall. The correlation coefficient ranges between  $-1$  and  $+1$ . The value of  $+1$  indicates a perfect positive fit, in other words, a perfect linear correlation. We use the term positive correlation when  $r > 0$ , in which case as  $P_G^i$  grows,  $P_S^i$  also increases, and negative correlation when  $r < 0$ , and in this case as  $P_G^i$  grows,  $P_S^i$  decreases on average.

Where:

$P_G^i$  is the gauge-based value at pixel  $i$

$P_S^i$  is the satellite-based precipitation value at pixel  $i$

$n$  is the number pixels included in the analysis.

$$r = \frac{\sum_{i=1}^n (P_S^i - P_S^{mean})(P_G^i - P_G^{mean})}{\sqrt{\sum_{i=1}^n (P_S^i - P_S^{mean})^2} \sqrt{\sum_{i=1}^n (P_G^i - P_G^{mean})^2}} \quad (3.1)$$

b) *RMSE: Root Mean Square Error* is one of the most commonly used methods to measure the absolute average error and is sensitive to larger errors.

$$RMSE = \sqrt{\frac{1}{n} \sum_{i=1}^n (P_S^i - P_G^i)^2} \quad (3.2)$$

c) *BIAS* indicates the average tendency of the satellite-based rainfall fields to be larger or smaller than the rain gauges; the best value is 0; negative (positive) values indicate an underestimation (overestimation).

$$BIAS = \frac{1}{n} \sum_{i=1}^n (P_S^i - P_G^i) \quad (3.3)$$

d) *Standard Deviation* is a measure of the amount of variation or dispersion of a set of values. A low standard deviation indicates that the values tend to be close to the mean of the set, while a high standard deviation indicates that the values are spread out over a wider range.

$$STD = \sqrt{\frac{1}{n} \sum_{i=1}^n (P_S^i - P_S^{mean})^2} \quad (3.4)$$

Taylor diagrams were used to facilitate comparison between the data estimated by different models and the reference data (TAYLOR, 2001); (LEMON, 2006); (GLECKLER et al., 2008). These diagrams are used to quantify the degree of correspondence between the modeled and observed data in terms of three statistics: Pearson correlation coefficient ( $r$ ), root mean square error (RMSE), and standard deviation (std). The x and y axes represent the standard deviation of the estimated and observed data, respectively. The green arc represents the RMSE and the

arc on the right side denotes positive Pearson correlation coefficient values. The colored circles inside the diagram represent the models (satellite products) and the white circle, over the x-axis, represents the reference data (INPE). The closer a model is to the observation point, the better the satellite product is. To compare the statistical behavior of the extreme precipitation values of the different satellite products, the graphs of the probability density function (PDF) and empirical cumulative distribution function (ECDF) of the maximum rainfall values and several percentile values were generated. To estimate the density curves, the non-parametric kernel method was used (WAND; MATT; JONES, 1994); (KUNG, 2014).

Denoted by  $f_x(x)$ , the PDF describes the behavior, in polygonal form, of the frequency distribution of a random variable. In this study, maximum rainfall and extreme rainfall threshold are represented by  $X$ . The probability (Prob) of the random variable being less than a given value of interest is calculated using the CDF ( $F_x(x)$ ), represented by Equation (5.1):

$$F_x(x) = Prob(X \leq x) = \int_{-\infty}^x f_x(x)dx \quad (3.5)$$

Inversely, the corresponding PDF can be obtained by differentiating Equation below:

$$f_x(x) = \frac{dF_x(x)}{dx} \quad (3.6)$$

The CDF of a continuous random variable is a non-decreasing function, and the validated expressions are:  $F_x(-\infty)=0$  and  $F_x(+\infty)=1$  (SHEATHER; JONES, 1991); (SILVERMAN, 1986); (VENABLES; RIPLEY, 2002); (SCOTT, 2015).

In addition to the statistical measures and graphical analysis of PDF and ECDF, a statistical test was also used. A preliminary analysis was carried out to choose between a parametric test, where the assumptions of normality, independence and constant variance must be satisfied, and a non-parametric test, where these assumptions do not all hold. The databases used were independent, but did not satisfy the other assumptions, so the Wilcoxon-Mann-Whitney test was chosen (MANN; WHITNEY, 1947). This is a non-parametric test employed as an alternative



to the Student t-test (parametric cases) for two independent samples (BERGMANN; LUDBROOK, 2000); (SPRENT; SMEETON, ); (HOLLANDER; WOLFE; CHICKEN, 2013). The objective is to test whether two distributions are equal in location, that is, whether the data distribution (observed and estimated) has the same median, where in this case the medians of the extreme values were evaluated. To apply the Wilcoxon-Mann-Whitney test, it is assumed that F and G are the distribution functions corresponding to the observed and estimated data, and the null hypothesis states that the distributions are equal,  $H_0: F(X) = G(Y)$ . The test statistic is calculated by the equation below, (MANN; WHITNEY, 1947):

$$U = mn + \frac{m(m+1)}{2} - S_m \quad (3.7)$$

Where m and n represent the number of elements in samples X and Y respectively; and  $S_m$  denotes the sum of the ranks related to the sample elements X. To decide whether or not to reject the null hypothesis, the p-value (probability of obtaining a test statistic equal to or greater than the value observed in a sample) is calculated. When this is below the desired significance level (here 5%), the null hypothesis is rejected.

### 3.2.3.2 Characterization of extreme rainfall

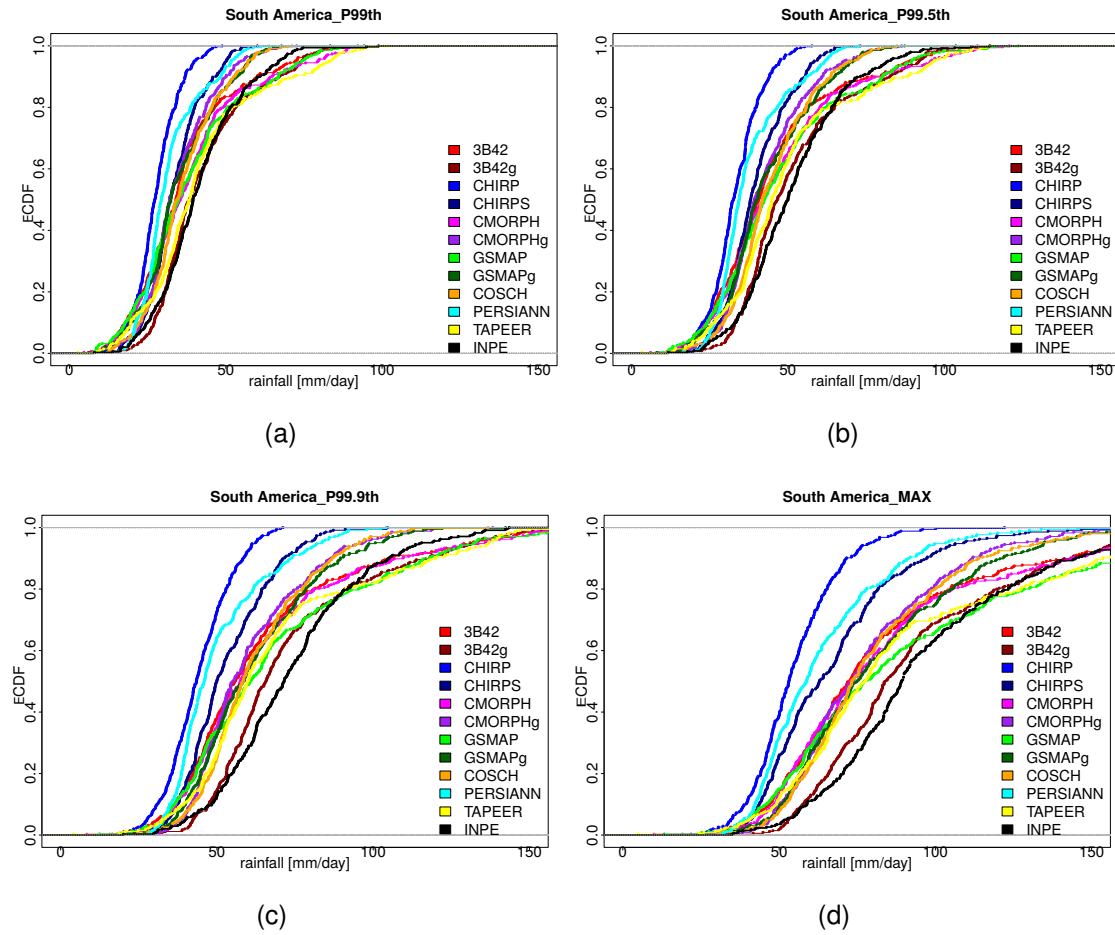
Extreme rainfall is one of the most severe weather hazards affecting the globe. To investigate these extreme events, statistical tools can be used to interpret a dataset and to find a constant threshold. This threshold is based on the empirical distribution of the variable at each location so as to ensure that a given fraction of events will by definition be extreme.

The most common way to choose a threshold is to use the quantiles as cutoff points that divide the range of a probability distribution into contiguous intervals with equal probabilities. But there is still no consensus in meteorology about the precipitation thresholds for the identification of extreme events, so this is highly variable. (LIEBMANN et al., 2001) studied the interannual variability of the events of daily extreme precipitation in the state of São Paulo and defined as extreme events those in which the daily precipitation exceeds a percentage of its seasonal or annual average. In turn, (TEIXEIRA; SATYAMURTY, 2007) defined the criterion of a 50 mm/day isohyetal line enclosing an area of not less than 10000 km<sup>2</sup> in

the domain of southern Brazil. (DERECZYNSKI et al., 2009) studied intense rainfall events in Rio de Janeiro during 1997 to 2006 and applied the percentile technique for each rain station. They observed a threshold higher than 30 mm for the daily precipitation totals corresponding to the 99th percentile of all rain stations considered. (ALVES et al., 2017) investigated the main atmospheric characteristics associated with extreme precipitation events in northeastern Brazil and defined extreme events as daily accumulation of precipitation with values greater than or equal to 50 mm.

In this work, we applied the quantile technique by establishing values above a certain threshold. Using the empirical cumulative distribution function (ECDF), we carried out a preliminary study with the thresholds of 99.0, 99.5 and 99.9 percentiles and the maximum value of the distribution of precipitation over tropical South America during the five-year period.

Figure 3.3 - ECDF of Percentiles (a) 99.0, (b) 99.5, (c) 99.9 and (d) MAX values from South America.



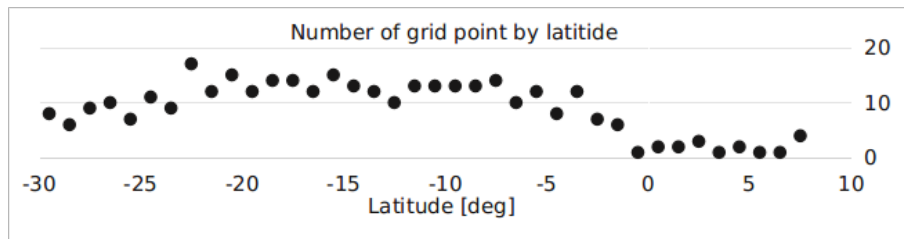
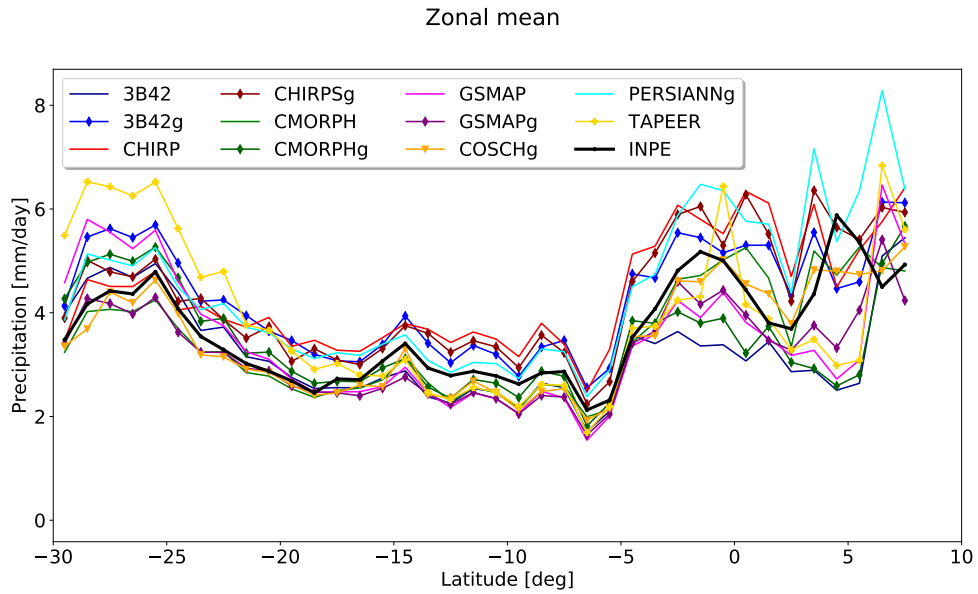
Source: Author's production.

In this study, the thresholds of 99.0 percentile (p99th, hereafter) and maximum value were chosen to characterize extreme precipitation events over South America. As shown in Figures 3.3 (a) and (d), there was a slight difference between the two approaches. While almost all algorithms underestimated the maximum value and there were large discrepancies among them, the p99th, even though considered to be an extreme value from a statistical point of view, showed better agreement among the algorithms when compared with the reference data. The first situation could be because the maximum values are highly sensitive to unfiltered outliers or very rare events in the probability distribution of the reference data and/or the FROGS dataset. The maximum and p99th are explored in section below.

### 3.3 Results and discussion

Since the launch of the first satellite completely focused on precipitation studies (TRMM), the academic community has been evaluating the performance of satellite precipitation estimates obtained by different algorithms (HUFFMAN et al., 2007);(EBERT et al., 2007);(ZHOU et al., 2015);(YONG et al., 2015);(HUFFMAN et al., 2019). For a long time, these efforts were focused on obtaining the average rainfall characteristics on a global basis. It was found that, for average values, the estimates showed a pattern similar to the observed rainfall (MELO et al., 2015). However, this does not happen with extreme rainfall values, where satellite estimates tend to underestimate or overestimate retrievals depending on the physical characteristics of rainfall systems (deep vs. shallow convection systems) and other regional factors like orography and local circulation patterns, among others (SALIO et al., 2015).

Figure 3.4 - Zonal mean precipitation over South America.



Source: Author's production.

To summarize the inter-product differences, zonal mean precipitation was performed (Figure 4) to aggregate the multiple measurements at each latitude band ( $2^\circ$  bins) by plotting the mean rainfall. Note that for the average values, the estimates are close to the reference values (in black), presenting larger dispersion in equatorial latitudes ( $5^\circ\text{S}$  to  $10^\circ\text{N}$ ) and close to the southern edge of the region between  $25^\circ\text{S}$  to  $30^\circ\text{S}$ . According to the climatology, these two regions presented the largest rain accumulation in the studied region (DINIZ et al., 2018). However, this disagreement among different algorithms and the reference data could be also due to a data sampling issue. While the central region has the largest amount of valid grid points per latitude band (see Figure 3.2-d), the equatorial region has the smallest number of valid grid points. The southern region is in an average

situation regarding the number of valid points (Figure 3.4).

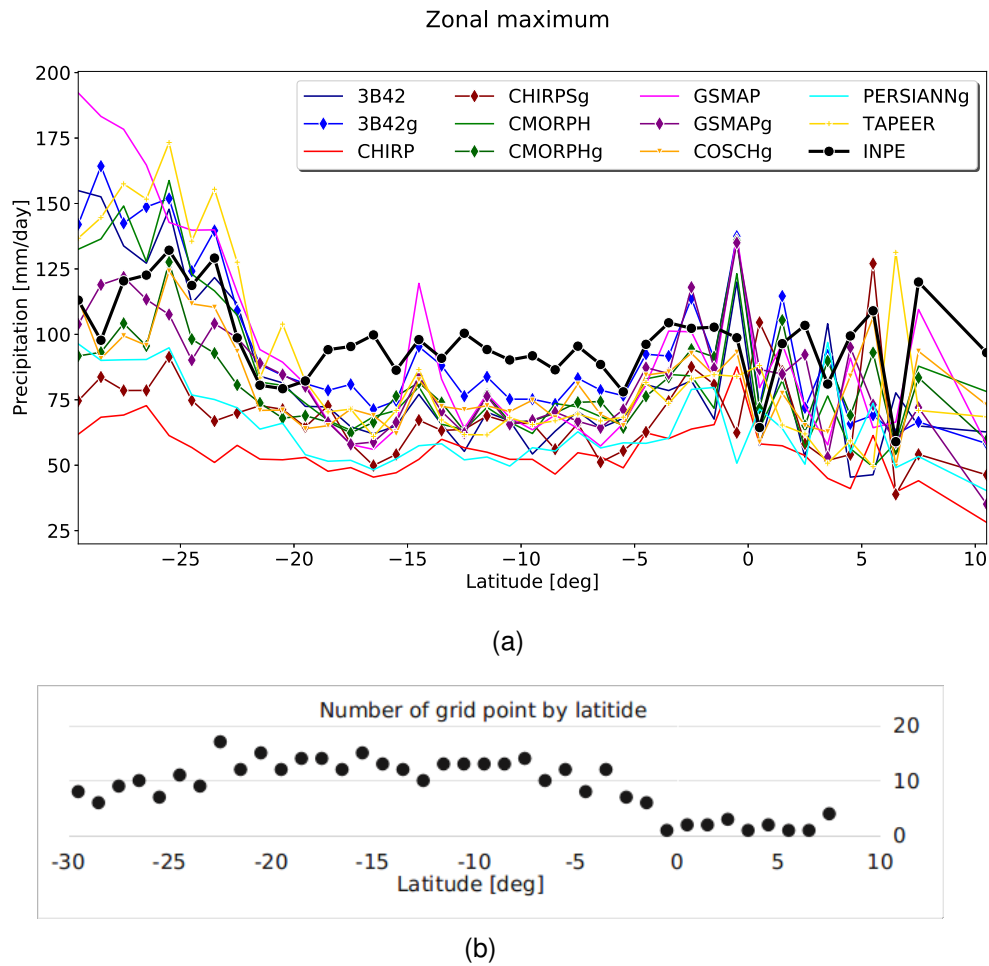
While there is a reasonable agreement for the mean values, large differences are observed in the ECDF of the extreme values, as can be noted in Figure 3.3. Therefore, approaches to extreme precipitation analysis are described in the next two subsections: (i) maximum daily values, and (ii) p99th obtained for each database and the reference.

### **3.3.1 Extreme rain from maximum daily values**

The same zonal mean analysis was performed for the maximum estimated values for each product and for the reference data, as shown in Figure 3.5. All products tended to underestimate the maximum precipitation values for almost all latitude bands, and larger dispersion was noticed for the same regions, as described for the mean values in Figure 3.4.

In equatorial latitudes ( $5^{\circ}\text{S}$  to  $10^{\circ}\text{N}$ ), there was an abrupt variation in the maximum values of rain, as can be seen in the reference data (black line), with variation from 60 mm to 120 mm in just a few degrees of latitude. This variation may be associated with the short-lived convective systems that are common in this region (BRITO, 2013). Also, the algorithms were unable to simulate the same behavior. In the region that comprises latitudes between  $5^{\circ}\text{S}$  to  $20^{\circ}\text{S}$ , there was minor variation of the maximum rainfall values, which were all near 100 mm. All algorithms underestimated the maximum rainfall in this central region of South America, but the dispersion among them was small. Latitudes between ( $20^{\circ}\text{S}$  to  $30^{\circ}\text{S}$ ) had the highest values for maximum rainfall and tended to underestimate these values, while others were overestimated. This behavior will be analyzed later in this section.

Figure 3.5 - Zonal precipitation (a) and number of grid points by latitude (b) of maximum values over South America.



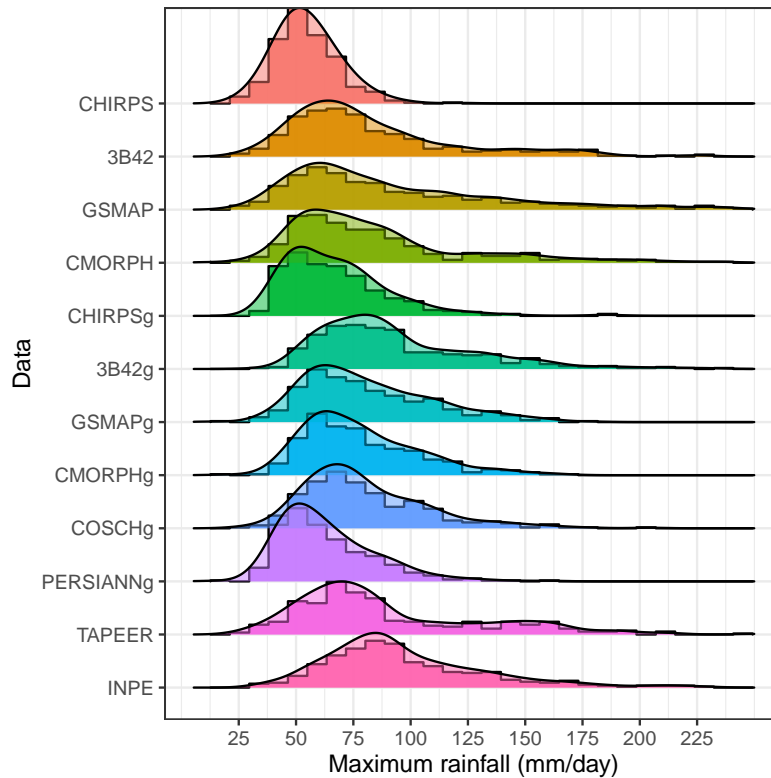
Source: Author's production.

Figure 3.6 shows the frequency of maximum rainfall using the probability distribution function (PDF) of satellite products in South America. According to this plot, the most frequent values were between approximately 75 mm/day and 100 mm/day for the studied region. As shown in the previous analysis, satellite estimates tended to underestimate, with several degrees of disagreement, the maximum values of the PDF.

According to the results, the distributions of the products 3B42, GSMAP, GSMAPg, CMORPHg, COSCHg presented the closest agreement with reference database's PDF, as shown in Figure 3.6. However, according to the Wilcoxon-Mann-Whitney test, the distributions of the maximum precipitation values esti-

mated by the GSMAP and 3B42g products were statistically equivalent to the distribution of the maximum precipitation values observed according to the reference database ( $p\text{-value} > 0.05$ ). The data distributions estimated by the 3B42g and GSMAP products had medians of 84.11 mm and 77.27 mm, respectively. The reference dataset (INPE) was closest to the median of the data distribution (89.20 mm). On average, the products with the smallest biases were 3B42g, GSMAP and TAPEER, with -3.05 mm, -3.82 mm, and -7.79 mm respectively.

Figure 3.6 - PDF of maximum rainfall [mm/day] of satellite products from South America (345 grid points). The histograms represent the empirical distribution. The curves represent the density estimated by the kernel method.



Source: Author's production.

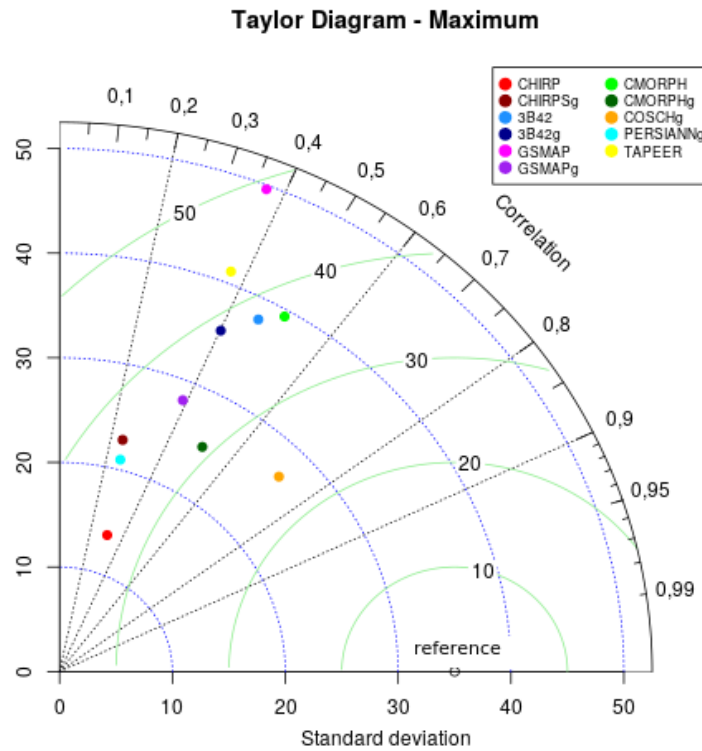
As mentioned, the Taylor diagram provides a concise statistical summary of how well patterns match each other in terms of their correlation, root mean-square error and standard deviation. In this case, the shortest Euclidean distance to the reference data represents the closest agreement. COSCHg presented the best agreement when compared with other algorithms, as shown in Figure 3.7. According to the plot, COSCHg presented the best metrics compared with other



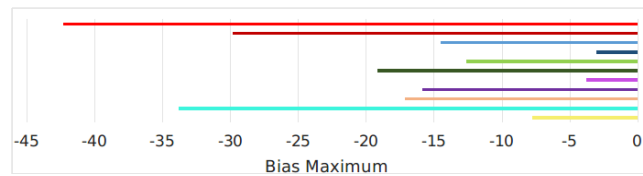
products, with the highest correlation coefficient ( $r = 0.72$ ) and the smallest standard deviation and root mean square error (std = 26.9 and RMSE = 24.5).

COSCHg presented the closest metrics when compared with the reference data, with correlation coefficient ( $r$ ) = 0.72, standard deviation (std) = 26.9, and root mean square error (RMSE) = 24.5 for the entire region. These results were expected based on (VILA et al., 2009), since the COSCHg product merges satellite estimates with daily gauge data. In this case, TMPA is used as a high-quality rainfall algorithm and a very similar database (that used as a reference), composed of daily rain gauge observations, is used to correct the bias of near real-time over South America. As shown in Figure 3.7, bias was negative for South America, indicating that all products tended to underestimate maximum rainfall values.

Figure 3.7 - Statistical comparison between gridded rain gauge data and satellite-derived rainfall products over a period of 5 years (2012-2016) described by Taylor Diagram of maximum rainfall (a) and Bias bars (b). RMSE is represented with curved lines in green, STD is represented with curved lines blue and  $r$  is represented with straight lines in black.



(a)



(b)

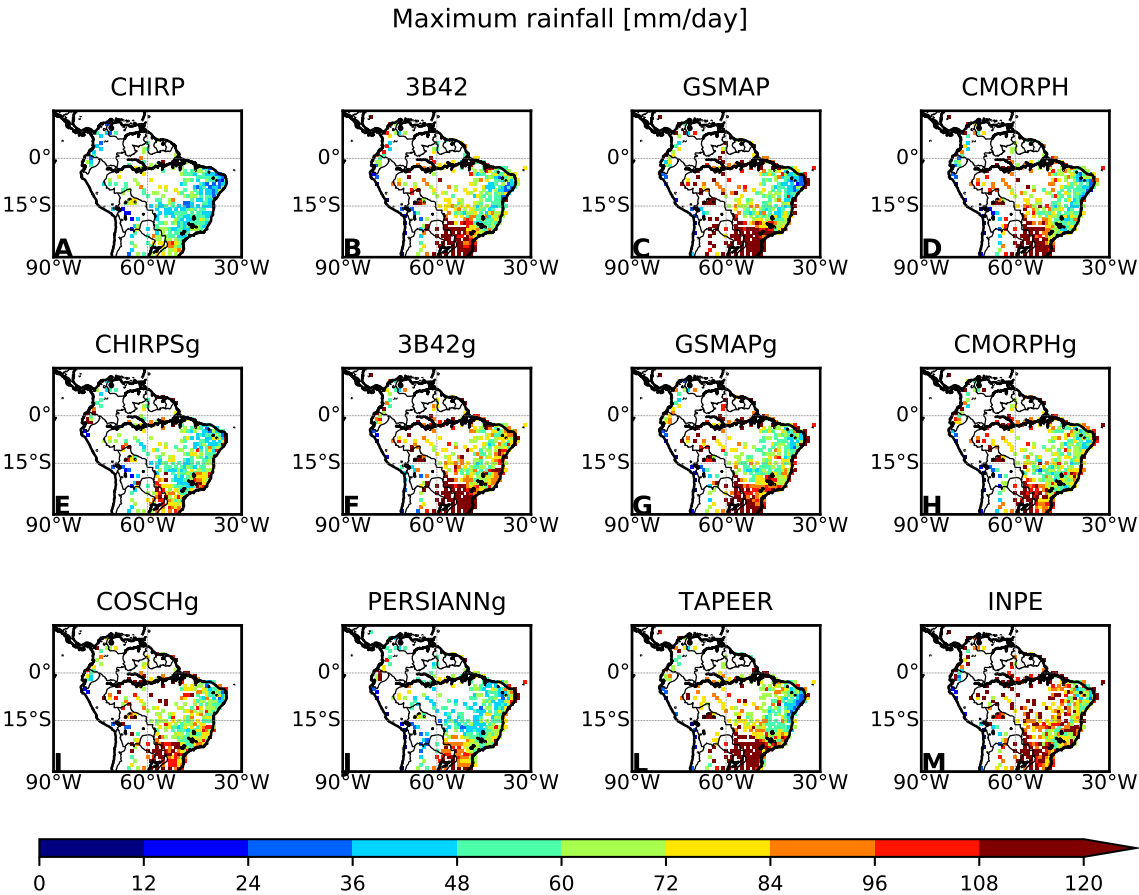
Source: Author's production.

Figure 3.5 shows the distribution of extreme rainfall differences with latitude and behaviors for each product. In Figure 3.8, the spatial distribution of maximum rainfall (mm/day) occurred in each valid pixel during the period analyzed for all SRPs and the reference data. The maximum spatial pattern values showed a clear delimitation of maximum values for almost all SRPs. In the reference dataset (Figure 3.8-M ), the largest maximum rainfall values were achieved in the southern and

northern regions of Brazil, while the smallest values were observed in the semi-arid region of northeastern Brazil. This pattern was also observed, with different degrees of agreement, in all studied algorithms.

The behavior mentioned above may be associated with the different types of meteorological systems that occur in each region (REBOITA et al., 2010) as well as the composition of hydrometeors within the clouds. In the southern region, clouds with significant ice content and deep convection, characteristics are typically observed (CALHEIROS, 2013), while at the northeastern region clouds generally have shallow convection with little or no ice content (PALHARINI; VILA, 2017).

Figure 3.8 - Spacial distribution of maximum rainfall [mm/day] of each products.



Still referring to Figure 3.8, it shows differences between the estimated maximum

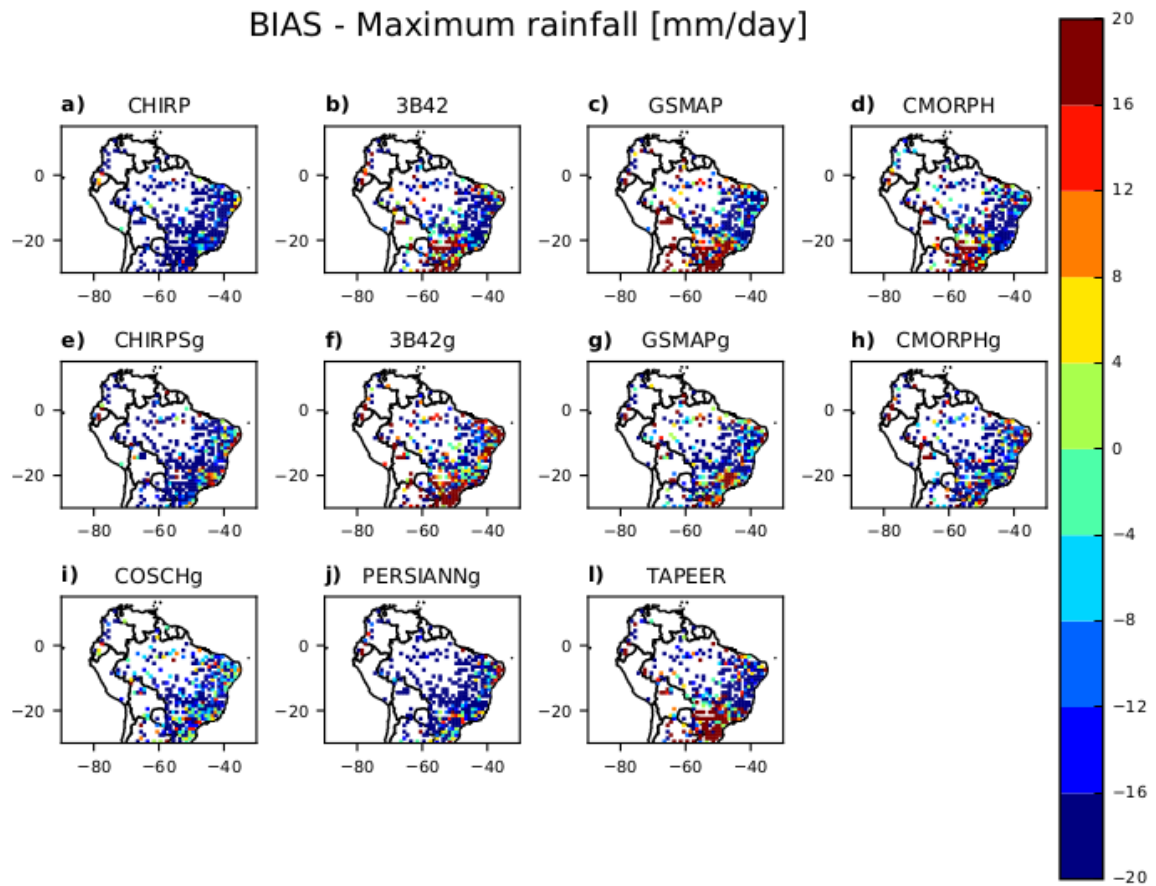
values and the observed maximum values. All products tended to underestimate extreme rainfall values. However, products such as CHIRP (Figure 3.8 A) and PERSIANN (Figure 3.8 J) tended to underestimate these values in all regions. This could be due to the fact that both rely on infrared information for rainfall retrieval. (HOBOUCHIAN, 2012) showed that other IR-based algorithms (Hydro Estimator in that case) have difficulty in retrieving the largest precipitation values.

The products without rainfall adjustments tended to underestimate the lowest values and overestimate the highest values, as it can be seen in the southern and the northeast regions of Brazil respectively, and as demonstrated in Figures 3.8 A-D and Figure 3.8 L). The results are similar to the results found by (KIMANI et al., 2017) for East Africa. According to the authors, the performance of satellite products is weaker when rainfall intensity is high, and after adjustments, they observed a closer estimate in some regions.

Figure 3.9 depicts the difference between the maximum rain in the reference data and the maximum rain estimated by each product at each grid point. Some products overestimated the maximum values in some regions (reddish colors) while underestimating them in others (bluish colors).

While some products (CHIRPS, CHIRP and PERSIANN, among others) underestimated the maximum value for almost the whole region, others had different behavior according to the region. GSMAP, 3B42g and TAPEER tended to overestimate the maximum values over the southern region while underestimating them in the central region. The regional analysis will be investigated in the near future to establish a relationship between anomalies of large and regional circulation patterns and extreme values.

Figure 3.9 - Spacial distribution of Estimated - Observed maximum precipitation [mm/day] of each products.



Source: Author's production.

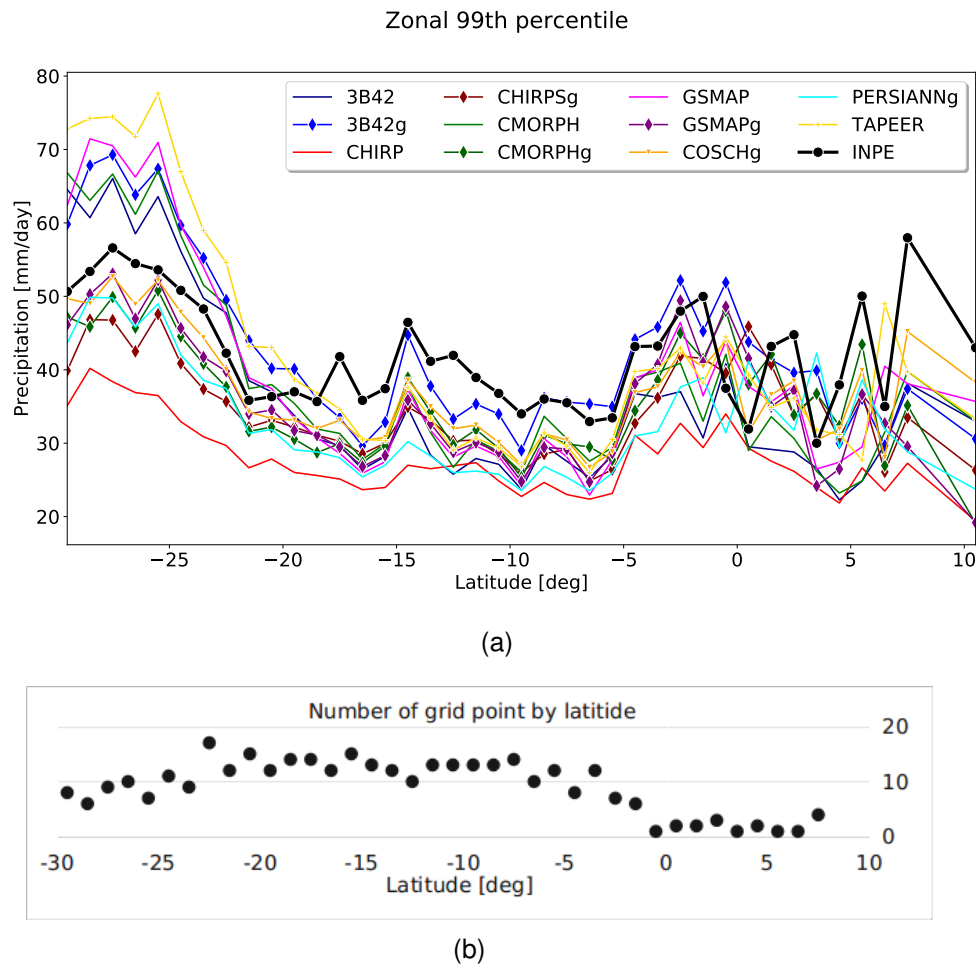
### 3.3.2 Extreme rain from 99th percentile threshold

The second approach used to analyze extreme precipitation over South America was application of the 99th percentile threshold. The zonal analysis was performed for the p99th values of each precipitation estimation product and reference data (in black), as shown in Figure 3.10. According to this plot, most of the products tended to underestimate p99th and the pattern is very similar to the maximum values with larger dispersion in the southern region between 30°S-25°S and close to the equator.

Figures 3.5 and 3.10 indicate that both maximum and p99th values for products such as GSMAP, CMORPH, 3B42 and TAPEER overestimated the reference values between 30°S-20°S. These results are similar to those obtained by

(MASUNAGA et al., 2019), who used other reference data sources (GPCC v2018 and CPC v1.0), considered all points on ocean/land and interpolated points. In the central region, underestimation is present in all products, with a smaller dispersion due to the larger number of valid points considered, while the equatorial region is noisier and has larger dispersion due to the smaller number of valid point considered in the comparison and the complex behavior of the rainfall systems over the Amazonian region.

Figure 3.10 - Zonal precipitation (a) and number of grid points by latitude of the mean values of all values above 99th percentile over South America.

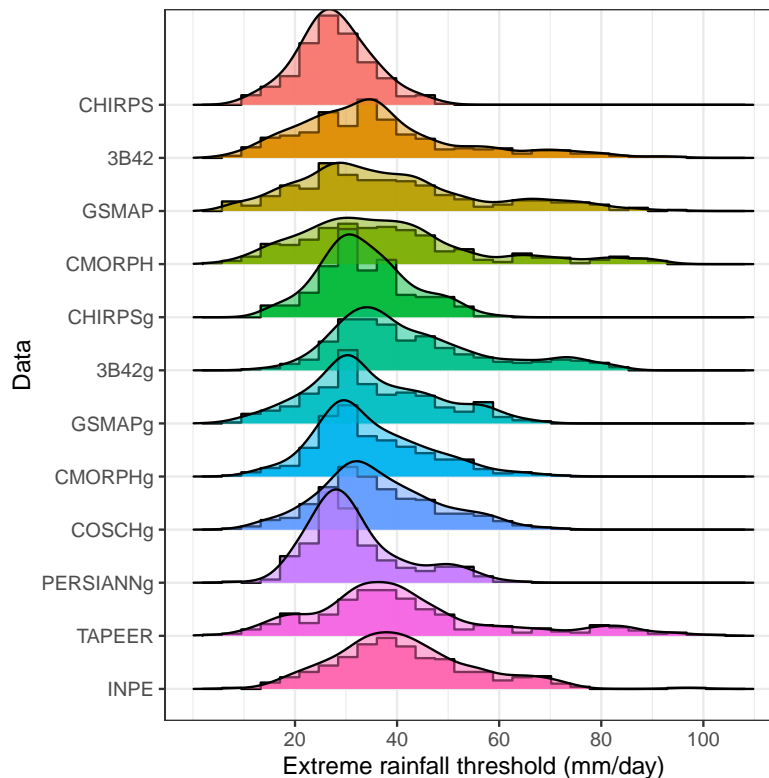


Source: Author's production.

A similar analysis was performed for the maximum values, as shown in Figure 3.11. This plot depicts the frequency of the 99th percentile for rainfall using the

probability distribution function (PDF) of satellite products from South America. According to the reference data, the most frequent p99th daily values were between 30 mm/day and 50 mm/day. This analysis considered daily rainfall values  $\geq 0.0$  mm in order to analyze the p99th for each grid point, and the same amount of data was present in each distribution.

Figure 3.11 - PDF of 99th percentile of rainfall [mm/day] of satellite products from South America (345 grid points). The histograms represent the empirical distribution. The curves represent the density estimated by the kernel method.



Source: Author's production.

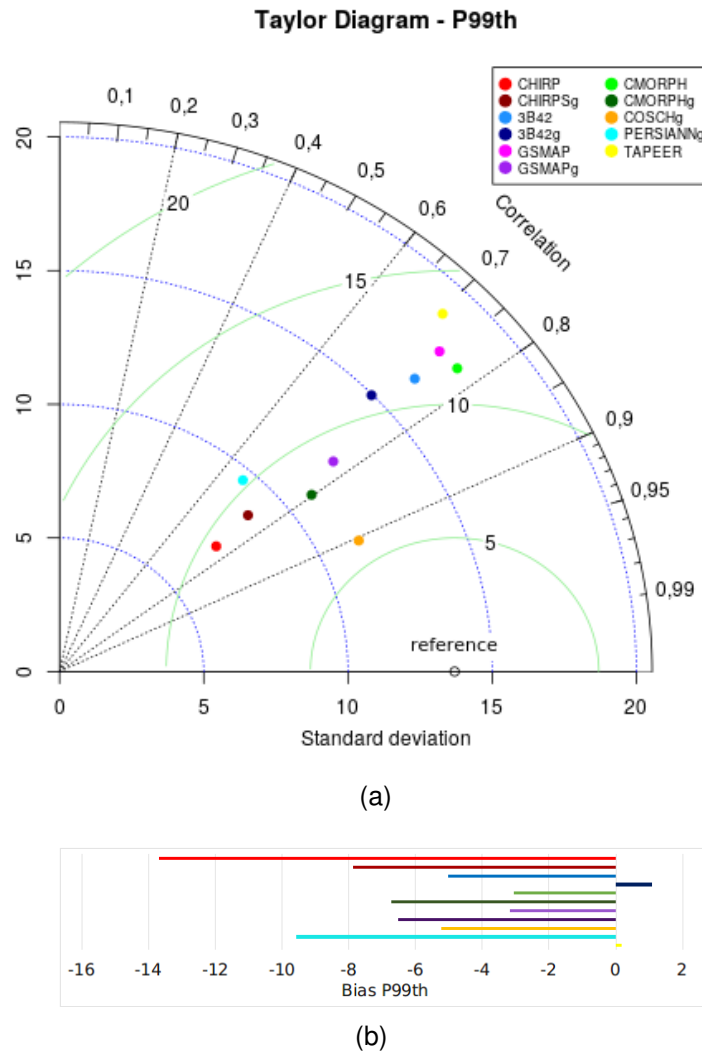
Still referring to Figure 3.11, according to the PRF's PDF, each product had a different maximum in the frequency (mode). In general, all products tended to underestimate the frequency of p99th rainfall values. The distributions of the products GSMAPg, CMORPHg, and COSCHg had the best agreement compared to the observed PDF (INPE) over South America. However, according to the results of the Wilcoxon-Mann-Whitney test, the distributions of the p99th threshold of precipitation values estimated by the 3B42g and TAPEER products were statistically equivalent to the distribution of the p99th precipitation values observed by

INPE, with p-value  $> 0.05$ . Other products had a p-value  $< 0.05$ . The data distributions estimated by the 3B42g and TAPEER products had a median of 38.5 mm and 38.6 mm, respectively, close to the median of the reference data distribution, which was 39.5 mm. On average, the products that showed the smallest biases were 3B42g and TAPEER, with 1.07 mm and 0.19 mm, respectively.

According to Figure 3.12, when statistical metrics such as correlation coefficient, mean square error and standard deviation were applied to the COSCHg product, better performance was achieved in comparison with the reference data. This Taylor diagram describes the performance of satellite-derived extreme rainfall estimates in comparison with gridded rain gauge data and shows the correlation coefficient, standard deviation and mean square error values. The bias of p99th over South America is negative for the majority of the products, indicating they tended to underestimate p99th threshold rainfall values. However, exceptions occurred for TAPEER (1.07 mm) and 3B42g (0.19 mm).



Figure 3.12 - Statistical comparison between gridded rain gauge data and satellite-derived rainfall products over a period of 5 years (2012-2016) described by Taylor Diagram of P99th rainfall (a) and Bias bars (b). RMSE is represented with curved lines in green, STD is represented with curved lines blue and  $r$  is represented with straight lines in black.



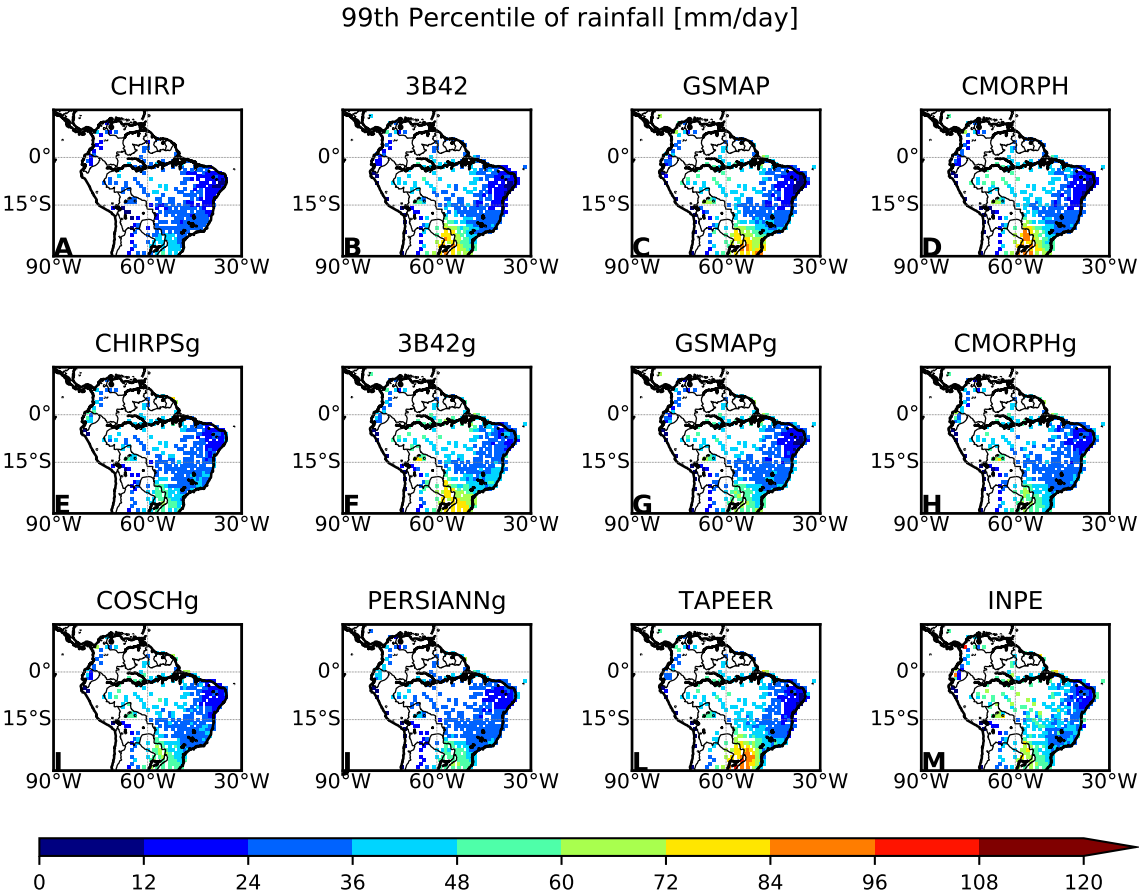
Source: Author's production.

Figure 3.13 shows the spatial distribution of the 99th percentile in each pixel for estimates and the reference data. In addition, Figure 3.9 shows the bias related to these data. While the spatial pattern observed is very similar to the maximum precipitation (Figure 3.8), the values are well below the maximum values with a smoother distribution. This situation can be explained because in this analysis, all rainfall values (including 0.0 mm) were considered in establishing the p99th. In very dry regions like the continental region of northeastern Brazil, where the

number of rainy days (defined as days with accumulated rainfall greater than 1 mm) is just 35 per year (DINIZ et al., 2018), the p99th could be affected by the fact that this situation does not represent an extreme value in terms of impacts on the society.

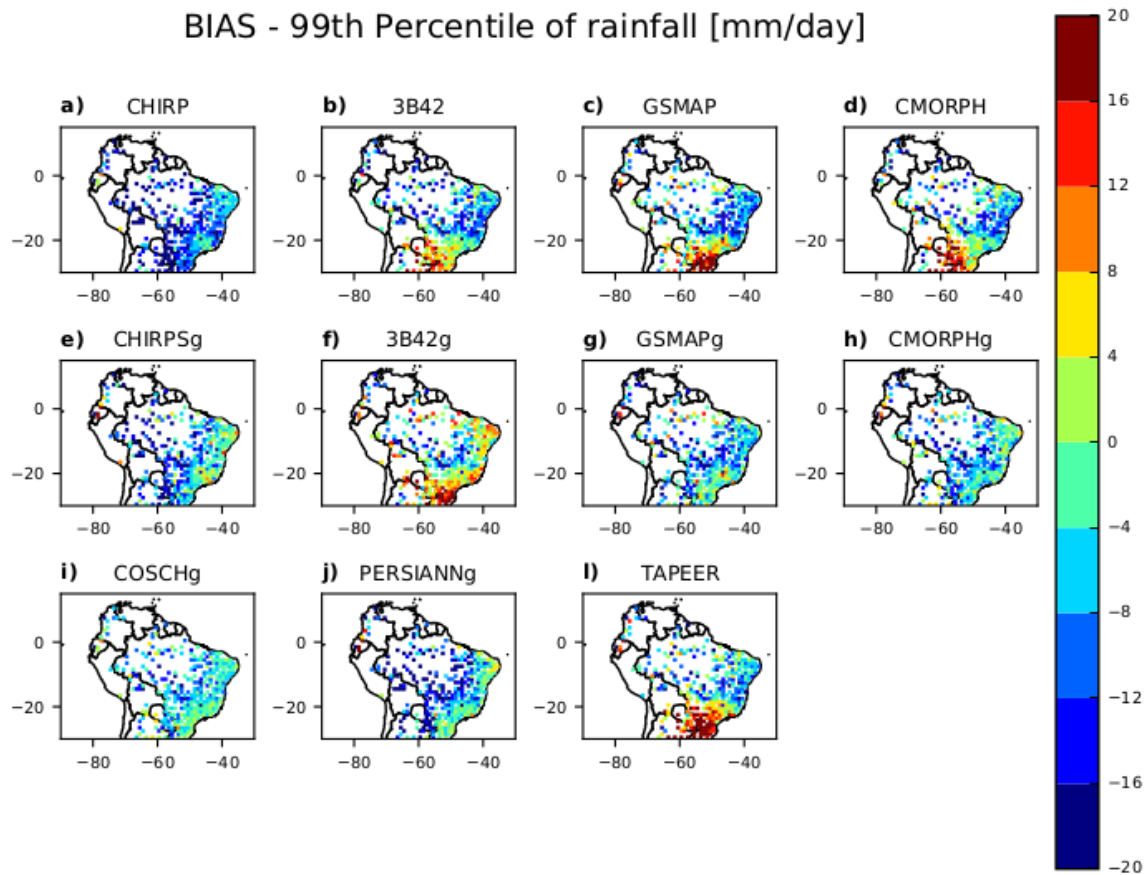
Figure 3.14 shows that some products overestimated the p99th values in some regions (reddish colors) while underestimating them in others (bluish colors), as observed by the maximum values. Some products, such as CHIRP, CHIRPSg, COSCHg, PERSIANNg, and CMORPHg, tended to underestimate the p99th value over South America, while 3B42, 3B42g, GSMAP, CMORPH and TAPEER tended to overestimate the p99th values over the southern region while underestimating then in the central region.

Figure 3.13 - Spacial distribution of 99th percentile rainfall [mm/day] of each products.



Source: Author's production.

Figure 3.14 - Spacial distribution of Estimated - Observed 99th percentile of rainfall [mm/day] of each products.



Source: Author's production.

### 3.4 Conclusions

Extreme rainfall events can cause several social, economic and environmental problems. Studies that improve understanding of the characteristics of these events are important. The main objective of this study was to evaluate a large number of satellite products and identify their capacity to detect extreme precipitation events. In addition, the extensive spatial coverage of data observed by the rain gauge network in South America was considered to compare these data with satellite products. In this scenario, the comparison between extreme precipitation values of 11 different satellite products and rain gauge data was carried out for the tropical region of South America. Precipitation extremes were defined by maximum values and the 99th percentile threshold in a daily  $1^\circ \times 1^\circ$  grid for the period from 2012 to 2016. The ability of the satellite-based precipitation products

to detect extreme precipitation was analyzed using statistical metrics. The SRPs evaluated were CHIRP v2.0, CHIRPS v2.0, 3B42 RT v7.0 uncalibrated, 3B42 RT v7.0, GSMAP-NRT-no gauges v6.0, GSMAP-NRT-gauges v6.0, CMORPH v1.0 RAW, CMORPH v1.0 CRT, PERSIANN CDR, CoSch, and TAPEER v1.5, using data from the rain gauges of the INPE database as the reference.

The evaluation of different SRPs showed that the adjusted rain gauge products had better performance than near real-time product versions. This suggests that satellite-based estimates combined with gauge information would be effective to identify extreme precipitation. Similar results were found by (WANG et al., 2017) and (LIU et al., 2019), who showed that post-real-time products agreed well with the gauge-based observations and presented satisfactory performance for China. In addition, (ROZANTE et al., 2018) compared the performance of TRMM, IMERG-F, and GSMAp-Gauge in Brazil and demonstrated that IMERG-F and GSMAp-Gauge presented better performance in comparison with near-real-time products. However, according to this investigation, this is most likely only in regions where rain gauge data are available.

The main findings of this study reveal that the products without rainfall adjustments tended to underestimate the lowest values and overestimate the highest values in the southern and northeastern regions of Brazil. This corroborates the results of (KIMANI et al., 2017) for East Africa, where the performance of satellite products was found to be weaker when rainfall intensity is high, and, after adjustments a closer estimate was observed in some regions. However, one of the big advantages of satellite data is availability for regions without rain gauges. In this study, we observed that GSMAP and TAPEER, which are SRPs that are not adjusted by rain gauge data, presented better performance when the maximum values occurred between 75 mm and 100 mm when compared with the other SRPs. We also observed that the performance of the SRPs that include MW measurements was better than those with IR information only. This was seen in the case of CHIRP, CHIRPSg and PERSIANNg, which were the products that most underestimated the extreme values of precipitation and that had the lowest correlation coefficient ( $r < 0.3$ ) for maximum values. In contrast, GSMAP, 3B42g and TAPEER, which have blended techniques, tended to overestimate the maximum values in the southern region. This leads to the hypothesis that the use of extreme precipitation estimates derived from satellite products should not be considered globally, but regionally, as the performance of each product varies according with the particularities of each region. In this way, extreme rain thresholds vary greatly

from region to region.

The most frequent values of extreme rainfall in South America were between 75 mm/day and 100 mm/day, but all products analyzed tended to underestimate extreme precipitation for almost all latitude bands in this region. In particular, we noted a spatial pattern of the extreme values of precipitation. The maximum and 99th percentile extreme rainfall estimates had similar features, where the extremes with the most intense volume were in the northern and southern regions of Brazil while the lowest values were observed in the semiarid region of northeastern Brazil. This spatial pattern was detected by all SRPs evaluated, with different degrees of agreement. This behavior may be associated with the different types of meteorological systems that occur in each region ([REBOITA et al., 2010](#)), as well as the composition of hydrometeors within the clouds. While in the southern region, clouds with significant ice content and deep convection characteristics are often observed ([CALHEIROS, 2013](#)), the northeastern region is characterized by shallow convection with little or no ice content ([PALHARINI; VILA, 2017](#)).

Our objective was to identify the characteristics of extreme rain events represented by different satellite databases. However, other analyses are necessary. In future works, the events of extreme precipitation for South America will be analyzed by date of occurrence, based on the observed rainfall data and for each specific event to validate satellite data, allowing us to show which product performs best according to the meteorological condition on the specific day. This will enable us to identify which physical thermodynamic processes favor the occurrence of rainfall extremes in different regions of South America.



## 4 ASSESSMENT OF THE EXTREME PRECIPITATION BY SATELLITE ESTIMATES - PART 2: REGIONAL ANALYSIS

### 4.1 Introduction

Precipitation is one of the main meteorological variables associated with the intensity and frequency of extreme events. In addition, precipitating cloud systems are an essential component of water reservoirs and have major impacts on the global and regional climate of the terrestrial system as a whole (STEPHENS; ELLIS, 2008). The latent heat released by precipitation is an important source of atmospheric heating that drives the general circulation of the atmosphere and the climate system. In this way, the worldwide population is vulnerable to the dangers caused by natural disasters triggered by extreme events. According to the Brazilian Atlas of Natural Disasters, in the period from 1991 to 2012 more than 57 million people were affected by extreme weather events across Brazil and a total of 38996 disasters were recorded in this period (UNIVERSIDADE FEDERAL DE SANTA CATARINA. CENTRO UNIVERSITÁRIO DE ESTUDOS E PESQUISAS SOBRE DESASTRES - UFSC.CEPED., 2012).

Due the several damages caused by extreme precipitation in Brazil over the last years, significant effort has been made in order to deep understand the causes and to propose plans to mitigate the impacts these extreme events (ALCÁNTARA-AYALA, 2002); (MARCELINO, 2008). In doing so, different techniques have been developed to monitor precipitation. Rain gauges, radars and satellites have be used to collect data at different regions of the world (TAPIADOR et al., 2012). With rain gauges, it is possible to make direct and immediate measurements at surfaces; however, these instruments cover a small area. It is required a more complete rain gauge network to efficiently monitor the rainfall. Weather radars can cover larger areas simultaneously and perform high spatial sampling. Despite their importance, rainfall networks and weather radars are scarce in many developing countries, especially due to the high cost of installing and maintaining their infrastructure (SALIO et al., 2015). In this scenario, several regions in Brazil do not have the necessary instrumentation to collect data from extreme events and the only way to monitor these areas is the use of satellite data available.

Since the end of the 90's, when the first satellite was launched with the objective of monitoring the rainfall in the tropical regions, great advances have been observed and a better understanding of extreme precipitation have been achieved. The Tropical Rainfall Measuring Mission (TRMM) provided 17 years of satellite data

with observations from November 1997 to April 2015. The TRMM was succeeded by the Global Precipitation Measurement (GPM) mission which has extended the satellite observation and data gathering to Arctic and Antarctic circles. The GPM are able to perform measurements using high quality passive/active microwaves and infrared (IR) at geostationary orbit ([LEVIZZANI et al., 2020a](#)).

The join effort of several space agencies around the world made possible the improvement of precipitation measurements through the better understanding of the physics and space-time variability of precipitation across the Earth ([LEVIZZANI et al., 2020b](#)). Different techniques have been developed to monitor precipitation using satellites and the physical principles of precipitation retrieval are based on Infrared (IR), Passive Microwave (PMW), and Active Microwave (AMW) sensors and the improvement of these techniques for data retrieval is essential to quantify extreme events in terms of frequency and intensity.

Some of the investigations have used information from Precipitation Radar (PR) and TRMM Microwave Imager (TMI) instruments on board of TRMM to quantify extreme events and their connection with convective activity. [Zipser et al. \(2006\)](#) detected and diagnosed extremely intense thunderstorms in the tropics; [Rasmussen et al. \(2013\)](#) studied extreme storms in South America; and [Rossow et al. \(2013\)](#) investigated the contributions of the average precipitation intensity and average daily accumulation rate generated by the different types of deep convective systems. Recently, [Sekaranom and Masunaga \(2019\)](#) studied the physical processes in the development of heavy precipitation clouds using the differences in TRMM active and passive sensors (PR-TMI) combined with the cloud structure information obtained from CloudSat and the background environmental conditions of ERA-Interim reanalysis.

Other studies mapped precipitation based on satellite observations using PMW/AMW sensors from several Low-Earth Orbit (LEO) satellites and Geosynchronous Equatorial Orbit (GEO) IR observations with rain gauges adjusts. These studies compared the differences between Satellite Precipitation Products (SPPs) in order to verify which one presented a better performance ([MASUNAGA et al., 2019](#));([LIU et al., 2019](#));([PALHARINI et al., 2020](#)). According to these investigations, it was observed that the average values of rain for different products presented similar results between them; however, a significant difference between the products were noticed for maximum or extreme values of rain. Perhaps because the SPPs were designed to detect a very wide spectrum of rain, ranging from light to heavy



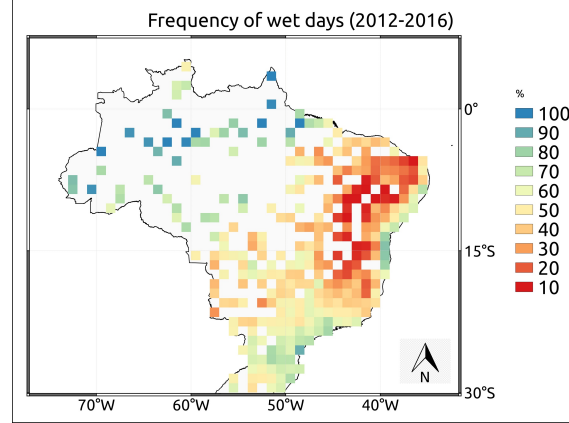
rainfall and globally, possibly without considering specific characteristics of each region. Given that some products are tailored for specific purposes and may not necessarily be optimal for all applications (MASUNAGA et al., 2019). There are numerous applications of SPPs are centred around precipitation extremes. Studies associated with tropical cyclones, El Niño-Southern Oscillation, convective systems, modelling of hydrological extremes including landslide; floods early warning and monitoring; extreme rainfall and streamflow predictions and others are extremely important. These studies can benefit if the next generation of SPPs, from GPM constellation for example, improve the algorithms for detecting extremes of rain or tailor some product with this specific purpose.

In Brazil, where different weather systems acts at different regions along the year, a deeper investigation become necessary in order to identify which of the current products have the best performance for extreme rainfall values across the country. In this way, the main goal of the work is to assess the performance of different products to detect extreme precipitation in five regions of Brazil using grided precipitation datasets.

## **4.2 Methodology**

In this investigation two thresholds were chosen to classify extreme rain events: maximum values and conditional 99th percentile (P99th). In this way, in the present work, it is considered only the values of rain above 1.0 mm/day. The P99th threshold was chosen since the number of rainy days over the time series used in this work have a significant difference from one region to another. In Figure 4.1 it is observed that in the north of Brazil some grid points have a frequency around 60% of rainy days while other points in the interior of the semi-arid northeast of Brazil have values around 10% of rainy days over the study period.

Figure 4.1 - Frequency of wet days (> 1.0 mm/day) over Brazil during the study period (2012-2016) using rain gauges dataset at National Institute for Space Research (INPE) .



Source: Author's production.

In order to compare satellite data with the gauged-based rainfall dataset for different regions of Brazil, a statistical analysis was performed. The main objective of comparing satellite products and the rain gauge dataset was to evaluate the ability of different algorithms to estimate extreme rainfall. The relevant statistical measures applied in this work were the correlation coefficient ( $r$ ); the root mean squared error (RMSE); and BIAS (WILKS, 2006). These metrics were calculated as follows:

$$r = \frac{\sum_{i=1}^n (P_S^i - P_S^{mean})(P_G^i - P_G^{mean})}{\sqrt{\sum_{i=1}^n (P_S^i - P_S^{mean})^2} \sqrt{\sum_{i=1}^n (P_G^i - P_G^{mean})^2}} \quad (4.1)$$

$$RMSE = \sqrt{\frac{1}{n} \sum_{i=1}^n (P_S^i - P_G^i)^2} \quad (4.2)$$

$$STD = \sqrt{\frac{1}{n} \sum_{i=1}^n (P_S^i - P_S^{mean})^2} \quad (4.3)$$

$$BIAS = \frac{1}{n} \sum_{i=1}^n (P_S^i - P_G^i) \quad (4.4)$$

Notation:  $n$  is the number pixels included in the analysis;  $P_G^i$  is the gauge-based value at pixel  $i$ ;  $P_S^i$  is the satellite-based precipitation value at pixel  $i$ .

To facilitate comparison between the data estimated by different satellite products and the reference data by rain gauges, Taylor diagrams are used (TAYLOR, 2001);(LEMON, 2006);(GLECKLER et al., 2008). These diagrams were applied to quantify the degree of correspondence between the modeled and observed data in terms of three statistics: Pearson correlation coefficient ( $r$ ), root mean square error (RMSE), and standard deviation (std). The  $x$  and  $y$  axes represents the standard deviation of the estimated and observed data, respectively. The green arc represents the RMSE and the arc on the right side denotes positive Pearson correlation coefficient values. The colorful circles inside the diagram represent the satellite products and the black diamond, over the  $x$ -axis, represents the reference data. The closer the satellite product is to the observation point, the better it is.

To compare the statistical behavior of the extreme precipitation values of the different satellite products, the graphs of the probability density function (PDF) and empirical cumulative distribution function (ECDF) of the maximum rainfall values and several percentile values were generated. To estimate the density curves, it was used the non-parametric kernel method(WAND; MATT; JONES, 1994); (KUNG, 2014).

Denoted by  $f_x(x)$ , the PDF describes the behavior, in polygonal form, of the frequency distribution of a random variable. In this study, maximum rainfall and extreme rainfall threshold are represented by  $X$ . The probability (Prob) of the random variable being less than a given value of interest is calculated using the CDF ( $F_x(x)$ ), represented by Equation (5.1):

$$F_x(x) = Prob(X \leq x) = \int_{-\infty}^x f_x(x)dx \quad (4.5)$$

Inversely, the corresponding PDF can be obtained by differentiating Equation be-

low:

$$f_x(x) = \frac{dF_x(x)}{dx} \quad (4.6)$$

The CDF of a continuous random variable is a non-decreasing function, and the validated expressions are:  $F_x(-\infty)=0$  and  $F_x(+\infty)=1$  (SHEATHER; JONES, 1991); (SILVERMAN, 1986); (VENABLES; RIPLEY, 2002); (SCOTT, 2015).

In addition to the statistical measures and graphical analysis of PDF and ECDF, a statistical test was applied to the data. A preliminary analysis was carried out to choose which test would be more appropriate, a parametric test or a non-parametric test. The assumptions of the parametric test, such as normality, independence and constant variance, must all be satisfied. Whereas the non-parametric test is not necessary for all the assumptions to be satisfied. Thus, the databases used were only independent and did not meet the other premises. Hence, the Wilcoxon-Mann-Whitney test was chosen (MANN; WHITNEY, 1947). This is a non-parametric test employed as an alternative to the Student-t test for two independent samples (BERGMANN; LUDBROOK, 2000); (SPRENT; SMEETON, ); (HOLLANDER; WOLFE; CHICKEN, 2013). The objective is to test whether two distributions are equal in location, that is, whether the data distribution (observed and estimated) has the same median, in this case, the medians of the extreme values were evaluated. To apply the Wilcoxon-Mann-Whitney test, it is assumed that  $F$  and  $G$  are the distribution functions corresponding to the observed and estimated data, and the null hypothesis states that the distributions are equal,  $H_0 : F(X) = G(Y)$ . The test statistic is calculated by the equation below, (MANN; WHITNEY, 1947):

$$U = mn + \frac{m(m+1)}{2} - S_m \quad (4.7)$$

Where  $m$  and  $n$  represent the number of elements in samples  $X$  and  $Y$  respectively; and  $S_m$  denotes the sum of the ranks related to the sample elements  $X$ . To decide whether or not to reject the null hypothesis, the probability of obtaining a test statistic equal to or greater than the value observed in a sample (p-value) is calculated. When p-value is below the desired significance level (5% in the

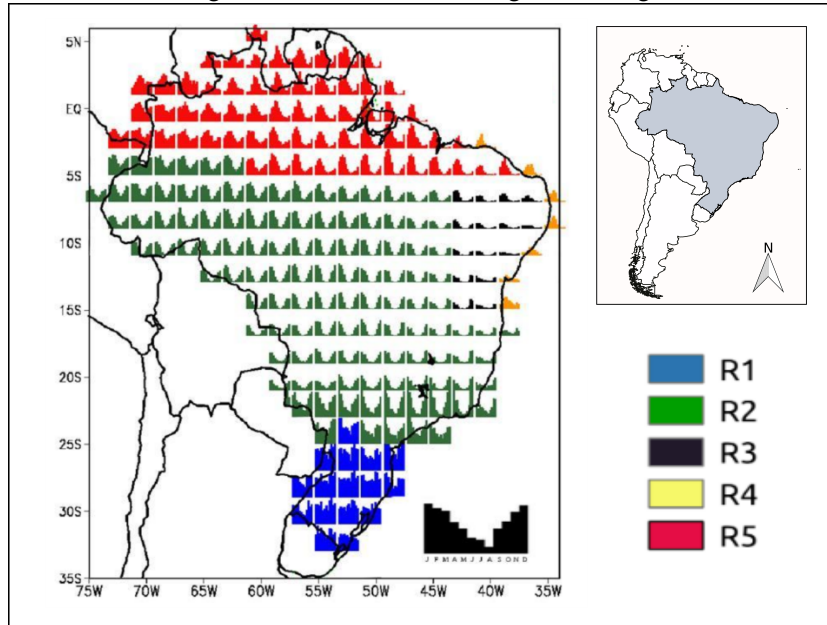
present work), the null hypothesis is rejected.

In order to understand the seasonality of the thresholds of rainfall studied in this research, seasonal ECDF was made. Grouped in every 3 months: austral summer that corresponds to December, January, February (DJF); austral autumn that corresponds to March, April, May (MAM); austral winter I that corresponds to June, July, August (JJA); and austral spring that corresponds September, October, November (SON).

#### **4.2.1 Study area**

Brazil is the biggest country of South America with an area of  $8.514.876 \text{ km}^2$ . This area corresponds to 48% of the continent South American according to the Brazilian Institute of Geography and Statistics (IBGE) data ([INSTITUTO BRASILEIRO DE GEOGRAFIA E ESTATÍSTICA - IBGE, 2010](#)). Due to Brazilian territorial extension, different meteorological systems are observed and have a significant effect on the rains regime in each of regions. In order to find regions with the same precipitation regime in Brazil, [Rozante et al. \(2018\)](#) used a climatology based on merge technique which consists in combines 3B42RT product with surface observations ([ROZANTE et al., 2010](#)). According to the results obtained by [Rozante et al. \(2018\)](#), the seasonal rainfall characteristics may be identified as five regions with distinct rainfall distribution. This regions named, after here, by R1, R2, R3, R4 and R5, are shown in Figure 6.1.

Figure 4.2 - The five regions of Brazil according to homogeneous rainfall regime.



Source: Adapt from Rozante et al. (2018)

The five regions identified by Rozante et al. (2018) were considered in this work in order to investigate extreme precipitation events under different meteorological systems influence and each region is explained in detail below:

The Southern region of Brazil (R1) is usually the stage of intense episodes of precipitation and the orography contributes primarily for these events to occur (MARENGO et al., 2008); (GRIMM; TEDESCHI, 2009); (REBOITA et al., 2010). The topography of the Andes mountain range blocks the low-level winds from the Pacific Ocean and directs the meteorological systems from the Atlantic to the tropical strip of the continent. This topography promote the transport of moisture to the South Region of Brazil. The meteorological systems operating in this region are the frontal systems, cyclones and Mesoscale Convective Systems (MCS) (VELASCO; FRITSCH, 1987); (GRIMM et al., 2000). During the spring and summer the MCS predominate, whereas in the autumn and winter the rains is caused by the frontal systems at mid-latitudes. In addition, during this period, the latitudinal temperature gradient generates baroclinic waves in the west winds in upper air (GRIMM et al., 2000) and the low-level jets stream are moved to the southeast through the Andes acting as an orographic barrier causing cyclogenesis (??).

The Central region of Brazil (R2) encompasses the south of the Amazon re-

gion, the central-west region and the southeastern region of Brazil. These regions have been combined since they presents a homogeneous annual rainfall regime (ROZANTE et al., 2018). R2 is characterized by 6 months of rain during the austral summer followed by 6 months of scanty rainfall in austral winter, the main characteristic of a monsoon region (ZHOU; LAU, 1998); (RAO et al., 2016). According to Neves et al. (2013), the rainy season in this region starts, on average, between mid-October and November due to the gradual increase in the latent heat flow and the decrease in the sensitive heat flow in the same proportion of this period. One of the most common meteorological systems in this region is the South Atlantic Convergence Zone where the flow from the northwest of the Low Level Jets can converge with the circulation of the subtropical high of the south Atlantic and still with the northeast trade winds, resulting in a band of cloudiness and intensification of precipitation in these regions (LENTERS; COOK, 1995); (ROSA et al., 2020).

The Northeastern region of Brazil (R3) is characterized as a semiarid region and presents scarce rainfall and have been affected by long periods of drought (ALTHOFF et al., 2016); (AWANGE et al., 2016). The biome present in this region is the Caatinga. CARVALHO DA COSTA et al. (2007) showed that the Caatinga biome is composed by a wide variety of herbaceous and arborescent vegetation where the prevalence of each component varies a function of climatic and soil factors. According to Köppen's classification developed specifically for Brazil by Alvares et al. (2013), the Caatinga biome presents a high temperature semi-arid climate with low latitude and altitude (BSh). The annual accumulated precipitation in this region does not exceed 500mm in some areas of the semiarid. The main meteorological systems acting in these region are the Inter-tropical Convergence Zone and the Upper Level Cyclonic Vortex (KOUSKY; GAN, 1981). The mean annual rainfall most of which registered from January to May and the rainfall is modulated by stratiform and deep convective precipitating clouds (PALHARINI; VILA, 2017).

The Northeast Coast region of Brazil (R4) presents Atlantic Forest biome that is affected by a tropical wet climate with dry summer (As) according to Köppen's classification (ALVARES et al., 2013). The annual cumulative rainfall is around 1000 mm in coastal, (KOUSKY; CHUG, 1978); (RAO et al., 2016) mostly concentrated from March to July ( 70%) and modulated by shallow convective precipitating clouds (PALHARINI; VILA, 2017). The main meteorological systems acting in this region are Intertropical Convergence Zone, Tropical Mesoscale Convective Systems, the Trade Winds, Upper Level Cyclonic Vortex, Easterly Waves and Sea Breeze Cir-

culatation ( (YAMAZAKI; RAO, 1977); (GOMES et al., 2015) ).

The North region of Brazil (R5) is covered by the Amazon rain-forest. At this region the climate is equatorial, warm and humid throughout the year. The period from November to April constitutes the rainfall season and the total annual rainfall ranges from 2000 to 3000 millimeters (RAO et al., 2016). This region exhibits large variability in rainfall and it is in general associated with El Niño or La Niña. During the years of La Niña the rainfall tends to increase. The mainly meteorological systems acting in this region are Intertropical Convergence Zone (MARENGO; HASTENRATH, 1993), the Tropical Squall Lines (COHEN et al., 1995) and the Trade Winds.

## **4.2.2 Analyzed data**

### **4.2.2.1 Satellite Precipitation Products (SPP)**

Blended techniques, such as the combination of Infrared (IR) with Passive Microwave (PMW) observations were developed to optimally include both estimates have presented performed better than alone (EBERT et al., 2007). In addition, surface information has been considered in order to calibrate this procedure (HUFFMAN et al., 2001); (XU et al., 1999); (MILLER et al., 2001); (KIDD et al., 2003); (SOROOSHIAN et al., 2000); (JOYCE et al., 2004). In doing so, eleven SPPs are analyzed in order to evaluate the performance of theses products for extreme rainfall at different regions of Brazil.

The products were grouped into a single dataset called Frequent Rainfall Observations on GridS (FROGS). FROGS dataset was developed with the objective of placing all products on a single temporal and spatial scale of 1 degree daily by Roca et al. (2019). The dataset was downloaded from the Institut Pierre Laplace Simon (IPSL) repository (<http://dx.doi.org/10.14768/06337394-73A9-407C-9997-0E380DAC5598>). FROGS database is formed by 32 products where the files are produced within NETCDF-4 format and contain information of longitude, latitude, time and rain intensity. In order to perform this investigation, the subset of SPPs from a period ranging from 2012 to 2016 was considered. More information about the product can be found in (ROCA et al., 2019). The Table 6.1 summarizes the information about the products used in the present investigation.

The short name of products from here on they will be called respectively 3B42g, 3B42, CMORPH, CMORPHg, GSMAP, GSMAPg, CHIRP, CHIRPSg,



PERSIANNg, COSCHg and TAPEER where sub-index 'g' represents those versions with gauge correction. The characteristics of SPPs considered in this work are described below:

The 3B42RT is a near-real-time product, also known as TRMM multi-satellite Precipitation Analysis (TMPA) algorithm - Real-Time (HUFFMAN et al., 2007). In this product, IR and PMW information are combined and the historical rain gauge information is incorporated in the calibrated product.

The Global Satellite Mapping of Precipitation (GSMAP) product (KUBOTA et al., 2006) is based on microwave estimation of rainfall. In addition, this product uses IR geostationary imagery to extrapolate the PMW estimates and rain gauges observations are applied to correct for bias.

The Climate Prediction Center morphing technique (CMORPH) (XIE et al., 2017) is a product that combines PMW and IR data to 'morphing' the PMW estimated fields. A bias correction technique, using Climate Prediction Center (CPC) rain gauge analysis (XIE et al., 2003), is applied over land surfaces for V1.0 CRT version.

The Combined Scheme approach (CoSch) (??) is a product that uses Real-Time (TRMM) Multi-satellite Precipitation Analysis (TMPA) algorithm. Rain gauge data from Global Telecommunications System (GTS) and multiple institutions over Latin America is used to remove the bias from TMPA.

The Tropical Amount of Precipitation with an Estimation of ERror (TAPEER) is a product based on GOES precipitation index technique (CHAMBON et al., 2013). This product merges geostationary infrared imagery with microwave instantaneous rain rates estimates.

The Climate Hazards Infrared Precipitation (CHIRP) (FUNK et al., 2015) is a product based on infrared observations from geostationary observations in a GOES. The CHIRPS product is a merge of rain stations information with the CHIRP estimates using a weighted average of the closest stations.

The Precipitation Estimation from Remotely Sensed Information using Artificial Neural Networks - Climate Data Record (PERSIANN-CDR) (ASHOURI et al., 2015) is an infrared-based product that use Neural Networks to obtain the rain rates information.

Table 4.1 - Description table of satellite products .

Satellite product version	Short name	Use rain gauges	Use IR sensor	Use MW sensor
CHIRP v2.0	CHIRP	No	Yes	No
CHIRPS v2.0	CHIRPSg	Yes	Yes	No
PERSIANN CDR v1 r1	PERSIANNg	Yes	Yes	No
3B42 RT v7.0 uncalibrated	3B42	No	Yes	Yes
3B42 RT v7.0	3B42g	Yes	Yes	Yes
GSMAP-NRT-no gauges v6.0	GSMAP	No	Yes	Yes
GSMAP-NRT-gauges v6.0	GSMAPg	Yes	Yes	Yes
CMORPH V1.0, RAW	CMORPH	No	Yes	Yes
CMORPH V1.0, CRT	CMORPHg	Yes	Yes	Yes
TAPEER v1.5	TAPEER	No	Yes	Yes
COSCH	COSCHg	Yes	Yes	Yes

Source: Adapted from [Roca et al. \(2019\)](#).

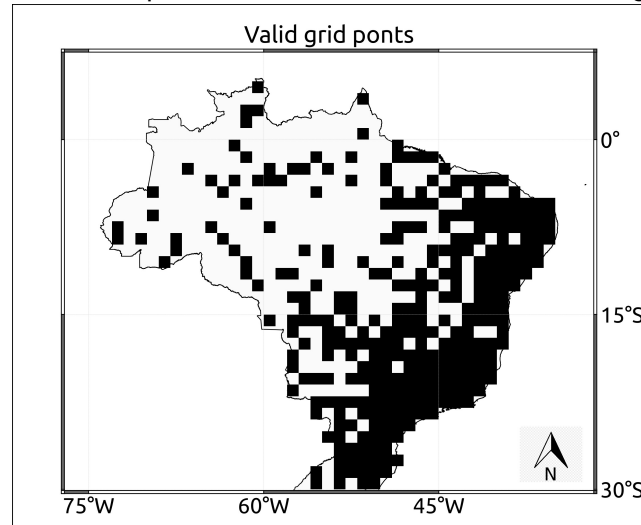
#### 4.2.2.2 Rainfall ground-based data

In this study, information from automatic and conventional rain gauges stations from different networks in Brazil was considered as reference data. The National Center for Space Research (INPE) is the institute responsible for receiving information from different agencies such as from National Institute of Meteorology (INMET), National Water Agency (ANA), Energetic Company of Minas Gerais (CEMIG), Agronomic Institute (IAC), Meteorological System of Paraná (SIMEPAR) among others and organize these information in a single database ([COSTA et al., 2017](#)).

INPE rainfall database is used hereafter as the reference data to validate the satellite analysis of precipitation estimates for different products. In order to ensure the data quality, INPE performs an automatic data quality control that considers 4 steps: (i) range test, which seeks to eliminate gross errors outside the confidence interval, (ii) step test, which considers a maximum difference value between consecutive values; (iii) internal consistency, which makes an association between different meteorological parameters; (iv) persistence test to identify the variability of measurements over a long period of time ([COSTA et al., 2017](#)).

This database of daily rainfall is in DAT format and has been interpolated for regular  $1^{\circ} \times 1^{\circ}$  grids using the simple average and converted to NETCDF format to ensure the consistency in spatial and temporal resolutions for inter-comparisons. In order to consider only the grid points representative for the entire time series period, only 10% of the missing data was allowed for each grid point. Figure 4.3 shows 317 valid grid points over the Brazilian territory.

Figure 4.3 - Grid points with more than 90% of rain gauges data in the temporal series for 2012 to 2016 period of INPE dataset with 317 valid grid points.



Source: Author's production.

### 4.3 Results and discussion

This section has noticed the behaviour of extreme rainfall over different regions of Brazil using statistical metrics. Also was evaluated eleven different satellite precipitation products in the relation to the capability to detect extreme rainfall in these regions of Brazil.

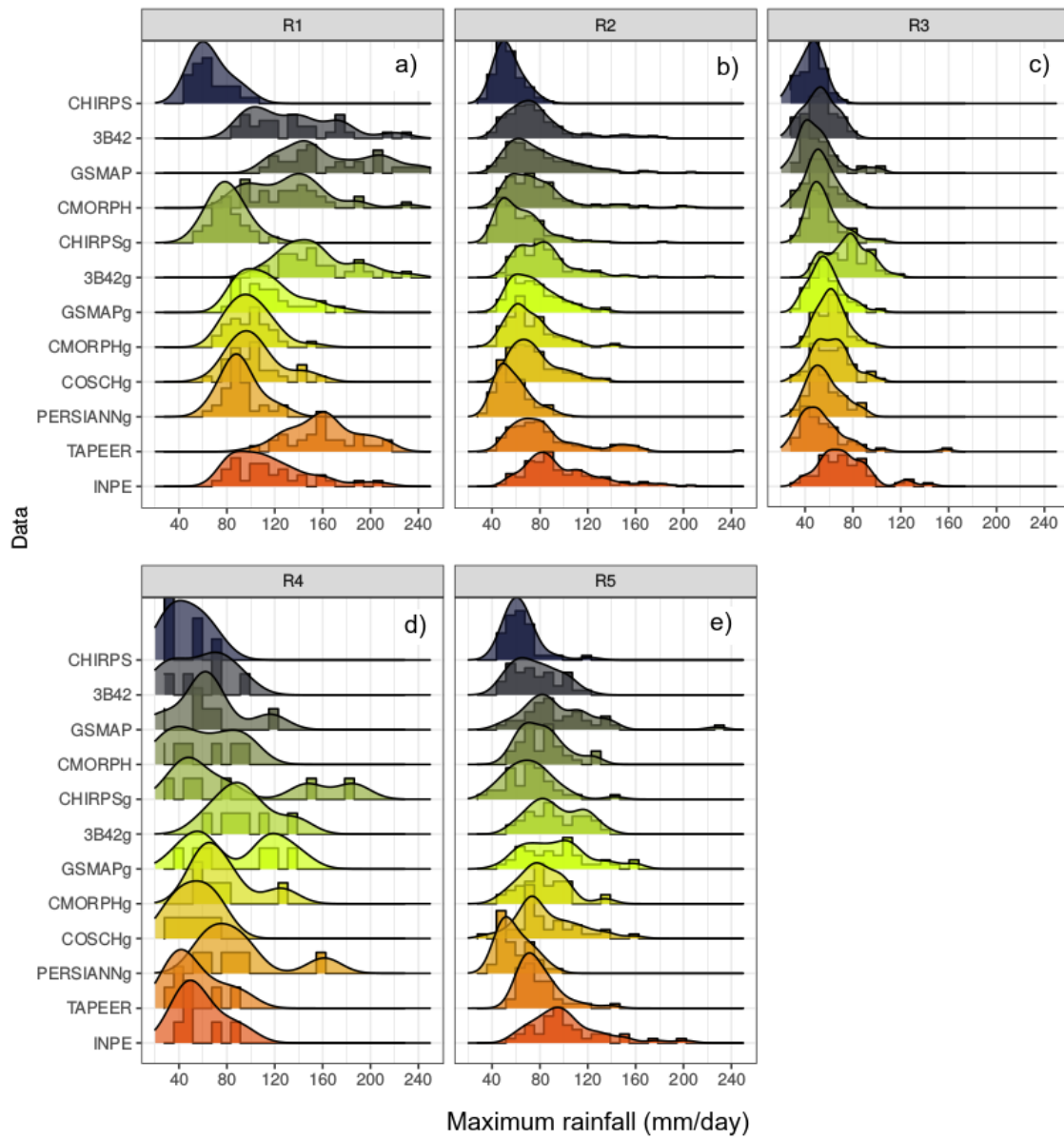
Figure 4.4 shows the frequency of maximum rainfall using the Probability Distribution Function (PDF) of satellite products over the 5 regions of Brazil. According to this plot, each region has a different range for the most frequent maximum rain values. The most frequent maximum values in the reference data (INPE product) are around: R1 = 100 mm/day; R2 = 85 mm/day; R3 = 70 mm/day; R4 = 50 mm/day; R5 = 100 mm/day. In general, the satellite estimates tend to overestimate at R1 and R4 while underestimate for the other regions, as seen in the Figure 4.4.

The same behaviour is noticed in Figure 4.5 considering P99th. However, the magnitude of rainfall is less than the maximum values. Analyzing the conditional P99th values, it was observed that the most frequent extreme values for each region considering the INPE reference database are approximately: R1 = 70 mm/day; R2 = 60 mm/day; R3 = 40 mm/day; R4 = 35 mm/day; R5 = 65 mm/day. By the fact that Brazil has continental dimensions covering different latitudes

and with different forms of relief, the development of different atmospheric systems occurs, such as Inter-tropical Convergence Zone; Upper Level Cyclonic Vortex; Trade Winds; Easterly Waves; Sea Breeze Circulation, South Atlantic Convergence Zone; Cold Fronts; Squall Lines and Mesoscale Convective Systems. These systems contribute to the rainfall inhomogeneity between the regions.

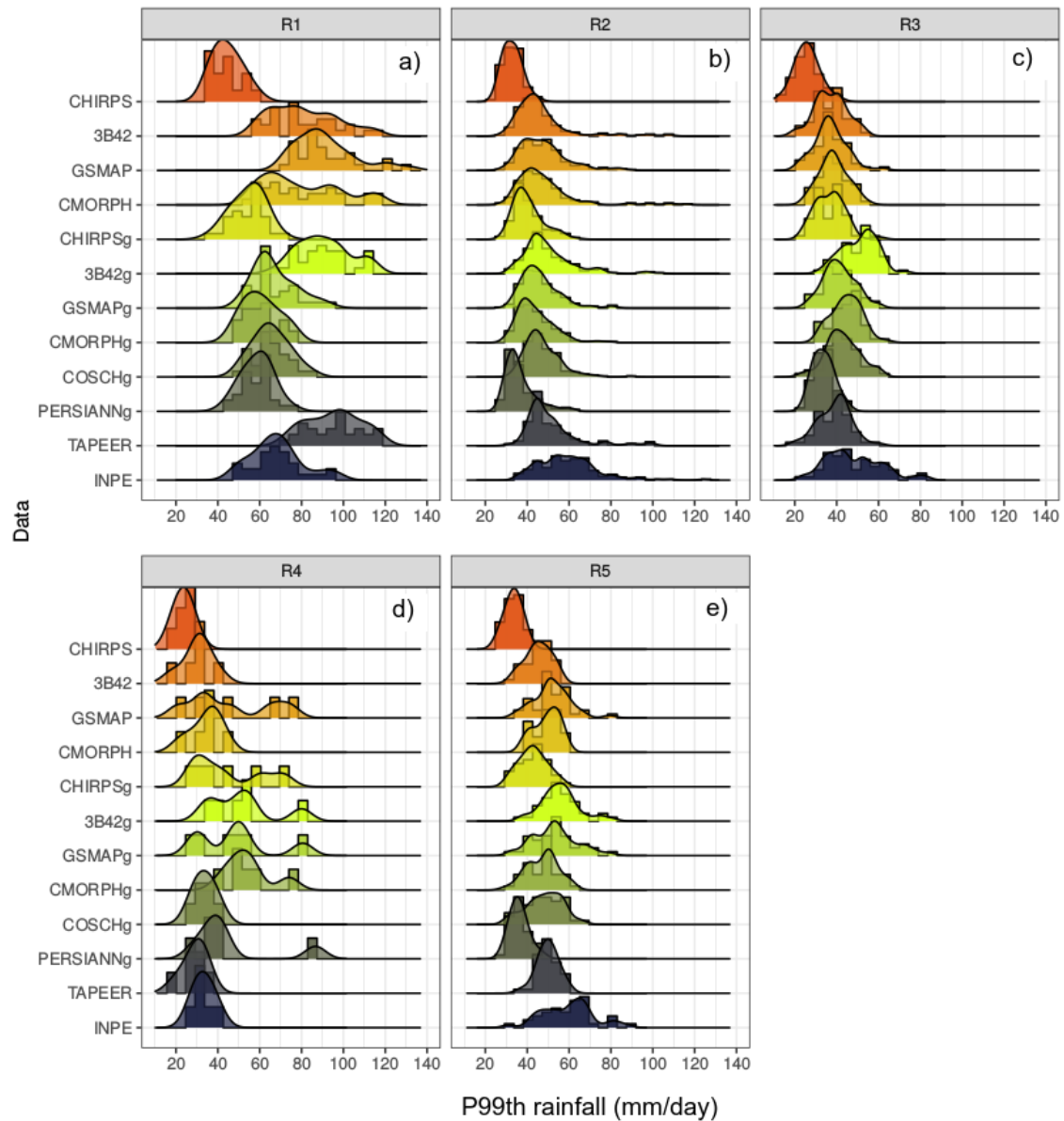
In this scenario, it is possible to identify that all regions presented extremes of rain during the period considered. Nonetheless, the extremes with greater intensities are more frequent in the regions R1 and R5 and do not necessarily cause disasters or generate impacts in these regions. These events are considered to be extreme from a statistical point of view and they are based on the database analysis. This shows us that the occurrence or not of natural disasters caused by rain is more related to the region's vulnerability than just the accumulated value of rain (RODRIGUES et al., 2020). Disasters are the materialization of hazard and are defined as a physical phenomenon or a potentially harmful natural process, which can cause serious socio-economic damage to exposed communities (TOBIN, 1997); (ISDR, 2004).

Figure 4.4 - PDF of Maximum rainfall [mm/day] from satellite products for five regions in Brazil: Southern Brazil (R1); Central Region (R2); Northeastern (R3); North-east Coast (R4); North Brazil (R5).



Source: Author's production.

Figure 4.5 - PDF of P99th rainfall [mm/day] from satellite products for five regions in Brazil: (a) Southern Brazil-R1; (b) Central Region-R2; (c) Northeastern-R3; (d) Northeast Coast-R4; (e) North Brazil-R5.



Source: Author's production.

#### 4.3.1 Southern Brazil - R1

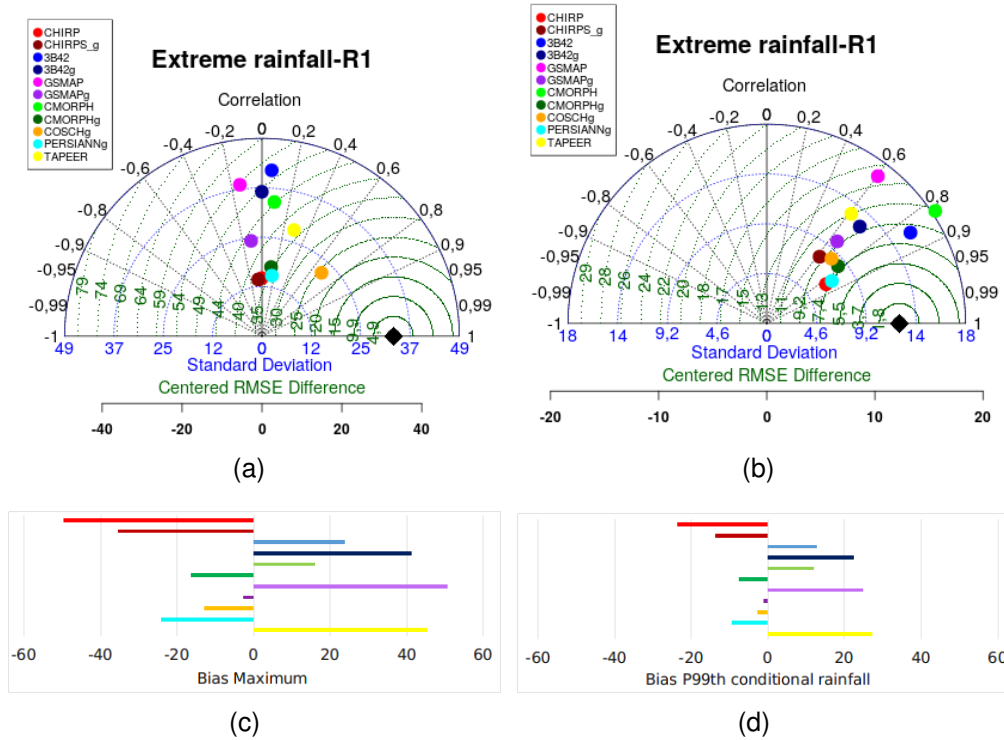
In the Taylor diagram for the maximum rainfall values, Figure 4.6-a, it was observed that the satellite estimation products have a correlation of less than 0.6 when compared with the observed data. A high dispersion of data is found when

the products have an STD ranging from 12.0 to 25.0 mm/day and RMSE ranging from 25.0 to 44.0 mm/day. As shown in the Taylor diagram, Figure 4.6-b, the 99th percentile values presented a correlation of greater than 0.6 when compared with the observed data, an STD of approximately 9.0 mm/day, and RMSE between 7.0 and 10.0 mm/day. Analyzing the bias, Figure 4.6 [c-d], it was noticed that half of the studied products underestimate the extreme rainfall while the other half overestimate it for R1.

According to the Wilcoxon-Mann-Whitney test, the distributions of the maximum and P99th precipitation values estimated by the GSMAPg, COSCHg and CMORPHg products were statistically equivalent to the distribution of the precipitation values from the reference database, i.e,  $p\text{-value} > 0.05$ . The data distributions estimated by the GSMAPg, COSCHg and CMORPHg products had medians of 108.2, 99.6 and 99.4 mm/day, respectively. It was observed that the reference dataset and the median of the data distribution have similar values of 108.2 mm/day. The statistical test confirms that these three products are the ones that present the best performance for R1 as seen in the Taylor diagram. On average, the products with the smallest biases were GSMAPg, COSCHg and CMORPHg (Figure 4.6 [c-d] ) showing a bias of -5.0, -15.0 and -18.0 mm/day respectively for maximum values and -2.0, -5.0 and -10.0 mm/day for P99th.

In order to understand in more details the behaviour of the threshold of rain, a seasonal analyse was made. Figure 4.7 [a-b] shows the R1 seasonal ECDF for maximum values and rainfall above P99th threshold, respectively. According to this figure, it was observed that the products GSMAPg, COSCHg and CMORPHg have a better agreement when compared with the reference data. In addition, these products perform better during the summer austral months (DJF), i.e, they are able to capture the extremes that occurred during the DJF period.

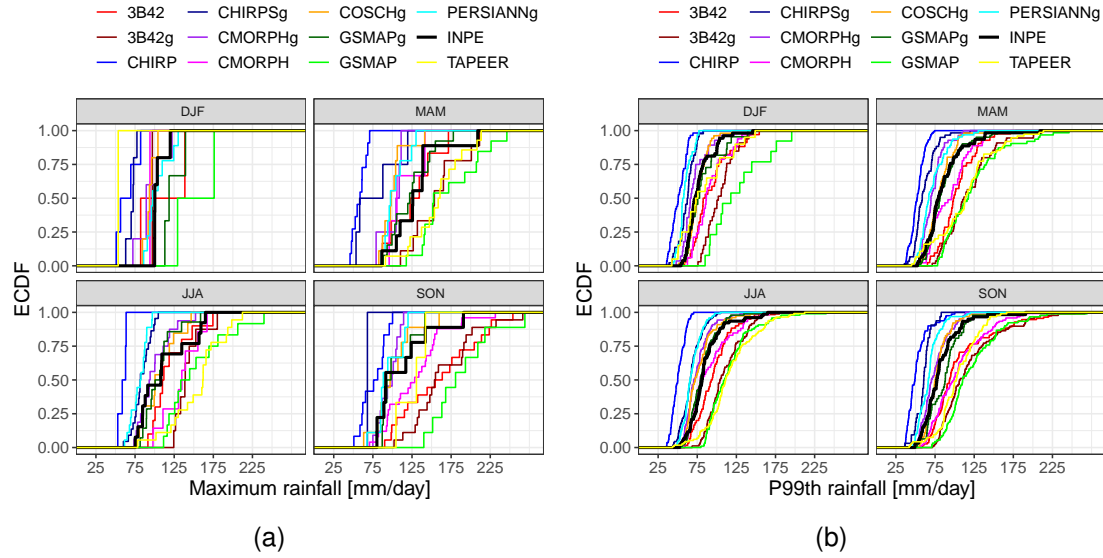
Figure 4.6 - Statistical comparison between gridded rain gauge data (INPE) and satellite-derived rainfall products over a period of 5 years (2012-2016): Taylor Diagram of Maximum (a), P99th rainfall (b), bias bars of Maximum (c), and P99th rainfall (d). RMSE is represented by green curved lines, STD is represented by blue curved lines and  $r$  is represented by black straight lines.



Source: Author's production.



Figure 4.7 - Seasonal empirical cumulative distribution function of (a) maximum rainfall and (b) extreme rainfall above P99th threshold [mm/day] of satellite products from R1 - Southern Brazil - 31 grid points.



Source: Author's production.

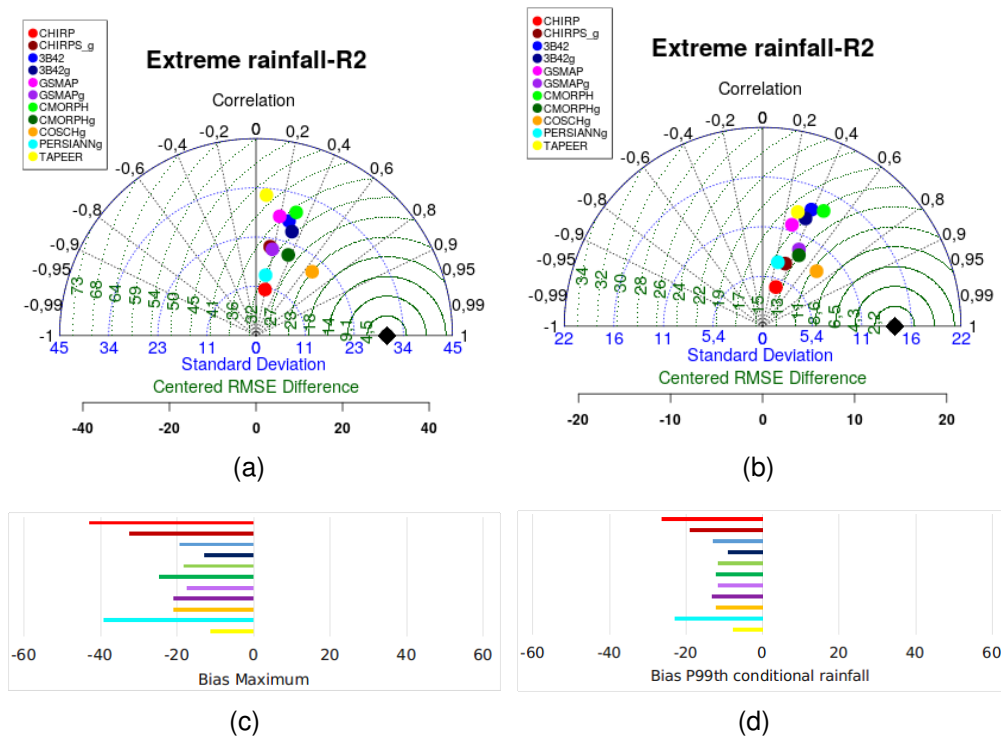
#### 4.3.2 Central Region - R2

Analyzing the bias for R2, Figure 4.8[c-d], it is noticed that all of the studied products underestimate the extreme rainfall values for maximum values and P99th values. The majority of products have a bias up to -20.0 mm/day, with the exception of CHIRPS and PERSIANN that exceed that value. The metrics for maximum and P99th thresholds showed similar behaviors with a correlation ranging from 0.6 to 0.1. This results contrast with those found for R1, where the estimates showed correlations greater than 0.6 for p99th threshold.

At R2 region, several products have similar metrics. As shown in Figure 4.8 in the Taylor diagram, the products with the smallest biases were TAPEER, 3B42g and CMORPH with -7.82, -9.11 and -11.69 mm/day for maximum values and -11.43, -12.82 and -18.27 mm/day for P99th. In doing so, these 3 products were considered to have the the best performance for this region. However, according to the Wilcoxon-Mann-Whitney test, the distributions of the maximum and P99th precipitation values estimated by the TAPEER product was the only one statistically equivalent to the distribution of the dataset precipitation values and obtained p-value > 0.05.

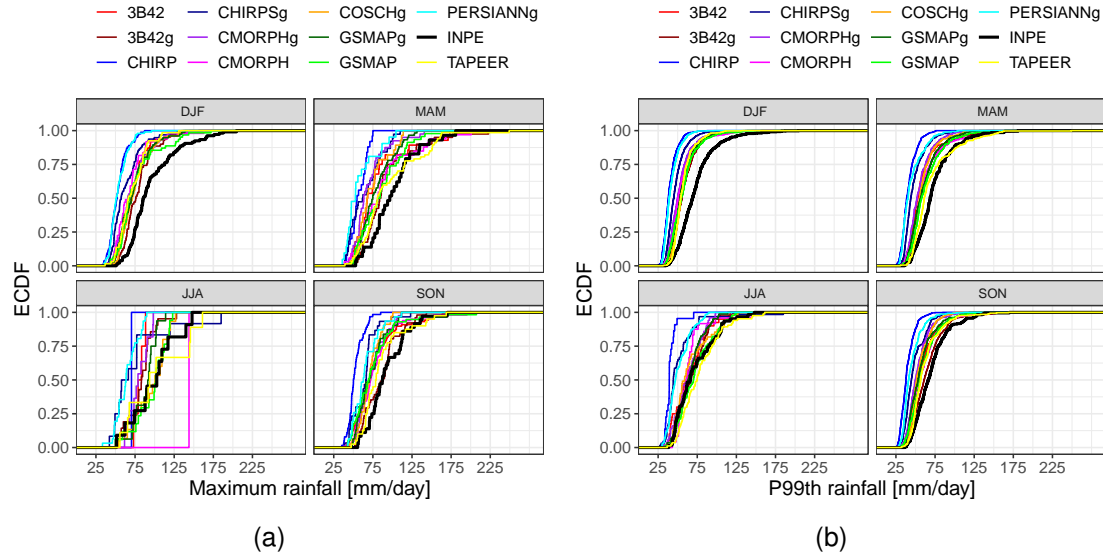
In order to understand in more details the behaviour of the threshold of rain, a seasonal analyse was made. Figure 4.9 [a-b] shows the seasonal ECDF at R2 for maximum values of rainfall and for values of rainfall above P99th threshold, respectively. In this region, the rainy season starts, on average, between mid-October and November and remains during the summer (NEVES et al., 2013). It is observed that in these months (SON and DJF) the products have a good agreement with each other, however in DJF where the most intense rains generally occur, the products tend to distance themselves from the reference curve (in black), thus underestimating the most intense values.

Figure 4.8 - Statistical comparison between gridded rain gauge data and satellite-derived rainfall products over a period of 5 years (2012-2016): Taylor Diagram of Maximum (a), P99th rainfall (b), bias bars of Maximum (c), and P99th rainfall (d). RMSE is represented by green curved lines, STD is represented by blue curved lines and  $r$  is represented by black straight lines.



Source: Author's production.

Figure 4.9 - Seasonal empirical cumulative distribution function of (a) maximum rainfall and (b) extreme rainfall above P99th threshold [mm/day] of satellite products from R2 - Central Region- 171 grid points.



Source: Author's production.

#### 4.3.3 Northeastern - R3

Figures 4.10 [a-b] presents the Taylor diagram for R3 regions. It is noticed from these plots, that the estimates show a correlation less than 0.6 for all estimation products at both the maximum and P99th thresholds. This results are similar to those found for R2 region. In addition, the STD varied from 8.5 and 25.0 mm/day and from 5.0 to 10.0 mm/day for maximum values and P99th values, respectively.

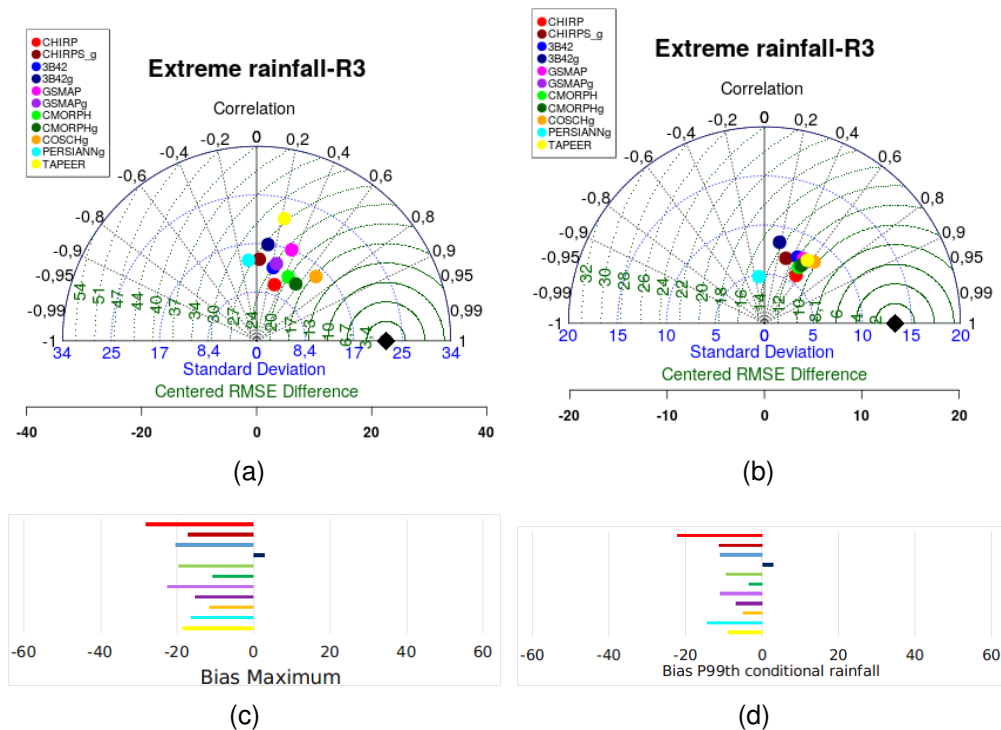
Analyzing the bias, Figures 4.10 [c-d], it is observed that most of precipitation estimation products underestimate the extreme rainfall at this region. However, the product 3B42g overestimated the precipitation. Similar results were found by the work conducted by [Rozante et al. \(2018\)](#), the authors compared the precipitation estimates of 3B42RT real time version with the 3B42 final version. According to this work, 3B42 final version product overestimate the precipitation in the wet season of this region.

Several products presented similar metrics at this region and, for the period investigated, the products 3B42g, CMORPHg and COSCHg showed the smallest bias with 2.82, -3.48 and -5.25 mm/day from maximum values and 2.92, -10.65 and -11.48 mm/day from P99th respectively. According to the Wilcoxon-Mann-Whitney

test, the distributions of the maximum and P99th precipitation values estimated by the 3B42g and CMORPHg product were statistically equivalent to the distribution of the precipitation values when compared with the reference database (INPE product).

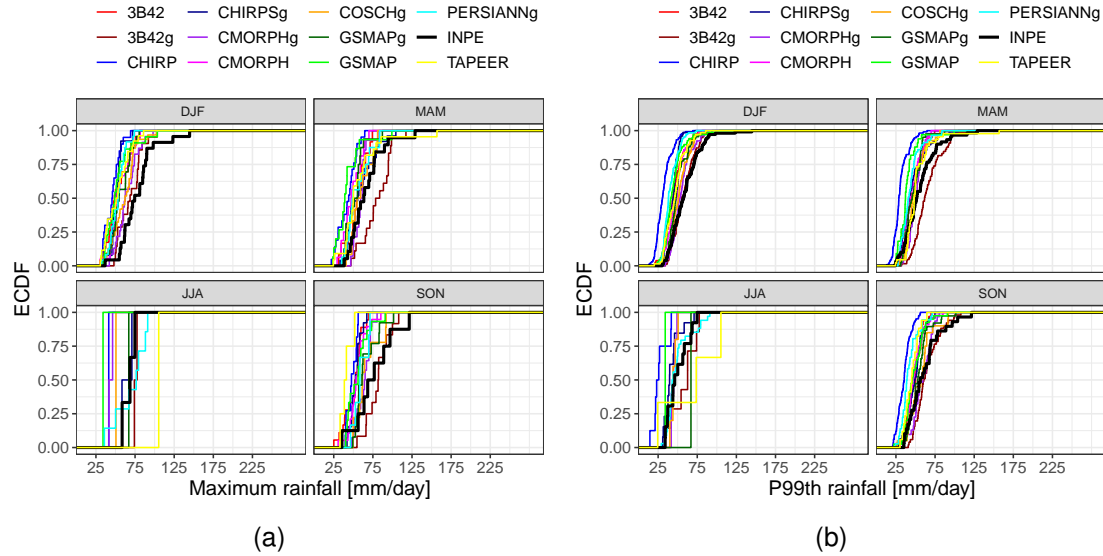
In order to understand in more details the behaviour of the threshold of rain, a seasonal analyse was made. Figure 4.11 [a-b] shows the seasonal ECDF for maximum values of rainfall and for values of rainfall above P99th threshold at R3 region. According to the results, the products 3B42g, CMORPHg and COSCHg presented a good agreement with the reference data. In addition, it was noticed that the product CMORPHg presented a good performance at this region for most of the months of the year. At June, due to scarce data available, all products present a poor performance.

Figure 4.10 - Statistical comparison between gridded rain gauge data and satellite-derived rainfall products over a period of 5 years (2012-2016): Taylor Diagram of Maximum (a), P99th rainfall (b), bias bars of Maximum (c), and P99th rainfall (d). RMSE is represented by green curved lines, STD is represented by blue curved lines and  $r$  is represented by black straight lines.



Source: Author's production.

Figure 4.11 - Seasonal empirical cumulative distribution function of (a) maximum rainfall and (b) extreme rainfall above P99th threshold [mm/day] of satellite products from R3 - Northeastern - 53 grid points.



Source: Author's production.

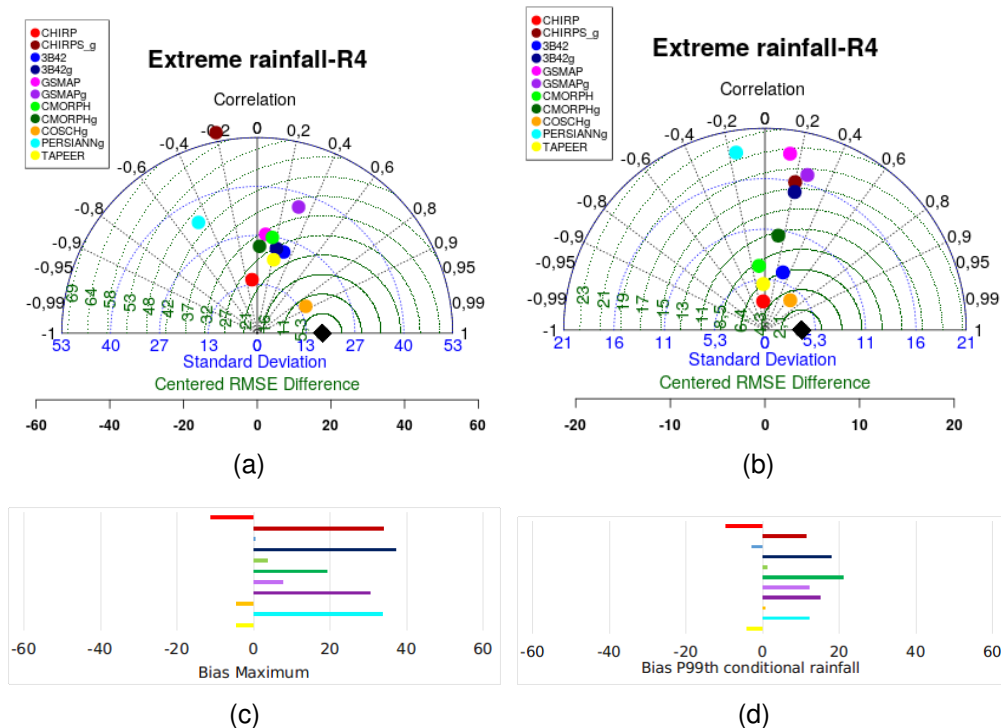
#### 4.3.4 Northeast Coast - R4

The Figure 4.12 shows that the R4 region is the only one where most products overestimate extreme rainfall. However, it was observed that the products COSCHg, TAPEER and CHIRP, underestimated the maximum values ( -4.68, -4.65 and -11.24, mm/day respectively) and 3B42, TAPEER and CHIRP products underestimated the P99th values(-2.94, -9.81 and -4.34 mm/day respectively ). Among the regions studied in this research, R4 presented the lowest correlation between the estimated data and the observed data ( $r < 0.4$ ). The low correlations is caused by the small number of valid points which are used to in the statistic metrics. Due to the small number of points, it was not possible to apply the Wilcoxon-Mann-Whitney test at this region. In addition, it is noticed at R4 that the 3B42, CMORPH and COSCHg products presented the smallest bias (0.14, 3.75 and -4.68 mm/day) among the analyzed products.

In order to understand in more details the behaviour of the threshold of rain, a seasonal analyse was made. Figure 4.13 [a-b] shows the seasonal ECDF for maximum values of rainfall and for values of rainfall above of P99th threshold at R4 region. In this region, the rainfall occurs with more frequency from March to

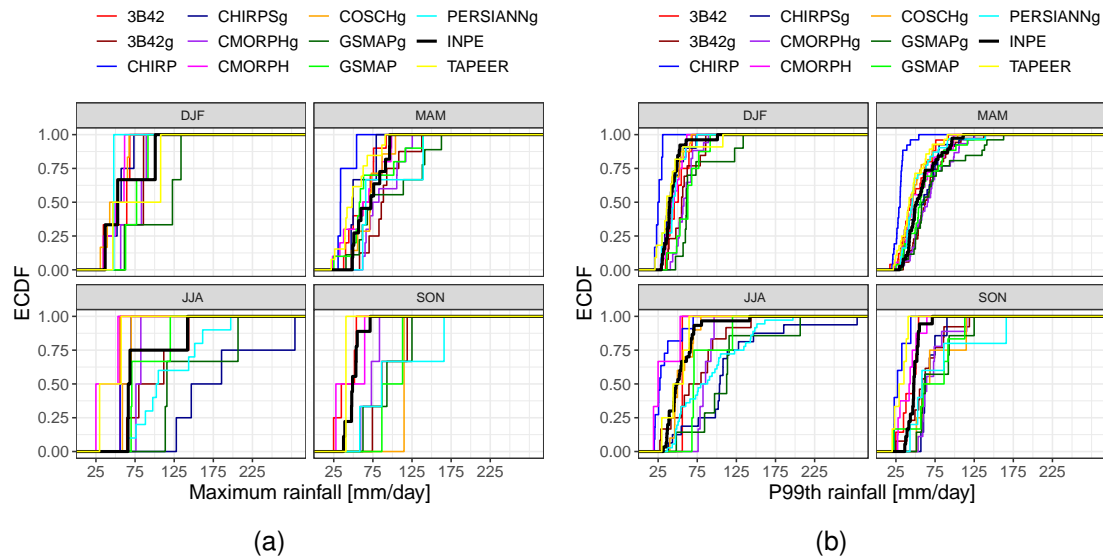
July (DINIZ et al., 2018). In the rainy season, the satellite products tend to similar behaviour between them; however at the dry season, these products there is no concordance between them where some overestimate and others underestimate the rain values. The products that have a distribution closer to the reference data are TAPEER, CHIRPSg, PERSIANN and COSCHg during DJF, but this is not the rainy season in this region. During the dry season, the events of rain in the R4 is rare, the number of grid points is small and maybe no make sense to do the inter-comparisons between the products. During MAM when the rainy season begins, the CMORPH and GSMAP without rain gauges adjustments performer better. During JJA when the rainy season ends, the COSCHg and TAPEER performer better.

Figure 4.12 - Statistical comparison between gridded rain gauge data and satellite-derived rainfall products over a period of 5 years (2012-2016): Taylor Diagram of Maximum (a), P99th rainfall (b), bias bars of Maximum (c), and P99th rainfall (d). RMSE is represented by green curved lines, STD is represented by blue curved lines and  $r$  is represented by black straight lines.



Source: Author's production.

Figure 4.13 - Seasonal empirical cumulative distribution function of (a) maximum rainfall and (b) extreme rainfall above P99th threshold [mm/day] of satellite products from R4 - Northeast Coast - 6 grid points.



Source: Author's production.

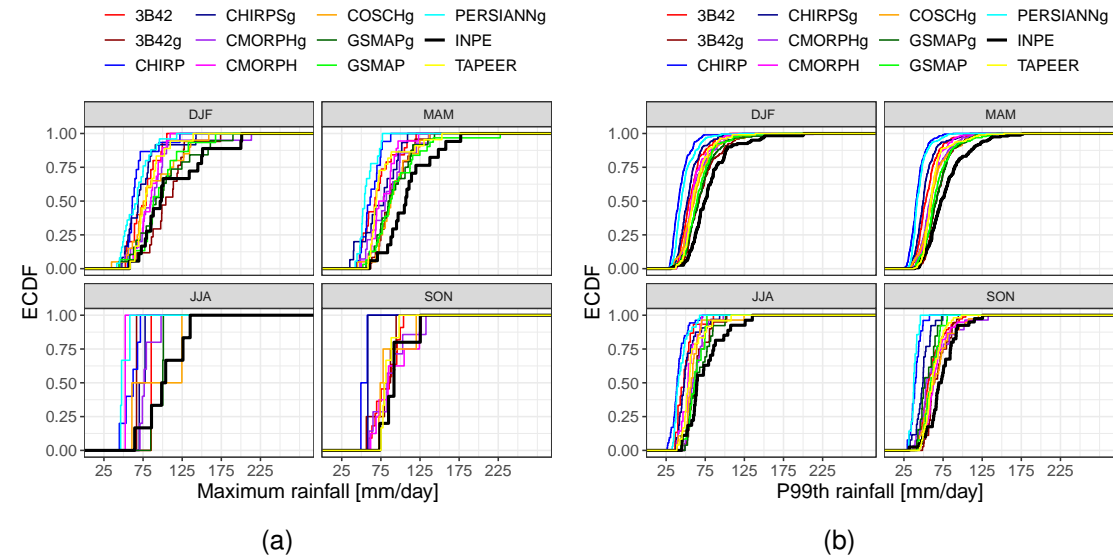
#### 4.3.5 North Brazil - R5

Analyzing the Taylor diagram, Figure 4.15, it is observed that on average, the products with the largest bias were CHIRP and PERSIANN and the products with smallest biases were 3B42g, GSMAP and GSMAPg ( -9.09, -6.90 and -8.27 mm/day for maximum values and -3.79, -7.54 and -6.48 mm/day for P99th respectively). According to the Wilcoxon-Mann-Whitney test, the distributions of the maximum and P99th precipitation values estimated by the 3B42g, GSMAP and GSMAPg products were statistically equivalent to the distribution of the precipitation values observed when compared with the reference database (INPE product).

In order to understand in more details the behaviour of the threshold of rain, a seasonal analyse was made. Figure 4.14 [a-b] shows the seasonal ECDF for maximum values of rainfall and for conditional P99th threshold of rainfall at R5 region. According to [Diniz et al. \(2018\)](#), the mean annual rainfall at this region occurs mainly from December to May ([DINIZ et al., 2018](#)). In this region, all products estimated by satellite tend to underestimate the extreme values of rain, both for the maximum values and for the values rainfall above of P99th threshold in all

seasons, presenting similar behaviors between them. The products that have a ECDF closer to the reference data are 3B42g, GSMAP and GSMAPg. In this way different analyzes indicate that these products are the ones that present a better performance for estimating extremes of rain in this region.

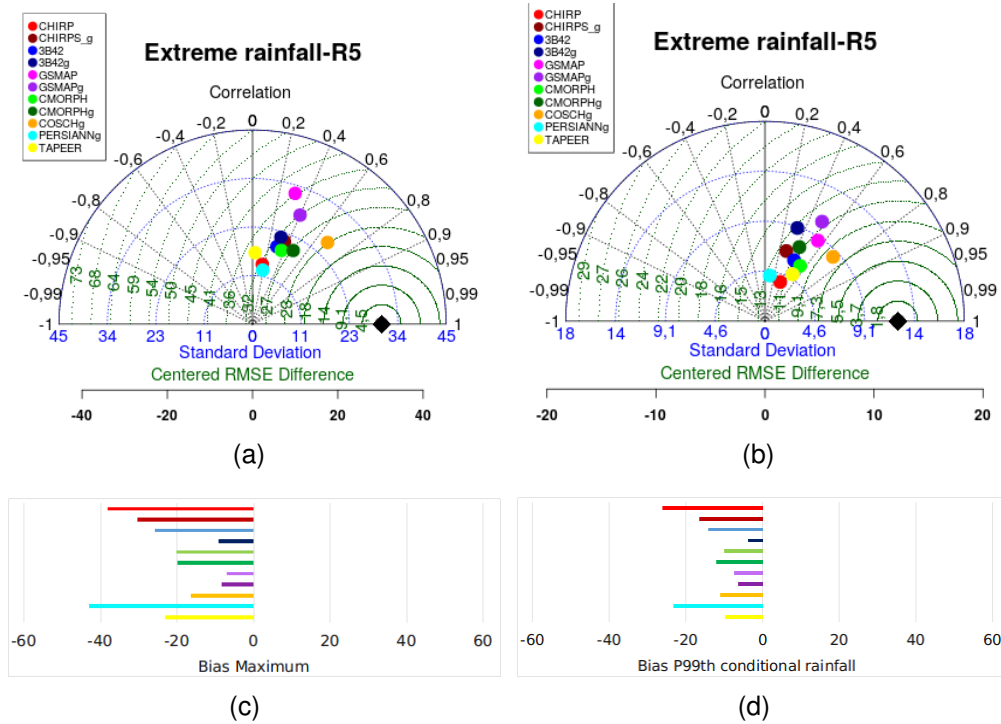
Figure 4.14 - Seasonal empirical cumulative distribution function of (a) maximum rainfall and (b) extreme rainfall above P99th threshold [mm/day] of satellite products from R5 - North Brazil- 39 grid points.



Source: Author's production.



Figure 4.15 - Statistical comparison between gridded rain gauge data and satellite-derived rainfall products over a period of 5 years (2012-2016): Taylor Diagram of Maximum (a), P99th rainfall (b), bias bars of Maximum (c), and P99th rainfall (d). RMSE is represented by green curved lines, STD is represented by blue curved lines and  $r$  is represented by black straight lines.



Source: Author's production.

#### 4.4 Conclusions

The main objective of this study was to evaluate a large number of Satellite Precipitation Products (SPP) and identify their capacity to detect extreme precipitation events. The comparison between extreme precipitation values of 11 different satellite products and rain gauge data was carried out for different regions of Brazil. The SPPs evaluated were CHIRP v2.0, CHIRPS v2.0, 3B42 RT v7.0 uncalibrated, 3B42 RT v7.0, GSMAP-NRT-no gauges v6.0, GSMAP-NRT-gauges v6.0, CMORPH v1.0 RAW, CMORPH v1.0 CRT, PERSIANN CDR, CoSch, and TAPEER v1.5, using data from the rain gauges of the INPE database as the reference. Similar to [Palharini et al. \(2020\)](#) precipitation extremes were defined by maximum values and the 99th percentile threshold in a daily  $1^\circ \times 1^\circ$  grid for the period from 2012 to 2016 and the ability of the satellite-based precipitation products to detect extreme precipitation was analyzed using statistical metrics.

An important characteristic of SPPs that must be considered is that these estimates tend to underestimate or overestimate rainfall mean values, as has been studied by some previous studies (HUFFMAN et al., 2001); (XU et al., 1999); (MILLER et al., 2001); (KIDD et al., 2003); (SOROOSHIAN et al., 2000); (JOYCE et al., 2004). The same occurs when talking about extreme rains, such as results found by Jiang et al. (2019) which shows on eastern coastal areas of China that satellite estimates tend to underestimate extreme rain values, as also Palharini et al. (2020) found that satellite estimates tend to underestimate extreme rainfall over South America.

However, these tendencies of overestimation or underestimation can vary from region to region. Especially when observed in smaller regions with specific characteristics of relief and land cover, as their effects influence the radiation, thermodynamics and the physics of clouds in each region. And also the meteorological systems of each region, which are different. These aspects consequently influence the response of the satellite sensors to capture the precipitation that occurred in the region. Considering that these sensors monitor the energy emissions of Earth captured in the infrared and microwave. These emissions generally correspond physically to the location and intensity of precipitation (FUNK et al., 2015).

In this work it was found that SPPs generally tend to underestimate the extreme values of rain in the regions R2-Central Region, R3-Northeastern and R5-North Brazil, while the region R4-Northeast Coast estimates tend to overestimate extreme rainfall. In the R1-Southern Brazil, there is a divergence of results between the products analyzed, where some tend to overestimate and others to underestimate. Thus, even though regions located within South America do not follow the same behavior of South America in general, that tend to underestimate (PALHARINI et al., 2020).

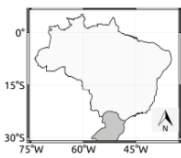
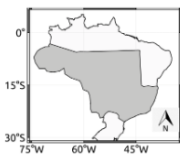
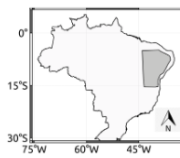
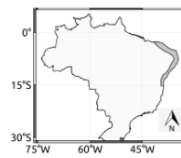
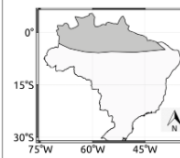
The main findings of this study reveal that each region of Brazil is characterized by extremes of rain with different intensities. The regions with the highest values are R1 and R5 around 125mm/day and the regions with the lowest intensities are R3 and R4 around the 35mm/day. However, these rainfall values do not necessarily cause natural disasters or generate impacts in these regions, they are considered to be extreme from a statistical point of view, considering the analyzed database. With that, it is clear that the same study with a longer series of temporal data can show a more accurate result for each region.

Another interesting result is that GSMAP product with and without rain gauges adjustments perform well in regions R1 and R5, which are the regions in Brazil that record the most intense rainfall values identified as extreme, mainly in the summer months, where the rainy season of these regions are characterized. A similar result was found by [Afonso et al. \(2020\)](#) that evaluating the diurnal precipitation cycle in these regions, also found that the GSMAP product presents a better performance and that this would be related to the fact that in those regions where thermal heating produce deep convective clouds, the diurnal cycle is better represented.

For the other regions, it is observed that other products obtained a better performance, as in the example of the R3-Northeastern region where the products that presented a better performance to detect extremes during the summer and autumn (DJF, MAM) were CMORPHg, COSCHg and 3B42g according to the metrics used that converge to this result. In the R4-Northeast Coast region, it was identified that the COSCHg and CMORPH products performed better during the rainy season (MAM, JJA). In the R2-Central Region, the metrics differ in terms of results, since the Wilcoxon-Mann-Whitney test indicates that the product with the greatest statistical similarity with the reference data is the TAPEER product, the Taylor diagram shows that the TAPEER products, 3B42g and CMORPH have a lower bias.

In general, the summary of products that showed the better performance to detect extreme rainfall that occurred in different regions of Brazil during the period from 2012 to 2016 was presented in [Figure 4.16](#). The present investigation showed that the ability of the satellite estimates depends on the location in which the precipitation events occur. As future work it is intended to analyze specific cases that have been recorded extreme rain and that have caused natural disasters in each of the regions analyzed here, thus identifying the performance of each product in specific events.

Figure 4.16 - Summary table indicating the products that showed a better performance over the different regions of Brazil.

R1	R2	R3	R4	R5
				
GSMAPg COSCHg CMORPHg	TAPEER 3B42g CMORPH	3B42g CMORPHg COSCHg	3B42 CMORPH COSCHg	GSMAP GSMAPg 3B42g

Source: Author´s production.

## 5 Characteristics of Mesoscale Convective Systems and its relation with extreme precipitation over South America using an Eulerian Tracking approach

### 5.1 Introduction

Precipitation is a key component of the hydrological water cycle around the world. It has been paramount to society by providing a source of freshwater and supporting agriculture. However, extreme precipitation may have a significant impact in larger metropolitan regions or small communities. Severe storms can cause flooding and structural damage. According to [Zipser et al. \(2006\)](#), South America is a region among the world's that occur most intense thunderstorms, and these storms can be classified as Mesoscale convective systems (MCS).

The MCS are defined as organized deep convective clouds. These clouds aggregate and interact to induce a large and almost contiguous area of precipitation. They can cover a horizontal range of hundreds to a few thousand kilometers and last for several hours ([ZIPSER, 1981](#); [HOUZE, 2018](#)).

Studies have shown that the timing and location of maximum precipitation across South America are modulated through the exchange tropical heat and moisture via the northerly low-level jet. The low-level jet plays a vital role in the development and maintenance of predominantly nocturnal MCS within the region ([MARENGO et al., 2004](#); [VERA et al., 2006](#); [ZIPSER et al., 2006](#); [SAULO et al., 2007](#)). The variability of MCS structures and spatial organizations, is strongly related to the larger scale meteorological forcing (([HOUZE JUNIOR, 1977](#); [HOUZE JUNIOR et al., 1990](#); [MACHADO; ROSSOW, 1993](#))).

The MCS are commonly analyzed using Lagrangian tracking techniques where the movement of the systems is followed in successive instants. The variation and the life cycle is observed over a time. According to the literature, satellites images can be used to measure the brightness temperature of the top of the cloud and identify the MCS. The first studies used manual tracking technique (i.e., visual inspection of all images to identify the systems ) is labour-intensive and somewhat subjective ([MARTIN; SCHREINER, 1981](#); [VELASCO; FRITSCH, 1987](#); [MILLER; FRITSCH,](#) ). Later studies developed automated techniques to do this tracking, some of the techniques used to detect MCS are described below.

MAximum Spatial Correlation Tracking TEchnique (MASCOTTE) ([CARVALHO;](#)

JONES, 2001) is a fully automated method used to determine the structural properties and evolution of cloud shields from convective systems. The method uses the brightness temperature of the satellite images obtained by the Geostationary Environmental Operational Satellite (GOES-8) based on the technique of maximum spatial correlation.

FORecast and TRAcking of Cloud Cluster (ForTraCC) (VILA et al., 2008) is a cloud cluster detection method based on a threshold temperature of 235 K. This tracking technique is based on MCS overlapping areas in successive images and a forecast module based on the evolution of each particular MCS in previous steps. This feature is based on the MCS's possible displacement, considering the center of the mass position of the cloud cluster in previous time steps, and its size evolution.

Cumulonimbus TRacking And Monitoring (Cb-TRAM) (ZINNER et al., 2008) is based on Meteosat-8 SEVIRI (Spinning Enhanced Visible and Infra-Red Imager) data from the broad band high resolution visible, water vapor(WV) 6.2  $\mu\text{m}$  , and the infrared (IR) 10.8  $\mu\text{m}$  channels. In addition, tropopause temperature data from ECMWF operational model analyses is utilised as an adaptive detection criterion. The tracking is based on geographical overlap between current detection and first guess patterns of cells predicted from preceding time steps.

Rapid Development Thunderstorm (RDT) (AUTONÈS; MOISSELIN, 2013) is an object-oriented diagnostics for convective clouds and it is based on geostationary satellite data. The RDT tracks clouds, identifies those that are convective, and provides some descriptive attributes for their dynamics. The main satellite channel is IR10.8  $\mu\text{m}$  (used for detection, tracking and discrimination). Additionally WV6.2  $\mu\text{m}$ , WV7.3  $\mu\text{m}$ , IR8.7  $\mu\text{m}$ , and IR12.0  $\mu\text{m}$  channels can be used for convective discrimination. RDT software has been developed by Météo-France within the EUMETSAT SAF/NWC (Satellite Application Facility for Nowcasting) framework.

However, the MCS tracking and monitoring technique considered in the present investigation uses the Eulerian approach. This approach is different from previous techniques, as it seeks to understand the behavior of MCS from a grid point and not from their trajectory like other techniques. In this way, it is possible to obtain a spatial and temporal analysis of the morphological characteristics of the MCS.

The MCS tracking and monitoring technique considered in the present investi-

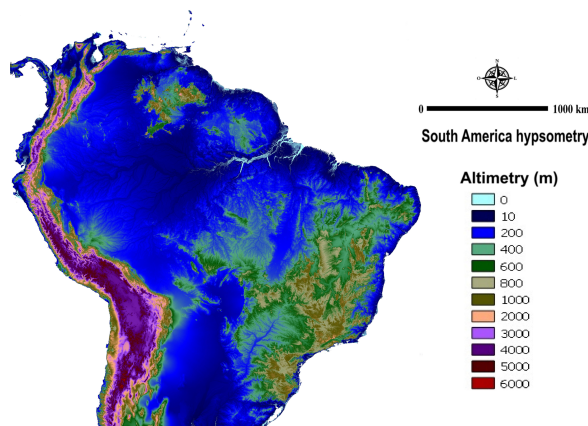
gation is the TOOCAN (Tracking Of Organized Convection Algorithm through 3D segmentationN) algorithm. TOOCAN was developed by (FIOLLEAU; ROCA, 2006) and the MCS tracking is conducted using an Eulerian approach. In this algorithm, a latitude and longitude grid point is fixed, and, in successive instants, the MCS variation is observed in the grid.

The main goal of this work is to describe the morphological characteristics of the MCS using TOOCAN outputs and identify the influence of these systems on extreme rain during the period 2012-2016 in the tropical region of South America.

## 5.2 Study area

South America has an area of about 17.8 million  $km^2$ , contains 6% of the world's population, and is divided into 12 countries. The topographic characteristics in the region can be seen in Figure 5.1. The area analyzed in this investigation is contained in the coordinates from 30°S to 15°N and from 90°W to 30°W, corresponding to the tropical region of South America. In this work, a period of five years, ranging from 2012 to 2016, is considered for analysis.

Figure 5.1 - Topography map of South America.



Source : Adapt from Base MDE SRTM corrigido  
Lab. de métricas da Paisagem -MEPA (UFRR)

## 5.3 Datasets

### 5.3.1 Mesoscale convective systems dataset

In order to analyse the characteristics of MCS over South America, the outputs of TOOCAN algorithm is used in the present investigation.

Developed by [Fiolleau and Roca \(2013\)](#), the TOOCAN use a 3-dimensional segmentation algorithm to detect and tracking of tropical Mesoscale Convective Systems from infrared images of a geostationary satellite. This algorithm works in a time sequence of infrared images to identify and track MCS in a single 3-D (spatial+time) segmentation step and detect the convective cores within a cold cloud shield defined at brightness temperature (Tb) less than 235 K (-38 °C). The minimum brightness temperature corresponds to the minimum temperature between all pixels belonging to the top of the same MCS. The algorithm apply an iterative process to detect the spread of convective seeds in segments individual convective systems. A Tb less than 235 K threshold is applied on the IR imagery to delineate the high cold clouds. In addition, pattern recognition techniques and tracking algorithms have been developed since the 1980s to detect and track the MCSs.

The TOOCAN database is a level-2 product available over the entire tropics for the period ranging from 2012 to 2016. It gives access to the integrated morphological parameters of each MCS at each 30 min-step of their life cycles. The TOOCAN database is available over the 5-year period for Eastern-Pacific, America, Africa, India, Western-Pacific. The CACATOES database is a level-3 product derived from the TOOCAN database. It allows the analyzes of MCS over the entire tropical belt by an Eulerian approach. The integrated morphological parameters of each MCS have been projected into a 1°/1day grid and the characteristics of all the MCSs occurring in a given grid point have been sorted according to the area occupied within this grid point. The MCS can be easily identified for a given 1°/1day grid point. The CACATOES database is available for the 5-year period over the whole tropical belt [30°S-30°N] and is composed by 1°/1day global monthly files in NETCDF. (<https://doi.org/10.14768/20191112002.1>)

In this work, the CACATOES dataset is used in order to analyse the characteristics of MCS over South America and to access the influence of MCS on the extreme rain events. The parameters such as a number of events, duration, size, brightness temperature, and eccentricity (ratio of the MCS minor axis to its major



axis) are analysed in this work. Table 5.1 shows these parameters in a detailed manner.

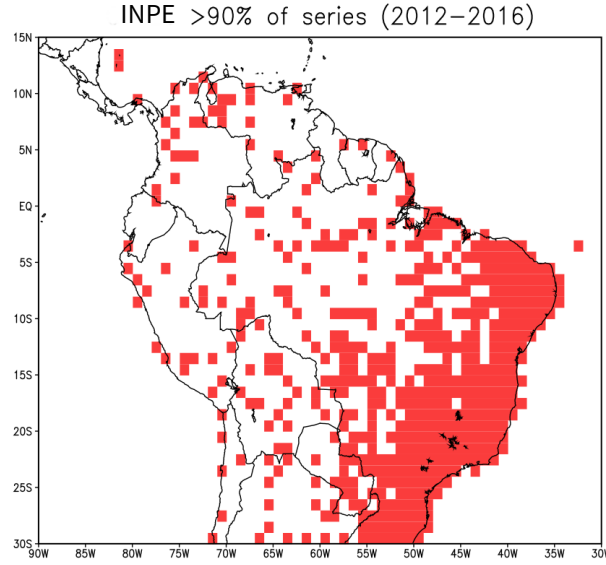
Table 5.1 - Description of parameters from TOOCAN dataset selected for analysis in this work. The dimensions Time and nmaxMCS represent the number of days within a month and the maximum number of MCS within a 1°/1day grid point (set at 25) respectively.

Parameters	Description	Units	Dimensions
Daylymcs_pop	Population of MCSs which are included partially or totally within a 1°/1day grid point	-	Time × lat × lon
Duration	Life time duration	hr	Time × nmaxMCS × lat × lon
Smax	Maximum cold cloud surface reached by the MCS along its life cycle at 235K	km <sup>2</sup>	Time × nmaxMCS × lat × lon
Ecc235K	Eccentricity of the ellipse at a 235K threshold and at Tmax	-	Time × nmaxMCS × lat × lon
Tbmin	Minimum brightness temperature	K	Time × nmaxMCS × lat × lon

### 5.3.2 Rain gauge dataset

The rain gauge database was provided by Brazil's National Center for Space Research (INPE). This contains data from automatic and conventional rain gauges/stations from different networks in South America. This database is in DAT format and has been interpolated for regular 1°x1° grids using the simple average and converted to NETCDF format to ensure the consistency of spatial and temporal for comparison with CACATOES database. To ensure data quality, INPE performs an automatic data quality control that considers four steps: (i) range test, which seeks to eliminate gross errors outside the confidence interval; (ii) step test, which considers a maximum difference between consecutive values; (iii) internal consistency test, which makes an association between different meteorological parameters; and (iv) persistence test, which identifies the variability of measurements over a long period of time (([COSTA et al., 2017](#))). It was considered 345 grid points from the INPE database and Figure 5.2 shows valid grid points over the tropical region of South America territory.

Figure 5.2 - Grid points with more than 90% of rain gauges data in the temporal series for 2012 to 2016 period of INPE dataset with 345 valid grid points.



Source: Author's production.

## 5.4 Methodology

In order to investigate the morphological attributes of MCS over tropical region of South America during 2012-2016 using a Eulerian approach, morphological attributes such as duration, maximum size, number of events occurred by day, eccentricity and minimum brightness temperature of the MCS were analyzed. To compare statistical behavior between these attributes over land and ocean, Probability density function (PDF) and Cumulative distribution function (CDF) plots were generated. In addition, non-parametric kernel method was used to estimate the density curves (WAND; MATT; JONES, 1994); (KUNG, 2014).

Denoted by  $f_x(x)$ , the PDF describes the behavior, in polygonal form, of the frequency distribution of a random variable. In this study, the morphological parameters are represented by  $X$ . The probability (Prob) of the random variable being less than a given value of interest is calculated using the CDF ( $F_x(x)$ ), represented by Equation (5.1):

$$F_x(x) = Prob(X \leq x) = \int_{-\infty}^x f_x(x) dx \quad (5.1)$$

The corresponding PDF can be obtained by differentiating Equation below:

$$f_x(x) = \frac{dF_x(x)}{dx} \quad (5.2)$$

The CDF of a continuous random variable is a non-decreasing function, and the validated expressions are:  $F_x(-\infty)=0$  and  $F_x(+\infty)=1$  ((SHEATHER; JONES, 1991); (SILVERMAN, 1986); (VENABLES; RIPLEY, 2002); (SCOTT, 2015)).

In addition, in order to find a relation between the variables, the probability distribution function bi-dimensional and the Pearson correlation coefficient ( $r$ ) was calculated. The ( $r$ ) refers to the agreement between two variables. The correlation coefficient ranges between  $-1$  and  $+1$ . The value of  $+1$  indicates a perfect positive fit, in other words, a perfect linear correlation. The term positive correlation,  $r > 0$  is applied when the variable represented by x-axis grows and the variable represented by y-axis grows also increases. The term negative correlation when  $r < 0$  is applied when the variable represented by x-axis grow and the variable represented by y-axis decreases.

Where:

$x_i$  is the values of the x-variable in a sample

$y_i$  is the values of the y-variable in a sample

$x^{mean}$  is the mean of the values of the x-variable

$y^{mean}$  is the mean of the values of the y-variable

$$r = \frac{\sum(x_i - x^{mean})(y_i - y^{mean})}{\sqrt{\sum(x_i - x^{mean})^2} \sqrt{\sum(y_i - y^{mean})^2}} \quad (5.3)$$

In order to understand the relation between the accumulated extreme rainfall during 2012-2016 and the extreme rainfall over influence of MCS, analyzes between both variables were made. In this study was considered extreme rainfall, values of rain above percentile 99th.

The contribution of the MCS on the extreme rain was subjectively defined as the ratio between the amount of extreme rain that was influenced by the MCS over the

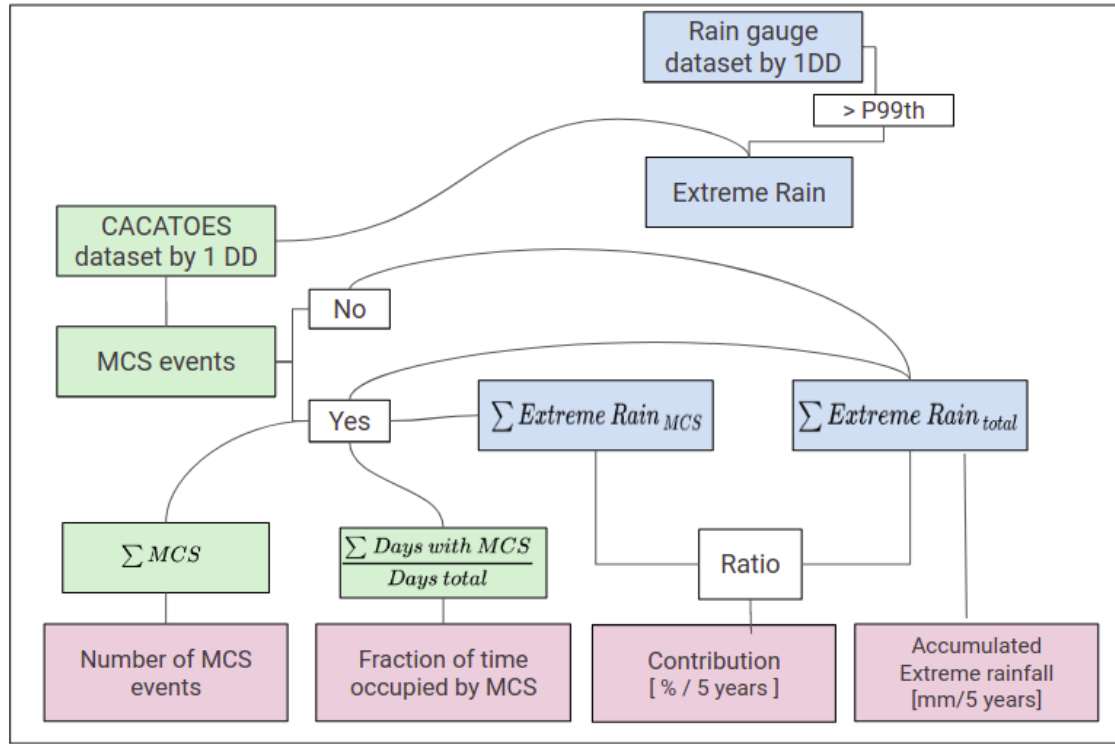
total amount of extreme rain recorded during the period of five years (2012-2016).

For obtain this contribution, that firstly was selected rainfall values above percentile 99th from rain gauges INPE dataset for one daily degree. Secondly, the CACATOES dataset with the population of MCSs within a 1°/1day grid point (Daylymcs\_pop) variable that recorded the MCS events occurred. In the cases that in each grid point were recorded at least one MCS event and a value of extreme rainfall associated, the information of rainfall was accumulated ( $\sum \text{Extreme Rain}_{MCS}$ ). Next, it was accumulated the extreme rainfall for five years at each grid point ( $\sum \text{Extreme Rain}_{total}$ ). Finally, it was obtained the ratio between both information (Figure 5.3). In doing so, the contribution of the MCS on the total extreme rainfall occurred during 2012-2016 is expressed by the following equation:

$$\text{Contribution } [\%/5 \text{ years}] = \frac{\sum \text{Extreme Rain}_{MCS}}{\sum_{1 \text{ day}}^{5 \text{ years}} \text{Extreme Rain}_{total}} * 100 \quad (5.4)$$

where the  $\text{Extreme Rain}_{MCS}$  represents the rain recorded at 1 daily degree for each grid point when MCS registered and  $\text{Extreme Rain}_{total}$  is the accumulated extreme rainfall for five years for each grid point.

Figure 5.3 - Schematic flowchart to describe variable extracted from CACATOES dataset and rain gauges dataset considering the rainfall values above percentile 99th (P99th).



Source: Author's production.

## 5.5 Results and discussion

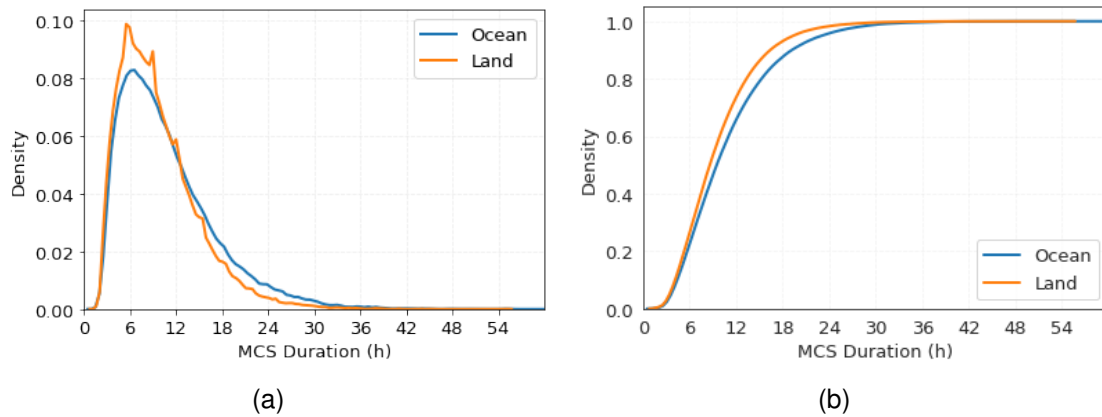
### 5.5.1 Characterization mesoscale convective systems over South America

The Figures (5.4-5.8) shows the PDF and CDF of the morphological attributes such as duration, maximum size achieved, number of events occurred by day, eccentricity and minimum brightness temperature of the MCS over land and over ocean separately. The period correspond to five years (2012-2016) and the domain analyzed contained in the coordinates from 30°S to 15°N and from 90°W to 30°W, corresponding to the tropical region of South America.

In Figure 5.4(a-b) it is possible to note interesting aspects of the MCS duration attribute: (i) MCS last longer over the oceans than over the continent; (ii) systems lasting up to 12 hours are the most frequent, corresponding to about 75% of the distribution over land and 65% of the distribution over the ocean; (ii) events lasting

more than 24 hours are less frequent both on the continent and in the ocean. Similar results were found by (ROCA; FIOLEAU, 2020) who studied the duration of MCS throughout the tropical belt regions.

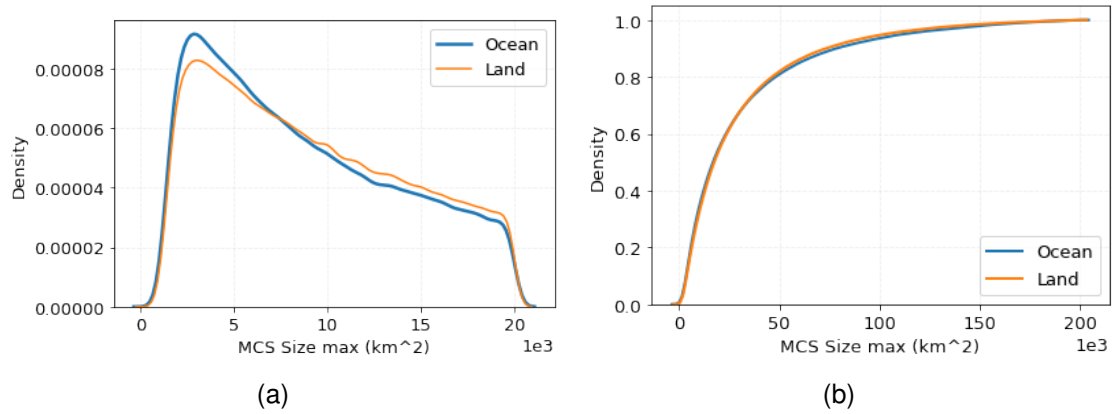
Figure 5.4 - Distribution of life time duration of MCS represented by (a) Probability distribution function and (b) Cumulative distribution function.



Source: Author's production.

Figure 5.5(a-b) represent the distribution of maximum size cold cloud surface reached by the MCS along its life cycle at  $T_b = 235$  K. It is noticed, that both continent and ocean distributions have a similar behavior. Even though, events that reach  $50 \times 10^3 \text{ km}^2$  of maximum area reached by the system represent 80% of the distribution, the highest frequency is of events that reach  $3 \times 10^3 \text{ km}^2$ , that is, small systems. According to Machado and Rossow (1993), on average a large tropical MCS has, during the maturation stage, approximately 80% of its area being composed of stratiform clouds. On the other hand, small systems would be more efficient in terms of the amount of rain and the occurrence of electrical activity of lightning, since the spatial development of the top of clusters of convective clouds has a strong dependence on the presence of ice particles (MORALES et al., 2004).

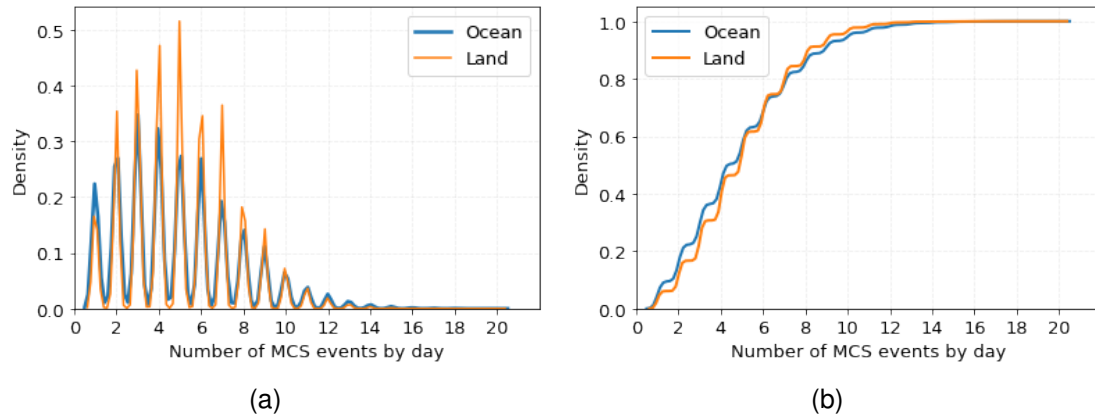
Figure 5.5 - Distribution of maximum cold cloud surface reached by the MCS along its life cycle at 235K represented by (a) Probability distribution function and (b) Cumulative distribution function.



Source: Author's production.

Figure 5.6(a-b) represents the distribution of the MCS population that is partially included or totally included in a 1 degree daily (1DD). Records above 15 by 1DD are rare to occur on land and the ocean. The most frequent number of MCS events recorded in 1DD is between 2 and 6 events for the ocean and between 2 and 7 events for land. However, the maximum of 20 MCS by 1DD records were verified in the analyzed database with a rare frequency. The developers of the CACATOES dataset (FOLLEAU; ROCA, 2013) set the number of 25 for this parameter since no larger values were found in any region of the globe that comprises a coverage area of the dataset.

Figure 5.6 - Distribution of population of MCS which are included partially or totally within a 1°/1day grid point represented by (a) Probability distribution function and (b) Cumulative distribution function.

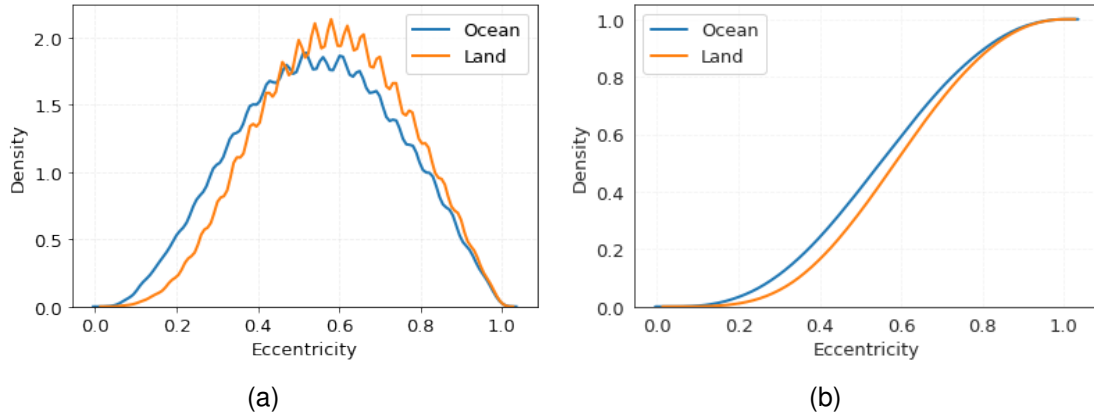


Source: Author's production.

Figure 5.7(a-b) represents the distribution of eccentricity (Ecc) of the ellipse at a  $T_b=235K$  threshold and at time of the maximum extent from MCS. It is noticed that (i) events with Ecc between 0.5 and 0.7 are more frequent; (ii) events with Ecc equals 1.0 are rare; (iii) events with Ecc less than 0.7 represent more than 75% of distribution. It indicates that, during the analyzed period, the MCS have a more elongated than circular shape, corroborating with the results found by (FERREIRA; ANABOR, 2015). On the other hand, 25% of distribution correspond to the events with Ecc greater than 0.7 and can represent more severe systems. According to Mattos and Machado (2009), the Ecc parameter characterizes MCS conducive to the occurrence of lightning, so that MCS that have lightning tend to have a more circular shape compared to those that do not have lightning. In general the electrical activity of lightning increases with the eccentricity of the MCS, this relationship being characterized by a quadratic function, with a high coefficient of determination. These results indicate that a more circular shape of the top of the MCS characterized by the occurrence of lightning is possibly due to the fact that they are associated with deep convection. However, for elongated systems they can be associated with less intense convective processes. The distributions over ocean and over land are similar although the eccentricity is slightly higher on the continent than on the ocean.



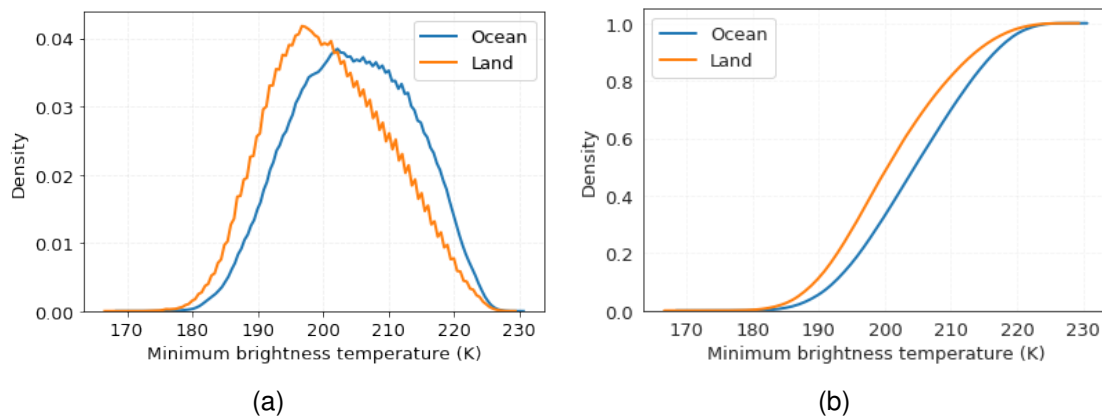
Figure 5.7 - Distribution of eccentricity of the ellipse at a 235K threshold and at time of the maximum extent from MCS represented by (a) Probability distribution function and (b) Cumulative distribution function.



Source: Author's production.

The IR Brightness Temperature at the top of the convective cloud clusters is a thermodynamic variable directly related to the formation of ice particles inside the MCS (GOODMAN; MACGORMAN, 1986; GARREAU; WALLACE, 1997; DOTZEK et al., 2005). Figure 5.8(a-b) represents the distribution of minimum brightness temperature ( $T_{bmin}$ ) of MCS. It is noticed that (i) the values of  $T_{bmin}$  are bigger over ocean than over land; (ii) the  $T_{bmin}$  more frequent varies between 195°K and 200°K over land while over ocean varies between 200°K and 210°K.

Figure 5.8 - Distribution of minimum brightness temperature of MCS represented by (a) Probability distribution function and (b) Cumulative distribution function.



Source: Author's production.

The Figures 5.9(a-d), shows the probability distribution function bi-dimensional of morphological attributes of MCS over tropical region of South America (land + ocean) during 2012-2016.

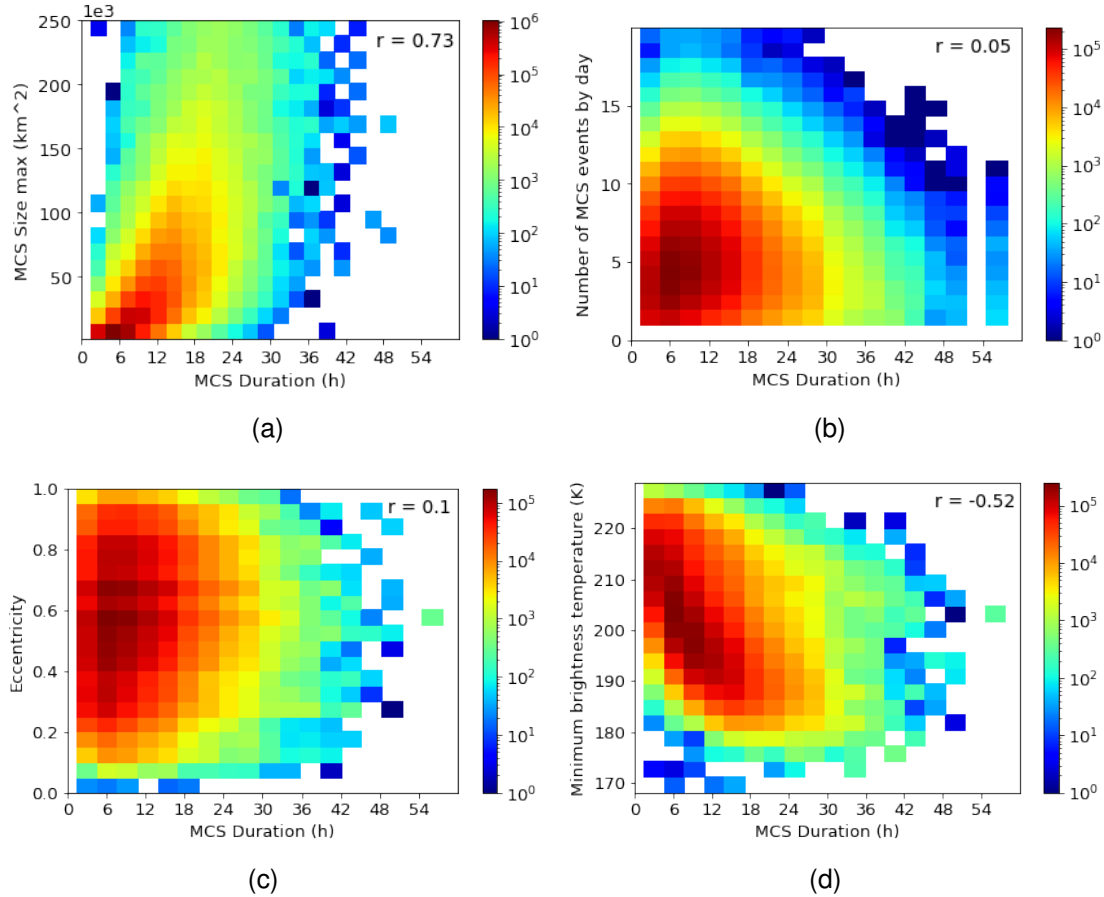
In the relation between duration and max size achieved by MCS, Figure 5.9(a), it is noticed that MCS with a life cycle of up to 12 hours is more frequent and that these systems are generally smaller than  $50 \times 10^3 \text{ km}^2$ . However, bigger MCS with long duration occur with less often. The correlation between these variables is  $r = 0.73$ .

Figure 5.9(b) shows the relationship between duration and number of MCS events per day. From this figure, it is noticed a low positive correlation of  $r = 0.05$ . In addition, for events that occurred up to 18 hours, it was record up to 10 events per 1DD.

Figure 5.9(c) shows the relation between duration and eccentricity. It is noticed that events with short duration, up to 12 hours, have a very large variation in eccentricity, ranging from 0.1 to 1.0, while longer systems ( $> 24$  hours) have an eccentricity between 0.4 and 0.9, that is, systems that have a longer life cycle tend to be more circular than elongated. The correlation between these variables is low positive ( $r = 0.1$ ).

Figure 5.9(d) shows the relation between duration and  $Tb\_min$ . It is noticed that warmer  $Tb\_min$  are more frequent (around  $210^\circ\text{K}$ ) in short duration systems of up to 3 hours. While the longer systems, i.e, the system that occurs during 12 hours or more  $Tb\_min$  is colder (around  $180^\circ\text{K}$ ). The correlation between these variables is negative,  $r = -0.52$ , indicating that as big system is colder.

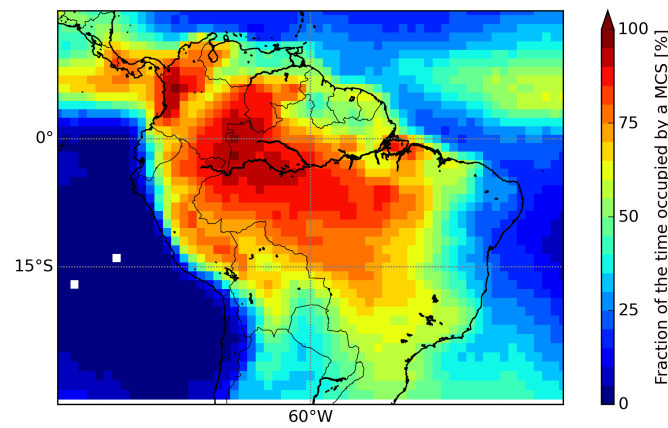
Figure 5.9 - Probability Distribution Function bi-dimensional of morphological attributes of MCS over South America (land + ocean). The colours shading corresponds to the joint frequency of variables in log-normal.



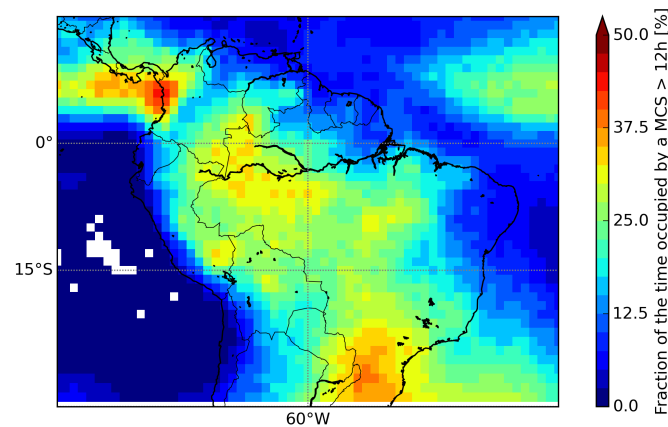
Source: Author's production.

According to Figure 5.4, MCS lasting up to 12 hours occurs more often. Figure 5.10(a-c) represents the spatial distribution of the time fraction occupied by a MCS. It is noticed that they occur, mostly, in the northern region of South America. Figures 5.10(a) and 5.10(b) indicates that the MCS over this region does not last more than one day. Over the entire South America region, the results show that systems lasting more than 24 hours are not frequent. However, these MCS occur mostly in the southern region, which may be explained by the synoptic pattern that facilitates the formation of these long-lived systems at mid-latitudes as shown in Figure 5.10(c).

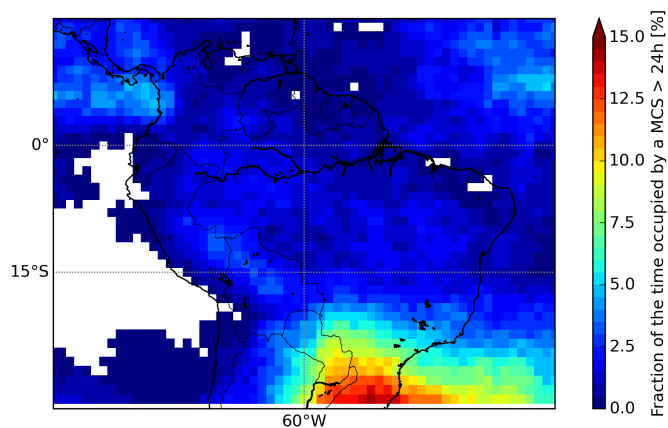
Figure 5.10 - (a) Spatial distribution of the fraction of the time occupied by MCS during all period of duration 2012-2016. (b) Spatial distribution of the fraction of the time occupied by MCS > 12 hr of duration. (c) Spatial distribution of the fraction of the time occupied by MCS > 24 hr of duration.



(a)



(b)



(c)

Source: Author's production.

The objective of the Eulerian tracking approach, represented in this investigation by TOOCAN, is to overcome the main problems of the existing tracking algorithms which are the artifacts of division and fusion. These problems generate complex MCS life cycles and disrupt the physical life cycle of convective systems. This approach tries to improve the description of the morphological parameters of the MCSs throughout their life cycles. However, the main results found in this investigation on the morphological attributes of MCS over South America show similar results if compared with results from previous studies such as Machado et al. (2002); Autonès and Moisselin (2013); Zinner et al. (2008); Vila et al. (2008); Carvalho and Jones (2001) who used a Lagrangian approach. In this way a more detailed study using the same data period comparing different algorithms is necessary so that the real differences are identified and quantified.

### 5.5.2 Influence of MCS on extreme rain

In order to understand the relation between the accumulated extreme rainfall occurred during 2012-2016 and the extreme rainfall over influence of MCS, a scatter plot and histogram of variables is shown in Figure 5.11(a). In this figure, it is observed that the most frequent value in the distribution is around 250 mm/5years. In addition, very high values of rain have a low frequency of occurrence. It is also observed that there is no perfect correlation between the variables. Some points show high values of extreme rain accumulated and a value low rainfall from MCS. It indicates that MCS does not have influence in extreme rain at all times everywhere.

Figure 5.11(b) show the relation between the contribution of MCS over extreme rainfall and the percentage of days with MCS. It is noticed a positive correlation between these variables. The greater the percentage of days with MCS the greater the contribution of MCS to extreme rain and the number of recorded MCS events.

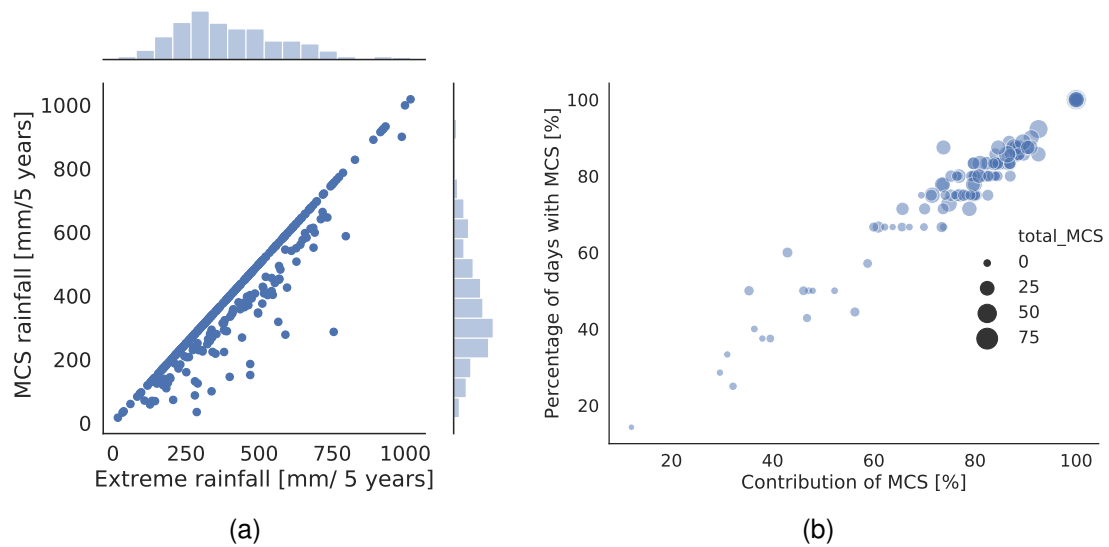
In order to visualize in more detail these relationships between extreme rain and the influence of the MCS on this rain, spatial maps shows the location of these events. The extreme rain accumulated during the 5 years analyzed is represented by Figure 5.12a. It is observed in this figure that the most intense rain is located north and south regions of Brazil. It can be observed that intense rain occurs in some grid points at east coast of Brazil and at the west coast of Colombia and Ecuador. Figure 5.12b represents the number of MCS events recorded by the TOOCAN algorithm. It is noticed that the largest number of registered MCS are

located at the grid points in the north, south, and southeast regions of Brazil. The grid points that had the lowest MCS record were in the northeast and southwest of the study area.

In doing so, Figure 5.12 represents the influence of the MCS on the extreme rain recorded during 2012-2016 in the tropical region of South America. According to this figure, a marked influence of the MCS during 2012-2016 period is observed since the ratio between the rain that occurred on the days when there was a MCS record and the total-extreme rain that occurred is 100% for most grid points analyzed. (Figure 5.12(c) ). In addition, at the northeast coast of Brazil and in some grid points in northern Argentina, the MCS contribution ranges from 20% to 60%.

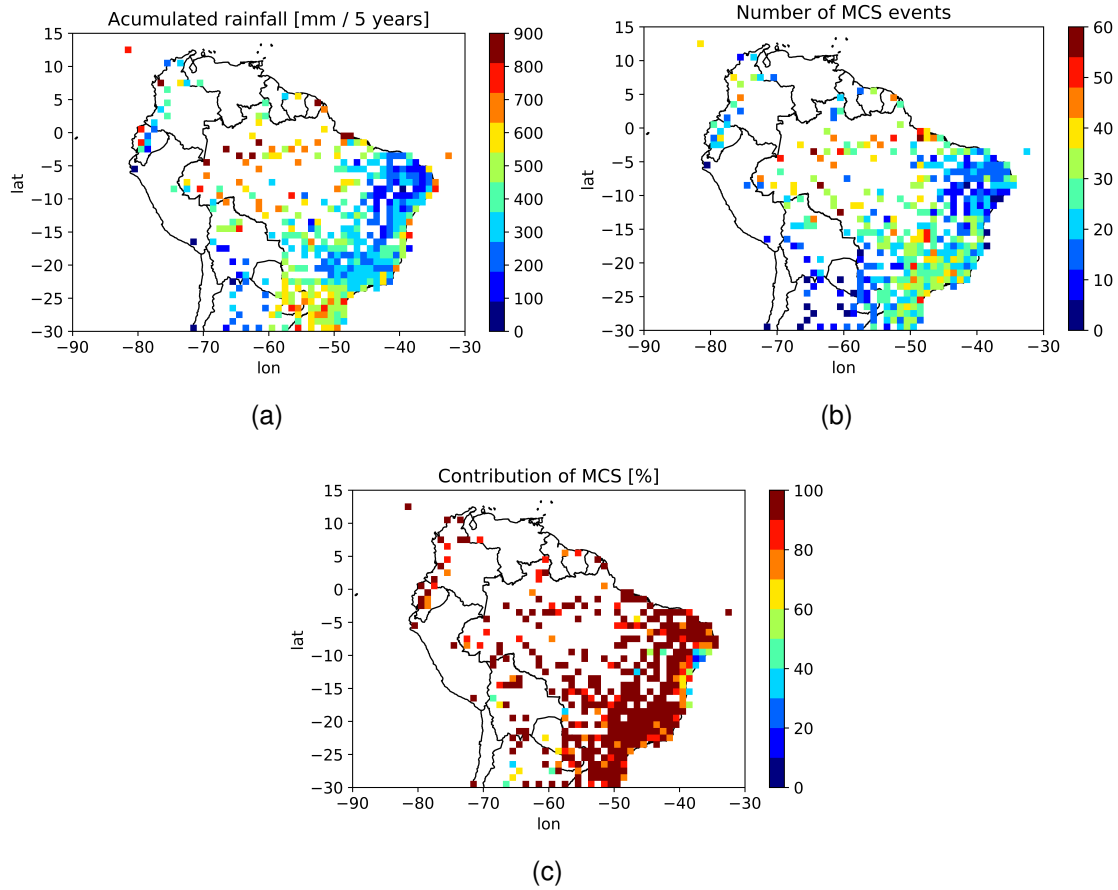
A hypothesis for this result is that the convection that occurs in these places is not deep or frequent and the  $Tb_{min}$  at the top of the clouds does not reach the 235K threshold used in the algorithm to identify an MCS. According to (PALHARINI; VILA, 2017), the eastern region of the northeast has a predominance of shallow convection that contributes to rainfall in this region. According to (CANCELADA et al., 2020), regions associated with topography, such as northwestern Argentina and western central Argentina, show a strong annual cycle of convection initiation with a maximum in the warm season December to February. In addition, according to the authors, almost no convection initiation is observed in the cool season, from May to August while the plains regions in south-central Argentina have a year-long annual convection initiation seasonal cycle. Which would explain the fact that the TOOCAN algorithm identify a smaller number of MCS and with a low contribution to the extreme rains in these regions.

Figure 5.11 - (a) Scatter plot of accumulated extreme rainfall (values above P99) and accumulated rainfall influenced by MCS occurred during 2012-2016 and marginal histograms of respectively variables. (b) Plot of relationship between contribution of MCS in extreme rainfall and fraction of time occupied by MCS, the size of points represent the total number of MCS occurred



Source: Author's production.

Figure 5.12 - (a) Accumulated extreme rainfall (values above P99) recorded during 2012 to 2016 over tropical region of South America. (b) Number of MCS events recorded in 5 years (2012-2016). (c) Contribution of MCS for extreme rainfall.



Source: Author's production.

## 5.6 Conclusions

This study provided a description of the morphological characteristics of the Mesoscale Convective Systems (MCS) through the use of Tracking Of Organized Convection Algorithm through 3D segmentationN (TOOCAN) algorithm in the first part of analysis. In the second part, this investigation identified the influence of MCS systems on extreme precipitation over the tropical region of South America. In to perform this analysis, rain gauges dataset and of CACATOES dataset was analyzed. Extreme precipitation was defined by 99th percentile threshold in a daily 1° X 1° grid for the period ranging from 2012 to 2016.

According to the results obtained in this investigation using a Eulerian tracking ap-



proach, small systems with a duration lower than 12 hours occurred with a higher frequency. However, the longer systems contributed to the extreme rain. These results corroborate with results obtained by (ROCA; FIOLEAU, 2020) that point to the importance of long-lived systems to extreme precipitation over the entire tropics. Similar results was found by previous studies that use a Lagrangian tracking approach, indicating that the characteristics of the MCS morphology can be obtained regardless of the method used and that the new algorithm represented these characteristics well.

The results also show that the MCS contributes substantially to extreme precipitation in South America. Although a great influence of the MCS has been identified over a large part of the South America regions, it is clear that there is a great degree of variability in the contributions of the MCS to the extreme rains in regions such as eastern Brazil and northern Argentina, where the contribution is lower than in other regions.

In the eastern region of the Northeast, there is a very strong presence of shallow convection (PALHARINI; VILA, 2017). Associated with topography, such as north-western Argentina and central-west Argentina, a strong annual cycle of initiation of convection with a maximum in the warm season from December to February and almost no start of convection in the cold season from May to August (CAN-CELADA et al., 2020), may justify the results found in this work. In addition, the study considered in this investigation is delimited between 30°S to 15°N due to a limitation in the TOOCAN database and it was not possible to verify deeper and intense systems that occurred in the central-south areas of Argentina.

In future work, it is intended to make a more detailed study using the same data period and comparing different algorithms so that the real differences between the Eulerian and Lagrangian approaches can be identified and quantified. In addition, a study on the morphological characteristics of MCS only in cases of extreme events is necessary.



## 6 Analysis of extreme rainfall events in different regions of Brazil : Case studies

### 6.1 Introduction

The occurrence of natural disasters have a significant impact in several regions around the world. According to the Intergovernmental Panel on Climate Change (IPCC) report extreme rainfall events will become more intense, concentrated, and poorly distributed in the next years (SENEVIRATNE et al., 2012). In another report on Managing the Risks of Extreme Events and Disasters to Advance Climate Change Adaptation (CHANGE, 2012). The IPCC surveyed disaster and death information since 1970-2008 and it was concluded that over 95.0% of natural-disaster-related deaths occurred in developing countries. According to the Brazilian Atlas of Natural Disasters from 1991 to 2012, it was observed almost 40 thousand disasters, caused by meteorological, hydrological and geological events (UNIVERSIDADE FEDERAL DE SANTA CATARINA. CENTRO UNIVERSITÁRIO DE ESTUDOS E PESQUISAS SOBRE DESASTRES - UFSC.CEPED., 2012). Unfortunately, these number have increased every year and a survey data with more updated information is necessary.

Most of the natural disasters that occurs in Brazil are triggered by precipitating meteorological systems (DEBORTOLI et al., 2017). The systems are capable of generating a large amount of rain in a generalized way and for a long period of time or are capable of generating rain in a more localized way and in a few hours. As an example, one can see the South Atlantic Convergence Zone (SACZ) and the Mesoscale Convective Systems (MCS) respectively (DURKEE et al., 2009). The main types of meteorological systems that occur and the most favorable seasons of the year may vary according to the regions analyzed. On South region of Brazil for example, are common the frontal systems, cyclones and Mesoscale Convective Systems (MCS) ((VELASCO; FRITSCH, 1987); (GRIMM et al., 2000)), whereas in North and Northeast regions are common the Intertropical Convergence Zone (MARENGO; HASTENRATH, 1993), the Tropical Squall Lines (COHEN et al., 1995), Upper Level Cyclonic Vortex, Easterly Waves and Sea Breeze Circulation (YAMAZAKI; RAO, 1977); (GOMES et al., 2015).

Due to the high spatial and temporal resolution, the use of satellite data is of fundamental importance in the analysis and understanding past extreme events in order to prevent or mitigate disasters that will occurs in near future. Nonetheless, a deeper investigation is necessary to extract the data in the best way as possible

to improve the performance of precipitation estimates using satellites precipitation products. In doing so, several studies have been performed to achieve this goal (XU et al., 1999); (TURK; MILLER, 2005); (KIDA et al., 2009);(??); (SHIGE et al., 2013); (KULIGOWSKI et al., 2016); (KIDD et al., 2020) (FUNK et al., 2020); (KUBOTA et al., 2020) among others.

The Global Precipitation Measurement Core Observatory (GPM-CO) mission is an international satellite mission to advance our knowledge and understanding of global precipitation (KIDD et al., 2020). The GPM-CO is a collaboration between NASA and JAXA and main goal of the mission is to improve precipitation measurements through understanding the physics and space-time variability of precipitation across the Earth. The most advanced precipitation instrumentation currently in orbit are a Dual-frequency Precipitation Radar (DPR) operating in 13.6 GHz and 35.5 GHz and the GPM Microwave Imager (GMI) that is composed by thirteen microwave channels ranging in frequency from 10 GHz to 183 GHz. Both instruments in the GPM-CO are designed to measure from light precipitation to the most intense precipitation (0.2-111.0 mm/h).

Using information from the newest GPM-CO satellite constellation, JAXA has been improving its product, the Global Satellite Mapping of Precipitation (GSMaP). According to (KUBOTA et al., 2020) this product is characterized by its careful treatment of precipitation types in its algorithm, fully utilizing the TRMM/PR, GPM/DPR, TMI and GMI observations. GSMaP employs precipitation regime classifications and precipitation profile information constructed from the TRMM/PR, GPM/DPR, and ancillary meteorological data. Careful classification of land/coast/ocean surface types and utilization of land surface emissivity obtained from TRMM data are included. In addition, severe underestimation of orographic precipitation in the original product is mitigated by incorporating an orographic rainfall scheme. A recent improvement is an implementation of a snow-fall estimation scheme that significantly extended the estimated data availability to higher latitudes.

Another example is the efforts made by Climate Hazards Center (CHC) at the University of California, Santa Barbara developed the Climate Hazards center InfraRed Precipitation with Stations (CHIRPS) dataset, in collaboration with the US Geological Survey and NASA SERVIR. This dataset is constantly improving in order to reduce the bias between the data observed in the rain stations and data estimated by satellite. In recent publication (FUNK et al., 2020) reveals that

development team is working in a new version of dataset in which the assumed 'prior' distribution is allowed to change with environmental conditions, such an approach could provide the long-term low bias performance of the current CHIRPS algorithm while allowing dry areas to receive high levels of precipitation when large-scale conditions indicate large weather disturbances.

In South America also is verified the efforts made by Satellite Division and Environmental Systems of National Center for Space Research (INPE) to create a satellite product using a Combined Scheme approach (CoSch) to provides a new high-resolution, gauge-satellite-based analysis of daily precipitation (??). This methodology is based on a combination of additive and multiplicative bias correction schemes to get the lowest bias when compared with the observed values (rain gauges). For that is used real-time TRMM Multi-satellite Precipitation Analysis (TMPA) and Integrated Multi-satellitE Retrievals for GPM (IMERG) products.

Although satellite information is important and in many regions the only existing one, it is far from perfect. The validation of satellite products using ground instruments can be helpful to understand the products strengths and limitations. Some studies have evaluated the performance of precipitation estimates using satellite products and have shown that products in general tend to underestimate or overestimate extreme rainfall (SCOFIELD; KULIGOWSKI, 2003); (FUNK et al., 2015); (SALIO et al., 2015); (AMITAI et al., 2012); (MASUNAGA et al., 2019);(LIU et al., 2019);(PALHARINI et al., 2020).

In the present investigation the main goal is to analyze the performance of different Satellite Precipitation Products (SPP) in detecting the extreme rainfall for 5 case studies in which caused natural disasters in 5 different regions of Brazil.

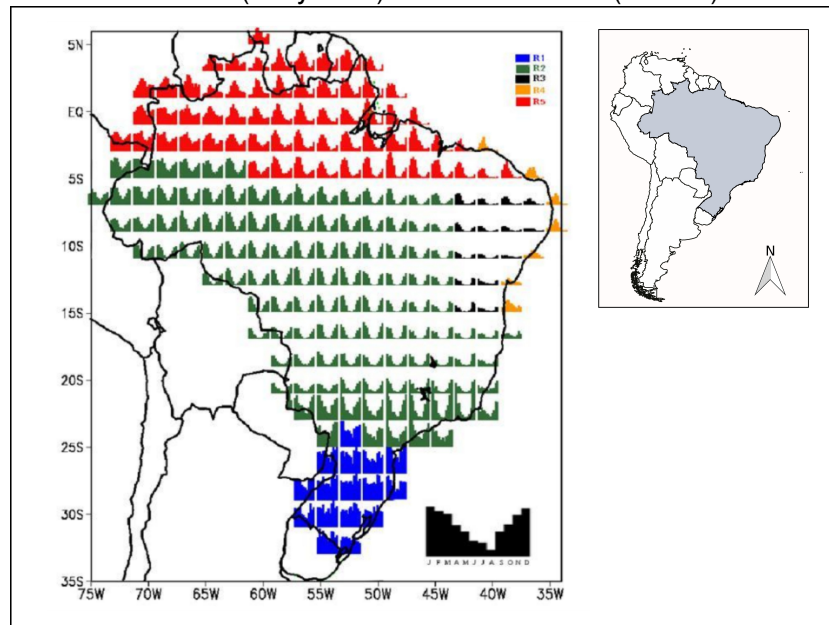
## **6.2 Materials and Methods**

### **6.2.1 Study area**

Brazil has a large territorial extension which contributes to the formation of different meteorological systems. This characteristic has a significant effect on the rainfall regime over the Brazilian territory. In order to investigate these meteorological system, the overall area was divide into five regions according to homogeneous rainfall regime (REBOITA et al., 2010); (ROZANTE et al., 2018). The seasonal rainfall characteristics may be identified with distinct rainfall distribution. According to the aforementioned works, these five regions are classified as: Southern Brazil (R1),

Central Region (R2), Northeastern (R3), Northeast Coast (R4) and North Brazil (R5). These regions and the predominant meteorological system that have influence in the rainfall regime is shown in Figure 6.1. According to the climatological rainfall averages (DINIZ et al., 2018) during the summer months (DJF) the rainfall varies between R1: 80.0 to 220.0 mm/month; R2: 100.0 to 420.0 mm/month; R3: 20.0 to 420.0 mm/month; R4: 30.0 to 140.0 mm/month; R5: 10.0 to 420.0 mm/month, while in the winter months (JJA) it varies between R1: 40.0 to 140.0 mm/month; R2: 10.0 to 80.0 mm/month; R3: 10.0 to 180.0 mm/month; R4: 10.0 to 180.0 mm/month; R5: 50.0 to 380.0 mm/month.

Figure 6.1 - The five regions of Brazil according to climatological rainfall regime. Southern Brazil (R1-blue), Central Region (R2-green), Northeastern (R3-black), Northeast Coast (R4-yellow) and North Brazil (R5-red).



Source: Adapted from Rozante et al. (2018).

On R1 are common the frontal systems, cyclones and Mesoscale Convective Systems (MCS) ((VELASCO; FRITSCH, 1987); (GRIMM et al., 2000)). During the autumn and winter the rains is caused by the frontal systems at mid-latitudes. In addition, during this period, the latitudinal temperature gradient generates baroclinic waves in the west winds in upper air (GRIMM et al., 2000) and the low-level jets stream are moved to the southeast through the Andes acting as an orographic barrier causing cyclogenesis (VERA et al., 2006). During the spring and summer the MCS

predominate.

On R2 one of the most common meteorological systems is the South Atlantic Convergence Zone (SACZ) where the flow from the northwest of the Low Level Jets can converge with the circulation of the subtropical high of the south Atlantic and still with the northeast trade winds, resulting in a band of cloudiness and intensification of precipitation in these regions (LENTERS; COOK, 1995); (ROSA et al., 2020). R2 is characterized by 6 months of rain during the austral summer followed by 6 months of scanty rainfall in austral winter, the main characteristic of a monsoon region ((ZHOU; LAU, 1998); (RAO et al., 2016)).

On R3 the main meteorological systems acting are the Inter-tropical Convergence Zone and the Upper Level Cyclonic Vortex (KOUSKY; GAN, 1981). The mean annual rainfall most of which registered from January to May and the rainfall is modulated by stratiform and deep convective precipitating clouds (PALHARINI; VILA, 2017).

On R4 the main meteorological systems acting are Intertropical Convergence Zone, Tropical Mesoscale Convective Systems, the Trade Winds, Upper Level Cyclonic Vortex, Easterly Waves and Sea Breeze Circulation (YAMAZAKI; RAO, 1977); (GOMES et al., 2015). The annual cumulative rainfall is around 1000 mm in coastal, ((KOUSKY; CHUG, 1978); (RAO et al., 2016)) mostly concentrated from March to July ( 70%) and modulated by shallow convective precipitating clouds (PALHARINI; VILA, 2017).

On R5 the mainly meteorological systems acting are Intertropical Convergence Zone (MARENGO; HASTENRATH, 1993), the Tropical Squall Lines (COHEN et al., 1995) and the Trade Winds. The period from November to April constitutes the rainfall season and the total annual rainfall ranges from 2000 to 3000 millimeters (RAO et al., 2016). This region exhibits large variability in rainfall and it is in general associated with El Niño or La Niña. During the years of La Niña the rainfall tends to increase.

### **6.2.2 Rain gauges dataset**

The National Center for Space Research (INPE) is the institute responsible to receive, store and organize rain gauges rainfall data from different agencies around the Brazil such as National Meteorological Institute (INMET; <http://www.inmet.gov.br>), the National Water Agency (ANA; [www.ana.gov.br](http://www.ana.gov.br)), the

Energy Company of Minas Gerais (CEMIG; <http://www.cemig.com.br/>), the Instituto Agrônômico (IAC; <http://www.iac.sp.gov.br/>) and the Meteorological System of Paraná (SIMEPAR; <http://www.simepar.br/>). In this study, a rainfall database was used as the reference data. This database of daily rainfall is organized in DAT format and has been interpolated for regular  $1^{\circ} \times 1^{\circ}$  grid using the simple average. The grid points with more than 90% of valid rain gauges data in the temporal series for 2012 to 2016 period of INPE dataset with 317 valid grid points was used.

### 6.2.3 Satellite Precipitation Products (SPP)

In order to evaluate the performance of some SPPs to detect extreme rainfall at different regions of Brazil, FROGS dataset was used. The FROGS is an acronym for Frequent Rainfall Observations on GridS dataset. This dataset is composed of daily precipitation gridded products that include satellites, ground-based and reanalysis products adjusted to a common  $1^{\circ} \times 1^{\circ}$  grid resolution. The dataset was downloaded from the Institut Pierre Laplace Simon (IPSL) repository (<http://dx.doi.org/10.14768/06337394-73A9-407C-9997-0E380DAC5598>). More information about the product contained within the database can be found in (ROCA et al., 2019). In the present investigation, eleven SPPs with one degree daily resolution (1DD) have been used: 3B42g, 3B42, CMORPH, CMORPHg, GSMAP, GSMAPg, CHIRP, CHIRPSg, PERSIANNg, COSCHg, and TAPEER. The sub-index 'g' indicates the products available with gauge correction. The full name and the version used are explained in detail in the Table 6.1.

Table 6.1 - Description table of satellite products.

Satellite product version	Short name	Use rain gauges	Use IR sensor	Use MW sensor
CHIRP v2.0	CHIRP	No	Yes	No
CHIRPS v2.0	CHIRPSg	Yes	Yes	No
PERSIANN CDR v1 r1	PERSIANNg	Yes	Yes	No
3B42 RT v7.0 uncalibrated	3B42	No	Yes	Yes
3B42 RT v7.0	3B42g	Yes	Yes	Yes
GSMAP-NRT-no gauges v6.0	GSMAP	No	Yes	Yes
GSMAP-NRT-gauges v6.0	GSMAPg	Yes	Yes	Yes
CMORPH V1.0, RAW	CMORPH	No	Yes	Yes
CMORPH V1.0, CRT	CMORPHg	Yes	Yes	Yes
TAPEER v1.5	TAPEER	No	Yes	Yes
COSCH	COSCHg	Yes	Yes	Yes

Source: Adapted from Roca et al. (2019).



#### 6.2.4 TOOCAN dataset

In order to access the influence of the Mesoscale Convective Systems (MCS) on the extreme rain events, the TOOCAN database, developed by (FIOLLEAU; ROCA, 2013), was considered in this work. TOOCAN is an acronym for Tracking Of Organized Convection Algorithm through a 3-D segmentation and it has been used to detect and track MCSs using infrared images from a geostationary satellite. This algorithm works in a time sequence of infrared images to identify and track MCSs in a single 3-D segmentation step, spatial and time resolution. To detect the convective nuclei within a 235K cold cloud shield, TOOCAN uses an iterative process of detection and propagation of convective seeds to segment individual convective systems.

#### 6.2.5 Methodology

In this study, five cases of extreme events were analyzed in order to evaluate eleven satellite precipitation products. These cases occurred in different regions of Brazil and were selected in three stages. Firstly, with the data of rain gauges already organized in a grid point, the 99th percentile threshold was calculated and only the rain values above this threshold were used, that is, the extreme rain. Second, for each proposed region, the mode of the dates corresponding to extreme rain was calculated. Mode represents the most frequent value in a data set. Finally, knowing which date was the most repeated, two days forward and two days back (D-2, D, D+2) were selected to compose the series of 5 days (rainy pentad) that will represent the extreme event of each region. The information and the impacts of each of the extreme rain event are available at newspapers, photos, and civil defence reports at the Integrated Disaster Information System - S2ID (<https://s2id.mi.gov.br/>) and was used in this investigation for describing each event. Table 6.2 summarize the information about each studied case.

Table 6.2 - Summarized table with the cases of extreme rainfall events analyzed from each region.

Region	Date	Rainfall	Affected People
R1	24/06/2014 to 28/06/2014	>300 mm/5days	1.600
R2	01/01/2012 to 05/01/2012	>140 mm/5days	200.000
R3	20/01/2016 to 24/01/2016	>200 mm/5days	No information in civil defence report
R4	14/04/2016 to 18/04/2016	>200 mm/5days	2.268
R5	29/04/2016 to 03/05/2016	>140 mm/5days	15.265

In addition, in order to complement the description of the events, the atmospheric pattern that occurred during the events that caused extreme rains was shown. For that it was conducted an analysis of the atmospheric fields 6-hourly and 0.5° of temporal and spatial resolutions respectively, using the Global Forecast System (GFS) and IR image employing the Geostationary Operational Environmental Satellite (GOES)-13.

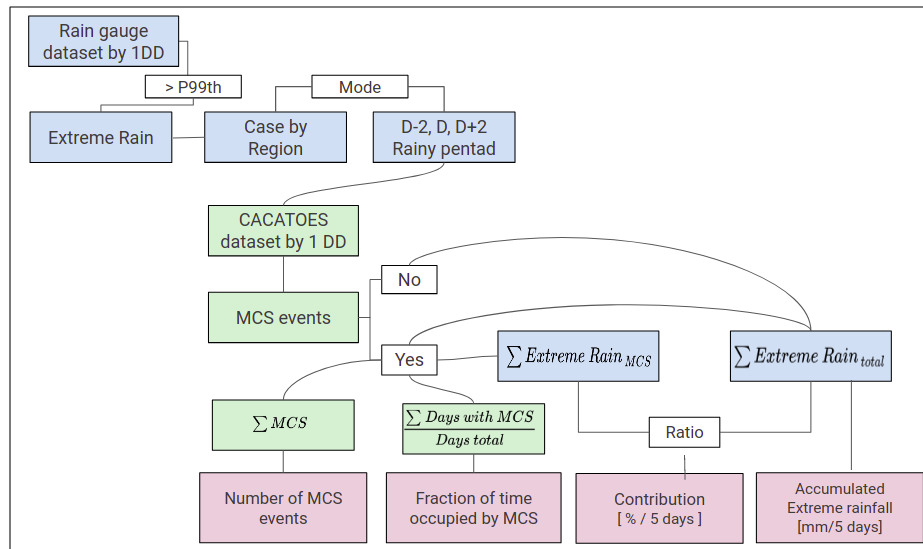
The influence of the MCS on the extreme rain was verified on a sub-synoptic scale. In order to perform the verification, it was analysed the ratio between the amount of extreme rain that was influenced by the MCS over the total extreme rain recorded during the events. Figure 6.2 shows a schematic flowchart with the necessary steps to obtain the analysis. These steps are: (i) accumulated rainfall in 5 days that from the rain gauge dataset; (ii) number of MCS events by grid point from CACATOES dataset; (iii) percentage of days with MCS that was made counting the days that recorded MCS events divided by five days; (iv) contribution of MCS in total rainfall of extreme event.

For obtain the contribution of MCS, that firstly was selected the rainy pentad for each region from rain gauges INPE dataset for one daily degree. Secondly, the CACATOES dataset with the population of MCSs within a 1°/1day grid point (Daylymcs\_pop) variable that recorded the MCS events occurred. In the cases that in each grid point were recorded at least one MCS event and a value of extreme rainfall associated, the information of rainfall was accumulated ( $\sum \text{Extreme Rain}_{MCS}$ ). Next, it was accumulated the extreme rainfall for five days at each grid point ( $\sum \text{Extreme Rain}_{total}$ ). Finally, it was obtained the ratio between both information (Figure 5.3). In doing so, the contribution of the MCS on the total extreme rainfall occurred during the rainy pentad is expressed by the following equation:

$$\text{Contribution}[\%/5 \text{ days}] = \frac{\sum \text{Extreme Rain}_{MCS}}{\sum \text{Extreme Rain}_{total}} * 100 \quad (6.1)$$

where the  $\text{Extreme Rain}_{MCS}$  represents the rain recorded at 1 daily degree for each grid point when MCS registered and  $\text{Extreme Rain}_{total}$  is the accumulated rain for 5 days for each grid point.

Figure 6.2 - Schematic flowchart to describe variable extracted from CACATOES dataset and rain gauges dataset considering the rainfall values above percentile 99th (P99th).



Source: Author's production.

A contingency table was generated based at the P99th threshold of rainfall at each grid point. The contingency table was employed to compute the number of Hits (A), False Alarms (B), Misses (C), and Correct Negatives (D) for study cases considered in this work (Table 6.3).

Table 6.3 - Contingency table considering P99th threshold by grid point

	Gauge $\geq$ Threshold	Gauge $<$ Threshold
Satellite $\geq$ Threshold	Hits (A)	False Alarms (B)
Satellite $<$ Threshold	Misses (C)	Correct Negatives (D)

Based in the information of contingency table, statistical measures such as Probability Of Detection (POD), Miss Rate (MR), False Alarm Ratio (FAR), Threat Score (TS), Frequency Bias Index (FBI) and Proportion Correct (PC) were used in the present investigation in order to demonstrate the performance of the eleven satellite products for each study case (WILKS, 2011). As can be seen in the Table 6.4, these measures are obtained from relations between A, B, C and D, where

MR and FAR show a perfect score = 0.0 and the other measures show a perfect score = 1.0.

Table 6.4 - Statistical measures obtained by contingency table

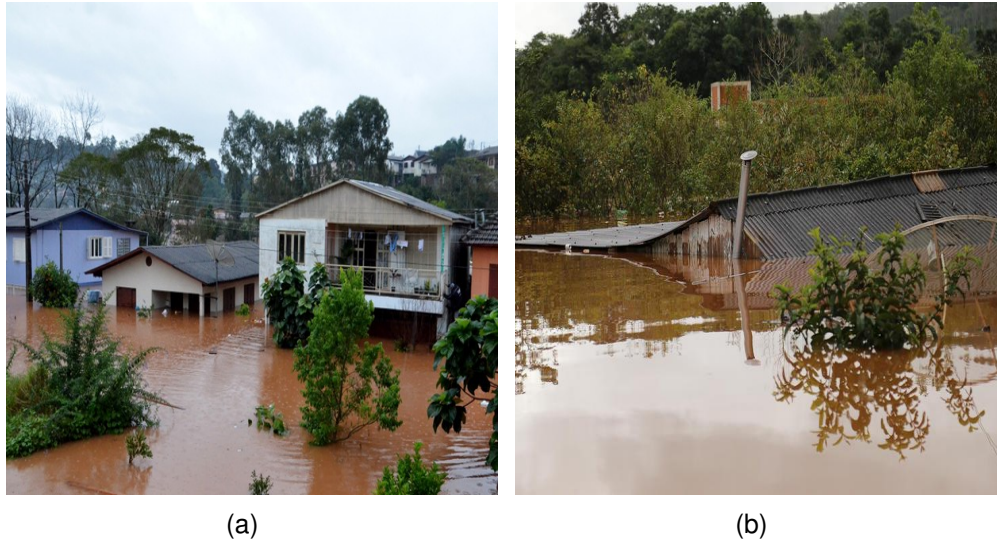
Statistical Measure	Equation	Range	Perfect Score
POD	$A/(A+C)$	0 to 1	1
MR	$C/(A+C)$	0 to 1	0
FAR	$B/(A+B)$	0 to 1	0
TS	$A/(A+B+C)$	0 to 1	1
FBI	$(A+B)/(A+C)$	0 to $\infty$	1
PC	$(A+D)/(A+B+C+D)$	0 to 1	1

## 6.3 Results and discussion

### 6.3.1 Case study for Southern Brazil - R1

In this work, the first case of extreme rain that caused a natural disaster occurred from 24/06/2014 to 28/06/2014 in R1. According to Figure 6.3, this event reached more than 300 mm in 5 days and caused several disasters in the region. At the municipality of Iraí, in the northern region of Rio Grande do Sul, it was reported the highest accumulated rainfall (467 mm/month) in the whole state during June 2014. According to the Civil Defense report (<https://s2id.mi.gov.br/>), the elevation of the Uruguay River left more than 600 people homeless and more than 1000 displaced. This event caused significant damage on the roads and harming the supply of essential services such as water, electricity, transportation, and medical assistance. About 36 houses were completely submerged and 400 houses flooded. More than 400 km of secondary roads were damaged and due to the destruction of 08 dams. Bridges destroyed by the flood isolating entire communities that only received aid by boat. The financial losses were incalculable for agriculture and livestock sectors. Large amounts of crops were washed away by the floods, destroying fertile soils, and causing erosion. The dairy farming sector was severely affected since the roads was not properly for use and it was not possible to access milk-producing properties for collection and processing the milk in a timely manner. Substantial efforts by government and civil society were necessary restore the damages caused by this extreme event in R1 region.

Figure 6.3 - Municipalities affected by extreme rains. (a) Flooding in municipality of Iraí located north of Rio Grande do Sul state. (b) Flooding in municipality of Chapecó located west of Santa Catarina state. Photographs: Fernando Sucolotti/G1 and Marcio Cunha/RBS.

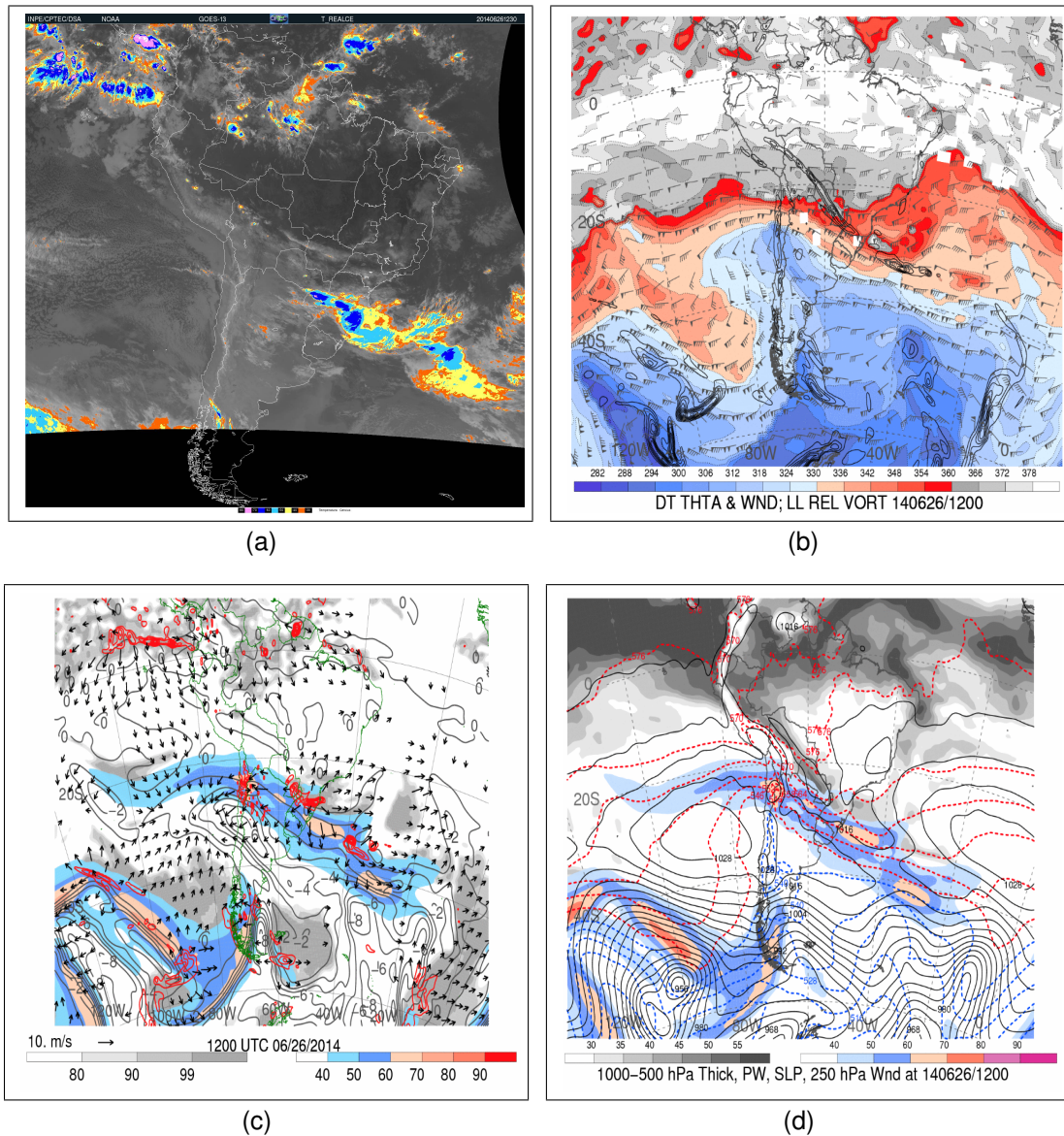


Source: G1 and RBS (2014).

Figure 6.4a shows an IR image with highlighted brightness temperature from GOES-13 over South America. According to this Figure, it is noted that a precipitating system over the R1 region and this system has a temperature ranging from  $-70$  to  $-60$  °C. It is an indication that the top of the clouds was cold and the system reached a great vertical development (XU et al., 1999);(MILLER et al., 2001);(KIDD et al., 2003). Figure 6.4b shows the field combination of wind and potential temperature in the dynamic troposphere. At this Figure, it is possible to track air masses and identify the advance of atmospheric ridges and troughs and as also cyclonic vorticity at low levels. In this study case, it is observed a trough intense over Argentina that advances eastwards from the 24th to the 28th of June. Associated with this trough it is also noticed from Figures 6.4 (c) and (d) a potential temperature gradient related to an intense wind jet at high levels that advances over the southern region of Brazil. In addition, there is a strong baroclinic situation that is identified by the proximity of the thick lines between the 1000-500 hPa layer and also the north flow. This flow carries warm temperature advection. High values of relative humidity and precipitable water are remarkable. These factors were maintained over the 5 days favouring the upward movement and the accumulation of significant rainfall at this region.



Figure 6.4 - Fields of atmospheric patterns from GFS model over South America for **20140626 12UTC**. **(a)** Satellite GOES-13 infrared image; **(b)** Potential temperature (shaded, K) and wind barbs (knots) in the dynamic tropopause, 925–850-hPa layer-averaged cyclonic relative vorticity (black contours); **(c)** 250-hPa wind speed (m s<sup>-1</sup>, shaded according to color bar), 250-hPa potential vorticity (gray contours), 250-hPa relative humidity (% , shaded according to gray scale), 600–400-hPa layer averaged ascent (red contours); **(d)** 250-hPa wind speed (m s<sup>-1</sup>, shaded according to color bar), 1000–500-hPa thickness (dashed contours), Sea Level Pressure (solid contours), total precipitable water (mm, shaded according to gray scale).

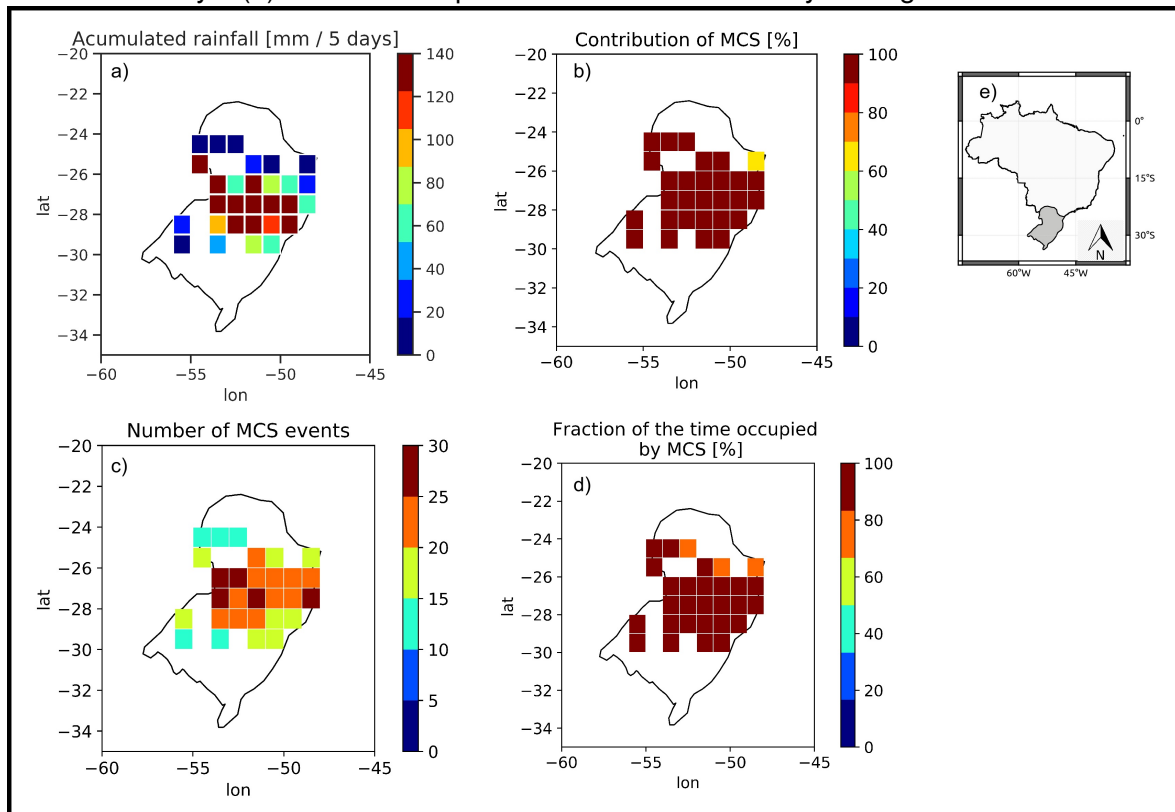


Source: CPTEC and Albany University (2014).

Figure 6.5 represents the influence of the MCS on the extreme rain recorded

from 24/06/2014 to 28/06/2014 in the southern region of Brazil (R1). The total rain accumulated over the 5 days is represented by Figure 6.5a. It is observed in this Figure that the most intense rain ( $> 120$  mm/5days) is located between the states of Rio Grande do Sul and Santa Catarina. It is perceived according to the proposed methodology, a marked influence of the MCS in this event since the contribution of MCS is above 90% for most grid points analyzed (Figure 6.5b ). Figure 6.5c represents the number of MCS events recorded by the TOOCAN algorithm over the 5 days analyzed. More than 20 MCS was registered during these 5 days. Observing the fraction of the time occupied by the MCSs it is noted that they remained for more than 80% of the time in this region (Figure 6.5d).

Figure 6.5 - (a) Accumulated rainfall recorded during 24/06/2014 to 28/06/2014 over South region of Brazil (R1). (b) Fraction of rain from rain gauges on days that had MCS record by rain accumulated in 5 days. (c) Number of MCS events recorded in 5 days. (d) Fraction of the days that had MCS record by 5 days. (e) Indicative map of the location of the analyzed region.

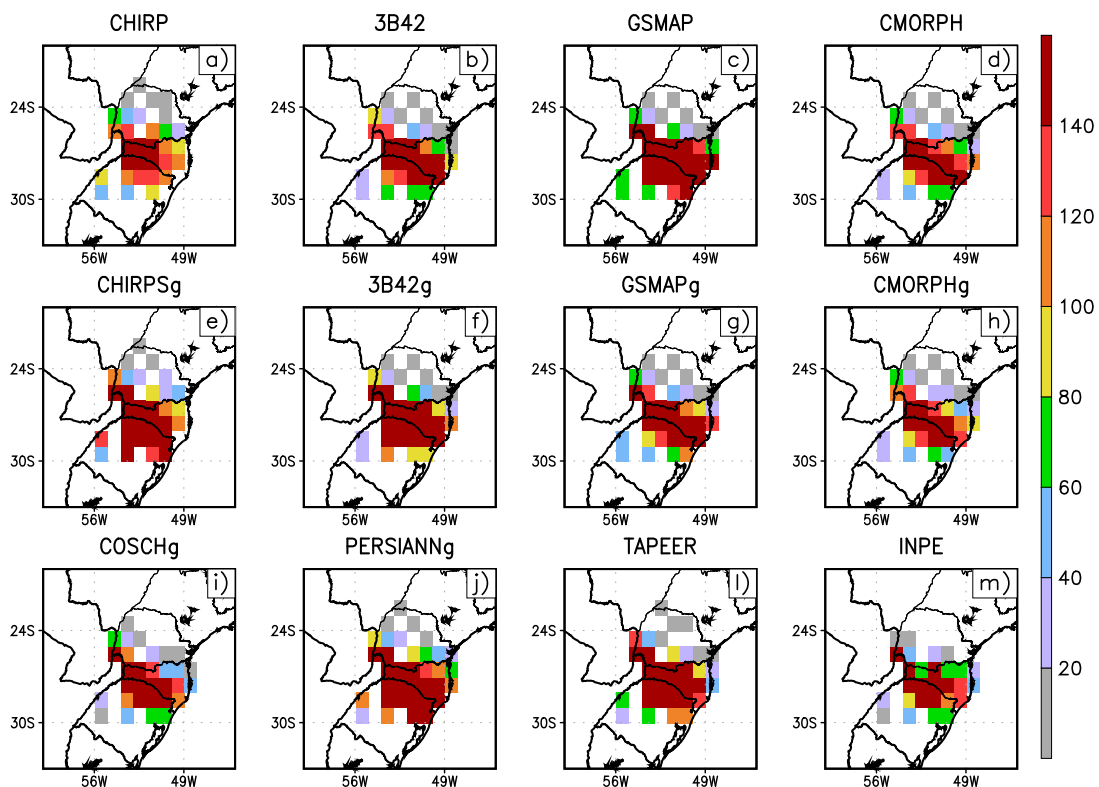


Source: Author's production.

In order to verify the performance of satellite rain estimation products, a specific case of extreme rain was chosen for R1. The case was selected considering the days when they presented a higher number of grid points with intense rainfall values. Figure 6.6 shows the spatial distribution of these precipitation event from different satellite products and noticed that the estimation products are able to identify the extreme rain that occurred in the region when compared to the reference (Figure 6.6m) data. According to Figures 6.6(c), 6.6(f) and 6.6(j), it is noticed that the products GSMAP, 3B42g, and PERSIANNg overestimate the area that occurred the event, because they have a larger number of pixels with rain values above 140.0 mm/5days.

Figure 6.6 - Case of extreme precipitation occurred over South region of Brazil (R1) during 24/06/2014 to 28/06/2014.

Extreme rainfall [mm/5days] : Case R1– 24JUN2014 to 28JUN2014



Source: Author's production.

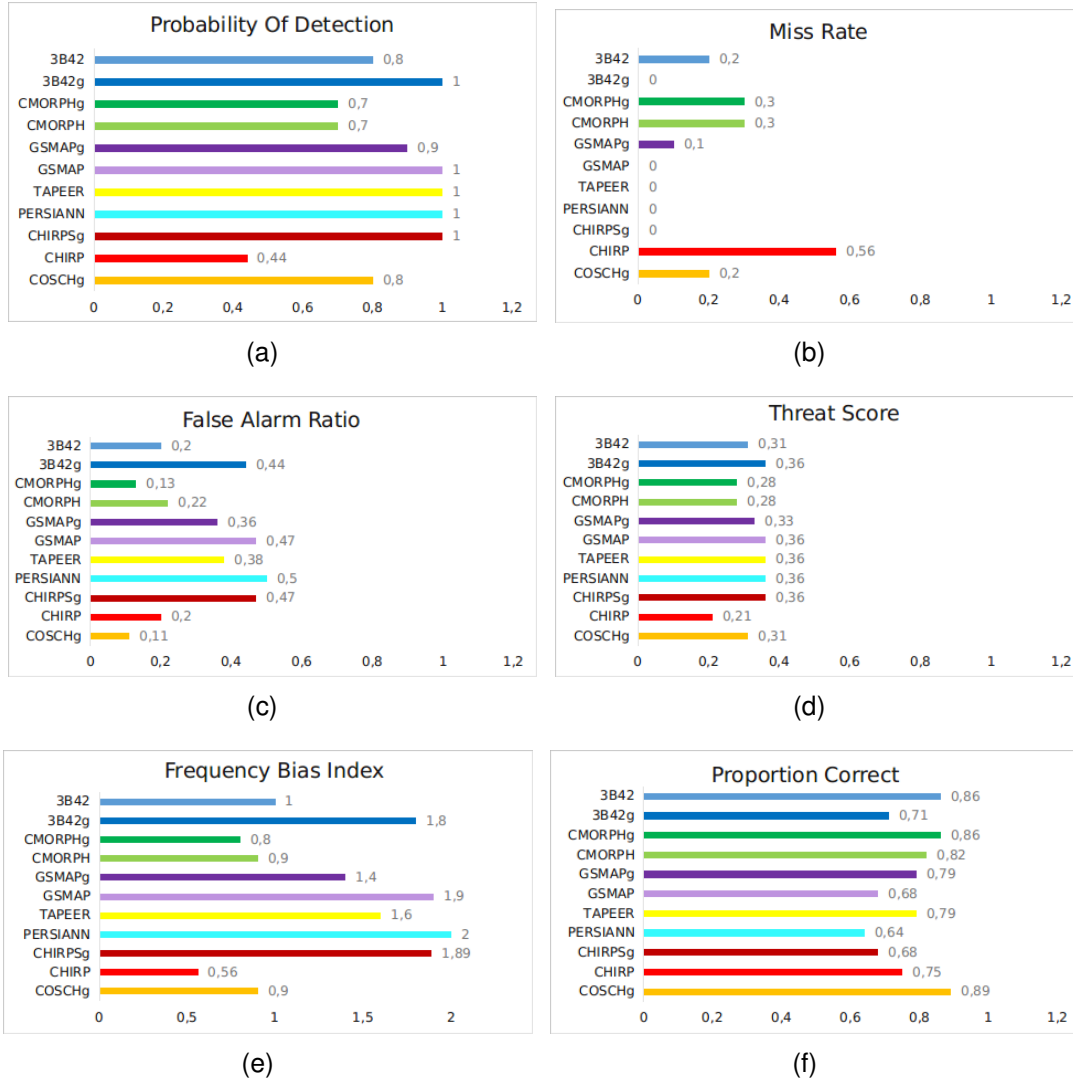
Better POD and MR scores were presented by 3B42g, GSMAP, TAPEER, PER-



SIANN and CHIRPSg products ( Figure 6.7a and 6.7b ). Threat Score (Figure 6.7d) also known as Critical Success Index, takes into account hits, misses and false alarms, there is a perfect score when  $TS = 1$ , so we see that the analyzed products reach a maximum value of 0.36, which corresponds to the same products that reached  $POD = 1$ . However, these products had a high rate of false alarms up to 0.5 (Figure 6.7c). The FBI (Figure 6.7e) is an index that shows us whether the products are overestimating ( $FBI > 1$ ) or underestimating ( $FBI < 1$ ), thereby we can see that the products 3B42 and CMORPH and COSCH were the presented a metrics closer to the perfect score. The product that showed the best Proportion Correct (Figure 6.7f) was COSCHg followed by CMORPHg and 3B42.

In this way, COSCHg, CMORPHg and 3B42 products performed better in that case of extreme rainfall event in R1, presenting a low FAR (0.11; 0.13; 0.2), a high POD (0.8; 0.7; 0.8), a high PC (0.89; 0.86; 0.86) and FBI nearby of 1.0 (0.9; 0.8; 1.0), respectively.

Figure 6.7 - Bar graphs of (a) Probability Of Detection (POD), (b) Miss Rate (MR), (c) False Alarm Ratio (FAR), (d) Threat Score (TS), (e) Frequency Bias Index (FBI) and (f) Proportion Correct (PC) for 5 days accumulated precipitation over South region of Brazil during 24/06/2014 to 28/06/2014.



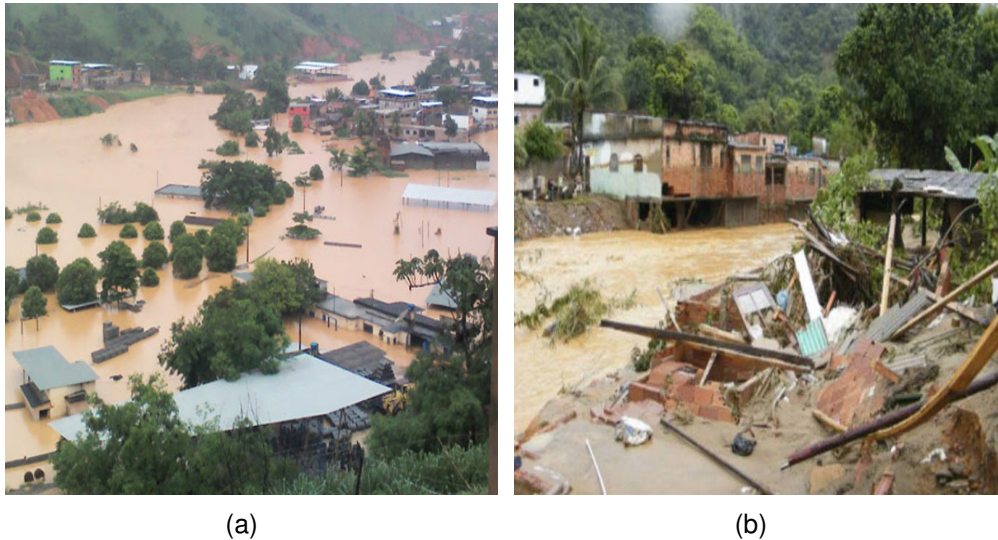
Source: Author's production.

### 6.3.2 Case study for Central Region - R2

In the Central Region of Brazil (R2), the rains from 01/01/2012 to 05/01/2012 affected several municipalities of Rio de Janeiro, Espírito Santo and Minas Gerais state, that declared a public calamity. According to Civil Defense report, more than 200 thousand people were affected and the estimated economic damage was greater than R\$ 20 million. With blocked roads, collapsing ravines and floods recorded in various places, human, material and environmental damage was

enormous. In the Figure 6.8 it shows one of the affected municipalities.

Figure 6.8 - Municipalities affected by the extreme rain. (a) Flooding in municipality of Muriaé on Minas Gerais state, (b) Collapse of houses in municipality of Duque de Caxias on Rio de Janeiro state. Photographs: Adir de Freitas Valentim Junior/VC no G1 and Vladimir Platonov/ABr/exame.com.



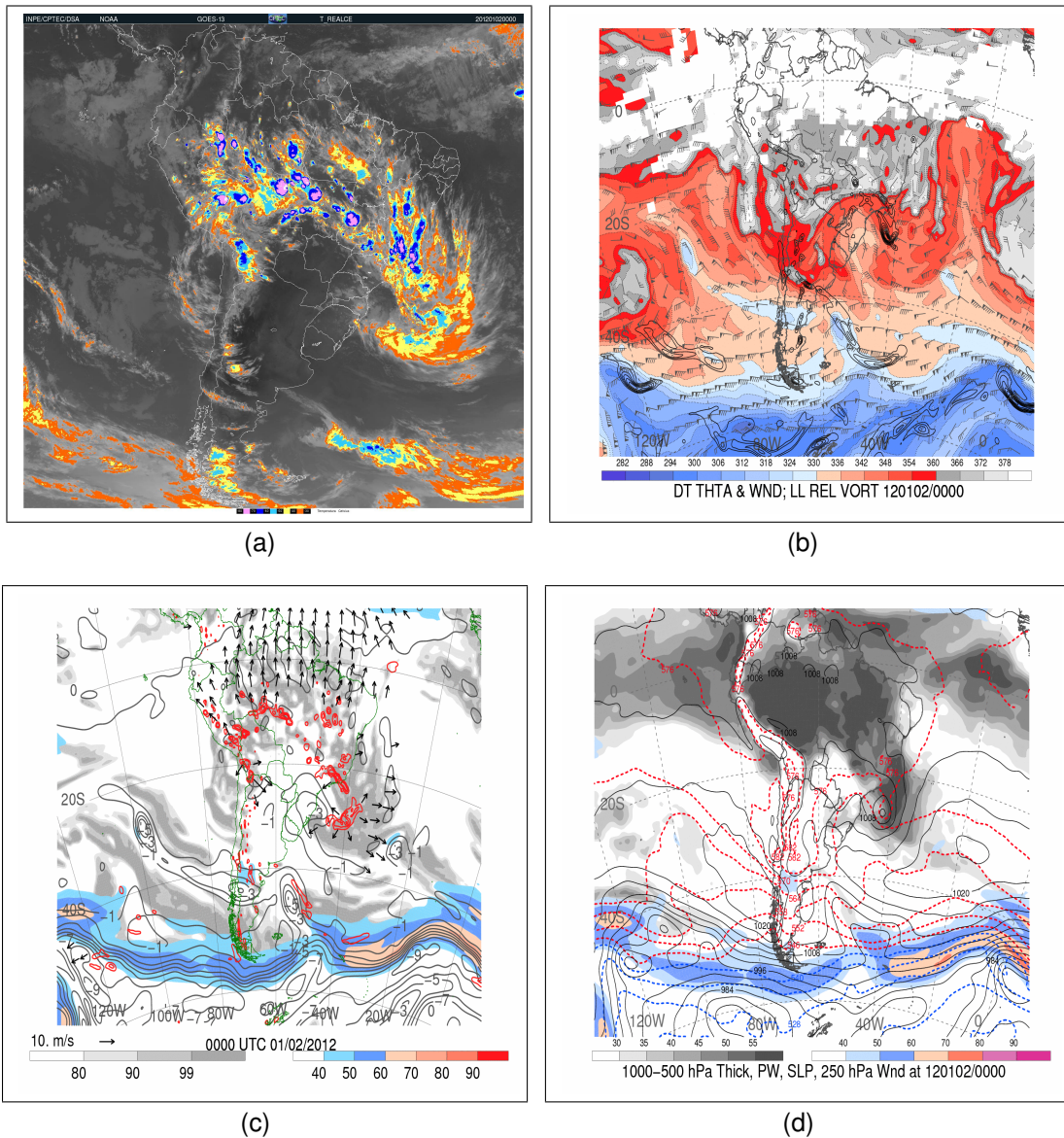
Source: G1 and Exame (2012).

For the purpose of describing the atmospheric pattern that occurred during this event, the Figure 6.9 show some fields 6-hourly  $0.5^\circ$  temporal and spacial resolutions from GFS model and analysis of IR image (represented here only by the 02/01/2012). In the Figure 6.9a noticed the existence of several convective systems which the brightness temperature were around  $-70^\circ \text{C}$  indicating that the top of the clouds was cold and consequently a system that reached a great vertical development with higher potential to produce rainfall.

Figure 6.9b shows a field that combines wind and potential temperature in the dynamic troposphere. In this event it is possible to see a troughs on the east of the South region extending to São Paulo. Advection of warm air just east/northeast of the cyclone in the ocean where the isobars are perpendicular to the thick lines. In this case, it seems that precipitation in the Southeast was associated with (i) differential advection of cyclonic vorticity by the medium/high levels (which was weak, since the troughs was further south and southwest) and (ii) the flow confluence at low levels associated with SACZ, where there was high relative humidity

(> 90.0%) with upward movement (Figure 6.9c) and probably high precipitable water. The cyclone probably caused winds from the south along the coast of Rio de Janeiro and Espírito Santo states, also favoring convergence at low levels along the SACZ (Figure 6.9d).

Figure 6.9 - Fields of atmospheric patterns from GFS model over South America for **20120102 00UTC**. **(a)** Satellite GOES image; **(b)** Potential temperature (shaded, K) and wind barbs (knots) in the dynamic tropopause, 925–850-hPa layer-averaged cyclonic relative vorticity (black contours); **(c)** 250-hPa wind speed (m s<sup>-1</sup>, shaded according to color bar), 250-hPa potential vorticity (gray contours), 250-hPa relative humidity (%), shaded according to gray scale), 600–400-hPa layer averaged ascent (red contours); **(d)** 250-hPa wind speed (m s<sup>-1</sup>, shaded according to color bar), 1000–500-hPa thickness (dashed contours), Sea Level Pressure (solid contours), total precipitable water (mm, shaded according to gray scale).

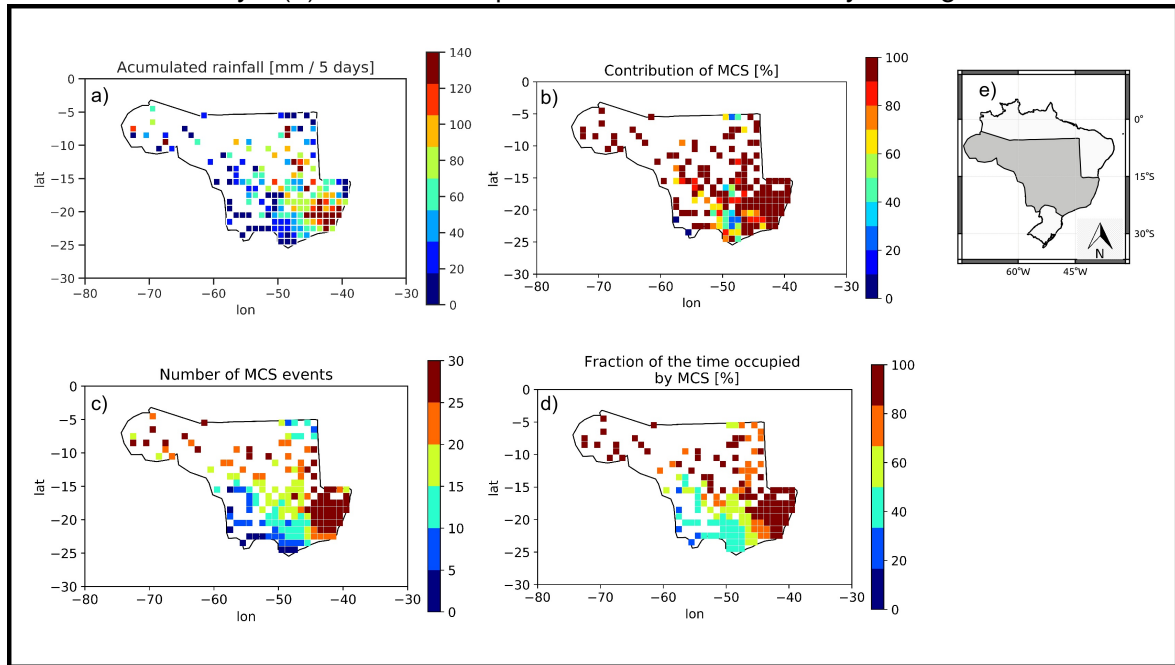


Source: CPTEC and Albany University (2012).

The influence of the MCS on the extreme rain recorded during 01/01/2012 to

05/01/2012 in Central region of Brazil (R2) is represented by Figure 6.10. It is perceived a large influence of the MCS in this event. The ratio between the rain that occurred on the days when there was a MCS record and the total rain that occurred in the 5 days is above 80.0% (Figure 6.10b) in regions such as Rio de Janeiro and south of Minas Gerais states that had the highest accumulated rainfall ( $> 140.0$  mm / 5 days) as can be seen in Figure 6.10a. In areas where the accumulated rainfall values are lower, the influence of the MCS is less ( $< 50.0$  %) as can be seen in Figure 6.10b. The Figure 6.10c represents the number of MCS events recorded by the TOOCAN algorithm over the 5 days analyzed and it is observed that the most affected area in this region recorded remained over 25 MCS during this event. Observing the fraction of the time occupied by the MCS in this region, it is noted that the MCS varied between 10.0% and 100.0% of the time (Figure 6.10d).

Figure 6.10 - (a) Accumulated rainfall recorded during 01/01/2012 to 05/01/2012 over Central Region of Brazil (R2). (b) Fraction of rain from rain gauges on days that had MCS record by rain accumulated in 5 days. (c) Number of MCS events recorded in 5 days. (d) Fraction of the days that had MCS record by 5 days. (e) Indicative map of the location of the analyzed region.



Source: Author's production.



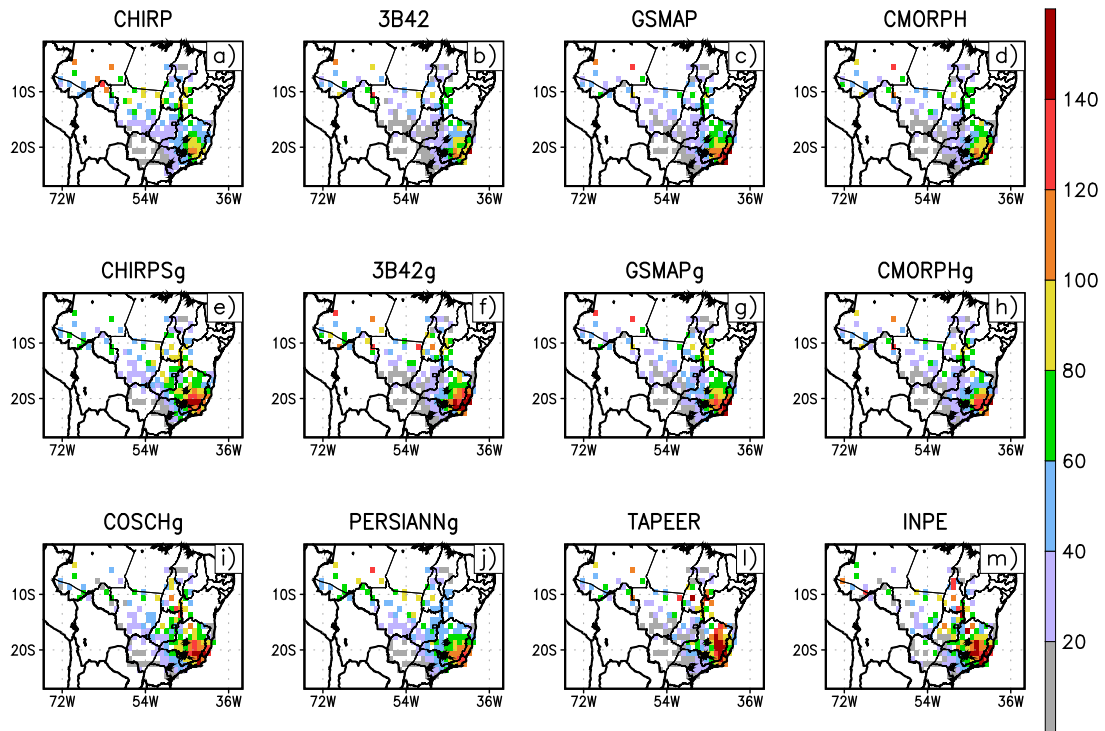
Figure 6.11 shows the spatial distribution of extreme rainfall estimate accumulated in 5 days. It is noted that in this period the rainy area occupies a large extension, going from the southeast to the northwest of Brazil, with the most intense rain occurring over the states of Rio de Janeiro, Espírito Santo and Minas Gerais. Also, note that all products were able to spatially identify the distribution of rain, however only products 3B42g, COSCHg and TAPEER (Figure 6.11(f), 6.11(i), 6.11(l) respectively) were the ones that presented similar spatial distribution to the reference data (Figure 6.11(m)), the others products underestimated the intensity of the rain ( $> 40.0$  mm). These results can be confirmed using categorical indices (Figure 6.12).

The indices show us that 3B42g, COSCHg and TAPEER were closer to the reference data, as they present a smaller bias with FBI values closer to the perfect score which is 1, even so all products underestimated the event because for all  $FBI < 1$  (Figure 6.12(e)). Looking at the other indices, it appears that the COSCHg product was the one that showed the best performance, since the MR and FAR (Figure 6.12(b), 6.12(c)) showed lower values than the other products, considering that the perfect score of these metrics are zero. Whereas POD, TS and PC (Figure 6.12(a), 6.12(d), 6.12(f)) showed higher values than the other products.

In this way, the COSCHg product performed better in this case of extreme rainfall event in R2, presenting a low FAR (0.0), a high POD (0.5) if compared with the other products, and a high PC (0.94), respectively.

Figure 6.11 - Case of extreme precipitation occurred over Central Region of Brazil (R2) during 01/01/2012 to 05/01/2012.

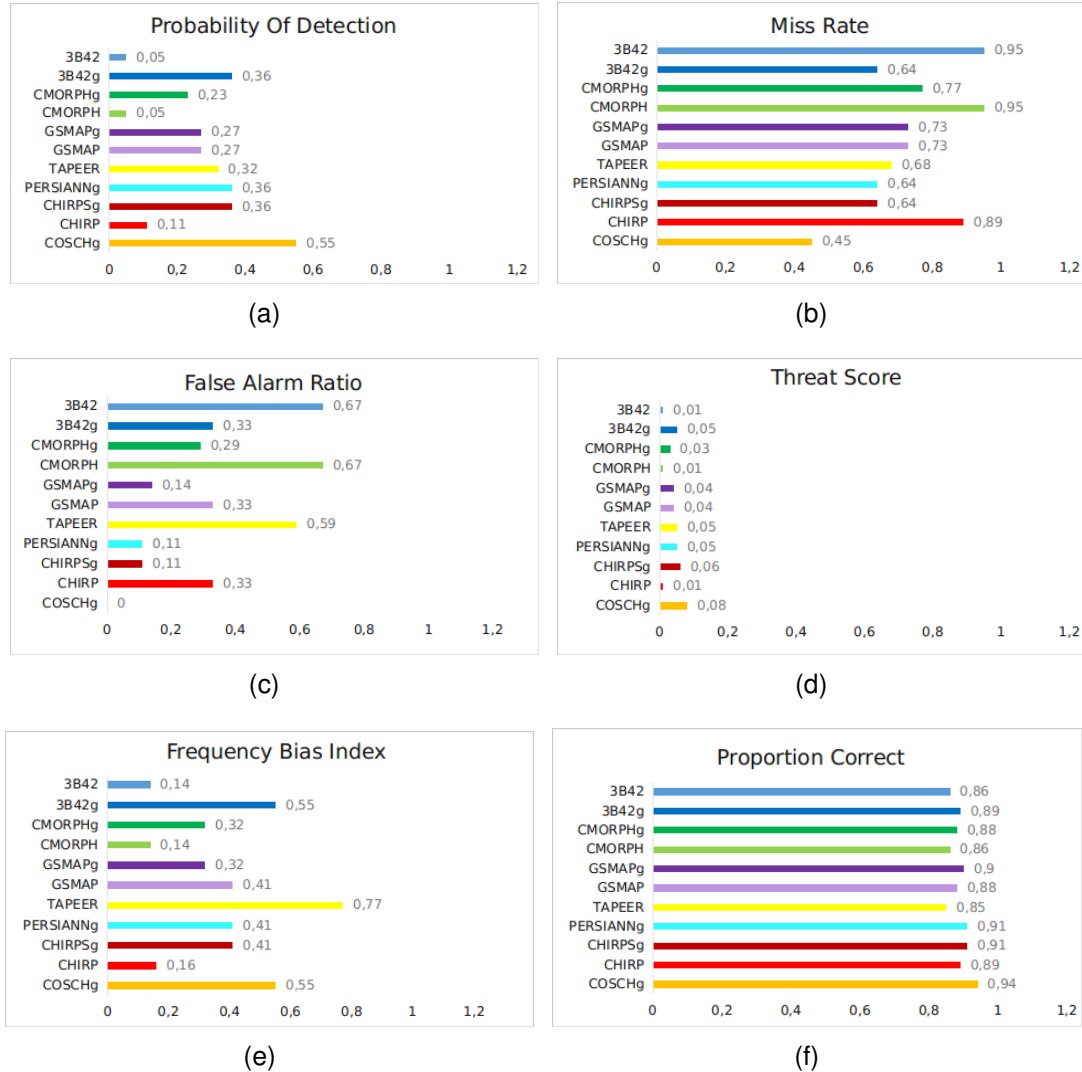
Extreme rainfall [mm/5days] : Case R2– 01JAN2012 to 05JAN2012



Source: Author's production.



Figure 6.12 - Bar graphs of (a) Probability Of Detection (POD), (b) Miss Rate (MR), (c) False Alarm Ratio (FAR), (d) Threat Score (TS), (e) Frequency Bias Index (FBI) and (e) Proportion Correct (PC) for 5 days accumulated precipitation over Central region of Brazil during 01/01/2012 to 05/01/2012.



Source: Author's production.

### 6.3.3 Case study for Northeastern - R3

In order to verify in more detail the performance of satellite rainfall estimation products over Northeastern region, a specific case of extreme rain occurred during 20/01/2016 to 24/01/2016 was identified. Under the influence of the large areas of instability associated with the SACZ, this case recorded a much higher rainfall than climatology average rainfall volume. The average precipitation for the period of January in this region is about 200 mm month (DINIZ et al., 2018),

however some regions recorded some 600 mm during January 2016. During the analyzed period it was observed that at least one-third of this rain was about 200 mm it was accumulated in just 5 days during January 20 to 24, 2016. Figure 6.13 shows if one of the affected municipalities in the west of the state of Bahia.

Figure 6.13 - Municipalities affected by the extreme rain. (a) Flooding in municipality of São Gabriel in Bahia state, (b) Flooding in municipality of Santa Maria da Vitoria in Bahia state. Photographs:Fabiano Pereira/Fotografe o tempo and Divulgação/Correios.

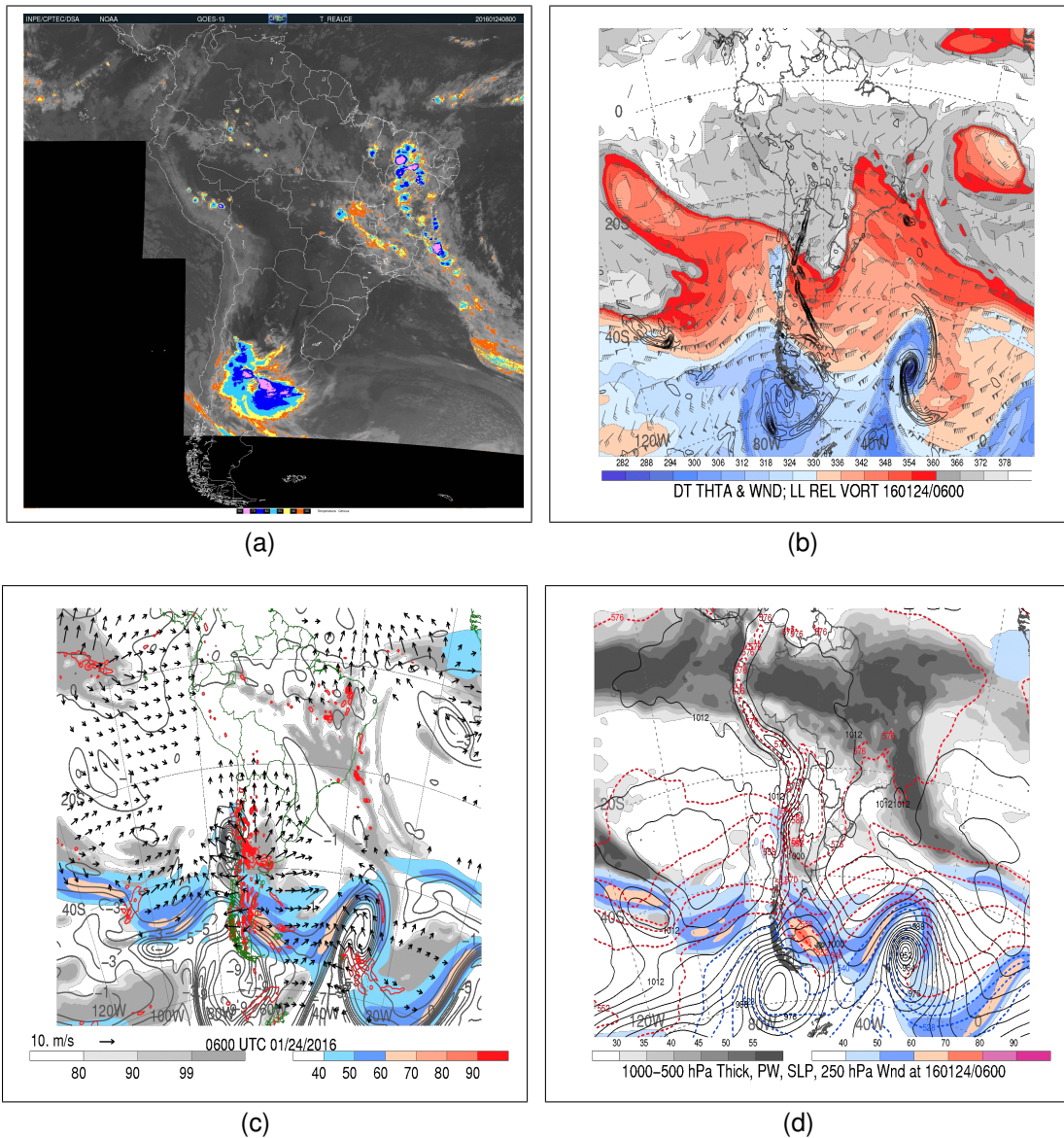


Source: Fotografe o tempo and Correios (2016).

In order to describe the atmospheric pattern that occurred during the event, Figure 6.14 shows some fields 6 hours 0.5° temporal and spatial resolutions of GFS model and an IR image analysis (represented here only by 24/01/2016). It is observed that the Intertropical Convergence Zone (ITCZ) is further south of its climatological position, contributing to the transport of moisture to the northeast region of Brazil (Figure 6.14a). It is also possible to observe an extensive trough in the dynamic troposphere operating in the center-south of Brazil. This trough in the dynamic tropopause seems to have been important. It is current above the center-north of Bahia state, where the most intense precipitation occurred. In addition, over Minas Gerais state and part of the Southeast region there is cold and dry air, which may have increased the baroclinia over Bahia state. This seems to be reflected in the jet, is noted in the dynamic tropopause map (Figure 6.14b) the north-central part of Bahia state is at the jet's equatorial entrance, although

in the Figure the jet does not appear in this area. This is because the jet is less intense than the initial 30.0 m/s of the scale (light blue) (Figure 6.14c). Therefore, still weak, the jet seems to have influenced precipitation in Bahia. The cyclonic circulation located over the equatorial Atlantic Ocean, favored the formation of a moisture convergence zone that ended up being trapped between these two systems during the 5 days analyzed. Intense divergence of winds at high levels, relative humidity above 90.0%, high values of precipitable water and intense upward movements are also seen in the R3 region (Figure 6.14c, 6.14d) . All of these factors favored the intense rains that occurred in the region.

Figure 6.14 - Fields of atmospheric patterns from GFS model over South America for **20160124 06UTC**. **(a)** Satellite GOES image; **(b)** Potential temperature (shaded, K) and wind barbs (knots) in the dynamic tropopause, 925–850-hPa layer-averaged cyclonic relative vorticity (black contours); **(c)** 250-hPa wind speed (m s<sup>-1</sup>, shaded according to color bar), 250-hPa potential vorticity (gray contours), 250-hPa relative humidity (%), shaded according to gray scale), 600–400-hPa layer averaged ascent (red contours); **(d)** 250-hPa wind speed (m s<sup>-1</sup>, shaded according to color bar), 1000–500-hPa thickness (dashed contours), Sea Level Pressure (solid contours), total precipitable water (mm, shaded according to gray scale).

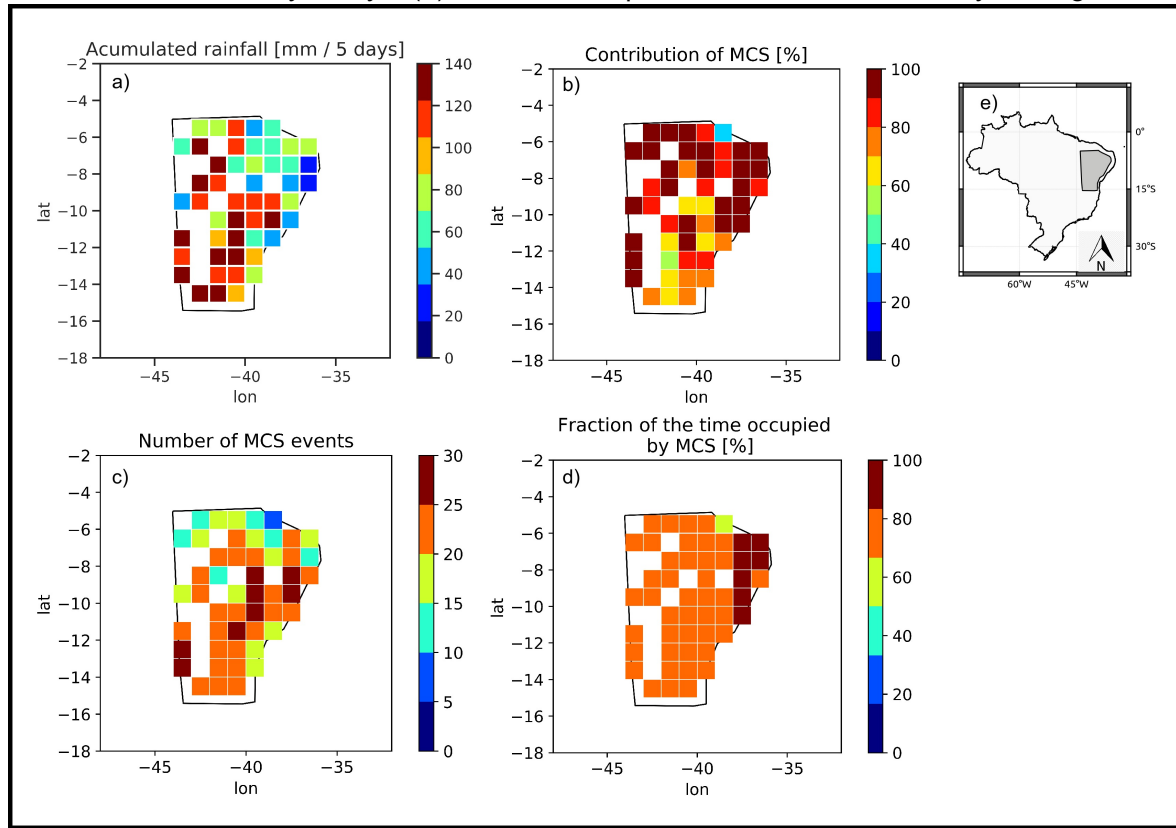


Source: CPTEC and Albany University (2016).

The influence of the MCS on the extreme rain in Northeastern region of Brazil

(R3) is represented by Figure 6.15. It is perceived the influence of the MCS in this event, however, a particularity is observed in this region. Some points of grid show a high accumulation of rain during the 5 days of the event (Figure 6.15a), but only 60.0% to 70.0% of this rain was influenced by MCS (Figure 6.15b). Therefore, the other 40.0% or 30.0% may have been generated by shallow convection that is not detected by the TOOCAN algorithm or by other systems with more stratiform characteristics. The number of MCS varied considerably in this region, being recorded more frequently from 15 to 25 MCS per grid point during the 5 days analyzed (Figure 6.15c). Over the 5 days the MCS identified by TOOCAN occupied between 80.0% and 100.0% of the time (Figure 6.15d). These results corroborate those found by (PALHARINI; VILA, 2017), where the authors analyzed the northeast region climatological behaviour of precipitating clouds. According to these authors and the stratiform clouds and shallow convective clouds are the most frequent in this region, but the associated rainfall is not as abundant as precipitation caused by deep convective clouds.

Figure 6.15 - (a) Accumulated rainfall recorded during 20/01/2016 to 24/01/2016 over Northeastern region of Brazil (R3). (b) Fraction of rain from rain gauges on days that had MCS record by rain accumulated in 5 days. (c) Number of MCS events recorded in 5 days. (d) Fraction of the days that had MCS record by 5 days. (e) Indicative map of the location of the analyzed region.



Source: Author's production.

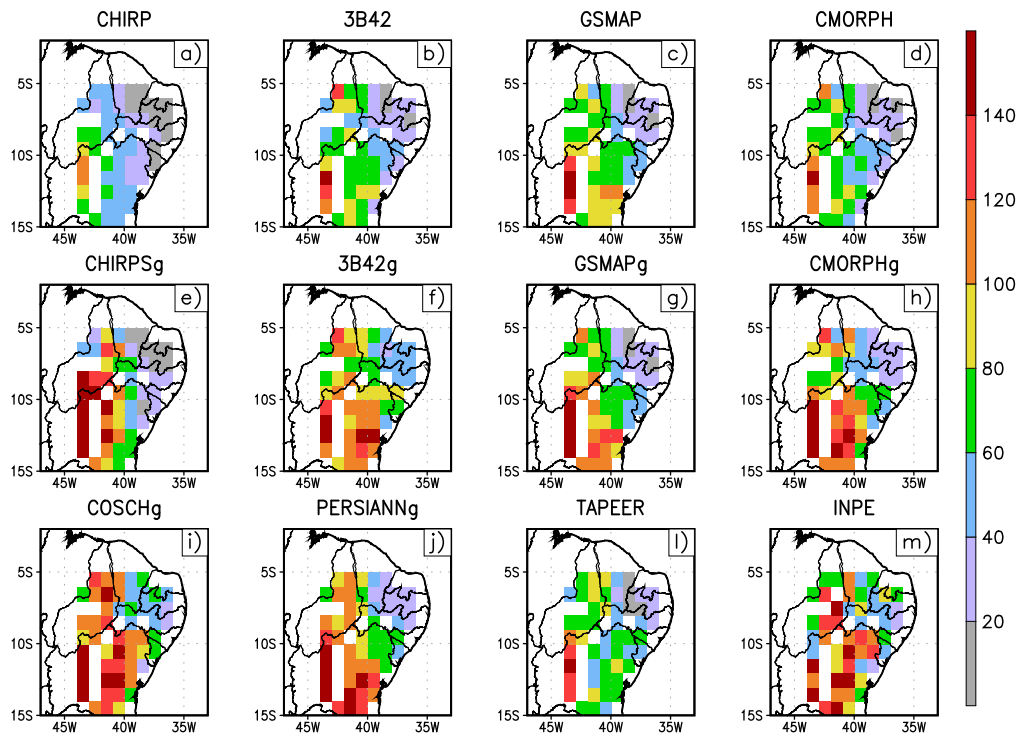
Figure 6.16 shows the spatial distribution of these precipitation event from different satellite products and noticed that the products with rain gauges adjustments (Figure 6.16e-j) performed better than the products without adjustments (Figure 6.16a-d and l) identifying the highest rainfall values as occurred in the reference data (Figure 6.16m). In this way it was analyzed some categorical metrics as POD, MR, FAR, TS, FBI and PC for this event that was analyzed considering an accumulated of 5 days from R3, as seen in the Figure 6.17. It can be seen that the products presented a perfect score for POD, TS and PC (Figure 6.17a, 6.17d and 6.17f) were COSCHg, CMORPHg and consequently are the same products that presented a perfect score in the MR and FAR (Figure 6.17b and 6.7c) for being a complementary metrics. The FBI (Figure 6.17e) is an index that shows



us whether the products are overestimating ( $FBI > 1$ ) or underestimating ( $FBI < 1$ ), with that we can see that the product CMORPHg was the presented a perfect score and the products 3B42g, PERSIANNg and COSCHg overestimate rainfall( in about 50.0 mm) and the others products underestimate ( in about 80.0 mm). In this way, the COSCHg and CMORPHg products performed better in this case of extreme rainfall event in R3, presenting a low FAR (0.35;0.39), a high POD (0.81; 0.61) if compared with the other products, and a high PC (0.73; 0.65), respectively.

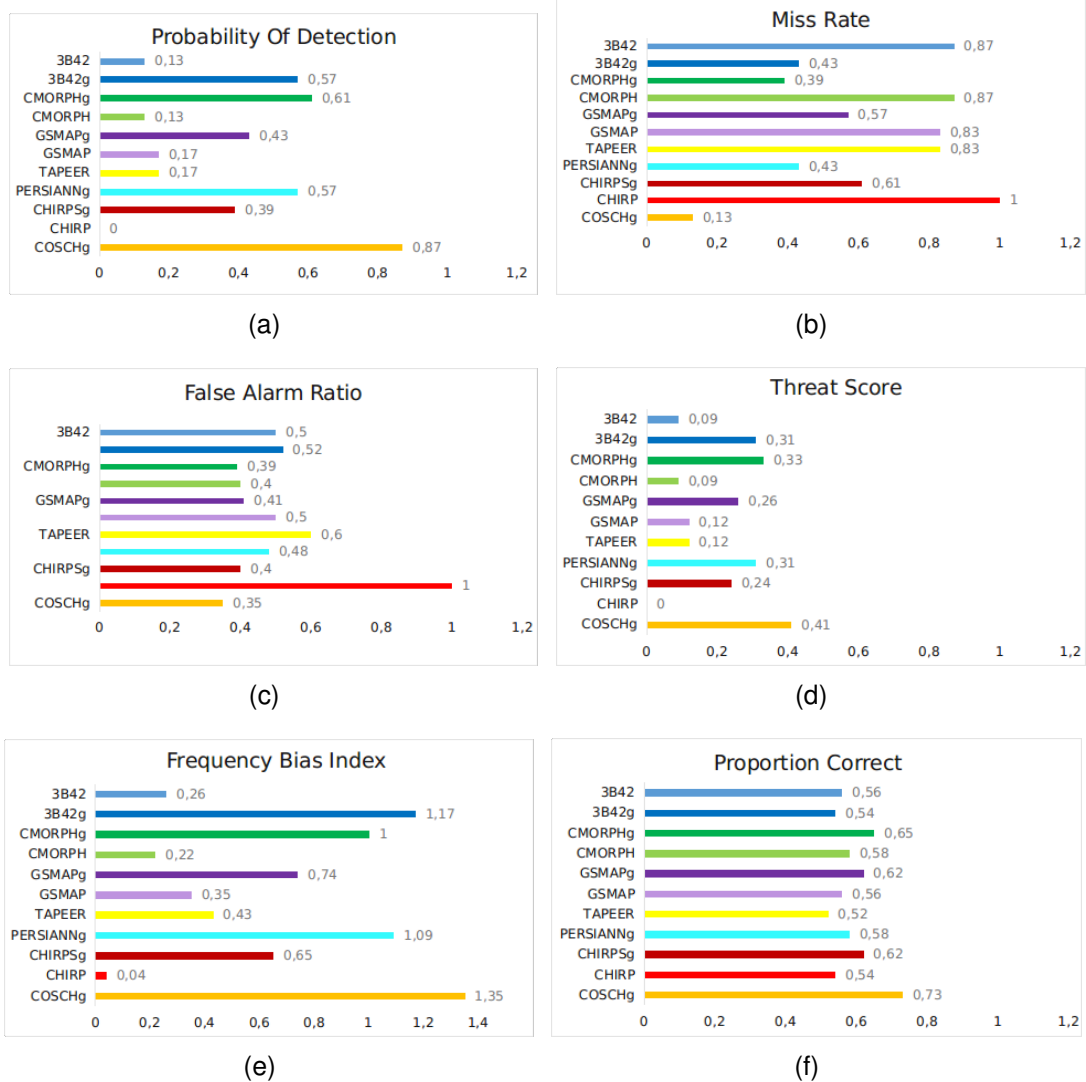
Figure 6.16 - Case of extreme precipitation occurred over Northeastern region of Brazil (R3) during 20/01/2016 to 24/01/2016.

Extreme rainfall [mm/5days] : Case R3– 20JAN2016 to 24JAN2016



Source: Author's production.

Figure 6.17 - Bar graphs of (a) Probability Of Detection (POD), (b) Miss Rate (MR), (c) False Alarm Ratio (FAR), (d) Threat Score (TS), (e) Frequency Bias Index (FBI) and (e) Proportion Correct (PC) for 5 days accumulated precipitation over Northeastern region of Brazil during 20/01/2016 to 24/01/2016.



Source: Author's production.

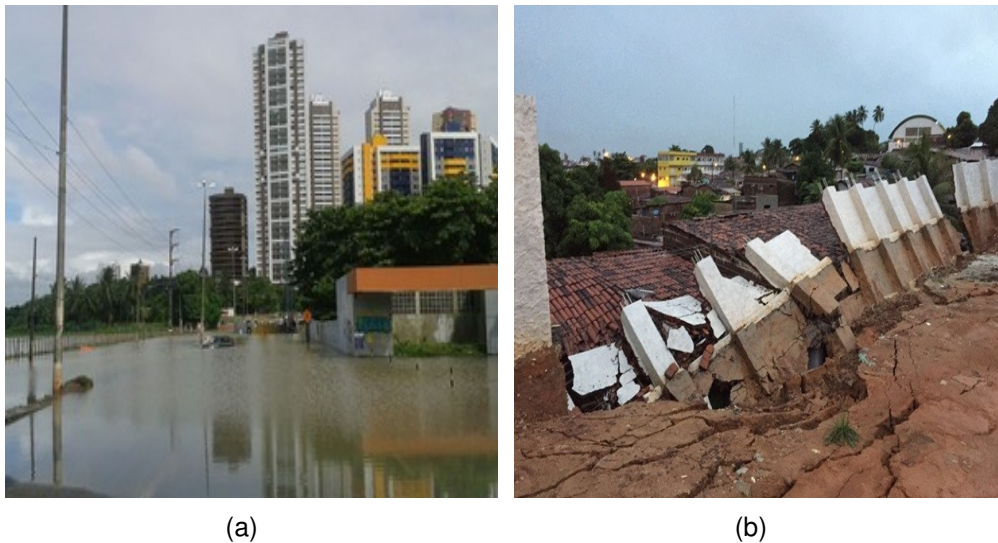
#### 6.3.4 Case study for Northeast Coast - R4

In order to verify in more detail the performance of satellite rainfall estimation products over Northeast Coast region of Brazil, a specific case of extreme rain occurred during 14/04/2016 to 18/04/2016 was chosen. The volume of rain recorded in the city of João Pessoa-PB, for example, was about 20% higher than historically expected for the months of April in this region. During 5 days analyzed was



recorded more than 200.0 mm of rainfall while the average historic is around 250.0 mm for entire month (DINIZ et al., 2018). According to the Civil Defense about 568 people were directly affected by the floods and landslides, and 1700 were without electricity.

Figure 6.18 - One of the municipalities affected by the extreme rain. (a) Flooding in Municipality of João Pessoa in Paraíba state, (b) Collapse of houses in municipality of João Pessoa in Paraíba state. Photograph: Natalia Xavier/G1 and Walter Paparazzo/G1).

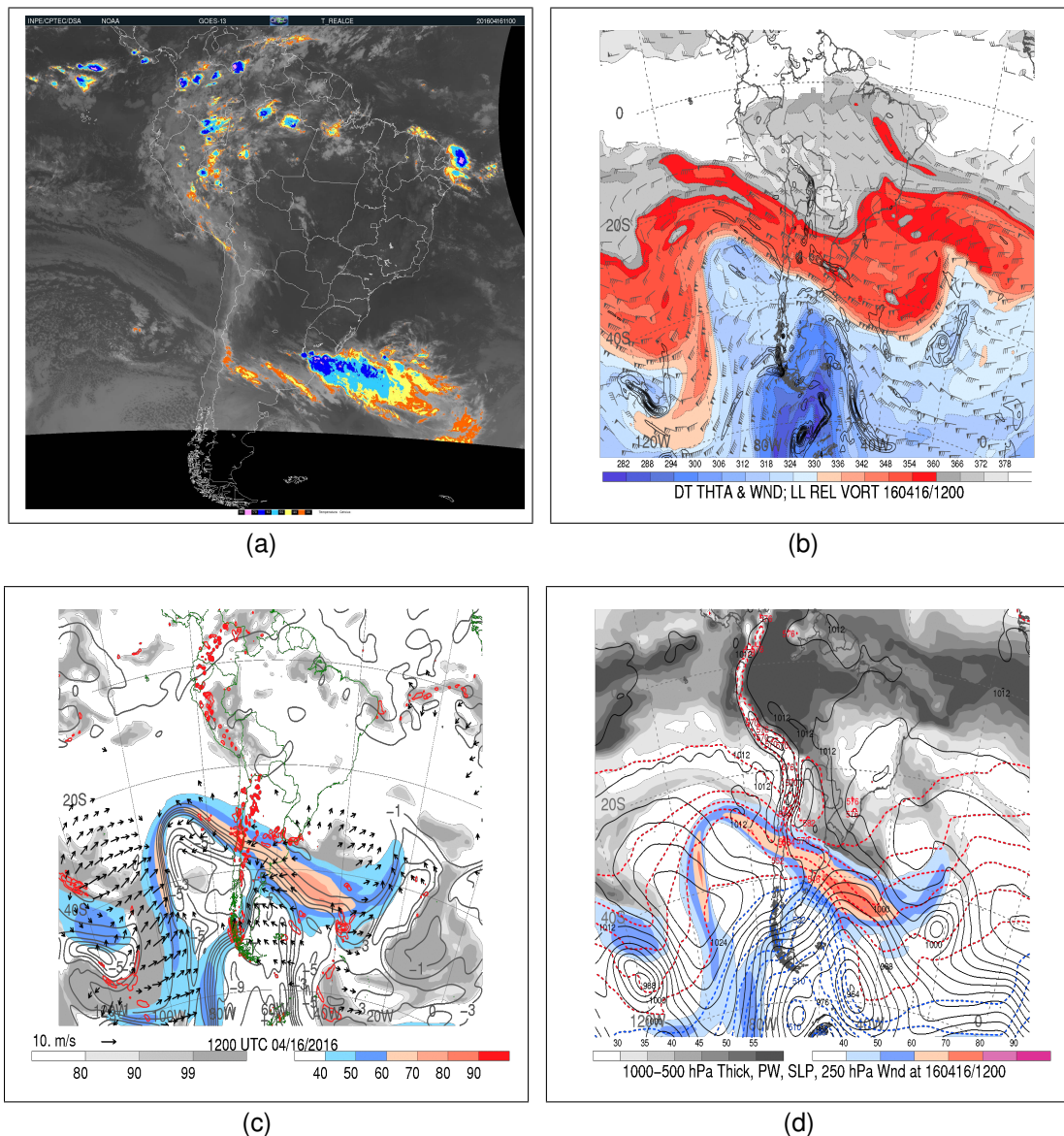


Source: G1 (2016).

For the purpose of describe the atmospheric pattern that occurred during the event, the Figure 6.19 show some fields 6-hourly  $0.5^\circ$  temporal and spatial resolutions of GFS model and an analysis of IR image (represented here only by the 16/04/2016). Figure 6.19a shows a IR image with the highlighted brightness temperature of GOES-13 over South America indicating that the top of the clouds were cold with some vertical development. It is noted that on a precipitating system with a temperature around  $-70.0$  to  $-60.0$  °C over the R4. The atmospheric pattern that occurred during this event of extreme rains on the Northeast coast can be analyzed from the atmospheric fields of the GFS, where a high level trough in the dynamic troposphere over the northeast region of Brazil was observed with a small potential temperature gradient due to advection of cooler air from the ocean to the interior of the continent (Figure 6.19b. In Figures 6.19c and 6.19d there is an upward movement and humidity above 90.0% concentrated in the

coastal zone in the Northeast, high values of precipitable water and the presence of the South Atlantic High at low levels favoring the advection of air perpendicular to the coast, these factors favor the formation of rains in this tropical region where the thermodynamics predominates.

Figure 6.19 - Fields of atmospheric patterns from GFS model over South America for **20160416 12UTC**. **(a)** Satellite GOES image; **(b)** Potential temperature (shaded, K) and wind barbs (knots) in the dynamic tropopause, 925–850-hPa layer-averaged cyclonic relative vorticity (black contours); **(c)** 250-hPa wind speed (m s<sup>-1</sup>, shaded according to color bar), 250-hPa potential vorticity (gray contours), 250-hPa relative humidity (%), 600–400-hPa layer averaged ascent (red contours); **(d)** 250-hPa wind speed (m s<sup>-1</sup>, shaded according to color bar), 1000–500-hPa thickness (dashed contours), Sea Level Pressure (solid contours), total precipitable water (mm, shaded according to gray scale).

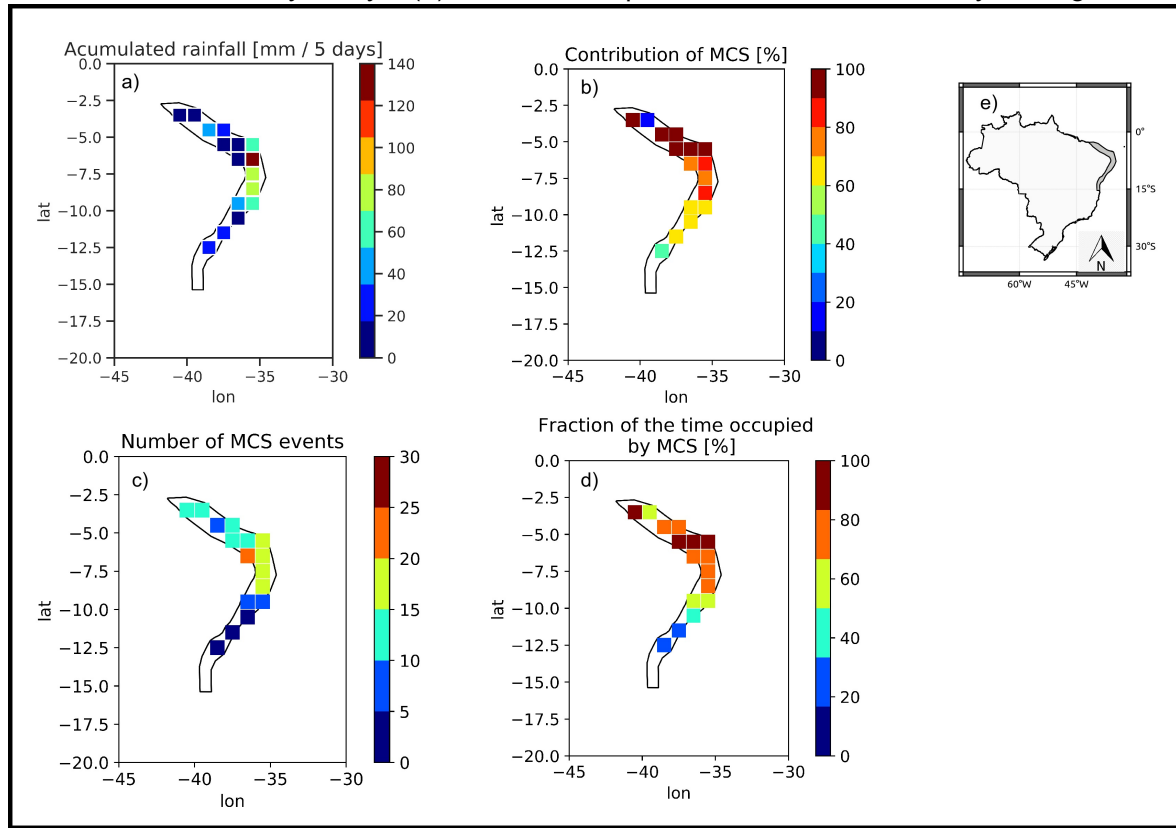


Source: CPTEC and Albany University (2016).

Figure 6.20 represents the influence of the MCS on the extreme rain recorded

during 14/04/2016 to 18/04/2016 over Northeast Coast of Brazil (R4). It is noticed in the Figure 6.20a that the accumulated rainfall in 5 days show a large variation according to the location (20.0 mm/5days to values greater than 140.0 mm/5days). As previously mentioned, the city most affected in this period was João Pessoa-PB and the surrounding municipalities, where the grid points with the highest values of accumulated rainfall are verified. It is noted in the Figure 6.20b that the fraction of rain influenced by the MCS was around 80.0%. However, areas further north of this municipality recorded less rainfall (between 10.0 mm/5days and 60.0 mm/5days) but with a greater contribution from the MCS (between 90.0% and 100.0%). While areas further south, accumulated less rainfall (between 10.0 mm/5days and 60.0 mm/5days) but with a smaller contribution from the MCS (between 50.0% and 70.0%). Deep convective systems are not frequent in this region, but when they occur they are one of the main responsible for the rains registered in this region (PALHARINI; VILA, 2017). The number of MCS varied considerably in this region, from 5 to 25 MCS per grid point during the 5 days analyzed (Figure 6.20c). The fraction of the time occupied by MCS varied from 80.0% to 100.0% in areas to the north of R4 and varied from 20.0% to 60.0% in areas to the south of R4.

Figure 6.20 - (a) Accumulated rainfall recorded during 14/04/2016 to 18/04/2016 over Northeast Coast of Brazil (R4). (b) Fraction of rain from rain gauges on days that had MCS record by rain accumulated in 5 days. (c) Number of MCS events recorded in 5 days. (d) Fraction of the days that had MCS record by 5 days. (e) Indicative map of the location of the analyzed region.

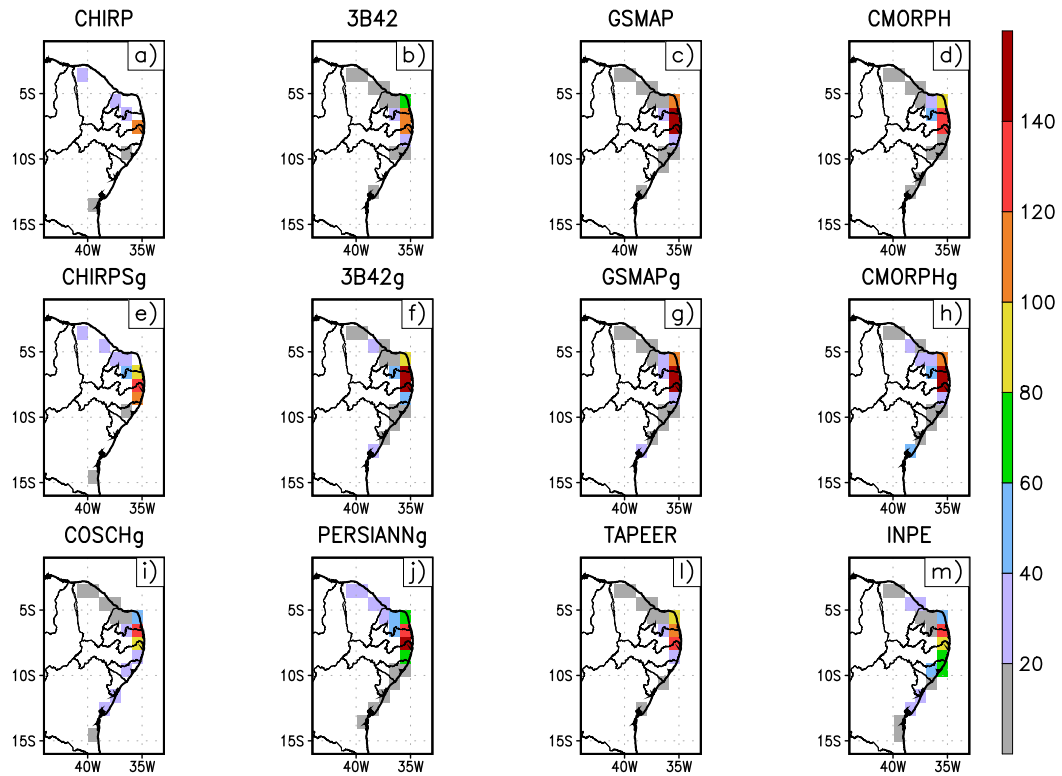


Source: Author's production.

Figure 6.21 shows the spatial distribution of these precipitation event from different satellite products. It is noticed that point of grid with more intense value of rain was located in coastal region of Paraíba state in the reference dataset (6.21m). In this region, the precipitation estimate products presented the categorical indexes was very close to the perfect score, as can be seen in Figure 6.22. The products 3B42g, CMORPH, CMORPHg, GSMAP, GSMAPg, PERSIANNg, CHIRP and COSCHg presented POD=1, MR=0 and FAR=0 indicating that these products showed a good performance over R4 region. However, the CHIRPg was the one that presented a lower performance in the estimation of this rain case in relation to the other analyzed products.

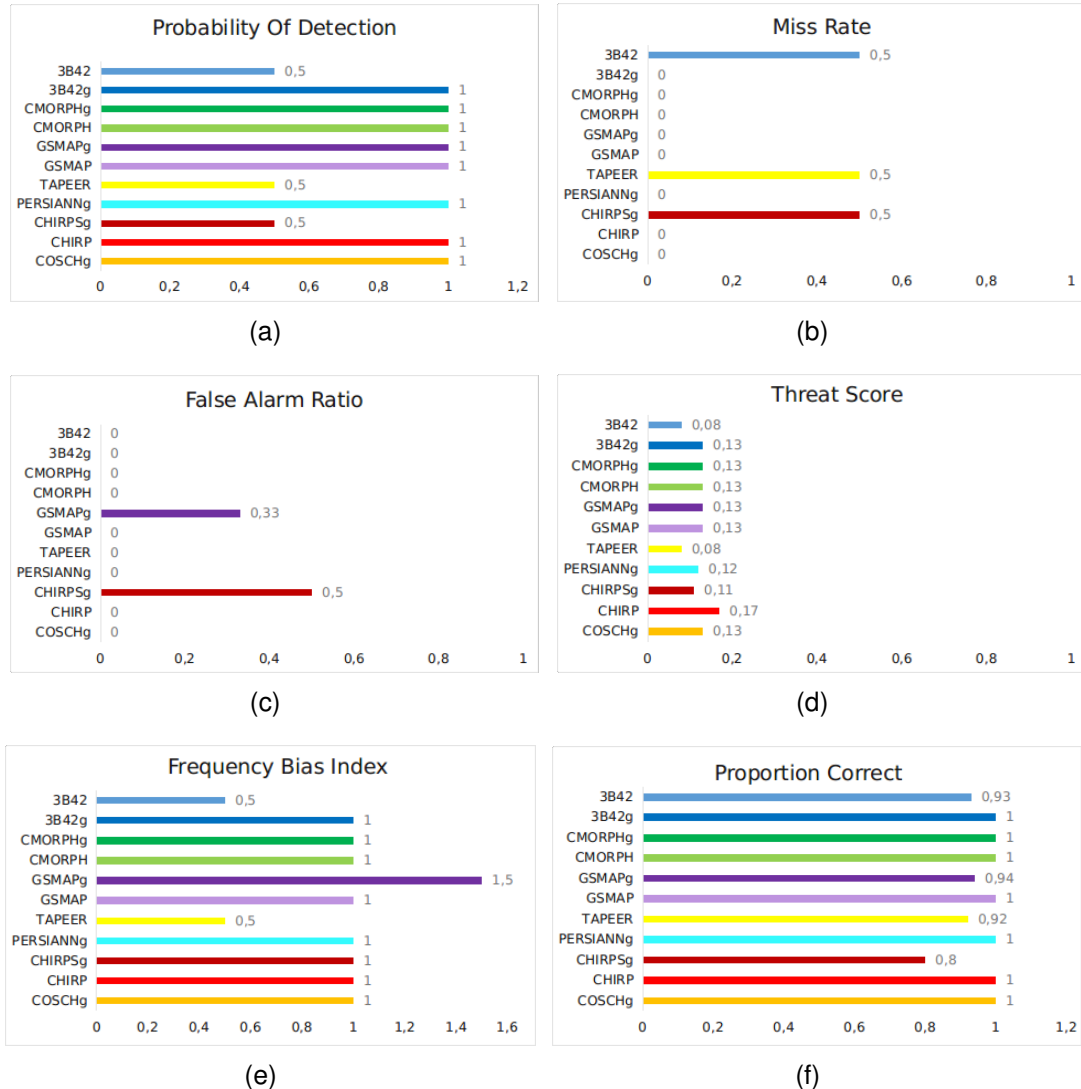
Figure 6.21 - Case of extreme precipitation occurred over Northeast Coast of Brazil (R4) during 14/04/2016 to 18/04/2016.

Extreme rainfall [mm/5days] : Case R4– 14APR2016 to 18APR2016



Source: Author's production.

Figure 6.22 - Bar graphs of **(a)** Probability Of Detection (POD), **(b)** Miss Rate (MR), **(c)** False Alarm Ratio (FAR), **(d)** Threat Score (TS), **(e)** Frequency Bias Index (FBI) and **(f)** Proportion Correct (PC) for 5 days accumulated precipitation over **Northeast Coast region of Brazil during 14/04/2016 to 18/04/2016**.



Source: Author's production.

### 6.3.5 Case study for North Brazil - R5

In order to verify in more detail the North region of Brazil, a specific case of extreme rain occurred during 29/04/2016 to 03/05/2016 was analysed. During these period the heavy rain wreaked havoc in several neighbourhoods in the municipality of Monte Alegre in western Pará, which registered about 130.0 mm in a single day. As it is a municipality with rugged topography, the slope of the terrain

favoured sudden floods in urban areas, where slopes collapsed and streets were flooded, causing inconvenience to the local population.

According to the Civil Defense disaster report, about 145 people were left homeless, 130 people were displaced and a total of 15265 people were affected in this event. Seven neighbourhoods in the urban area were affected, where 08 homes were completely destroyed, 42 were damaged and 2700 were in the situation of isolation due to the destruction and damage of bridges. In addition to the damage that occurred in the public patrimony, such as in schools, health centres, daycare centres, water supply systems, energy, education, health, streets and streets.

According to National System of Protection and Civil Defense (SINPDEC), a projection was made of the use of approximately 580 thousand US dollars in the public sector to fully restore damage to equipment and health posts, to provide urgent and emergency services to the population, to reform damaged health posts, to restore the system water supply, to carry out the removal of debris and garbage, as well as the reconstruction of streets and public areas and normalize the flow of transport of the population as well as access to daycare centres and education.

In the private sector, the damage was slightly greater, approximately 870 thousand US dollars, because with the destruction of several bridges and secondary roads that gave access to the communities, the agricultural and agricultural inputs did not reach the municipality. This caused great losses to the commerce sector, which is based on the strong agriculture of the region, which stopped moving a large financial volume in all sectors of commerce. This situation was aggravated by the great destruction that occurred in the urban area of the city, affecting businesses, homes and the purchasing power of the population that was affected by the disaster.



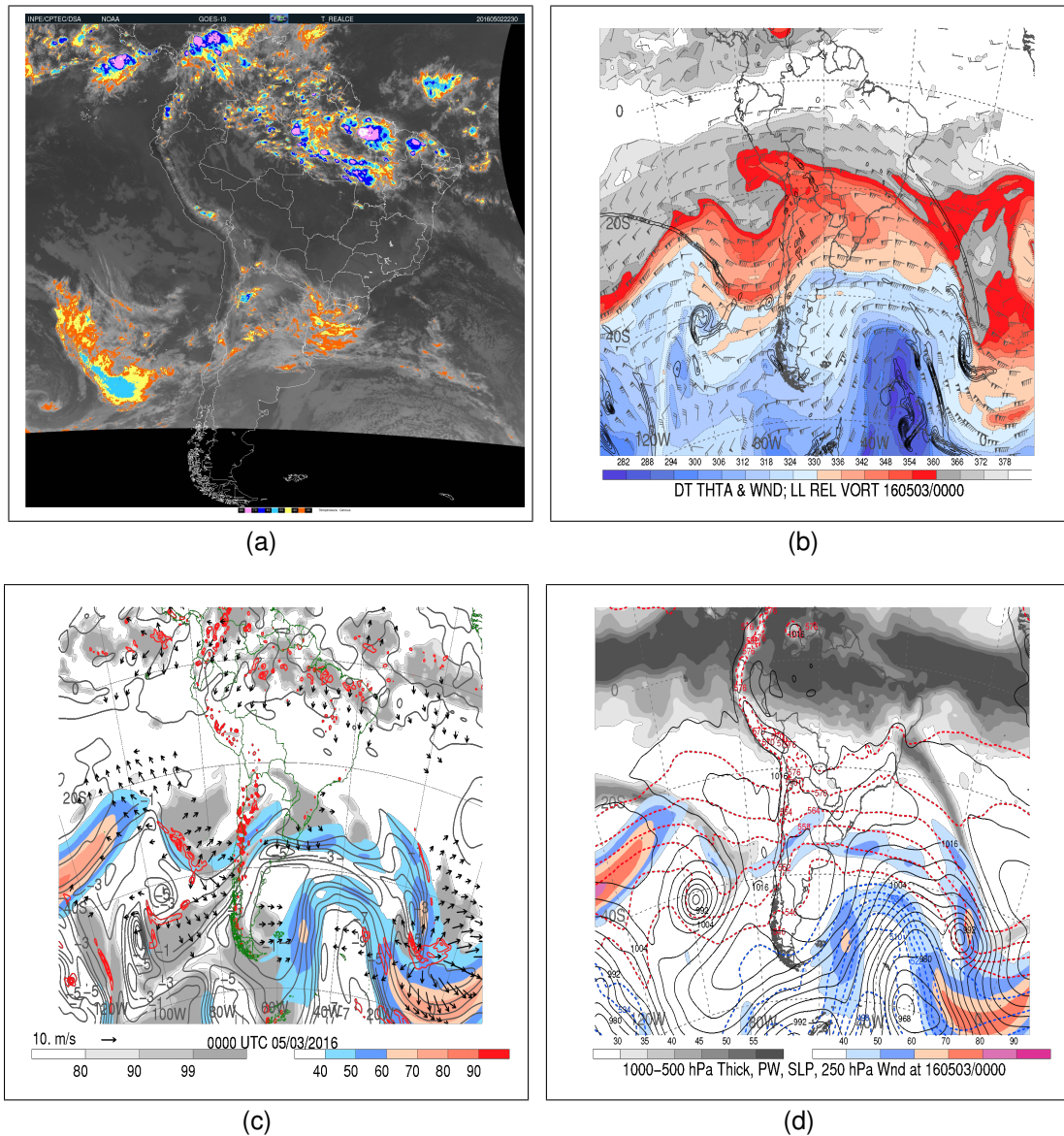
Figure 6.23 - One of the municipalities affected by the extreme rain. (a) and (b) Collapse of houses in municipality of Monte Alegre in Pará state. Photographs: Arney Barreto/G1 and Reprodução/TV Tapajós).



Source: G1 and TV Tapajós (2016).

For the purpose of describe the atmospheric pattern that occurred during the event, the Figure 6.24 show some fields 6-hourly  $0.5^\circ$  temporal and spatial of GFS model and an analysis of IR image (represented here only by the 03/05/2016). Figure 6.24a shows a IR image with the highlighted brightness temperature of GOES-13 over South America where it is noted that on a precipitating system with a temperature around  $-70$  to  $-80^\circ\text{C}$  or less over the North region of Brazil - R5, indicating that the top of the clouds were very cold and consequently a system that reached a great vertical development. This image shows several convective systems with large and small in extension. This region is characterized by having a moist atmosphere with large and intense convective activity due to the diabatic heating from the solar energy throughout the year in association with mechanisms, such as the Intertropical Convergence Zone (ITCZ) migration and Coastal Squall Lines propagation. The average life span of an Amazonian Squall Lines is 10 h (COHEN et al., 1995) and can be associated with the circulation of sea breeze. In the Figure 6.24c and 6.24d there is an upward movement, humidity above 90% and high values of precipitable water.

Figure 6.24 - Fields of atmospheric patterns from GFS model over South America for **20160503 00UTC**. **(a)** Satellite GOES image; **(b)** Potential temperature (shaded, K) and wind barbs (knots) in the dynamic tropopause, 925–850-hPa layer-averaged cyclonic relative vorticity (black contours); **(c)** 250-hPa wind speed (m s<sup>-1</sup>, shaded according to color bar), 250-hPa potential vorticity (gray contours), 250-hPa relative humidity (%), shaded according to gray scale), 600–400-hPa layer averaged ascent (red contours); **(d)** 250-hPa wind speed (m s<sup>-1</sup>, shaded according to color bar), 1000–500-hPa thickness (dashed contours), Sea Level Pressure (solid contours), total precipitable water (mm, shaded according to gray scale).

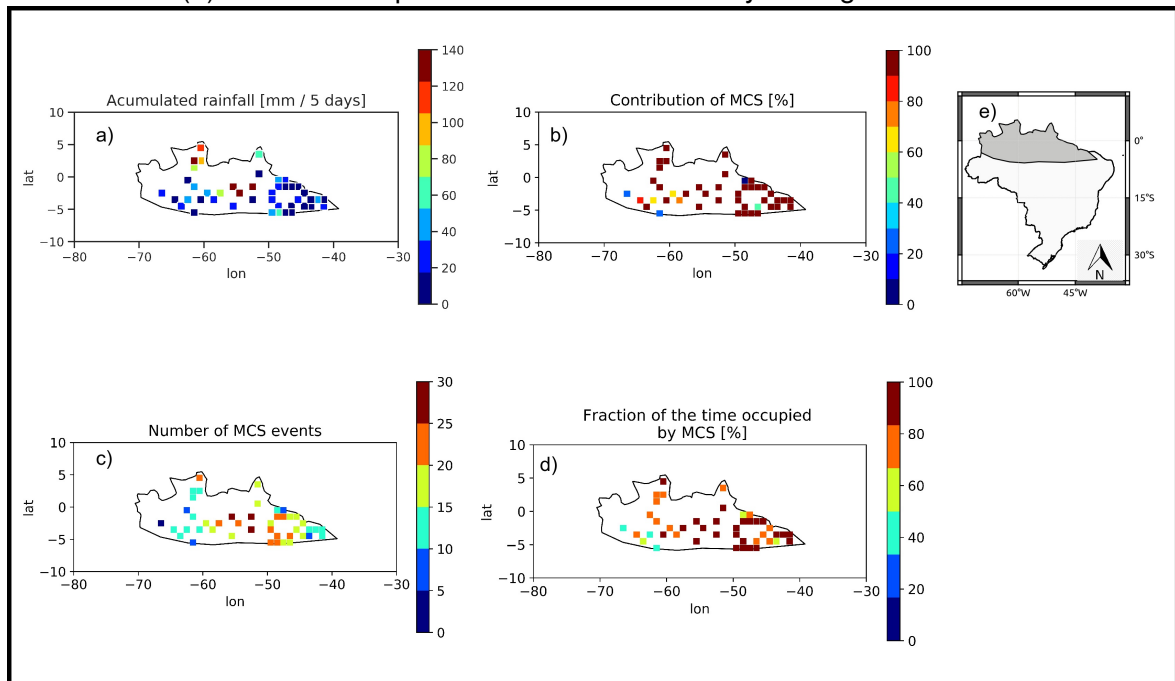


Source: CPTEC and Albany University (2016).

Figure 6.25 represents the influence of the MCS on the extreme rain recorded

during 29/04/2016 to 03/05/2016 over North region of Brazil (R5). In this region it is noted that a large influence of MCS both for the grid points that presented high values of accumulated rainfall ( $> 140.0$  mm/5days) and for the grid points with low accumulated rainfall values (between  $10.0$  mm/5days and  $40.0$  mm/5days) (Figures 6.25a-b). The number of MCS varied from 5 to 30 and the fraction of the time occupied by MCS varied from  $40.0\%$  to  $100.0\%$  (Figures 6.25c-d). An interesting result is that the areas to the east of the R5 region recorded low amounts of accumulated rain (between  $10.0$  to  $40$  mm/5 days) but this rain is highly influenced by the MCS ( $100\%$ ), with a high number of MCS registered by grid point ( $10 - 25$ ) and with the fraction of time occupied by the MCS also high ( $80.0\%$  to  $100.0\%$ ). While areas to the west of the R5 region that also registered low values of accumulated rain (between  $10.0$  and  $40.0$  mm/5 days) presented MCS contribution values varying between  $30\%$  and  $100\%$ , with a low number of MCS registered ( $10-15$ ) and with the smaller fraction of time occupied by MCS (between  $40.0\%$  and  $80\%$ ).

Figure 6.25 - (a) Accumulated rainfall recorded during 29/04/2016 to 03/05/2016 over North Brazil (R5). (b) Fraction of rain from rain gauges on days that had MCS record by rain accumulated in 5 days. (c) Number of MCS events recorded in 5 days. (d) Fraction of the days that had MCS record by 5 days. (e) Indicative map of the location of the analyzed region.

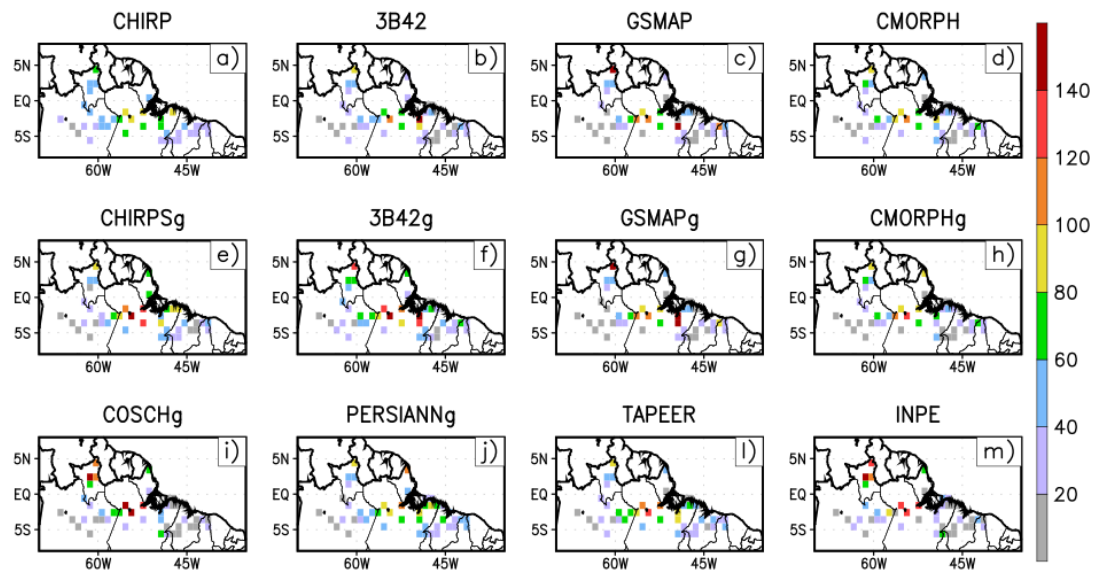


Source: Author's production.

Figure 6.26 shows the spatial distribution of these precipitation event from different satellite products. It is noticed that points of grid with more intense value of rain was located in center of Pará state and in north of Amapá state as can be seen in reference dataset (6.26m). Observing the categorical indexes for the case of extreme rain occurring in the R5 region, it is noted that the COSCHg product presents a better performance (6.26i), as it presents values closer to the perfect score in all POD, MR, FAR, TS, FBI and PC indices (Figure 6.27). However, all products underestimated the rain that occurred, considering that the  $FBI < 1$  for all products. The products with the highest false alarm and Miss Rate were the 3B42 and the CMORPH, thus the products with the lowest POD. In this way, the COSCHg product performed better in this case of extreme rainfall event in R5, presenting a low FAR (0.0), a high POD (0.55) if compared with the other products, and a high PC (0.94).

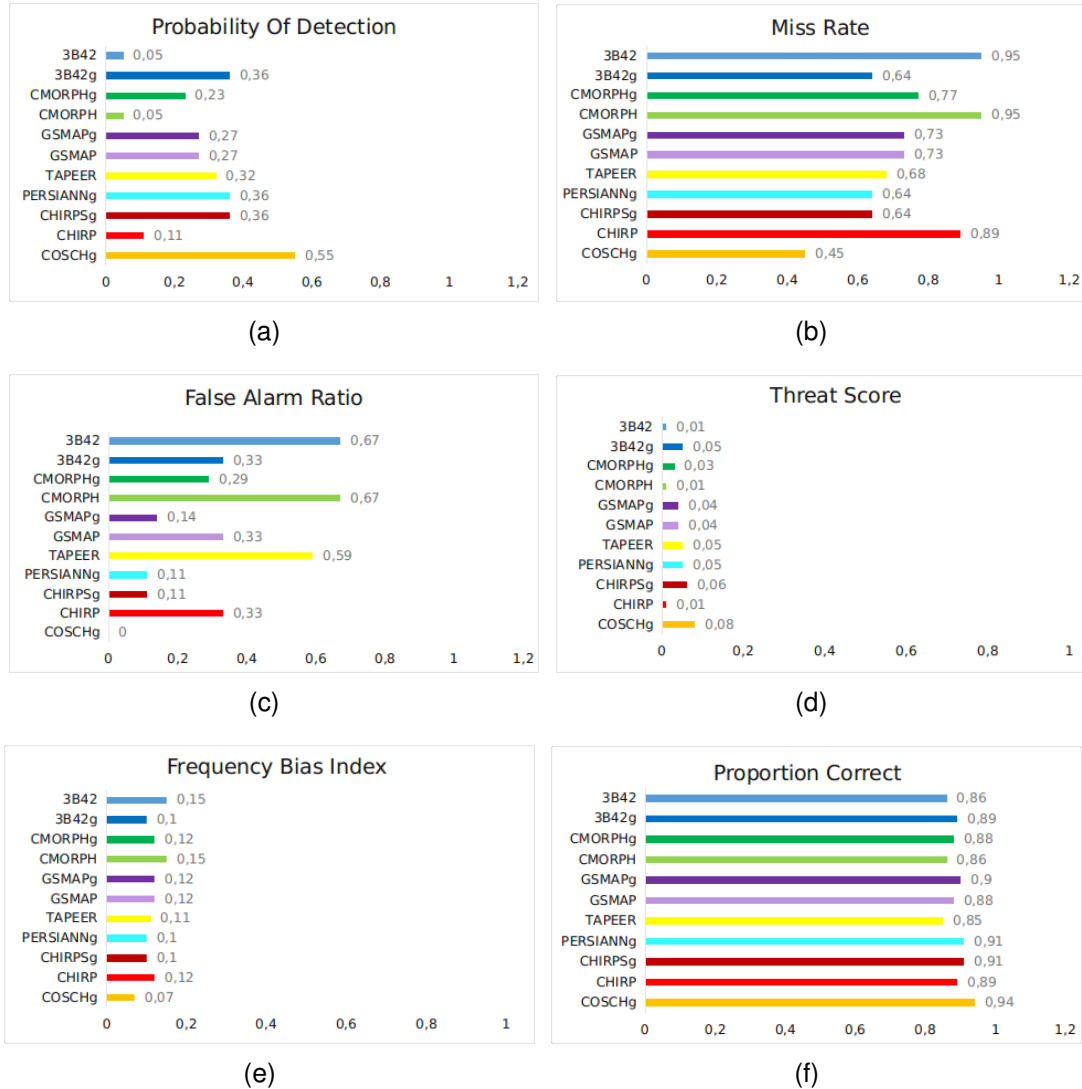
Figure 6.26 - Case of extreme precipitation occurred over North Brazil (R5) during 29/04/2016 to 03/05/2016.

Extreme rainfall [mm/5days] : Case R5– 29APR2016 to 03MAY2016



Source: Author's production.

Figure 6.27 - Bar graphs of (a) Probability Of Detection (POD), (b) Miss Rate (MR), (c) False Alarm Ratio (FAR), (d) Threat Score (TS), (e) Frequency Bias Index (FBI) and (e) Proportion Correct (PC) for 5 days accumulated precipitation over North region of Brazil during 29/04/2016 to 03/05/2016.



Source: Author's production.

## 6.4 Conclusions

The main objective of this study was to describe cases of extreme precipitation events that caused natural disasters in Brazil. Identifying whether there was an influence of Mesoscale Convective Systems (MCS) in the occurrence of these events and analyzing the performance of different Satellite Precipitation Products (SPP) in detecting the extreme rain that occurred.



For each region, the date with the highest number of grid points with maximum rainfall values was identified. The accumulated rainfall in a period of 5 days was defined as an event, being two days before and two days after the date with the highest maximum values. For this study, the observed dataset of rain gauges from INPE was used as a reference during the period from 2012 to 2016.

The description of the chosen events was made from reports in newspapers that had photographic records of the impacts caused by rain events in their archives. Another important source for describing the events was the official documents of the civil defense that report in a quantitative way the losses occurred in the affected municipalities. To describe the behavior of the atmosphere on a synoptic scale, GFS model reanalysis fields were used.

With the description of these events, it is clear that extreme rain is capable of causing great damage, regardless of which region it takes place. However, some civil defenses report this information in more detail than others. Perhaps due to the fact that natural disasters due to extreme rains are somewhat more recurrent in certain regions. For example the R1 region is characterized by registering several episodes of severe storms that end up causing damage to the municipalities that are there. For this region, it is easy to find official civil defense documents reporting the phenomenon occurred and calculations with the estimates of losses generated by the event. However, in the R3 region, characterized by being a semi-arid region, where extreme rain events occur less frequently, it was not possible to find any official civil defense document reporting the event.

With this work it was possible to identify that all regions of Brazil are prone to the occurrence of natural disasters caused by extreme rains. Although the rainfall accumulations have different intensities, the impacts affect a large part of the population, indicating that the vulnerability factor must be taken into consideration by public authorities and decision makers.

Several meteorological systems are capable of causing rain in a given region. In this work, special attention was given to the MCS, which are systems formed from deep convection that are generally responsible for severe storms. With this research, it was possible to realize that the occurrence of MCS and its contribution to the extreme rain that occurred in the analyzed cases presented different behaviors depending on the region.

In the event analyzed in the region R1 great influence of the MCS was noticed,

because over the 5 days the presence of these events in the region was identified. In the R2 region it was possible to notice a positive relationship between the MCS and the rain that occurred, because where there were the highest values of rain, there was also a high number of MCS records and where the accumulated values of rain were lower, the number of MCS were also lower. The R3 and R4 regions located in northeastern Brazil, have presented different results from the others analyzed regions, because in some grid points that presented high accumulated rain values, the contribution of the MCS existed but was not marked as in the other regions. This suggests that the extreme rain that was occurred during the events was influenced by shallow convective systems or stratiform systems that are not identified by the MCS tracking algorithm used in this work. The R5 region also had a marked influence from the MCS during the event analyzed.

In order to identify the capacity to detect extreme precipitation events in specific cases the comparison between extreme precipitation values of 11 different satellite products and rain gauge data was carried out for different regions of Brazil. For this purpose some categorical statistics such as (A), (B), (C), (D), (POD), (MR), (FAR), (TS), (FBI), (PC) was computed. The SPPs evaluated were CHIRP v2.0, CHIRPS v2.0, 3B42 RT v7.0 uncalibrated, 3B42 RT v7.0, GSMAP-NRT-no gauges v6.0, GSMAP-NRT-gauges v6.0, CMORPH v1.0 RAW, CMORPH v1.0 CRT, PERSIANN CDR, CoSch, and TAPEER v1.5, using data from the rain gauges of the INPE database as the reference. The results showed that the products that had the indexes closest to the perfect score and performer better in all regions analyzed were COSCHg and CMORPHg.

It is important to emphasize that in future analyzes it would be interesting to evaluate a greater number of events with similar characteristics for the same regions. In addition, it would be interesting, if data is available, to analyze double-polarized radar data in order to obtain a physical characterization of the storms, such as the different types of hydrometeors, the amount of ice and the electrical activity prevalent in the events extremes of rain.





## 7 MAIN CONCLUSIONS AND FUTURE WORK

This investigation aimed to obtain answers to the following questions:

- Are the satellites able to correctly estimate extreme rainfall values?
- What is the influence of MCS for extreme rainfall South America?

In order to answer these questions, the present investigation evaluated a large number of satellite products using statistical metrics and comparisons with rain data measured by rain gauges over the region considered in this work.

It was found that satellite products are capable of detecting extreme rain; however, the adjusted rain gauge products had better performance than near-real-time product versions. It is expected that the new GPM satellite constellation and the products derived from it will improve the estimation of these events. The new GPM satellite constellation will be extremely important for monitoring extreme events with the potential to cause natural disasters.

It was observed that the performance of the satellite precipitation products that include MW measurements were better than those with IR information only. In addition, this study reveals that the products without rainfall adjustments tended to underestimate the lowest values and overestimate the highest values in the southern and northeastern regions of Brazil. For this reason, a regional analysis was made and it was found that the ability of the satellite estimates depends on the location in which the precipitation events occur. The same product may perform well in one region and not in other. These results are extremely important to know which product has a better performance and the region where it occurs.

In order to answer the second scientific question, it was performed an analysis of morphological characteristics of the Mesoscale Convective Systems using CA-CATOES dataset.

According to the results, it was noticed that small systems with a duration lower than 12 hours are the ones that occur with a higher frequency. However, the systems that have a duration higher than 12 hours, play an important role in the development of extreme rain. In addition, it was observed a significant contribution of MCS on extreme precipitation in South America.

In order to have a better understanding of the results mentioned above, it was

analyzed 5 cases of natural disasters occurred in Brazil. According to the results, the accumulations of rains have different intensities and the impacts affect a large part of the population. Thus, the vulnerability factor must be taken into account by public authorities and decision makers.

Taking into account that some studies suggest that the resolution of precipitation products estimates by satellite can alter the analysis of extreme events (MA-SUNAGA et al., 2019). In future work, it is intended to carry out the validation analyzes of these products in different time scales and with a more refined resolution, in order to verify if there is an improvement in their performances. As well as a study with products that already use sensors in the new GPM satellite constellation and compare with results obtained in this investigation.

Regarding the mesoscale convective systems, it is intended make a comparison with the results obtained by TOOCAN with other tracking techniques, such as ForTraCC for example, in order to check if there is any difference compared with the results obtained in this study.

## REFERENCES

- AFONSO, J. M. S.; VILA, D. A.; GAN, M. A.; QUISPE, D. P.; BARRETO, N.; CHINCHAY, J. H.; PALHIRINI, R. Diurnal cycle assessment of hourly satellite precipitation estimates over Brazil. **Remote Sensing**, p. 1–22, 2020. 77
- AGHAKOUCHAK, A.; BEHRANGI, A.; SOROOSHIAN, S.; HSU, K.; AMITAI, E. Evaluation of satellite-retrieved extreme precipitation rates across the central United States. **Journal of Geophysics Research Atmospheric**, v. 116, n. 2, p. 1–11, 2011. ISSN 01480227. 8
- ALCÁNTARA-AYALA, I. Geomorphology, natural hazards, vulnerability and prevention of natural disasters in developing countries. **Geomorphology**, v. 47, n. 2-4, p. 107–124, 2002. ISSN 0169555X. 1, 17, 49
- ALEXANDER, D. E. **Natural disasters**. London: Springer Science., 1993. ISSN 00405736. ISBN 1581152833. Available from:  
<[https://doi.org/10.1163/{\\_}q3{\\_-}SIM{\\_-}0037](https://doi.org/10.1163/{_}q3{_-}SIM{_-}0037)>. 1
- ALTHOFF; MENEZES; CEZAR; CARVALHO; PINTO de S.; CHAGAS; OMETTO; BALBAUD; RANDOW von; SAMPAIO de S. B.; VALADARES. Climate change impacts on the sustainability of the firewood harvest and vegetation and soil carbon stocks in a tropical dry forest in Santa Teresinha Municipality, Northeast Brazil. **Forest, Ecology and Management**, v. 360, p. 367–375, 2016. ISSN 03781127. Available from:  
<<http://dx.doi.org/10.1016/j.foreco.2015.10.001>>. 57
- ALVARES, C. A.; STAPE, J. L.; SENTELHAS, P. C.; GONÇALVES, J. M.; LEONARDO; SPAROVEK, G. Köppen's climate classification map for Brazil. **Meteorologische Zeitschrift**, p. 711–728, dec 2013. 57
- ALVES, J. M. B.; SILVA, E. M. da; SOMBRA, S. S.; BARBOSA, A. C. B.; SANTOS, A. C. S. dos; LIRA, M. A. T. Eventos extremos diários de chuva no nordeste do Brasil e características atmosféricas. **Revista Brasileira de Meteorologia**, v. 32, n. 2, p. 227–233, 2017. ISSN 19824351. 28
- AMITAI, E.; PETERSEN, W.; LLORT, X.; VASILOFF, S. Multiplatform comparisons of rain intensity for extreme precipitation events. **IEEE Transactions Geoscience Remote Sensing**, v. 50, n. 3, p. 675–686, 2012. ISSN 01962892. 103

ASHOURI, H.; HSU, K. L.; SOROOSHIAN, S.; BRAITHWAITE, D. K.; KNAPP, K. R.; CECIL, L. D.; NELSON, B. R.; PRAT, O. P. PERSIANN-CDR: Daily precipitation climate data record from multisatellite observations for hydrological and climate studies. **Bulletin of the American Meteorological Society**, v. 96, n. 1, p. 69–83, 2015. ISSN 00030007. 21, 59

AUTONÈS, F.; MOISSELIN, J. **Algorithm Theoretical Basis Document for “Rapid Development Thunderstorms” (RDT-PGE11 v3.0)**. [s.n.], 2013. 73 p. Available from:

<<https://www.nwcsaf.org/AemetWebContents/ScientificDocumentation/Documentation/MSG/SAF-NWC-CDOP2-MFT-SCI-ATBD-11{ }v3.0.pdf>>. 80, 95

AWANGE, J. L.; MPELASOKA, F.; GONCALVES, R. M. When every drop counts: analysis of droughts in Brazil for the 1901-2013 period. **Science of Total Environment**, v. 566-567, p. 1472–1488, 2016. ISSN 18791026. Available from: <<http://dx.doi.org/10.1016/j.scitotenv.2016.06.031>>. 57

BECKER, A.; FINGER, P.; MEYER-CHRISTOFFER, A.; RUDOLF, B.; SCHAMM, K.; SCHNEIDER, U.; ZIESE, M. A description of the global land-surface precipitation data products of the Global Precipitation Climatology Centre with sample applications including centennial (trend) analysis from 1901-present. **Earth System Science Data**., v. 5, n. 1, p. 71–99, 2013. ISSN 18663508. 22

BERGMANN, R.; LUDBROOK, J. Different outcomes of the wilcoxon—mann—whitney test from different statistics packages. **American Statistics**, v. 54, n. 1, p. 72–77, 2000. ISSN 15372731. 27, 54

BONACHEA PICO, J. **Desarrollo, aplicación y validación de procedimientos y modelos para la evaluación de amenazas, vulnerabilidad y riesgo debidos a procesos geomorfológicos**. 1–7 p. PhD Thesis (PhD), 2006. 16

BRITO, S. S. d. B. **Ciclo diário de precipitação no norte do Brasil**. 180 p. Tese (Doutorado em Meteorologia) — Instituto Nacional de Pesquisas Espaciais (INPE), Sao José dos Campos, 2013. Available from: <<http://urlib.net/rep/8JMKD3MGP7W/3FBM5BS>>. 32

CALHEIROS, A. J. P. **Propriedades radiativas e microfísicas das nuvens continentais: uma contribuição para a estimativa da precipitação de nuvens quentes por satélite**. Tese (Doutorado em Meteorologia), 2013. 2, 18, 37, 47

CANCELADA, M.; SALIO, P.; VILA, D.; NESBITT, S. W.; VIDAL, L. Backward Adaptive Brightness Temperature Threshold Technique (BAB3T): a methodology to determine extreme convective initiation regions using satellite infrared imagery. **Remote Sensing**, v. 12, n. 2, p. 1–19, 2020. ISSN 20724292. [96](#), [99](#)

CARVALHO DA COSTA, R.; SOARES DE ARAUJO, F.; LIMA VERDE, L. Flora and life-form spectrum in an area of deciduous thorn woodland (caatinga) in northeastern, Brazil. **Journal of Arid Environments**., v. 68, n. 2, p. 237–247, 2007. ISSN 01401963. [57](#)

CARVALHO, L. M. V.; JONES, C. A satellite method to identify structural properties of mesoscale convective systems based on maximum spatial correlation tracking technique. **Journal Applied Meteorology**., v. 40, p. 1683–1701, 2001. [80](#), [95](#)

CHAMBON, P.; JOBARD, I.; ROCA, R.; VILTARD, N. An investigation of the error budget of tropical rainfall accumulation derived from merged passive microwave and infrared satellite measurements. **Quartely Journal of the Royal Meteorological Society**., v. 139, n. 673, p. 879–893, 2013. ISSN 00359009. [21](#), [59](#)

CHANGE, I. P. on C. **Managing the risks of extreme events and disasters to advance climate change adaptation. A special report of working groups I and II of the Intergovernmental Panel on Climate Change**. [S.l.: s.n.], 2012. 582 p. [101](#)

CHEN, R.; LI, Z.; KULIGOWSKI, R. J.; FERRARO, R.; WENG, F. A study of warm rain detection using A-Train satellite data. **Geophysical Research Letters**., v. 38, n. 4, p. 1–5, 2011. ISSN 00948276. [2](#), [18](#)

COHEN, J. C. P.; SILVA DIAS, M. A. F.; NOBRE, C. A. Environmental conditions associated with Amazonian squall lines: a case study. **Monthly Weather Review**, v. 123, n. 11, p. 3163–3174, 1995. ISSN 0027-0644. [58](#), [101](#), [105](#), [139](#)

COSTA, T. P. D.; CARVALHO, L. D. S. M.; MORAES, E. B. B. de. **Controle de qualidade para dados observacionais de estações meteorológicas automáticas**. Cachoeira Paulista: INPE, 2017. [24](#), [60](#), [83](#)

COTTON, W. R. Storm and cloud dynamics. **Choice Reviews Online**, v. 27, n. 07, p. 27–3929–27–3929, 1990. ISSN 0009-4978. [14](#)

DEBORTOLI, N. S.; CAMARINHA, P. I. M.; MARENGO, J. A.; RODRIGUES, R. R. An index of Brazil's vulnerability to expected increases in natural flash flooding and landslide disasters in the context of climate change. **Natural Hazards**, v. 86, n. 2, p. 557–582, 2017. ISSN 15730840. [101](#)

DEMBÉLÉ, M.; ZWART, S. J. Evaluation and comparison of satellite-based rainfall products in Burkina Faso, West Africa. **International Journal of Remote Sensing**, v. 37, n. 17, p. 3995–4014, 2016. ISSN 13665901. [18](#)

DEMIRDJIAN, L.; ZHOU, Y.; HUFFMAN, G. J. Statistical modeling of extreme precipitation with TRMM data. **Journal Applied Meteorology and Climatology**, v. 57, n. 1, p. 15–30, 2018. ISSN 15588432. [13](#)

DERECZYNSKI, C. P.; OLIVEIRA, J. S.; MACHADO, C. O. Climatologia da precipitação no município do Rio de Janeiro. **Revista Brasileira de Meteorologia**, v. 24, n. 1, p. 24–38, 2009. [28](#)

DIAZ, H. F.; MURNANE, R. J. The significance of weather and climate extremes to society: an introduction. In: DIAZ, H. F.; MURNANE, R. J. (Ed.). **Climate extreme society**. Cambridge: Cambridge University Press, 2008. p. 1–8. ISBN 9780511535840. Available from:  
<<http://ebooks.cambridge.org/ref/id/CB09780511535840A009>>. [12](#)

DINIZ, F. d. A.; RAMOS, A. M.; REBELLO, E. R. G. Brazilian climate normals for 1981-2010. **Pesquisa Agropecuaria Brasileira**, v. 53, n. 2, p. 131–143, 2018. ISSN 16783921. [31](#), [44](#), [72](#), [73](#), [104](#), [123](#), [131](#)

DONAT, M. G.; LOWRY, A. L.; ALEXANDER, L. V.; O’GORMAN, P. A.; MAHER, N. More extreme precipitation in the world’s dry and wet regions. **Nature Climate Change**, v. 6, n. 5, p. 508–513, 2016. ISSN 17586798. [1](#)

DOTZEK, N.; RABIN, R. M.; CAREY, L. D.; MACGORMAN, D. R.; MCCORMICK, T. L.; DEMETRIADES, N. W.; MURPHY, M. J.; HOLLE, R. L. Lightning activity related to satellite and radar observations of a mesoscale convective system over Texas on 7-8 April 2002. **Atmospheric Research**, v. 76, n. 1-4, p. 127–166, 2005. ISSN 01698095. [91](#)

DURKEE, J. D.; MOTE, T. L.; SHEPHERD, J. M. The contribution of mesoscale convective complexes to rainfall across subtropical South America. **Journal of Climate**, v. 22, n. 17, p. 4590–4605, 2009. ISSN 08948755. [3](#), [101](#)

EASTERLING, D. R. Climate extremes: observations, modeling, and impacts. **Science.**, v. 289, n. 5487, p. 2068–2074, 2000. ISSN 00368075. Available from: <<http://www.sciencemag.org/cgi/doi/10.1126/science.289.5487.2068>>. 15

EBERT, E. E.; JANOWIAK, J. E.; KIDD, C. Comparison of near real time precipitation estimates from satellite observations and numerical. v. 88, n. 1, p. 47–64, 2007. 30, 58

FALCK, A. S.; VILA, D.; TOMASELLA, J.; MAGGIONI, V.; DINIZ, F. L. Avaliação de um Modelo Estocástico de Erro Multidimensional Aplicado a Estimativas de Precipitação por Satélite. **Revista Brasileira de Meteorologia.**, v. 31, n. 1, p. 52–63, 2016. ISSN 0102-7786. Available from: <[http://www.scielo.br/scielo.php?script=sci\\_arttext&pid=S0102-77862016000100052&lng=pt&tlng=pt](http://www.scielo.br/scielo.php?script=sci_arttext&pid=S0102-77862016000100052&lng=pt&tlng=pt)>. 8

FERRARO, R. R. Past, present and future of microwave operational rainfall algorithms. In: LEVIZZANI V., BAUER P., TURK F.J. (Ed.). **Measuring precipitation from space. Advanced Global Change Research.** 28. ed. Springer, Dordrecht, 2007. chapter 15. ISBN 78-1-4020-5835-6. Available from: <[https://doi.org/10.1007/978-1-4020-5835-6\\_15](https://doi.org/10.1007/978-1-4020-5835-6_15)>. 2

FERREIRA, V.; ANABOR, V. Climatologia de sistemas convectivos de mesoescala ocorridos sobre a América do Sul no período de 2005 a 2006. **Ciência e Natura**, v. 37, n. 0, 2015. ISSN 0100-8307. 90

FIELD, C. B.; BARROS, V.; STOCKER, T. F.; QIN, D.; DOKKEN, D. J.; EBI, K. L.; MASTRANDREA, M. D.; MACH, K. J.; PLATTNER, G. K.; ALLEN, S. K.; TIGNOR, M.; MIDGLEY, P. M. Managing the risks of extreme events disasters to advance climate change adaptation. In: . [S.l.: s.n.], 2012. p. 555–564. ISBN 9780470511343. 12

FIOLLEAU, T.; ROCA, R. Further investigation on the tooCan algorithm to detect and track convective systems in the tropics. 2006. Available from: <[https://www-cdn.eumetsat.int/files/2020-04/pdf\\_conf\\_p56\\_s6\\_08\\_fiolleau.pdf](https://www-cdn.eumetsat.int/files/2020-04/pdf_conf_p56_s6_08_fiolleau.pdf)>. 81

\_\_\_\_\_. An algorithm for the detection and tracking of tropical mesoscale convective systems using infrared images from geostationary satellite. **IEEE Transactions on Geoscience and Remote Sensing**, v. 51, n. 7, p. 4302–4315, 2013. ISSN 01962892. 82, 89, 107

FRANK, W. M. The life cycles of GATE systems. **Journal of Atmospheric Science.**, v. 35, 1978. [14](#)

FUNK, C.; PETERSON, P.; LANDSFELD, M.; PEDREROS, D.; VERDIN, J.; SHUKLA, S.; HUSAK, G.; ROWLAND, J.; HARRISON, L.; HOELL, A.; MICHAELSEN, J. The climate hazards infrared precipitation with stations - a new environmental record for monitoring extremes. **Science Data**, v. 2, p. 1–21, 2015. ISSN 20524463. [21](#), [59](#), [103](#)

FUNK, C.; PETERSON, P.; LANDSFELD, M.; DAVENPORT, F.; BECKER, A.; SCHNEIDER, U.; PEDREROS, D.; MCNALLY, A.; ARSENAULT, K.; HARRISON, L.; SHUKLA, S. **Algorithm and data improvements for version 2.1 of the Climate Hazards Center's InfraRed Precipitation with Stations Dataset**. [S.l.]: Springer, 2020. 209–427 p. ISBN 9783030245672. [102](#)

FUNK, C.; VERDIN, A.; MICHAELSEN, J.; PETERSON, P.; PEDREROS, D.; HUSAK, G. A global satellite assisted precipitation climatology. **Earth System Science Data Discussions**, v. 8, n. 1, p. 401–425, 2015. [76](#)

GARREAU, R. D.; WALLACE, J. M. The diurnal march of convective cloudiness over the Americas. **Monthly Weather Review**, v. 125, n. 12, p. 3157–3171, 1997. ISSN 00270644. [91](#)

GLECKLER, P. J.; TAYLOR, K. E.; DOUTRIAUX, C. Performance metrics for climate models. **Journal Geophysics Research Atmospheric**, v. 113, n. 6, p. 1–20, 2008. ISSN 01480227. [25](#), [53](#)

GOMES, H. B.; AMBRIZZI, T.; HERDIES, D. L.; HODGES, K.; PONTES DA SILVA, B. F. Easterly wave disturbances over Northeast Brazil: an observational analysis. **Advances in Meteorology**, v. 2015, 2015. ISSN 16879317. [58](#), [101](#), [105](#)

GOODMAN, S. J. **GOES-R series introduction**. [S.l.: s.n.], 2019. 1–3 p. ISBN 9780128143285. [6](#)

GOODMAN, S. J.; GURKA, J.; DE MARIA, M.; SCHMIT, T. J.; MOSTEK, A.; JEDLOVEC, G.; SIEWERT, C.; FELTZ, W.; GERTH, J.; BRUMMER, R.; MILLER, S.; REED, B.; REYNOLDS, R. R. The goes-R proving ground: accelerating user readiness for the next-generation geostationary environmental satellite system. **Bulletin of American Meteorological Society**, v. 93, n. 7, p. 1029–1040, 2012. ISSN 00030007. [2](#)



GOODMAN, S. J.; MACGORMAN, D. R. Cloud to ground lightning activity in Mesoscale Complexes Convective. **Monthly Weather Review**, v. 114, p. 2320—2328, 1986. 91

GRIMM, A. M.; BARROS, V. R.; DOYLE, M. E. Climate variability in southern South America associated with El Niño and La Niña events. **Journal of Climate**, v. 13, n. 1, p. 35–58, jan 2000. ISSN 0894-8755. Available from: <[http://journals.ametsoc.org/doi/abs/10.1175/1520-0442\(2000\)29013:3C0035:3ACVISSA3E2.0.CO;3B2](http://journals.ametsoc.org/doi/abs/10.1175/1520-0442(2000)29013:3C0035:3ACVISSA3E2.0.CO;3B2)>. 56, 101, 104

GRIMM, A. M.; TEDESCHI, R. G. ENSO and extreme rainfall events in South America. **Journal of Climate**, v. 22, n. 7, p. 1589–1609, 2009. ISSN 08948755. 56

HALLEGATTE, S.; VOGT-SCHILB, A.; BANGALORE, M.; ROZENBERG, J. Unbreakable: building the resilience of the poor in the face of natural disasters. 2016. Available from: <<http://elibrary.worldbank.org/doi/book/10.1596/978-1-4648-1003-9>>. 15

HOBOUCHIAN, P. Validation of satellite precipitation estimates over south america with a network of high spatial. In: **Proceedings of IPWG**. São José dos Campos: [s.n.], 2012. 38

HOLLANDER; WOLFE; CHICKEN, E. **Nonparametric statistical methods**. 3. ed. [S.l.: s.n.], 2013. 347–353 p. ISBN 9780080448947. 27, 54

HOU, A. Y.; KAKAR, R. K.; NEECK, S.; AZARBARZIN, A. A.; KUMMEROW, C. D.; KOJIMA, M.; OKI, R.; NAKAMURA, K.; IGUCHI, T. The global precipitation measurement mission. **Bulletin of American Meteorological Society**, v. 95, n. 5, p. 701–722, 2014. ISSN 00030007. 2, 6, 17

HOUZE JUNIOR. Mesoscale convective systems. **Review Geophysics**, v. 42, p. 101–132, 2004. 13

HOUZE JUNIOR; SMULL, B. F.; DODGE, P. Mesoscale organization of springtime rainstorms in Oklahoma. **Monthly Weather Review**, v. 118, n. 3, 1990. Available from: <[https://journals.ametsoc.org/view/journals/mwre/118/3/1520-0493\(1990\)118:0613:moosri20co2.xml](https://journals.ametsoc.org/view/journals/mwre/118/3/1520-0493(1990)118:0613:moosri20co2.xml)>. 79

HOUZE JUNIOR, R. A. Structure and dynamics of a tropical squall–line system. **Monthly Weather Review**, v. 105, n. 12, 1977. Available from:

<[https://journals.ametsoc.org/view/journals/mwre/105/12/1520-0493\\_{\\_}1977\\_{\\_}105\\_{\\_}1540\\_{\\_}sadoat\\_{\\_}2\\_{\\_}0\\_{\\_}co\\_{\\_}2.xml](https://journals.ametsoc.org/view/journals/mwre/105/12/1520-0493_{_}1977_{_}105_{_}1540_{_}sadoat_{_}2_{_}0_{_}co_{_}2.xml)>. 79

HOUZE, R. A. 100 years of research on mesoscale convective systems.

**Meteorology Monograph**, v. 59, p. 17.1–17.54, 2018. ISSN 0065-9401. 13, 79

HUFFMAN, G. J.; ADLER, R. F.; MORRISSEY, M. M.; BOLVIN, D. T.; CURTIS, S.; JOYCE, R.; MCGAVOCK, B.; SUSSKIND, J. Global precipitation at one-degree daily resolution from multisatellite observations. **Journal of Hydrometeorology**, v. 2, n. 1, p. 36–50, 2001. ISSN 1525755X. 18, 58, 76

HUFFMAN, G. J.; BOLVIN, D. T.; BRAITHWAITE, D.; HSU, K.-L.; JOYCE, R.; KIDD, C.; NELKIN, E. J.; SOROOSHIAN, S.; TAN, J.; XIE, P. **Algorithm Theoretical Basis Document (ATBD) version 06 NASA Global Precipitation Measurement (GPM) Integrated Multi-satellitE Retrievals for GPM (IMERG)**. [s.n.], 2019. 1–34 p. Available from: <[https://pmm.nasa.gov/sites/default/files/document\\_{\\_}files/IMERG\\_{\\_}ATBD\\_{\\_}V06.pdf](https://pmm.nasa.gov/sites/default/files/document_{_}files/IMERG_{_}ATBD_{_}V06.pdf)>. 30

HUFFMAN, G. J.; BOLVIN, D. T.; NELKIN, E. J.; WOLFF, D. B.; ADLER, R. F.; GU, G.; HONG, Y.; BOWMAN, K. P.; STOCKER, E. F. The TRMM Multisatellite Precipitation Analysis (TMPA): quasi-global, multiyear, combined-sensor precipitation estimates at fine scales. **Journal of Hydrometeorology**, v. 8, n. 1, p. 38–55, 2007. ISSN 1525-755X. Available from:

<<http://journals.ametsoc.org/doi/abs/10.1175/JHM560.1>>. 20, 30, 59

INSTITUTO BRASILEIRO DE GEOGRAFIA E ESTATÍSTICA - IBGE. **Censo demográfico**. Rio de Janeiro, 2010. 55

ISDR, I. S. F. D. R. **Living with risk: a global review of disaster reduction initiatives**. 2004. 152 p. Available from:

<<https://www.un.org/press/en/2004/iha922.doc.htm>>. 62

JIANG, Q.; LI, W.; WEN, J.; FAN, Z.; CHEN, Y.; SCAIONI, M.; WANG, J. Evaluation of satellite-based products for extreme rainfall estimations in the eastern coastal areas of China. **Journal Integrate Environment Science**, v. 16, n. 1, p. 191–207, 2019. ISSN 19438168. Available from:

<<https://doi.org/10.1080/1943815X.2019.1707233>>. 76

JOYCE, R. J.; JANOWIAK, J. E.; ARKIN, P. A.; XIE, P. CMORPH: a method that produces global precipitation estimates from passive microwave and infrared

data at high spatial and temporal resolution. **Journal of Hydrometeorology**, v. 5, n. 3, p. 487–503, 2004. ISSN 1525755X. 58, 76

KIDA, S.; SHIGE, S.; KUBOTA, T.; AONASHI, K.; OKAMOTO, K. Improvement of rain/no-rain classification methods for microwave radiometer observations over the ocean using a 37 Ghz emission signature. **Journal of Meteorological Society Japan**, v. 87 A, p. 165–181, 2009. ISSN 00261165. 102

KIDD, C.; ; TAKAYABU, Y. N.; ; SKOFRONICK-JACKSON, G. M.; ; HUFFMAN, G. J.; ; BRAUN, S. A.; ; KUBOTA, T.; ; TURK, F. J. The Global Precipitation Measurement (GPM) mission. In: LEVIZZANI, V.; KIDD, C.; KIRSCHBAUM, D. B.; KUMMEROW, C. D.; NAKAMURA, K.; TURK, F. J. (Ed.). **Satellite precipitation measurements vol. 1**. Springer International Publishing, 2020. chapter 1, p. 3—23. ISBN 978-3-030-24568-9. Available from: <[https://doi.org/10.1007/978-3-030-24568-9\\_{\\_}1](https://doi.org/10.1007/978-3-030-24568-9_{_}1)>. 102

KIDD, C.; KNIVETON, D. R.; TODD, M. C.; BELLERBY, T. J. Satellite rainfall estimation using combined passive microwave and infrared algorithms. **Journal of Hydrometeorology**, v. 4, n. 6, p. 1088–1104, 2003. ISSN 1525-755X. Available from: <[http://journals.ametsoc.org/doi/abs/10.1175/1525-7541{\\_%}282003{\\_%}29004{\\_%}3C1088{\\_%}3ASREUCP{\\_%}3E2.0.CO{\\_%}3B2](http://journals.ametsoc.org/doi/abs/10.1175/1525-7541{_%}282003{_%}29004{_%}3C1088{_%}3ASREUCP{_%}3E2.0.CO{_%}3B2)>. 58, 76, 111

KIMANI, M. W.; HOEDJES, J. C.; SU, Z. An assessment of satellite-derived rainfall products relative to ground observations over East Africa. **Remote Sensing**, v. 9, n. 5, 2017. ISSN 20724292. 38, 46

KIRSCHBAUM, D.; STANLEY, T. A global landslide hazard assessment model for situational awareness. **Earth's Future**, v. 1, p. 10–35, 2017. ISSN 23284277. 1

KIRSCHBAUM, D. B.; STANLEY, T.; SIMMONS, J. A dynamic landslide hazard assessment system for Central America and Hispaniola. **Earth's Future**, v. 1, p. 2257–2272, 2015. 1

KOUSKY, V. E.; CHUG, P. S. Fluctuations in annual rainfall for northeast Brazil. **Journal of Meteorological Society Japan**, v. 56, n. 5, p. 457–465, 1978. ISSN 0026-1165. Available from: <[https://www.jstage.jst.go.jp/article/jmsj1965/56/5/56\\_{\\_}5\\_{\\_}457/{\\_}article](https://www.jstage.jst.go.jp/article/jmsj1965/56/5/56_{_}5_{_}457/{_}article)>. 57, 105

KOUSKY, V. E.; GAN, M. A. Upper tropospheric cyclonic vortices in the tropical South Atlantic. **Tellus**, v. 33, n. 6, p. 538–551, 1981. ISSN 00402826. 57, 105

KUBOTA, T.; AONASHI, K.; USHIO, T.; SHIGE, S.; TAKAYABU, Y. N.; KACHI, M.; ARAI, Y.; TASHIMA, T.; MASAKI, T.; KAWAMOTO, N.; MEGA, T.; YAMAMOTO, M. K.; HAMADA, A.; YAMAJI, M.; LIU, G.; OKI, R. Global Satellite Mapping of Precipitation (GSMaP) products in the GPM Era. In: LEVIZZANI, V.; ; KIDD, C.; ; KIRSCHBAUM, D. B.; ; KUMMEROW, C. D.; ; NAKAMURA, K.; ; TURK, F. J. (Ed.). **Satellite precipitation measurements vol. 1**. Springer International Publishing, 2020. chapter 20, p. 355—373. ISBN 978-3-030-24568-9. Available from: <[https://doi.org/10.1007/978-3-030-24568-9\\_{ }20](https://doi.org/10.1007/978-3-030-24568-9_{ }20)>. 102

KUBOTA, T.; HASHIZUME, H.; SHIGE, S.; OKAMOTO, K.; AONASHI, K.; TAKAHASHI, N.; USHIO, T.; KACHI, M. Global precipitation map using satellite borne microwave radiometers by the GSMaP project: production and validation. **International GeoScience Remote Sensing Symposium**, v. 45, n. 7, p. 2584–2587, 2006. ISSN 01962892. 20, 59

KULIGOWSKI, R. J.; LI, Y.; HAO, Y.; ZHANG, Y. Improvements to the GOES-R rainfall rate algorithm. **Journal of Hydrometeorology**, v. 17, n. 6, p. 1693–1704, 2016. ISSN 15257541. 102

KUMMEROW, C.; BARNES, W.; KOZU, T.; SHIUE, J.; SIMPSON, J. The Tropical Rainfall Measuring Mission (TRMM) sensor package. **Journal Atmospheric Ocean Tecnology**, v. 15, n. 3, p. 809–817, 1998. ISSN 07390572. 2, 6, 17

KUNG, S. Y. **Kernel methods and machine learning**. [S.l.: s.n.], 2014. ISBN 978-1107024960. 26, 53, 84

LAU, K. M.; WU, H. T. Warm rain processes over tropical oceans and climate implications. **Geophysics Research Letter**, v. 30, n. 24, p. 2–6, 2003. ISSN 00948276. Available from: <<http://doi.wiley.com/10.1029/2003GL018567>>. 1, 17

LEMON, J. Plotrix: a package in the red light district of R. **R-News**, v. 6, n. January 2006, p. 8–12, 2006. 25, 53

LENTERS, J. D.; COOK, K. H. Simulation and diagnosis of the regional summertime precipitation climatology of South America. **Journal of Climate**, v. 8, p. 2988–3005, 1995. 57, 105

LEVIZZANI, V.; KIDD, C.; KIRSCHBAUM, D. B.; KUMMEROW, C. D.; NAKAMURA, K.; TURK, J. **Satellite precipitation measurement**. [S.l.: s.n.], 2020. 500 p. ISBN 9783030245672. 50

LEVIZZANI, V.; KIDD, C.; KIRSCHBAUM, D. B.; KUMMEROW, C. D.; NAKAMURA, K.; TURK, F. J. **Satellite precipitation measurement volume 2**. [s.n.], 2020. ISBN 9783030357979. Available from: <http://www.springer.com/series/5588>. 50

LIEBMANN, B.; JONES, C.; CARVALHO, L. M. V. de. Interannual variability of daily extreme precipitation events in the state of São Paulo, Brazil. **Journal of Climate**, v. 14, n. 2, p. 208–18, 2001. ISSN 15200442. Available from: [http://journals.ametsoc.org/doi/abs/10.1175/1520-0442\(2001\)014\(014\)3C0208:IVODEP\(2\)3E2.0.CO;2](http://journals.ametsoc.org/doi/abs/10.1175/1520-0442(2001)014(014)3C0208:IVODEP(2)3E2.0.CO;2). 13, 27

LIU, C.; ZIPSER, E. J. "Warm rain" in the tropics: seasonal and regional distributions based on 9 yr of TRMM data. **Journal of Climate**, v. 22, n. 3, p. 767–779, 2009. ISSN 08948755. 18

LIU, J.; XIA, J.; SHE, D.; LI, L.; WANG, Q.; ZOU, L. Evaluation of six satellite-based precipitation products and their ability for capturing characteristics of extreme precipitation events over a climate transition area in China. **Remote Sensing**, v. 11, n. 12, jun 2019. ISSN 20724292. 24, 46, 50, 103

MACHADO; ROSSOW. Structural characteristics and radiative properties of tropical cloud clusters. **Monthly Weather Review**, n. 121, p. 3234–3260, 1993. Available from: [file:///C:/Users/youhe/Downloads/kdoc\\_o\\_00042\\_01.pdf](file:///C:/Users/youhe/Downloads/kdoc_o_00042_01.pdf). 79, 88

MACHADO, L. A. T. **Previsão imediata de tempestades intensas e entendimento dos processos físicos no interior das nuvens: o SOS-CHUVA**. Cachoeira Paulista: INPE, 2015. 1–49 p. 16

MACHADO, L. A. T.; LAURENT, H. The convective system area expansion over Amazonia and its relationships with convective system life duration and high-level wind divergence. **Monthly Weather Review**, v. 132, n. 3, p. 714–725, 2004. ISSN 00270644. 1

MACHADO, L. A. T.; ROSSOW, W. B.; GUEDES, R. L.; WALKER, A. W. Life cycle variations of mesoscale convective systems over the Americas. **Monthly Weather Review**, v. 126, n. 6, p. 1630–1654, 2002. ISSN 0027-0644. 95

MADDOX, R. **Mesoscale Convective Complexes - MCC**. [S.l.]: American Meteorological Society, 1980. 14 p. 14

MANN, H. B.; WHITNEY, D. R. On a test of whether one of two random variables is stochastically larger than the other. **Annual Mathematics Statistics**, v. 18, n. 1, p. 50–60, 1947. ISSN 0003-4851. [26](#), [27](#), [54](#)

MANTON, M. J.; HAYLOCK, M. R.; HENNESSY, K. J.; NICHOLLS, N.; CHAMBERS, L. E.; COLLINS, D. A.; DAW, G.; FINET, A.; GUNAWAN, D.; INAPE, K.; ISOBE, H.; KESTIN, T. S.; LEFALE, P.; LEYU, C. H.; LWIN, T.; MAITREPIERRE, L.; OUPRASITWONG, N.; PAGE, C. M.; PAHALAD, J.; PLUMMER, N.; SALINGER, M. J.; SUPPIAH, R.; TRAN, V. L.; TREWIN, B.; TIBIG, I.; YEE, D. Trends in extreme daily rainfall and temperature in southeast Asia and the South Pacific : 1961 – 1998. **International Journal of Climatology**, v. 284, p. 269–284, 2001. [13](#)

MARCELINO, E. V. **Desastres naturais e conceitos básicos**. 193. ed. Santa Maria: INPE, 2008. 37 p. [1](#), [17](#), [49](#)

MARENGO, J. A.; HASTENRATH, S. Case studies of extreme climatic events in the Amazon Basin. **Journal of Climate**, v. 6, n. 4, p. 617–627, 1993. ISSN 08948755. [58](#), [101](#), [105](#)

MARENGO, J. A.; JONES, R.; ALVESA, L. M.; VALVERDEA, M. C. Future change of temperature and precipitation extremes in South America as derived from the PRECIS regional climate modeling system. **International Journal of Climatology**, v. 2029, p. 2011–2029, 2008. [56](#)

MARENGO, J. A.; SOARES, W. R.; SAULO, C.; NICOLINI, M. Climatology of the low-level jet east of the Andes as derived from the NCEP-NCAR reanalyses: characteristics and temporal variability. **Journal of Climate**, v. 17, n. 12, p. 2261–2280, 2004. ISSN 08948755. [79](#)

MARTIN, D. W.; SCHREINER, A. J. Characteristics of West African and East Atlantic cloud clusters: a survey from GATE. **Monthly Weather Review**, v. 109, n. 8, p. 1671–1688, 1981. ISSN 00270644. Available from:  
<<https://journals.ametsoc.org/view/journals/mwre/109/8/1520-0493{ }1981{ }109{ }1671{ }cowaae{ }2{ }0{ }co{ }2.xml?tab{ }body=fulltext-display>>. [79](#)

MASSARI, C.; MAGGIONI, V. Error and uncertainty characterization. In: LEVIZZANI, V.; KIDD, C.; KIRSCHBAUM, D.; KUMMEROW, C.; K, N.; TURK, F. (Ed.). **Satellite precipitation measurements advance global change**

**research**. 69. ed. [S.l.]: Springer, Cham, 2020. chapter 4. ISBN 978-3-030-35798-6. 2

MASUNAGA, H.; SCHRÖDER, M.; FURUZAWA, F. A.; KUMMEROW, C.; RUSTEMEIER, E.; SCHNEIDER, U. Inter-product biases in global precipitation extremes. **Environment Research Letter**, v. 14, 2019. Available from: <<https://doi.org/10.1088/1748-9326/ab5da9>>. 17, 18, 40, 50, 51, 103, 148

MATTOS, E. V.; MACHADO, L. A. T. Relações das propriedades físicas das nuvens convectivas com as descargas elétricas. **Bolletín da Sociedade Brasileira Meteorologica**, p. 72–73, 2009. 3, 90

MEHRAN, A.; AGHAKOUCHAK, A. Capabilities of satellite precipitation datasets to estimate heavy precipitation rates at different temporal accumulations. **Hydrology Process**, v. 1, p. 217–247, 2014. ISSN 08856087. 8, 24

MELO, D. D. C. D.; XAVIER, A. C.; BIANCHI, T.; OLIVEIRA, P. T. S.; SCANLON, B. R.; LUCAS, M. C.; WENDLAND, E. Performance evaluation of rainfall estimates by trmm multi-satellite precipitation analysis 3b42v6 and v7 over brazil. **Journal of Geophysical Research : Atmospheres**, p. 9426–9436, 2015. 30

MILLER, D.; FRITSCH, J. M. Mesoscale convective complexes in the Western Pacific region . **Monthly Weather Review**, v. 119, n. 12. Available from: <[https://journals.ametsoc.org/view/journals/mwre/119/12/1520-0493\\_{\\_}1991\\_{\\_}119\\_{\\_}2978\\_{\\_}mccitw\\_{\\_}2\\_{\\_}0\\_{\\_}co\\_{\\_}2.xml](https://journals.ametsoc.org/view/journals/mwre/119/12/1520-0493_{_}1991_{_}119_{_}2978_{_}mccitw_{_}2_{_}0_{_}co_{_}2.xml)>. 79

MILLER, S. W.; ARKIN, P. A.; JOYCE, R. A combined microwave/infrared rain rate algorithm. **International Journal of Remote Sensing**, v. 22, n. 17, p. 3285–3307, 2001. ISSN 01431161. 58, 76, 111

MIN, S. K.; ZHANG, X.; ZWIERS, F. W.; HEGERL, G. C. Human contribution to more-intense precipitation extremes. **Nature**, v. 470, n. 7334, p. 378–381, 2011. ISSN 00280836. Available from: <<http://dx.doi.org/10.1038/nature09763>>. 1

MORALES, C. A.; FREDIANI, M. E.; MACHADO, L. A. T. Thunderstorm characteristics during the 2002 RACCI/LBA field campaign. **Conference Meteorology Applied Light Data**, v. 53, n. 9, p. 1689–1699, 2004. ISSN 1098-6596. Available from: <<http://ams.confex.com/ams/pdfpapers/85605.pdf>>. 88



MUHAMMAD, W.; YANG, H.; LEI, H.; MUHAMMAD, A.; YANG, D. Improving the regional applicability of satellite precipitation products by ensemble algorithm. **Remote Sensing**, n. 4, 2018. ISSN 2072-4292. 7, 24

NATIONAL WEATHER SERVICES. **Automated Flood Warning Systems ( AFWS )**. [S.l.], 2009. 1–17 p. 16

NEVES, D.; ARAÚJO, R.; ARAVÉQUIA, J. Análise da água precipitável e dos fluxos de calor latente/sensível no início da estação chuvosa das regiões sudeste e centro-oeste do Brasil. **Ciência e Nature**, p. 222–226, 2013. ISSN 0100-8307. 57, 68

ORLANSKI, I. A rational subdivision of scales for atmospheric processes. **Bulletin of American Meteorological Society**, v. 56, p. 527–530, 1975. 13

PALHARINI, R. S. A.; VILA, D. A. Climatological behavior of precipitating clouds in the northeast region of Brazil. **Advances in Meteorology**, v. 2017, p. 17–21, 2017. ISSN 16879317. 3, 18, 37, 47, 57, 96, 99, 105, 127, 134

PALHARINI, R. S. A.; VILA, D. A.; RODRIGUES, D. T.; QUISPE, D. P.; PALHARINI, R. C.; SIQUEIRA, R. A. D.; AFONSO, J. M. D. S. Assessment of the extreme precipitation by satellite estimates over South America. **Remote Sensing**, v. 12, p. 1–24, 2020. Available from: <<https://www.mdpi.com/2072-4292/12/13/2085>>. 50, 75, 76, 103

PEREIRA, A.; QUEIROZ FILHO, D.; GALVANI, E. Precipitação e eventos extremos: mapeamento bibliométrico de artigos científicos internacionais. **Os Desafios da Geografia Física na Fronteira do Conhecimento**, p. 1811–1821, 2017. 13

PEREIRA FILHO, A. J.; SANTOS, C. C. dos. Modeling a densely urbanized watershed with an artificial neural network, weather radar and telemetric data. **Journal of Hydrometeorology**, v. 317, n. 1-2, p. 31–48, 2006. ISSN 00221694. 16

PETKOVIĆ, V.; KUMMEROW, C. D. Understanding the sources of satellite passive microwave rainfall retrieval systematic errors over land. **Journal Applied Meteorology and Climatology**, v. 56, n. 3, p. 597–614, 2017. ISSN 15588432. 2, 18

PRAKASH, S.; MITRA, A. K.; PAI, D.; AGHAKOUCHAK, A. From trmm to gpm: how well can heavy rainfall be detected from space? **Advances Water**



**Resources**, v. 88, p. 1–7, feb 2016. ISSN 03091708. Available from:  
<<http://linkinghub.elsevier.com/retrieve/pii/S0309170815002675>>. 8

RAO, V. B.; FRANCHITO, S. H.; SANTO, C. M.; GAN, M. A. An update on the rainfall characteristics of brazil: seasonal variations and trends in 1979-2011. **International Journal of Climatology**, v. 36, n. 1, p. 291–302, 2016. ISSN 10970088. 57, 58, 105

RASMUSSEN, K. L.; CHOI, S. L.; ZULUAGA, M. D.; HOUZE, R. A. TRMM precipitation bias in extreme storms in South America. **Geophysics Research Letter**, v. 40, n. 13, p. 3457–3461, 2013. ISSN 00948276. 50

REBOITA, M. S.; GAN, M. A.; ROCHA, R. P. da; AMBRIZZI, T. Regimes de precipitação na América do Sul: uma revisão bibliográfica. **Revista Brasileira de Meteorologia**, v. 25, n. 2, p. 185–204, 2010. 19, 37, 47, 56, 103

ROCA, R.; ALEXANDER, L. V.; POTTER, G.; BADOR, M.; JUCÁ, R.; CONTRACTOR, S.; BOSILOVICH, M. G.; CLOCHÉ, S. FROGS: A daily 1° × 1° gridded precipitation database of rain gauge, satellite and reanalysis products. **Earth System Science Data**, v. 11, n. 3, p. 1017–1035, 2019. ISSN 18663516. 19, 20, 58, 60, 106

ROCA, R.; FIOLEAU, T. Extreme precipitation in the tropics is closely associated with long-lived convective systems. **Communication Earth Environment**, v. 1, n. 1, p. 1–6, 2020. ISSN 2662-4435. Available from:  
<<http://dx.doi.org/10.1038/s43247-020-00015-4>>. 3, 88, 99

RODRIGUES, D. T.; GONÇALVES, W. A.; SPYRIDES, M. H.; SANTOS E SILVA, C. M.; SOUZA, D. O. de. Spatial distribution of the level of return of extreme precipitation events in northeast brazil. **International Journal of Climatology**, p. 1–16, 2020. ISSN 10970088. 62

RODRIGUES, D. T.; GONÇALVES, W. A.; SPYRIDES, M. H. C.; SANTOS E SILVA, C. M. Spatial and temporal assessment of the extreme and daily precipitation of the tropical rainfall measuring mission satellite in northeast brazil. **International Journal Remote Sensing**, p. 1–24, 2019. ISSN 0143-1161. Available from:  
<<https://www.tandfonline.com/doi/full/10.1080/01431161.2019.1643940>>. 18

- ROSA, E. B.; PEZZI, L. P.; QUADRO, M. F. L. de; BRUNSELL, N. Automated detection algorithm for SACZ, oceanic SACZ, and their climatological features. **Frontiers Environment Science**, v. 8, 2020. ISSN 2296665X. 57, 105
- ROSSOW, W. B.; MEKONNEN, A.; PEARL, C.; GONCALVES, W. Tropical precipitation extremes. **Journal of Climate**, v. 26, n. 4, p. 1457–1466, 2013. ISSN 08948755. 50
- ROZANTE, J. R.; MOREIRA, D. S.; GONCALVES, L. G. G. de; VILA, D. A. Combining TRMM and surface observations of precipitation: technique and validation over South America. **Weather Forecast**, v. 25, n. 3, p. 885–894, 2010. ISSN 08828156. 55
- ROZANTE, J. R.; VILA, D. A.; CHIQUELTO, J. B.; FERNANDES, A.; ALVIM, D. S. Evaluation of TRMM/GPM blended daily products over Brazil. **Remote Sensing**, v. 15, n. 6, p. 814–815, 2018. ISSN 01918141. Available from: <<http://www.mdpi.com/2072-4292/10/6/882>>. 46, 55, 56, 57, 69, 103, 104
- SALIO, P.; HOBOUCHIAN, M. P.; GARCÍA SKABAR, Y.; VILA, D. Evaluation of high-resolution satellite precipitation estimates over southern South America using a dense rain gauge network. **Atmospheric Research**, v. 163, p. 146–161, 2015. ISSN 01698095. Available from: <<http://dx.doi.org/10.1016/j.atmosResearch2014.11.017>>. 18, 30, 49, 103
- SANÒ, P.; CASELLA, D.; PANEGROSSI, G.; MARRA, A.; PETRACCA, M.; DIETRICH, S. The Passive Microwave Neural Network Precipitation Retrieval (PNPR) for the cross-track scanning ATMS radiometer. **Remote Sensing**, 2018. 9
- SAPIANO, M. R. P.; ARKIN, P. A. An intercomparison and validation of high-resolution satellite precipitation estimates with 3-Hourly gauge data. **Journal of Hydrometeorology**, v. 10, n. 1, p. 149–166, 2009. ISSN 1525-755X. Available from: <<http://journals.ametsoc.org/doi/abs/10.1175/2008JHM1052.1>>. 8
- SAULO, C.; RUIZ, J.; GARCÍA SKABAR, Y. Synergism between the low-level jet and organized convection at its exit region. **Monthly Weather Review**, v. 135, n. 4, p. 1310–1326, 2007. ISSN 00270644. 79
- SCOFIELD, R. A.; KULIGOWSKI, R. J. Status and outlook of operational satellite precipitation algorithms for extreme precipitation events. **Weather**

**Forecast**, v. 18, n. 6, p. 1037–1051, 2003. ISSN 0882-8156. Available from:  
<[http://journals.ametsoc.org/doi/abs/10.1175/1520-0434\(2003\)29018:3C1037:3ASA000S;3E2.0.CO;3B2](http://journals.ametsoc.org/doi/abs/10.1175/1520-0434(2003)29018:3C1037:3ASA000S;3E2.0.CO;3B2)>. 103

SCOTT, D. W. W. **Multivariate density estimation and visualization**. 2. ed.  
[S.l.: s.n.], 2015. 26, 54, 85

SEKARANOM, A. B.; MASUNAGA, H. Origins of heavy precipitation biases in the TRMM PR and TMI products assessed with cloudsat and reanalysis data. **Journal Applied Meteorology and Climatology**, v. 58, n. 1, p. 37–54, 2019. ISSN 15588432. 50

SENEVIRATNE, S. I.; NICHOLLS, N.; EASTERLING, D.; GOODESS, C. M.; KANAE, S.; KOSSIN, J.; LUO, Y.; MARENGO, J.; Mc Innes, K.; RAHIMI, M.; REICHSTEIN, M.; SORTEBERG, A.; VERA, C.; ZHANG, X.; RUSTICUCCI, M.; SEMENOV, V.; ALEXANDER, L. V.; ALLEN, S.; BENITO, G.; CAVAZOS, T.; CLAGUE, J.; CONWAY, D.; DELLA-MARTA, P. M.; GERBER, M.; GONG, S.; GOSWAMI, B. N.; HEMER, M.; HUGGEL, C.; VAN DEN HURK, B.; KHARIN, V. V.; KITO, A.; KLEIN TANK, A. M.; LI, G.; MASON, S.; MC GUIRE, W.; VAN OLDDENBORGH, G. J.; ORLOWSKY, B.; SMITH, S.; THIAW, W.; VELEGRAKIS, A.; YIOU, P.; ZHANG, T.; ZHOU, T.; ZWIERS, F. W. Changes in climate extremes and their impacts on the natural physical environment. **Management Risks Extreme Events Disasters to Advances Climate Change Adaptation**, v. 9781107025, p. 109–230, 2012. Available from: <[https://www.ipcc.ch/site/assets/uploads/2018/03/SREX-Chap3\\_FINAL-1.pdf](https://www.ipcc.ch/site/assets/uploads/2018/03/SREX-Chap3_FINAL-1.pdf)>. 1, 101

SHARIFI, E.; STEINACKER, R.; SAGHAFIAN, B. Multi time-scale evaluation of high-resolution satellite-based precipitation products over northeast of Austria. **Atmospheric Research**, v. 206, n. 1, p. 46–63, 2018. ISSN 01698095. 18

SHEATHER, S. J.; JONES, M. C. A reliable data-based bandwidth selection method for kernel density estimation. **Journal Statistics Society**, v. 53, n. 3, p. 683–690, 1991. 26, 54, 85

SHI, J.; YUAN, F.; SHI, C.; ZHAO, C.; ZHANG, L.; REN, L.; ZHU, Y.; JIANG, S.; LIU, Y. Statistical evaluation of the latest GPM-Era IMERG and GSMaP satellite precipitation products in the Yellow River Source region. **Water**, v. 12, n. 4, p. 1006, 2020. ISSN 2073-4441. 18

SHIGE, S.; KIDA, S.; ASHIWAKE, H.; KUBOTA, T.; AONASHI, K. Improvement of TMI rain retrievals in mountainous areas. **Journal Applied Meteorology and Climatology**, v. 52, n. 1, p. 242–254, 2013. ISSN 15588424. 102

SILVERMAN, B. Density estimation for statistics and data analysis. **Journal of Mathematics**, v. 33, n. 1, p. 43–54, 1986. ISSN 03009858. 26, 54, 85

SMITH; WARD. Book review. **Research Policy**, v. 28, n. 4, p. 441–443, 1999. Available from:

<<http://linkinghub.elsevier.com/retrieve/pii/S0048733398001218>>. 1

SORENSEN, J. Hazard warning systems: review of 20 years of progress. **Nature Hazards Review**, v. 1, n. 2, p. 119–125, 2000. ISSN 15276988. Available from: <[http://dx.doi.org/10.1061/\(ASCE\)1527-6988\(2000\)1:2\(119\)](http://dx.doi.org/10.1061/(ASCE)1527-6988(2000)1:2(119))>. 15

SOROOSHIAN, S.; HSU, K. L.; GAO, X.; GUPTA, H. V.; IMAM, B.; BRAITHWAITE, D. Evaluation of PERSIANN system satellite-based estimates of tropical rainfall. **Bulletin of American Meteorological Society**, v. 81, n. 9, p. 2035–2046, 2000. ISSN 00030007. 58, 76

SPRENT; SMEETON. Applied non parametric statistical methods. **Statistics**, n. 1, p. 219–220. ISSN 0932-5026. 27, 54

STEPHENS, G. L.; ELLIS, T. D. Controls of global-mean precipitation increases in global warming GCM experiments. **Journal of Climate**, v. 21, n. 23, p. 6141–6155, 2008. ISSN 08948755. 49

TAPIADOR, F. J.; TURK, F. J.; PETERSEN, W.; HOU, A. Y.; GARCÍA-ORTEGA, E.; MACHADO, L. A.; ANGELIS, C. F.; SALIO, P.; KIDD, C.; HUFFMAN, G. J.; CASTRO, M. de. Global precipitation measurement: methods, datasets and applications. **Atmospheric Research**, v. 104-105, p. 70–97, 2012. ISSN 01698095. Available from: <<http://dx.doi.org/10.1016/j.atmosResearch2011.10.021>>. 49

TAYLOR, K. E. In a single diagram. **Journal of Geophysics Research**, v. 106, n. D7, p. 7183–7192, 2001. ISSN 0148-0227. 25, 53

TEIXEIRA, M. d. S.; SATYAMURTY, P. Trends in the frequency of intense precipitation events in southern and southeastern Brazil during 1960-2004. **Journal of Climate**, v. 24, n. 7, p. 1913–1921, 2011. ISSN 08948755. 13

TEIXEIRA, M. S.; SATYAMURTY, P. Dynamical and synoptic characteristics of heavy rainfall episodes in southern Brazil. **Monthly Weather Review**, v. 135, n. 2, p. 598–617, 2007. ISSN 0027-0644. Available from:

<<http://journals.ametsoc.org/doi/abs/10.1175/MWR3302.1>>. 27

THIELEN, J.; BARTHOLMES, J.; RAMOS, M.-H.; ROO, A. de. The european flood alert system: concept and development. **Hydrology Earth System Science Discuss**, v. 5, n. 1, p. 257–287, 2008. ISSN 1812-2116. Available from:

<<http://www.hydrol-earth-syst-sci-discuss.net/5/257/2008/>>. 16

TIAN, Y.; PETERS-LIDARD, C. D.; EYLANDER, J. B.; JOYCE, R. J.; HUFFMAN, G. J.; ADLER, R. F.; HSU, K.-I.; TURK, F. J.; GARCIA, M.; ZENG, J. Component analysis of errors in satellite-based precipitation estimates. **Journal of Geophysics Research**, v. 114, n. D24, p. D24101, 2009. ISSN 0148-0227.

Available from: <<http://doi.wiley.com/10.1029/2009JD011949>>. 8

TOBIN, M. **Natural hazards: explanation and integration**. New York:: The Guilford Press., 1997. 388 p. ISBN 1-57230-061-2. 62

TORO, J.; MATERA, M.; MOURA, F. S. d.; PEDROSO, F. F. Coping with losses: options for disaster risk financing in Brazil. **Global Facilities Disaster Reduction Recover - World Bank**, p. 86, 2014. Available from:

<<https://www.gfdrr.org/sites/default/files/publication/Options-for-Disaster-Risk-Financing-in-Brazil-English.pdf>>. 15

TURK, F. J.; MILLER, S. D. Toward improved characterization of remotely sensed precipitation regimes with MODIS/AMSR-E blended data techniques.

**IEEE Transactions on Geoscience and Remote Sensing**, v. 43, n. 5, p. 1059–1069, 2005. ISSN 01962892. 102

UNDP, U. N. D. P. **Reducing disaster risk**. [s.n.], 2004. 1 p. ISBN 9211261600.

Available from: <<http://www.ifrc.org/en/what-we-do/disaster-management/preparing-for-disaster/risk-reduction/reducing-disaster-risk/>>. 1

UNIVERSIDADE FEDERAL DE SANTA CATARINA. CENTRO UNIVERSITÁRIO DE ESTUDOS E PESQUISAS SOBRE DESASTRES - UFSC.CEPED. **Atlas brasileiro de desastres naturais 1991 a 2010: volume Brasil**. [S.l.: s.n.], 2012. 94 p. ISBN 9788564695085. 49, 101

VELASCO, I.; FRITSCH, J. M. Mesoscale convective complexes in the Americas. **Journal of Geophysical Research**, v. 92, n. 7, p. 9591–9613, 1987.

1, 14, 56, 79, 101, 104

VENABLES; RIPLEY, B. D. Modern applied statistics. **Annual Mathematics Statistics**, v. 40, n. 4, p. 1386–1400, 2002. ISSN 0003-4851. 26, 54, 85

VERA, C.; BAEZ, J.; DOUGLAS, M.; EMMANUEL, C. B.; MARENGO, J.; MEITIN, J.; NICOLINI, M.; NOGUES-PAEGLE, J.; PAEGLE, J.; PENALBA, O.; SALIO, P.; SAULO, C.; SILVA DIAS, M. A.; SILVA DIAS, P.; ZIPSER, E. The South American low-level jet experiment. **Bulletin of American Meteorological Society**, v. 87, n. 1, p. 63–77, 2006. ISSN 00030007. 79, 104

VILA, D. A.; GONCALVES, L. G. G. de; TOLL, D. L.; ROZANTE, J. R. Statistical evaluation of combined daily gauge observations and rainfall satellite estimates over continental South America. **Journal of Hydrometeorology**, v. 10, n. 2, p. 533–543, 2009. ISSN 1525755X. Available from:  
<<http://journals.ametsoc.org/doi/abs/10.1175/2008JHM1048.1>>. 21, 35

VILA, D. A.; MACHADO, L. A. T.; LAURENT, H.; VELASCO, I. Forecast and tracking the evolution of cloud clusters (ForTraCC) using satellite infrared imagery: methodology and validation. **Weather Forecast**, v. 23, n. 2, p. 233–245, 2008. ISSN 08828156. 80, 95

WAND; MATT; JONES, M. C. **Kernel smoothing**. [S.l.: s.n.], 1994. 26, 53, 84

WANG, Z.; ZENG, Z.; LAI, C.; LIN, W.; WU, X.; CHEN, X. A regional frequency analysis of precipitation extremes in Mainland China with fuzzy c-means and L-moments approaches. **International Journal of Climatology**, v. 37, n. March, p. 429–444, 2017. ISSN 10970088. 13, 18, 46

WERNER, M.; CRANSTON, M.; HARRISON, T.; WHITFIELD, D.; SCHELLEKENS, J. Recent developments in operational flood forecasting in England, Wales and Scotland. **Meteorology Applied**, v. 114, p. 103–114, 2009. ISSN 13504827. 16

WILKS, D. **Statistical methods in the atmospheric sciences**. 3. ed. Cambridge, MA, USA: Elsevier, 2011. ISBN 9780123850225. 24, 109

WILKS, D. S. . **Statistical methods in the atmospheric sciences**. [S.l.: s.n.], 2006. 627 p. ISSN 13504827. ISBN 978-0-12-751966-1. 52

XIE, P.; JANOWIAK, J. E.; ARKIN, P. A.; ADLER, R.; GRUBER, A.; FERRARO, R.; HUFFMAN, G. J.; CURTIS, S. GPCP pentad precipitation analyses: an experimental dataset based on gauge observations and satellite estimates. **Journal of Climate**, v. 16, n. 13, p. 2197–2214, 2003. ISSN 08948755. 21, 59

XIE, P.; JOYCE, R.; WU, S.; YOO, S. H.; YAROSH, Y.; SUN, F.; LIN, R. Reprocessed, bias-corrected CMORPH global high-resolution precipitation estimates from 1998. **Journal of Hydrometeorology**, v. 18, n. 6, p. 1617–1641, 2017. ISSN 15257541. [21](#), [59](#)

XU, L.; GAO, X.; SOROOSHIAN, S.; ARKIN, P. A.; IMAM, B. A microwave infrared threshold technique to improve the GOES precipitation index. **Journal Applied of Meteorology**, v. 38, n. 5, p. 569–579, 1999. ISSN 0894-8763. [58](#), [76](#), [102](#), [111](#)

YAMASOE, M. A.; CORRÊA, M. d. P. **Processos radiativos na atmosfera - Fundamentos**. São Paulo: Oficina de Textos, 2016. 142 p. ISBN 978-85-7975-229-2. [5](#)

YAMAZAKI, Y.; RAO, V. B. Tropical cloudiness over the South Atlantic ocean. **Journal of Meteorological Society Japan**, v. 55, n. 2, p. 205–207, 1977. ISSN 0026-1165. [58](#), [101](#), [105](#)

YONG, B.; LIU, D.; GOURLEY, J. J.; TIAN, Y.; HUFFMAN, G. J.; REN, L.; HONG, Y. Global view of real-time TRMM multisatellite precipitation analysis: implications for its successor global precipitation measurement mission. **Bulletin of American Meteorological Society**, v. 96, n. 2, p. 283–296, 2015. ISSN 00030007. [30](#)

ZAMBRANO-BIGIARINI, M.; NAUDITT, A.; BIRKEL, C.; VERBIST, K.; RIBBE, L. Temporal and spatial evaluation of satellite-based rainfall estimates across the complex topographical and climatic gradients of Chile. **Hydrology Earth System Science**, v. 21, n. 2, p. 1295–1320, 2017. ISSN 16077938. [18](#)

ZHOU, J.; LAU, K. M. Does a monsoon climate exist over South America? **Journal of Climate**, v. 11, n. 5, p. 1020–1040, 1998. ISSN 08948755. [57](#), [105](#)

ZHOU, Y.; LAU, W. K. M.; HUFFMAN, G. J. Mapping TRMM TMPA into average recurrence interval for monitoring extreme precipitation events. **Journal Applied Meteorology and Climatology**, v. 54, n. 5, p. 979–995, 2015. ISSN 15588432. [13](#), [30](#)

ZINNER, T.; MANNSTEIN, H.; TAFFERNER, A. Cb-TRAM : tracking and monitoring severe convection from onset over rapid development to mature phase using multi-channel Meteosat-8 SEVIRI data. **Meteorology Atmospheric Physics**, v. 210, p. 191–210, 2008. [80](#), [95](#)



ZIPSER, E. J. Life cycle of mesoscale convective systems. **Proceedings an International Symposium**, v. 165, p. 381, 1981. Available from:  
<[file:///C:/Users/youhe/Downloads/kdoc{}\\_o{}\\_00042{}\\_01.pdf](file:///C:/Users/youhe/Downloads/kdoc{}_o{}_00042{}_01.pdf)>. 13, 79

ZIPSER, E. J.; CECIL, D. J.; LIU, C.; NESBITT, S. W.; YORTY, D. P. Where are the most: intense thunderstorms on Earth? **Bulletin of American Meteorological Society**, v. 87, n. 8, p. 1057–1071, 2006. ISSN 00030007. 17, 50, 79